ALBERTA OIL SANDS ENVIRONMENTAL RESEARCH PROGRAM

Plume Dispersion Measurements from an Oil Sands Extraction Plant

ME 2.3.1

May 1977

Sponsored jointly by

Alberta ENVIRONMENT

Environment Canada

Environnement Canada

15th Floor, Oxbridge Place
9820 - 106 Street
Edmonton, Alberta T5K 2J6
Phone 403/427-3943

91-03678/

ALBERTA OIL SANDS ENVIRONMENTAL RESEARCH PROGRAM

RESEARCH REPORTS

These research reports describe the results of investigations funded under the Alberta Oil Sands Environmental Research Program, which was established by agreement between the Governments of Alberta and Canada in February 1975. AOSERP is a 10-year Program designed to direct and coordinate research projects into the environmental effects of the development of the Athabasca oil sands in Alberta.

Enquiries pertaining to the Alberta-Canada Agreement or the AOSERP research reports should be directed to:

Alberta Oil Sands Environmental Research Program
15th Floor, Oxbridge Place
9820 - 106 Street, Edmonton, Alberta T5K 2J6
Phone (403) 427-3943.

Plume Dispersion Measurements
from an Oil Sands Extraction Plant
Sub-project ME 2.3.1

AOSERP Report 13

LETTER OF TRANSMITTAL

The Hon. D. J. Russell
Minister of the Environment
Legislative Building
Edmonton, Alberta

and

The Hon. R. LeBlanc
Minister of Fisheries and Environment
Parliament Buildings
Ottawa, Ontario.

Sirs:

Enclosed is the report on "Plume Dispersion Measurements from an Oil Sands Extraction Plant".

This report was prepared for the Meteorology and Air Quality Technical Research Committee of the Alberta Oil Sands Environmental Research Program, under the Alberta-Canada Agreement of 28 February 1975.

Respectfully,

W. Solodzuk, P.Eng.
Chairman, Steering Committee, AOSERP
Deputy Minister, Alberta Environment

for J. S. Tener, Ph.D.
Member, Steering Committee, AOSERP
Assistant Deputy Minister
Environmental Management Services
Environment Canada.

PLUME DISPERSON MEASUREMENTS FROM AN OIL SANDS EXTRACTION PLANT

Descriptive Summary

ABSTRACT

During March 1976, a plume survey program was conducted to determine the diffusion coefficients and turbulence parameters associated with the GCOS effluent plume. Airborne measurements were conducted under various meteorological conditions ranging from stable inversions to neutral stability cases.

Five cases were selected for detailed analysis of plume geometry, mass flux calculations, and turbulence characteristics. Comparisons were made between observed plume structure and the Gaussian-predicted profiles. Lateral and vertical plume spread was derived from each case and compared with the Pasquill-Gifford stability classes. Significant comparisons were made between observed diffusion estimates and the estimates of the standard deviations of the horizontal and vertical wind components.

BACKGROUND AND PERSPECTIVE

As part of the air quality data acquisition system of the Meteorology and Air Quality Technical Research Committee Sector Program, a consultant was commissioned to conduct plume dispersion surveys. The surveys were designed to be an integral part of short duration intensive field studies during which climatology data would be gathered and related to plume disperson and turbulence measurements.

Plume behavior is generally regarded to be unique to geographical areas. In order to establish a comparison to popular theoretical/empirical plume rise models, to normal Gaussian profiles, and to standard deviations as determined from the Pasquill-Gifford stability classes, it was deemed necessary to conduct, by means of a consultant, measurements of SO_2 concentration and turbulence in the plume.

ASSESSMENT

During the two week intensive field study in March 1976 the consultant has been successful in acquiring sufficient data to satisfy the terms of reference as briefly outlined above.

The report has been reviewed by the Meteorology and Air Quality Technical Research Committee and the Oil Sands Environmental Study Group, and has been recommended for publication. The content of this report does not necessarily reflect the views of Alberta Environment, Fisheries and Environment Canada, or the Oil Sands Environmental Study Group.

The report, "Plume Dispersion Measurements from an Oil Sands Extraction Plant" is accepted by the Meteorology and Air Quality Technical Research Committee as having significant input to the concepts of air quality modelling and as such is recommended for publication. The Committee will give the author's recommendation due consideration in planning future studies and the Committee thanks the researchers for their scientific contributions.

F. E. Burbidge

F. E. Burbidge, Chairman
Meteorology and Air Quality
Technical Research Committee.

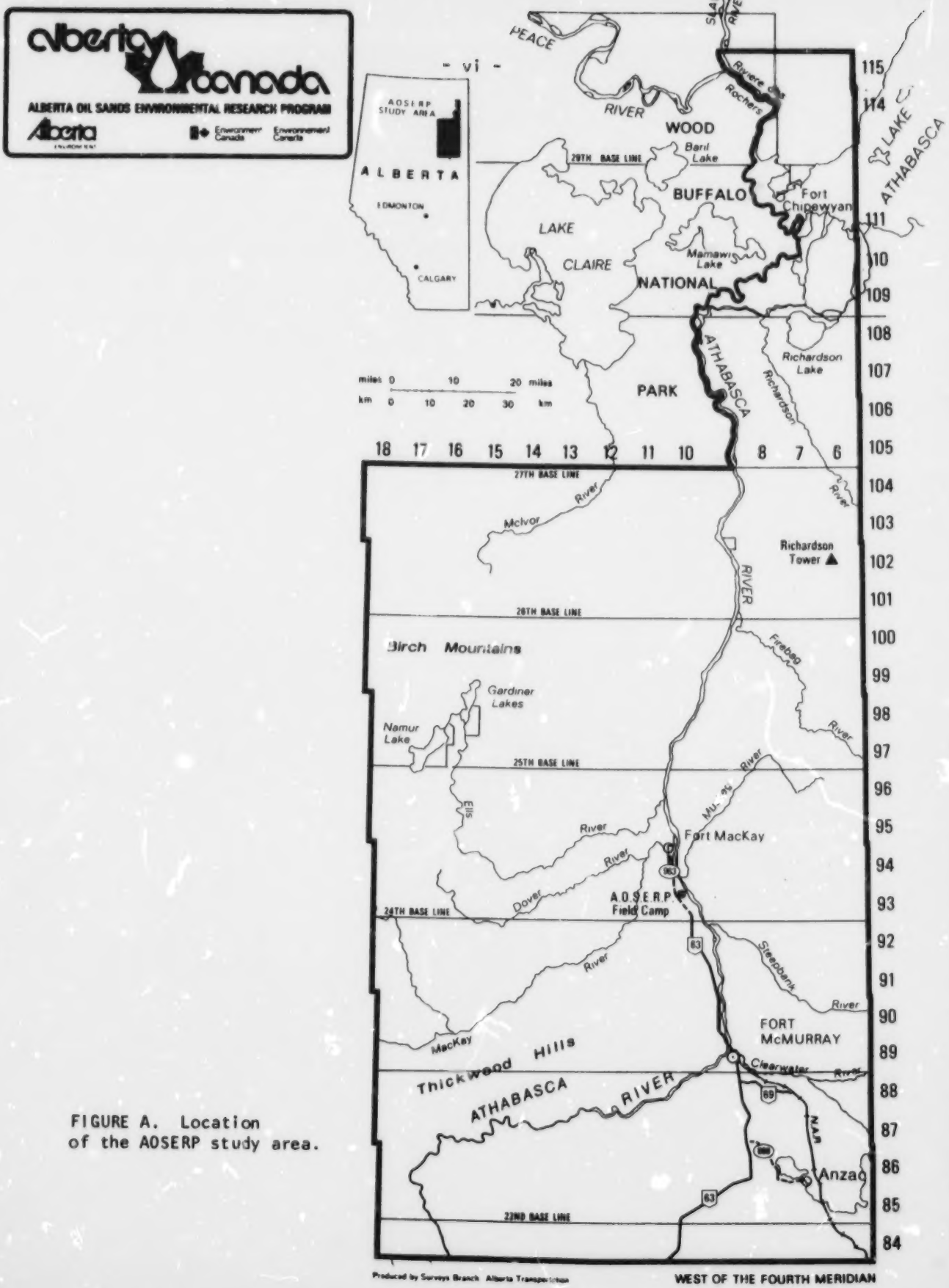

FIGURE A. Location of the AOSERP study area.

PLUME DISPERSION MEASUREMENTS FROM AN OIL SANDS EXTRACTION PLANT, MARCH 1976

by

D.S. DAVISON, Ph.D.;
C.J. FORTEMS, P.Eng., M.Sc.; and K.L. GRANDIA, M.Sc.

INTERA ENVIRONMENTAL CONSULTANTS LTD.
CALGARY, ALBERTA

for

METEOROLOGY AND AIR QUALITY TECHNICAL RESEARCH COMMITTEE
ALBERTA OIL SANDS ENVIRONMENTAL RESEARCH PROGRAM

PROJECT ME 2.3.1

November 1976

TABLE OF CONTENTS

Declaration		ii
Letter of Transmittal		iii
Descriptive Summary		iv
List of Illustrations		x
Abstract		xv
1.	INTRODUCTION	1
2.	EQUIPMENT	3
2.1	Air Chemistry Package	3
2.2	Airborne Turbulence Package	7
2.3	Position Recovery and Other Observations	9
2.4	Airborne Data Acquisition System	9
3.	EXPERIMENTAL PROCEDURES	11
4.	CASE STUDY ANALYSES	13
4.1	Methodology Used in the Analysis of the Case Studies	13
4.2	Case Study for the Flight of March 10, 1976 (1415 - 1705)	22
4.3	Case Study for the Flight of March 11, 1976 (0750 - 1050)	38
4.4	Case Study for the Flight of March 11, 1976 (1250 - 1655)	53
4.5	Case Study for the Flight of March 12, 1976 (1420 - 1650)	68
4.6	Case Study for the Flight of March 15, 1976 (0740 - 0940)	82
5.	DISCUSSION OF THE CASE STUDY RESULTS	98
5.1	A Comparison of Plume Geometry with Pasquill-Gifford Results	98
5.2	The Effects of Topography on Dispersion	103
5.3	Summary of Plume Rise Data	105
5.4	The Relationship between the Standard Deviations of the Plume Dispersion and the Turbulent Statistics	107
5.5	A Recommended Procedure for Relating Turbulence and Plume Dispersion	113
6.	CONCLUSIONS	114
7.	RECOMMENDATIONS	116
8.	LIST OF REFERENCES	118

APPENDICES

1.	SO_2 Traverses for March 10, 1976 (1415 - 1705)	119
2.	SO_2 Traverses for March 11, 1976 (0750 - 1050)	137
3.	SO_2 Traverses for March 11, 1976 (1250 - 1655)	150
4.	SO_2 Traverses for March 12, 1976 (1420 - 1650)	167
5.	SO_2 Traverses for March 15, 1976 (0740 - 0940)	182
6.	Emission Characteristics from GCOS Plant	193
7.	The Appropriate Gaussian Equation for Normalized Axial Centre Line Concentrations	194

LIST OF ILLUSTRATIONS

Figure A	Location of the AOSERP study area	vi
Figure 1	Sign-X SO_2 Analyzer Flow Diagram	5
Figure 2	Schematic of Co-Spec III Internal Operation	6
Figure 3	Flow chart of Airborne Data Recovery System	10
Figure 4	Flight profile for Mar. 10, 1976 (1415-1705).	23
Figure 5	SO_2 concentration isopleths for March 10, 1976 (1415-1705 MST).	25
Figure 6	Normalized SO_2 concentrations for run 5 on the flight of March 10, 1976 (1415-1705).	26
Figure 7	Normalized SO_2 concentrations for run 14 on the flight of March 10, 1976 (1415-1705).	28
Figure 8	Normalized SO_2 concentrations for run 15 on the flight of March 10, 1976 (1415-1705).	29
Figure 9	Observed lateral plume dispersion coefficients compared to Pasquill-Gifford curves for the flight of March 10, 1976 (1415-1705).	31
Figure 10	Observed vertical dispersion coefficient compared to Pasquill-Gifford curves for the flight of March 10, 1976 (1415-1705).	32
Figure 11	Comparison of observed normalized centreline concentrations with Pasquill-Gifford curves for stability C for the flight of March 10, 1976 (1415-1705)	33
Figure 12	Observed centreline SO_2 concentrations shown as a function of altitude for the flight of March 10, 1976 (1415-1705).	35
Figure 13	Flight profile for March 11, 1976 (0750-1050).	39
Figure 14	SO_2 concentration isopleths for March 11, 1976 (0745-1050).	42
Figure 15	Normalized SO_2 concentrations for run 11 on the flight of March 11, 1976 (0750-1050).	43
Figure 16	Normalized SO_2 concentrations for run 8 on the flight of March 11, 1976 (0750-1050).	44
Figure 17	Observed horizontal dispersion coefficients compared with Pasquill-Gifford curves for the flight of March 11, 1976 (0750-1050).	46
Figure 18	Observed vertical dispersion coefficient compared to Pasquill-Gifford for the flight of March 11, 1976 (0750-1050).	47

Figure 19	Comparison of observed normalized centreline concentrations with Pasquill-Gifford curves for Stability C for the flight of March 11, 1976 (0750-1050).	48
Figure 20	Observed centreline SO_2 concentrations as a function of altitide for the flight of March 11, 1976 (0750-1050).	50
Figure 21	Flight profile for March 11, 1976 (1250-1655).	54
Figure 22	SO_2 concentration isopleths for March 11, 1976 (1250-1655).	56
Figure 23	Normalized SO_2 concentrations for run 11 on the flight of March 11, 1976 (1250-1655).	58
Figure 24	Normalized SO_2 concentrations for run 6 on the flight of March 11, 1976 (1250-1655).	59
Figure 25	Observed horizontal dispersion coefficient compared to Pasquill-Gifford curves for the flight of March 11, 1976 (1250-1655).	60
Figure 26	Observed vertical dispersion coefficient compared to Pasquill-Gifford curves for the flight of March 11, 1976 (1250-1655).	61
Figure 27	Comparison of observed normalized centreline concentrations with Pasquill-Gifford curves for Stability C for the flight of March 11, 1976 (1250-1655).	62
Figure 28	Observed centreline SO_2 concentrations as a function of altitude for the flight of March 11, 1976 (1250-1655).	63
Figure 29	Flight profile for March 12, 1976 (1420-1650).	69
Figure 30	SO_2 concentration isopleths for March 12, 1976 (1420-1650).	71
Figure 31	Normalized SO_2 concentrations for run 10 the flight of March 12, 1976 (1420-1650).	75
Figure 32	Normalized SO_2 concentrations for run 15 on the flight of March 12, 1976 (1420-1650).	76
Figure 33	Observed horizontal dispersion coefficients compared to Pasquill-Gifford curves for the flight of March 12, 1976 (1420-1650).	77
Figure 34	Observed vertical dispersion coefficient compared with Pasquill-Gifford curves for the flight of March 12, 1976 (1420-1650).	78
Figure 35	Comparison of observed normalized centreline SO_2 concentrations with Pasquill-Gifford curves for Stability B for the flight of March 12, 1976 (1420-1650).	79

Figure 36	Observed centreline SO_2 concentrations shown as a function of altitude for the flight of March 12, 1976 (1420-1650).	80
Figure 37	Flight profile for March 15, 1976 (0740-0940).	83
Figure 38	SO_2 concentration isopleths for March 15, 1976 (0740-0940).	85
Figure 39	Normalized SO_2 concentrations for run 11 on the flight of March 15, 1976 (0740-0940).	87
Figure 40	Normalized SO_2 concentrations for run 8 on the flight of March 15, 1976 (0740-0940).	88
Figure 41	Normalized SO_2 concentrations for run 9 on the flight of March 15, 1976 (0740-0940).	89
Figure 42	Observed centreline of SO_2 concentrations for the flight of March 15, 1976 (0740-0940).	90
Figure 43	Observed horizontal dispersion coefficients compared to Pasquill-Gifford curves for the flight of March 15 (0740-0940).	93
Figure 44	Observed vertical dispersion coefficient compared to Pasquill-Gifford curves for the flight of March 15, 1976 (0740-0940).	94
Figure 45	Comparison of observed normalized centreline SO_2 concentrations with Pasquill-Gifford curves for Stability D for the flight of March 15, 1976 (0740-0940).	95
Figure 46	Comparison of observed σ_y values with Pasquill-Gifford.	100
Figure 47	Vertical dispersion coefficient as a function of downwind distance from the source as compared with Pasquill-Gifford values.	101
Figure 48	Comparison of observed normalized centreline concentrations with Pasquill-Gifford curves for stability C.	102
Figure 49	Summary of ratios of calculated to observed plume rises.	106
Figure 50	Horizontal plume spread versus the root of the dispersion time.	109
Figure 51	Vertical plume spread versus the root of dispersion time.	110
Figure 52	Schematic velocity spectral shape.	112

TABLES

Table 1	Run information for flight of March 10, 1976 (1415-1705).	24
Table 2	Plume geometry and mass flux as function of downwind distance from source for flight of March 10, 1976 (1415-1705).	30
Table 3	Observed and calculated plume rises for the powerhouse stack for the flight of March 10, 1976	36
Table 4	Summary of turbulence data for the flight of March 10, 1976	37
Table 5	Run information for the flight of March 11, 1976 (0750-1050).	40
Table 6	Plume geometry and mass flux as function of downwind distance from source for flight of March 11,1976 (0750-1050).	45
Table 7	Observed and calculated plume rises for the powerhouse stack for the flight of March 11, 1976 (0750-1050).	51
Table 8	Summary of turbulence data for the flight of March 11, 1976 (0750-1050).	52
Table 9	Run information for flight of March 11, 1976 (1250-1655).	55
Table 10	Plume geometry and mass flux as function of downwind distance from source for flight of March 11, 1976 (1250-1655).	64
Table 11	Observed and calculated plume rises for the powerhouse stack for the flight of March 11, 1976 (1250-1655).	65
Table 12	Summary of turbulence data for the flight of March 11, 1976 (1250-1655).	66
Table 13	Run information for flight of March 12, 1976 (1420-1650).	70
Table 14	Plume geometry and mass flux as function of downwind distance from source for flight of March 12, 1976 (1420-1650).	73
Table 15	Observed and calculated plume rises for the powerhouse stack for the flight of March 12, 1976 (1420-1650).	74

Table 16	Summary of turbulence data for the flight of March 12, 1976 (1420-1650).	81
Table 17	Run information for flight of March 15, 1976 (0740-0940).	84
Table 18	Plume geometry and mass flux as function of downwind distance from source for flight of March 15, 1976 (0740-0940).	91
Table 19	Observed and calculated plume rises for the powerhouse stack for the flight of March 15, 1976 (0740-0940).	92
Table 20	Summary of turbulence data for the flight of March 15, 1976 (0740-0940).	97
Table 21	Assigned Pasquill-Gifford stability classes for each case study.	99
Table 22	A comparison of the effective stack heights with the Pasquill-Gifford σ_z values.	195

ABSTRACT

During March 1976, a plume survey field program was conducted to determine the diffusion coefficients and turbulence parameters associated with the GCOS effluent plume. Airborne measurements were conducted under various meteorological conditions ranging from stable inversions to neutral stability cases.

Five cases were selected for detailed analysis of plume geometry, mass flux calculations, and turbulence characteristics. Comparisons were made between observed plume structure and the Gaussian-predicted profiles. Lateral and vertical plume spread was derived for each case and compared with the Pasquill-Gifford stability classes. Significant comparisons were made between observed diffusion estimates and the estimates of the standard deviations of the horizontal and vertical wind components.

1. INTRODUCTION

In January 1976, Intera entered contract with the Alberta Oil Sands Environmental Research Program to design and conduct a field program, and to analyze specific data from that program. The field program consisted of a three-week aerial gas-tracer sampling program in the Athabasca Oil Sands area, using SO_2 emissions from the G.C.O.S. plant as a tracer.

This final report is submitted to the AOSERP Meteorology and Air Quality Technical Research Committee as part of the terms of the contract. This report presents a review of the terms of reference of the contract, a description of the equipment and experimental techniques used during the field program, summaries of the data collected and discussions of the results of the data analysis.

1.1 TERMS OF REFERENCE

The terms of reference of the study as specified in the attachment to the AOSERP letter to INTERA dated January 19, 1976, are summarized in the following.

1) Design and conduct a three-week aerial gas tracer sampling program using SO_2 emissions from the G.C.O.S. plant as a tracer. The instrumentation and aircraft proposed must determine statistically reliable values of
   - plume width, depth and cross-sectional areas,
   - plume height above groundlevel and downwind trajectory from source,
   - three-dimensional concentration fields and flux of SO_2 and various downwind location for mass balance considerations, and
   - associated turbulence levels.
2) Analyze the level of plume dispersion over complex terrain by
   - presenting three-dimensional concentration profiles and deriving their deviation from the Gaussian distributions of simple plume diffusion models, and
   - deriving standard deviations of horizontal and vertical distributions as functions of downwind distance, comparing of these values with the standard deviations

reported in the literature and correlating these values with measured levels of turbulence.

3) Determine the effects of topography on the plume trajectory by comparing observed plume rise with that predicted by popular theoretical/empirical models.

4) Carry out other analysis as appropriate to extract maximum amount of usable information from the data.

5) Make recommendations for improving subsequent aerial sampling programs.

2. EQUIPMENT

The specific objectives of this study required the accurate determination and recording of various meteorological state parameters, atmospheric turbulence data, and effluent SO_2 plume characteristics. The sensing and recording platforms for this field study were mounted on a light twin-engine aircraft, a Cessna 411. The five-seat passenger configuration was modified considerably to accommodate two standard 19" instrument racks and a technician's station. These racks housed the sensing and recording control units, and the primary power distribution panel.

An external sampling panel was fabricated to mount the sampling probes and intake lines. This panel served the dual role of aircraft escape hatch and instrument mounting panel, which facilitated the installation of numerous instrument mounts without having to cut additional holes in the skin of the aircraft. The panel supported the isokinetic probes for the Sign-X SO_2 Analyzer, viewing ports for the COSPEC monitor, and the E.G.&G. Dew Point Hygrometer.

The turbulence probe was mounted through the nose of the aircraft, parallel to the longitudinal axis. This probe consisted of isolated pitot and static pressure sources and two vanes. The vanes were orthogonally-mounted pitch and yaw vanes. A sliding instrument tray was installed in the part nose compartment to house the pressure transducers and power distribution panel for the probe system. It was desirable to reduce the distance between the pressure sensors and signal tranducers as much as possible, to prevent pressure surges from developing along the lines.

2.1 AIR CHEMISTRY PACKAGE

The effective measurement of an effluent plume structure by an airborne platform requires sensitive, accurate and fast-response samplers that are relatively easy to operate in the air. The accuracy and sensitivity requirements are common to any sampling device. However, the response characterisitics become critical whenever considering a mobile sampling platform. The aircraft is normally operated at 60 m/sec (120 kts) which places a considerable constraint on establishing plume boundaries whenever using a slow-response instrument.

The air chemistry instrumentation used for the SO_2 measurements was the Sign-X SO_2 Analyzer and the Barringer COSPEC III Remote Sensing

Correlation Spectrometer. The Sign X system provides a continuous measurement of SO_2 concentration along a flight traverse. The COSPEC system, on the other hand, provides an integral value along the optical beam volume. For this study the COSPEC beam was sampling vertically upward, so that the resultant signal would yield the total SO_2 burden upward from the aircraft level.

The Sign X SO_2 Analyzer continuously measures the electroconductivity of a sample of deionized water which dissolves all incoming SO_2 gases. Once the conductivity of this sample is measured, the SO_2 solution is converted back to deionized water, which is then recycled through the flow system. The threshold sensitivity of the analyzer is 0.02 ppm, and the SO_2 readings have an accuracy of $\pm$15% of the calibrated range. The time constant for the readings is 2.5 seconds, which is adequate for aerial sampling. The operation of this analyzer is shown schematically in Figure 1 .

During the field study the output signal from the Sign X was monitored on an MFE chart record as well as being digitized and recorded with all the other sensor outputs. The visual display of SO_2 concentration was used extensively by the crew to reference plume positioning and maximum or centreline plume concentration along a traverse. The Sign X system was laboratory calibrated before and after the field program.

The complementary air chemistry unit used for this study was the Barringer Correlation Spectrometer (COSPEC III). This system provides an estimate of the total burden, or integral value, of SO_2 along an optical beam. For the airborne installation, the optical beam was directed vertically, so that the output signal is an estimate of the SO_2 burden upward from the aircraft flight level.

As seen in Figure 2, the sensor contains two telescopes to collect light from a distant source, a spectrometer for dispersing the incoming light, and a correlator. The correlator provides a high contrast reference spectrum for matching against the incoming spectra, in the absorption bands of the target gas. The resulting light modulations are detected by photo-multiplier tubes which produce a voltage output proportional to the optical depth or burden of the gas under observation. The unit contains a reference sample of the SO_2 gas which can be selected by

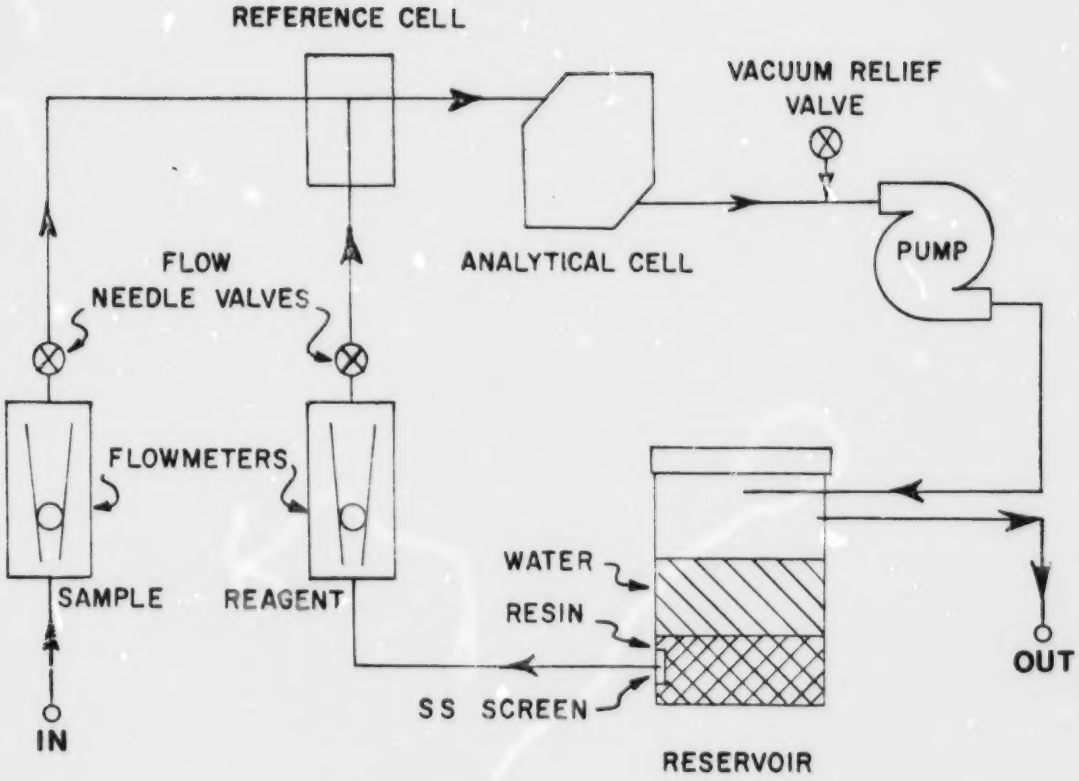

FIGURE 1 Sign-X SO_2 Analyzer Flow Diagram

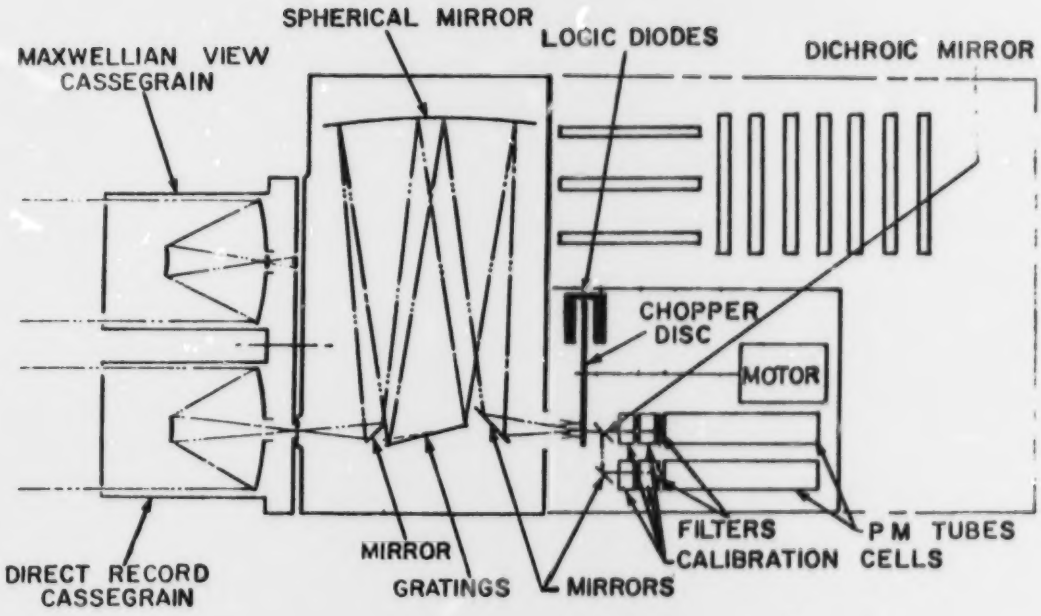

FIGURE: 2 Schematic of Co-Spec III Internal Operation

the technician. Frequently during the flight traverses this reference sample was selected in order to maintain an on-going field calibration. Additionally, the unit was shop-calibrated prior to installation on the aircraft.

The dynamic range of the COSPEC is from $1\text{-}10^4$ ppm-m with a threshold of 6 ppm-m for an 8 second integration time. The response time is as fast as 1 second, with selectable integrating time-steps up to 32 seconds. As with the out put signal from the Sign X, the signal from the COSPEC was monitored on a chart record as well as recorded via the data acquisition system.

INTERA originally proposed a second point SO_2 sampler for this study, a Thermo-Electron pulsed fluorescent analyzer (TECO-43). A TECO system was graciously made available by the Alberta Department of Environment during the field study. However, the response time of 2-4 minutes associated with that particular model of the TECO system precluded its application in an airborne mode, and it was not installed in the aircraft.

A back up Sign X SO_2 monitor was taken to the field study to be available in event of malfunction of the principal Sign X monitor. While it was not needed for the airborne system, it did serve as a temporary replacement for an AES Sign X monitor that was damaged in transit from Toronto.

2.2 AIRBORNE TURBULENCE PACKAGE

The measurement of turbulence is important in an assessment of plume diffusion by turbulent mixing. It is possible to measure the total amount of turbulent energy simply by measuring dissipation through the measurement of band-limited high-frequency pitot pressures. However, this technique of measuring turbulence levels is not advantageous if a careful study of plume dispersion is desired. In trying to relate observed plume geometry to the turbulent mixing mechanisms, it is important to know how the turbulent energy is distributed at the larger size scales which dominate the mixing process. In addition terrain-induced vertical mixing is difficult to document using just dissipation measurements.

The system used by Intera can resolve the actual gust velocities. Once the gust velocities are available the statistics for the horizontal

and vertical components of turbulence can be examined separately. Direct measurement of stability as a function of height can be made using Flux Richardson Numbers or Monin Obukhov length scales. Such stability information is very beneficial in the interpretation of plume isopleths.

To measure the environmental gusts, it is necessary to determine the complete motion forces acting on an aircraft in flight, in order to differentiate those wind components that are attributable to aircraft motion from those due to the environmental gusts. The rates of aircraft pitch, roll, and yaw were measured by three mutually orthogonal miniature gyroscopes aligned to the three axes of the aircraft. A three-axis accelerometer is used to measure motions in the x, y, and z directions. The gyros and accelerometers which together measure all six possible modes of motion were mounted on a platform close to the aircraft centre of gravity.

Pitch and yaw vanes were mounted on an instrument probe extended through the nose of the aircraft. The shaft from each vane drove a miniature autosyn motor, which related a vane deflection to a phase shift of the induced 400 hz signal. The output signal was fed to a demodulator unit which produced a DC voltage according to the amount of phase shift between the vane-controlled 400 hz signal and a reference 400 hz signal.

Accurate static and dynamic pressures are required for the gust calculations. As mentioned above, the static and dynamic ports were mounted on the nose probe, outside the influence of the aircraft itself. Pressure lines from the ports were directed to transducers located at the base of the probe, in order to reduce the length of the pressure lines.

The measurement of temperature and dew point permit determination of heat and water vapor fluxes and of stability. The Rosemount Model 102U2U Total Temperature Probe is a fast-response platinum resistance element, and was mounted under the port wing. The E.G.&G. Dew Point Hygrometer, also a fast-response system, was mounted on the instrument panel. After compensation for the effects of dynamic heating, absolute accuracies from these sensors are of the order of $\pm 0.5C^{\circ}$ with relative accuracies close to $\pm 0.1C^{\circ}$

2.3 POSITION RECOVERY AND OTHER OBSERVATIONS

Position recovery for the aircraft flight profiles was accomplished by hand records of the starting and ending points of each run. Visual land references were used to ensure superposition of the stacked plume traverses.

It became evident during the field trip that a meteorologist/observer was very beneficial to ensure optimum flight profiles and adequate meteorological and plume geometry observations. Navigation proved to be very difficult, so that neither pilot nor co-pilot/navigator had sufficient time to observe the plume carefully.

2.4 AIRBORNE DATA ACQUISITION SYSTEM

The analog signals from the various sensors were directed to the data acquisition system for subsequent recording. This system consisted of the Signal Conditioning Unit (SCU), the Monitor Labs 9400 Data Logger, and the Cipher Incremental Tape Drive. Figure 3 shows a schematic diagram of the Data Acquisition System.

The SCU included a bank of low pass filters designed to eliminate any significant aliasing effects on the incoming signal. Subsequent to the filters was a bank of amplifiers to provide good dynamic range. After passing through the SCU, the signals were fed into the Monitor Labs 9400 Data Logger for digitization and formatting. The digital sampling period for an entire cross-channel sequence plus time and the positions of 10 sense switches was 0.6 seconds.

The digitized, formatted channel sequence was then directed to the Cipher Incremental Tape Drive. This tape drive produced a 9-track, 800 bpi computer compatible tape in EBCDIC format for post-flight computer processing.

Two signals were monitored on an MFE chart recorder for in-flight monitoring. These signals were from the Sign X SO_2 Monitor and the COSPEC III. The chart recorders were mounted for ease-of-access to the technician, to permit hand annotations.

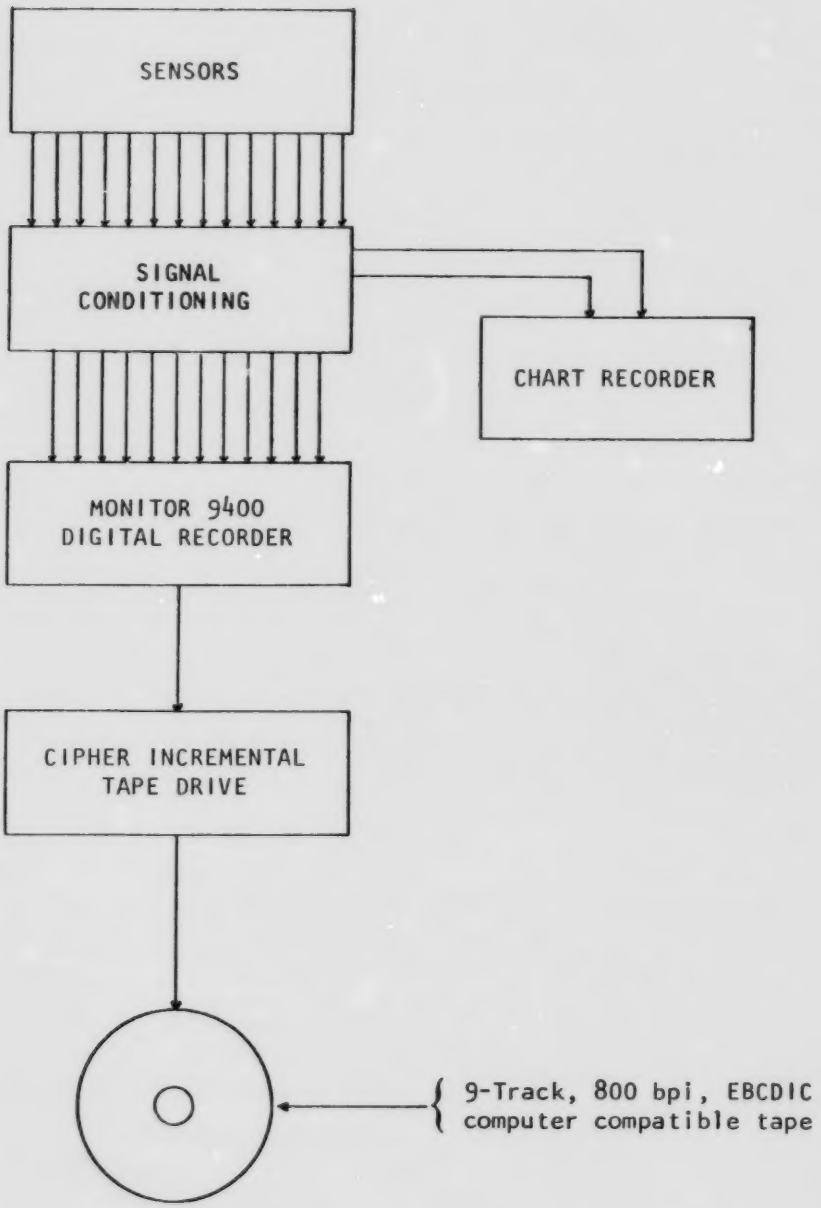

FIGURE 3 Flow chart of Airborne data recovery system

3. EXPERIMENTAL PROCEDURES

The flight profiles used in this study consisted of two phases. One phase examined the effluent SO_2 plume in a rigorous manner to determine the desired plume characteristics. The other phase of the flight profile investigated the characteristics of atmospheric turbulence associated with the plume structure.

To make the greatest number of plume traverses in a given time, short stacked traverses across the plume were flown downwind from the plant. The turbulence runs, on the other hand, required a total of 30 minutes of data, preferably in uninterrupted blocks of about five minutes, in order to obtain stable turbulent statistics. Thus two types of runs were adopted.

It was originally intended to conduct a series of vertically-stacked rectangular patterns downwind from the SO_2 source for the plume traverses. The proposed downwind distances were 0.5, 2, 5, and 10 miles from the source. However, it was observed on several days that the plume at 0.5 miles was still rising to its effective height. Furthermore, the time required to complete two separate rectangular patterns, at all the desired heights to encompass the plume, was approaching 1.5 hours. Within such a length of time, the plume could undergo significant changes. It was thus decided in the field to routinely conduct only one rectangular pattern for the SO_2 plume measurements. The downwind distances were typically 2 and 5-8 miles from the source. This pattern could be flown within 45 minutes, which is a reasonable time to assume steady-state conditions. On some occasions, when conditions warranted, another series of stacked traverses was flown at a third downwind distance.

The cross-wind legs of the rectangular pattern were oriented normal to the plume axis, as best determined by the flight crew, from visual observations of the plume. Topographic maps (scale 1:50,000) were marked for turning points and run numbers for the passes.

The order of the flight levels was mixed to avoid a fixed incremental change. Thus, a typical sequence of altitudes might be 2500', 4000', 3000', 1500', 3500', and 2000' MSL, which would further test the stationarity of the plume structure.

Typically an additional flight segment was flown, visually near centreline level, to ensure that the transects were normal or perpendicular to the plume. This segment was flown at 45° to the assumed plume axis. The relative sizes of the plume cross-sections for the normal and 45° traverses were compared in order to verify that the normal traverses were indeed perpendicular to the plume axis.

Turbulence measurements were made using 2-minute data segments. This length of data permitted the use of the plume traverses as turbulence runs. However, two or three 2-minute segments are not generally considered valid for stable averages of turbulent parameters (see for example Wyngaard (1973) page 140). Thus longer turbulence runs were flown to provide at least a couple of levels of reliable turbulent statistics. A typical turbulence run at one level lasted some twenty minutes and was flown immediately before or after the SO_2 plume runs.

The single dominant terrain feature in the vicinity of the GCOS plant is the Athabasca River valley. The turbulence measurements were designed to relate the plume diffusion coefficients with certain turbulence characteristics, and, further, to evaluate the influence of the topography on turbulence generation. Turbulence runs were generally flown parallel to the river valley. When the mean wind was from the western quadrant, runs were made both upwind and downwind of the valley at the same altitude. In this way the effect of the Athabasca River valley on the turbulence levels at typical plume center line heights could be examined. On other days turbulence runs were flown at two or more heights over the same ground track to examine the vertical changes in the turbulence levels particularly as related to stability consideration.

On case days with light winds, or winds parallel to the riverbed, the aircraft was flown for turbulence runs parallel to, and at the same altitude as the plume centreline.

In order to estimate the stationarity of the turbulence generation, the typical flight sequence consisted of a turbulence run after the aircraft arrived at the SO_2 plume source. Upon completion of this phase the aircraft was flown in the plume sampling mode, after which a second turbulence sequence was made. The typical flight time, then, was about 4 hours per case, as weather permitted.

4. CASE STUDY ANALYSES

4.1 METHODOLOGY USED IN THE ANALYSIS OF THE CASE STUDIES

4.1.1 Criteria for the selection of the case studies

There were two major criteria for the selection of the case studies. The first was the requirement for relatively stationary meteorological conditions. The second was the completeness of the profiles.

By the nature of the data collection procedure, stationary conditions were required. In order to be able to determine concentration isopleths, mass flux and plume geometry all the traverses had to be assumed to be describing the same plume. For example, the rapid visual changes in the plume structure during the flight of March 14 precluded that day. The early morning inversion cases had to be completed before the mixing height rose high enough to begin fumigation.

The flight profiles and the data set needed to be complete in order to obtain reliable plume interpretations. This criteria precluded days in which there were serious instrument malfunctions or in which poor visibility led to large variations in the ground track of the stacked traverses.

The five case studies which were chosen provide a fairly representative range of meteorological conditions for early March period.

4.1.2 Isopleth analysis

On the individual plume traverses, the SO_2 concentrations were sampled as a function of time and recorded along with the turbulence data on magnetic tape. The data were calibrated and normalized and the SO_2 concentrations were printed and plotted by the computer. From these traverses (the complete set is included in the appendices) the intercepts of SO_2 concentration levels could be determined as a function of distance along the traverse. The corresponding intercepts at each flight level were then joined to form the isopleths. On most days, there was little ambiguity; however in well mixed cases, some subjective judgment had to be used. The intercepts along each flight level are the data; all interpolations are subjective.

4.1.3 Determination of plume geometry and mass flux

The center line trajectory was determined from observer notes in the field and from photographs of the plume taken during the flights. The horizontal plume dispersion coefficient, σ_y, was computed for each traverse on the basis of the area under the SO_2 concentration curve. For a Gaussian distribution, minus and plus one standard deviation occur at distances such that the accumulated fractions of the total area under the curve are 0.159 and 0.841 respectively. The σ_y values were computed using the same area criteria. This procedure meant that the observed concentrations were being compared with a Gaussian distribution of the same area. Often the σ_y values are computed in terms of the second moment of the distribution. However this latter method puts extra weighting on secondary peaks removed from the main peak. At the GCOS site there were many minor sources of SO_2 such that secondary peaks were common particularly well downwind of the source. In such a situation the use of a second moment technique leads to very large σ_y values; whereas the area technique minimized the effects of small displaced peaks.

The vertical plume dispersion coefficients, σ_z, were computed by assuming that each traverse was representative of the layer from midway to the flight level above to midway to the one below. The upper and lower limits were estimated from observer field notes and photographs. The σ_z values were then computed by the area method described above for the σ_y values.

The mass flux was calculated from the horizontally integrated concentrations along each traverse with the same layer representation as for σ_z. The mean wind speed, $\bar{U}$, was obtained from the tethersonde data as provided by Dr. R. Mickle of AES, Downsview. It is interesting to note that even the 10-minute averages of the tethersonde wind speeds showed considerable change from 10-minute block to 10-minute block. The large degree of variability in meteorological parameters at the typical heights of the plume center line is not unexpected from both theoretical and previous experimental results. This variability means that winds obtained by theodolite from free rising balloons are not adequate for mass flux computations.

4.1.4 Plume rise formulations

Atmospheric dispersion of a gas plume is most easily discussed as two separate aspects: (1) the plume rise relative to the mean motion of the air because of buoyancy and initial vertical momentum and (2) diffusion because of turbulence in the air. Briggs (1969) discusses plume rise in this manner and indicates that although in reality these aspects occur simultaneously, they are generally assumed not to interact. In this discussion only the aspect of plume rise is reviewed.

When a less dense plume is emitted into the atmosphere it has momentum and buoyancy. The momentum, which generates mechanical turbulence because of the velocity shear between the emitted gases and the air, causes mixing with the ambient air. This mixing, termed entrainment, dilutes the plume and in turn diminishes its momentum and buoyancy. Once the initial vertical velocity is eliminated, the plume acquires the horizontal momentum of the entrained air. However, the plume can continue to rise because of residual buoyancy. The duration of these buoyancy effects is dependent on the rate of dilution and the stability of the atmosphere. If the atmosphere is well mixed it is said to be neutral or adiabatic with a negative temperature gradient of $0.98^{o}C$ per 100 m. This adiabatic lapse rate is indicative of the rate air adiabatically cools because of expansion as the ambient atmospheric pressure decreases. Thus a plume rising through adiabatic air, entraining ambient air of constant potential temperature as it ascends, is quickly diluted losing buoyancy and momentum to reach a state of equilibrium. In contrast, if the lapse rate is less than adiabatic (ie. stable), the air entrained in the plume will have negative buoyancy causing the plume to sink to a lower altitude until equilibrium is attained. The buoyancy of a plume increases as it rises if the temperature lapse rate is greater than adiabatic, which in turn accentuates the plume rise.

The various parameters integral to the assessment of plume rise are given a detailed discussion by Briggs (1969) and will not be repeated here. However the formulations or models to be used in the comparative analysis with the observed plume rises will be listed. Of the various models available, the following were selected primarily because of their extensive usage.

1) Briggs
2) TVA (1972)
3) Bosanquet, Carey and Holton
4) Holland

The methods of TVA (1972), and Holland are empirical derivations based from published source data while those of Briggs and Bosanquet et al are theoretical developments with the Briggs method being verified by data. In addition the Briggs model recognizes the dependency of plume rise on downwind distance when downwind distances are less than that corresponding to the final rise. The others estimate ultimate or maximum height only. Momentum rise is not considered separately by Briggs and TVA (1972) because of its negligible contributions. In summary the equations making up these models are as follows.

1) **Briggs model**

a) Unstable or neutral conditions

$$\Delta h = 1.6\, F^{1/3}\, (3.5\, X^*)^{2/3}\, U^{-1}$$

wherein

$X^* = 14F^{5/8}$ when $F < 55 m^4 s^{-3}$

$X^* = 34F^{2/5}$ when $F \geq 55 m^4 s^{-3}$

and the downwind distance to the final rise given by $X_f = 3.5X^*$

b) Stable windy conditions

$$\Delta h = 2.4 \left(\frac{F}{US}\right)^{1/3}$$

c) Stable calm conditions

$$\Delta h = 5.0\, F^{1/4}\, S^{-3/8}$$

wherein

$$S = \frac{g}{Ta} \frac{\Delta\theta}{\Delta Z}$$

and the downwind distance to the final rise given by $X_f = \pi U S^{-1/2}$

2) TVA (1972) model

$$\Delta h = 173\, F^{1/3}\, (U\, E)^{-1}$$

wherein

$$E = \exp\left(64 \frac{\Delta\theta}{\Delta Z}\right)$$

3) Bosanquet, Carey and Halton

a) Unstable and neutral conditions

momentum rise is

$$\Delta h_v = \Delta h_{vmax}\left(1 - 0.8\,\frac{\Delta h_{vmax}}{x}\right)$$

wherein

$$\Delta h_{vmax} = \frac{1.45}{1 + 0.43\ U/V_s}\cdot(Q_1 Vs)^{1/2}\ U^{-1}$$

and buoyancy rise is

$$\Delta h_b = \frac{1.94\ g\ Q_1\ \Delta T_1\ Z}{U^3 T_1}$$

wherein

$$Z = -1.7 + 4.5\ \text{Log}\ X$$

$$X = 0.08\ xU\ (Q_1 V_s)^{-1/2}$$

b) Stable conditions

$$\Delta h_b = \frac{1.94\ g\ Q_1\ \Delta T_1 Z}{U^3\ T_1}\ (\log J^2 + \frac{2}{J} - 2)$$

wherein

$$J = U^2\ (Q_1\ V_s)^{-1/2}\ \left(0.43\left(\frac{T_1}{g\frac{\Delta\theta}{\Delta Z}}\right)^{1/2} - 0.28\ \frac{V_s}{g}\ \frac{T_1}{\Delta T_1}\right) + 1$$

giving a total plume rise of

$$\Delta h = 0.75\ (\Delta h_v + \Delta h_b)$$

4) Holland model

$$\Delta h = (1.5\ V_s d + 1.102\ F)\ U^{-1}$$

wherein

Δh = plume rise, m

U = wind speed, m/sec

g = acceleration due to gravity, m/sec^2

$\Delta\theta/\Delta Z$ = lapse rate of potential temperature °C/m

x = downwind distance from stack, m

V_s = stack exit velocity, m/sec

d = stack diameter, m

T_s = stack exit temperature, °K

T_a = ambient temperature, °K

$\Delta T = T_s - T_a$, °K

T_1 = temperature at which the stack gas density is equivalent to that of air, °K

$\Delta T_1 = T_s - T_1$

$F = 2.45 \quad V_s \, d^2 \, \Delta T/T_s$, m^4/sec^3

$Q = 0.785 \, V_s \, d^2 \, T_1/T_s$, m^3/sec

X^*, X_f, S, E, X, and J defined as above

For each case analyzed emission data provided by Great Canadian Oil Sands Limited were reduced to generate average stack exit temperature and flow rate. These data are summarized in the Appendix 6. Ambient temperature, wind speed and temperature gradient were abstracted from the tethered balloon data collected by the Atmospheric Environment Service. Generally there was more than one set of data over the plume survey period which was averaged for the layer of the atmosphere between stack top and observed plume tops. For those cases where one of the meteorological parameters varied significantly during the survey separate calculations were made. The observed effective stack heights were derived from the center line or maximum sulphur dioxide concentration as measured by the analyzer mounted in the aircraft. Photographs taken by the aircraft complemented this analysis.

4.1.5 Analysis procedures for and interpretation of the turbulence data

The turbulence data were analysed in 2-minute data segments to avoid any serious drift problems with the gyros. The data segments correspond to a distance of about 7 km (4.3 miles) and so are long enough to resolve eddies that would influence the plume.

The turbulence system measures the wind with respect to a moving platform (the aircraft) whose motion is measured. Hence it is possible to resolve the environmental gust velocities by computer reduction of the data. The same basic technique has been used by several groups around the world to obtain turbulence data and is well accepted in the meteorological literature (see, for example, McBean and MacPherson (1976),

Donelan and Miyake (1973)).

It is interesting to note that since the air speed of the aircraft was typically 20 times faster than the wind speed, a 2-minute aircraft data segment was equivalent to a 40-minute ground based observation. Even so, there were major averaging problems due to the inherent increase in intermittency of turbulence with increasing height; so that several 2-minute data segments were usually required for a reliable averaged turbulent quantity. Where a sufficient number of data segments were available, the standard deviation of the mean value was calculated.

There was a problem with unreliable pitot pressure values in several of the case studies. It was decided that these data, when questionable, would not be used. In such cases, only the vertical and transverse turbulent components but not the longitudinal component (with respect to the aircraft) were computed. There were usually sufficient runs parallel and perpendicular to the wind direction so that all three turbulent components could be estimated. Frequently there were more crosswind turbulence runs than along-wind runs and so the longitudinal environmental gusts (transverse gusts with respect to the aircraft) were better defined. The momentum stress is largely in the longitudinal-vertical plane and so the estimates of the momentum stress were probably not seriously degraded. The standard deviations of the lateral wind component would be more seriously affected. However the assumption of equi-partition of energy in the two horizontal directions is a reasonable approximation and so the average standard deviations of the horizontal wind components denoted by the subscript "UH" was often used in place of σ_v. On the March 12 case study, reliable pitot pressure were available and the data validated these approximations.

It is important to recognize some of the differences in the turbulent quantities presented. The standard deviations of the wind components are very frequently used to relate plume dispersion coefficients to turbulence (for example Pasquill (1971) and Draxler (1976)). However, there are two important considerations to keep in mind when interpreting such data.

Firstly, the standard deviations are sensitive to all velocity changes whether turbulent or laminar. For example, wave motion would contribute to the standard deviations of the wind components but would

have very little turbulent mixing effect since the existence of the waves indicates the presence of stable layers. The same contribution to the standard deviations from truly turbulent eddies would cause significantly more mixing. In any region of irregular topography, the use of the standard deviations must be carefully examined. In one of the case studies, turbulence runs on both sides of the Athabasca River failed to show statistically significant differences which suggests that the use of standard deviations in the Athabasca oil sands area is most probably valid.

The second consideration is whether the horizontal wind components have a low frequency fall-off. The length of the turbulence runs was probably long enough to give stable σ_u and σ_v values which are insensitive to the exact length of the run. Calculations using 60-second, 90-second and 120-second data segments showed no significant differences.

The momentum fluxes are $\overline{W'U'}$ and $\overline{W'V'}$ (where the primes indicate fluctuating quantities, the overbar is a time average, and U, V, and W are the x, y, z wind velocities following standard meteorological sign conventions and nomenclature). These quantities are an indication of the amount of smaller scale turbulent energy. In a mixed surface boundary layer $\overline{W'U'}$ is negative indicating transfer of momentum toward the ground; that is, the wind feels the effects of the ground drag. If $\overline{W'U'}$ and $\overline{W'V'}$ are near zero then there is very little mechanical turbulence. If $\overline{W'U'}$ is positive then there may be a low level jet. Obtaining a stable average value for the momentum flux requires a lot of data because of intermittency (see for example Wyngaard (1973)). Thus only the values from heights with at least five 2-minute segments can be considered representative.

The heat flux, $\overline{W'T'}$ is a measure of the local thermal stability. If the heat flux is positive then heat is moving upward and so the air mass is unstable. It is important to realize that even in very unstable conditions, the temperature profile above the near surface layer is adiabatic and hence indistinguishable from a neutral case.

The stability of an air mass is often defined in terms of the ratio of the mechanical to convective energy; the exact forms may be Richardson Numbers, Flux Richardson Numbers, Monin Obukhov Lengths or

some other less frequently used parameters. The advantages of the above forms compared to Pasquill-Gifford stability classes is that the above forms are continuous variables that can be directly measured as opposed to somewhat subjective classes. The Monin-Obukhov stability formulation has the widest use in the literature and so was often used in the discussions of the case studies. Stability is determined by the value of Z/L where Z is height above ground and L is the Monin-Obukhov Length defined as

$$L = - \frac{U_*^3 T}{Kg \overline{W'T'}}$$

where

U_* is the friction velocity: $U_*^2 = ((\overline{U'W'})^2 + (\overline{V'W'})^2)^{1/2}$ following McBean and MacPherson (1976)

T is the absolute temperature

g is acceleration due to gravity

K is von Karman's constant, (0.4)

A negative Z/L value is unstable; a positive value is stable. In some cases turbulent levels were so small that reliable values for Z/L could not be calculated. In such cases, it was clear that the suppression of turbulence in the presence of a wind could only rise from very stable conditions.

4.1.6 Use of the Cospec Data

Because of low sun angle, the signal-to-noise ratio for the Cospec data was very poor. The Automatic Gain Compensation value for the Cospec was very often at a level of 8.5 to 9 which indicates unreliable data. However, the Cospec data were used to check the calibration of the Sign X and the degree of veering of the plume for isopleth and mass flux analysis. The method to determine the amount of SO_2 in the layer between stacked traverses from Cospec data involves the difference between two poorly defined large values to obtain a smaller value. Data quality was not considered good enough to follow such a procedure and so routine computer analysis was not done on the Cospec data. The use of the Cospec in subsequent field trips is still considered valuable, but an improved signal-to-noise ratio is essential.

4.2 CASE STUDY FOR THE FLIGHT OF MARCH 10, 1976 (1415-1705)

4.2.1 General meteorology and visual plume description

The visual plume was moving south along the west bank of the Athabasca River with very little meandering; (see Figure 4). There were obvious capping inversion effects with clear air above the visual plume. A concentration of visual plume was noted near the capping inversion but fumigation to the ground was also visible. There was some layering near the top of the visual plume.

Low level emissions from the GCOS site were seen to be flowing northward down the valley, almost directly opposed to the main plume. These visual observations were confirmed by the data from the AES tethersonde. The tethersonde wind records showed a southerly wind near the surface veering through a westerly wind to a northerly wind by 200 meters (640 feet) above ground. The wind speed was 1 to 2 m/sec (3 to 6 ft/sec) under a clear sky.

4.2.2 Flight profiles

A race track pattern was set up with stacked crosswind traverses at 1.6 km (1 mile) and 14.6 km (9 miles) (see Figure 4 and Table 1). Run 11 was flown at approximately 45° to the plume axis as a orthogonality check. Run 12 was flown for a stationarity check. It also served as a check on any instrumental response effects. A series of stacked traverses were then flown at 6.4 km (4 miles) downwind. Then turbulence runs were made parallel to the river on the west side.

4.2.3 Isopleths and selected traverses

Figure 5 shows the isopleths of SO_2 concentrations at 1.6 km (1 mile) and 14.6 km (9 miles). As discussed in Section 4.1, the isopleths were sketched in from the crosswind traverses indicated on the isopleth diagram. Normalized plots of the SO_2 concentration for every traverse are indicated in the Appendix.

Secondary emissions cause an apparently broad plume particularly at low levels. A layering observed at the top of the inversion may explain the isolated peak at 14.6 km (9 miles).

Figure 6 is a plot of the normalized SO_2 concentrations for run 5 near the center line at 1.6 km (1 mile). It can be seen that there is excellent agreement with a Gaussian distribution.

Figure 4 Flight profile for Mar. 10, 1976 (1415-1705). Solid lines denote numbered runs and dashed lines denote interconnecting legs. Plume centerline for 1430 is superimposed.

TABLE 1 Run information for flight of March 10, 1976 (1415-1705)

RUN NUMBER	TIME (MST)	ALTITUDE (m-MSL) ±20	DOWNWIND DISTANCE (km) ±0.3	σ_y (m) ±100	MAX CONC. (ppm) ±0.02	INTEGRATED CONC. (ppm-m) ±50	FLIGHT DIR. (From-to)
1	1431 - 1435	1220	1.6	3350	0.06	210	W - E
2	1441 - 1448	1220	14.5	5640	0.11	700	E - W
3	1453 - 1457	760	1.6	3420	0.26	510	W - E
4	1500 - 1505	760	14.5	3710	0.11	610	E - W
5	1508 - 1512	910	1.6	790	0.60	1100	W - E
6	1516 - 1521	910	14.5	*	0.11	*	E - W
7	1525 - 1528	490	1.6	*	0.10	*	W - E
8	1533 - 1537	490	9.7	*	0.08	*	E - W
9	1540 - 1544	980	1.6	920	0.83	1440	W - E
10	1548 - 1553	980	14.5	2300	0.25	480	E - W
11	1555 - 1600	980	-	2030	0.32	890	SW-NE
12	1602 - 1606	980	1.6	1130	0.73	1300	E - W
13	1610 - 1616	910	6.4	4010	0.30	1130	W - E
14	1618 - 1622	760	6.4	3580	0.20	770	E - W
15	1624 - 1628	760	6.4	2840	0.27	840	W - E
16	1630 - 1633	460	6.4	*	0.27	*	E - W
17	1638 - 1644	760	-	T	T	T	N - S
18	1645 - 1651	760	-	T	T	T	S - N
19	1652 - 1658	760	-	T	T	T	N - S

- flight not perpendicular to plume (i.e. not crosswind)
* incomplete sectioning of plume so that reliable values not available
T turbulence run

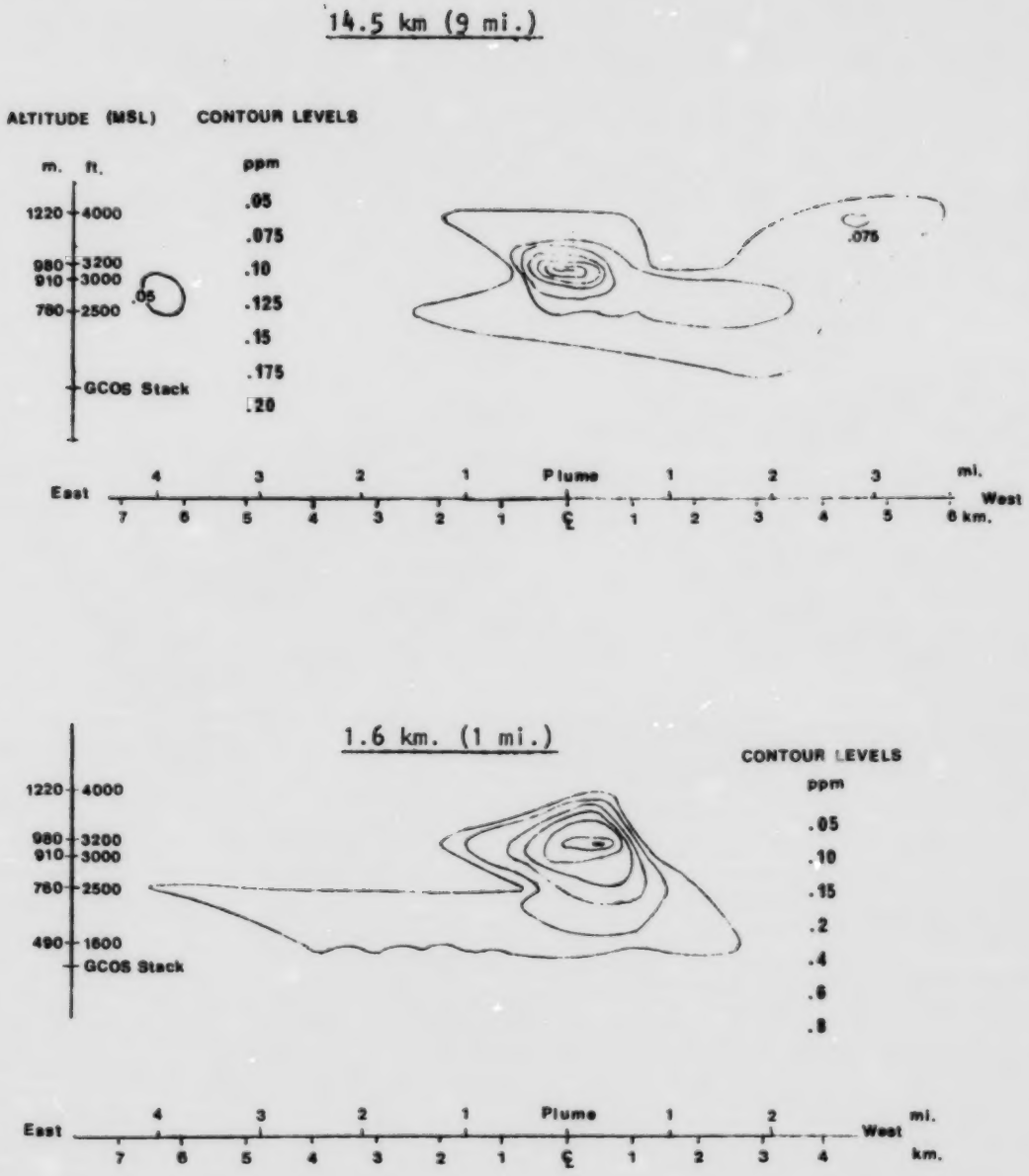

FIGURE 5 SO_2 Concentration Isopleths for March 10, 1976 (1415-1705 MST). Transects were flown downwind of GCOS Stack at 1.6 km. (1 mi.) and 14.5 km. (9 mi.).

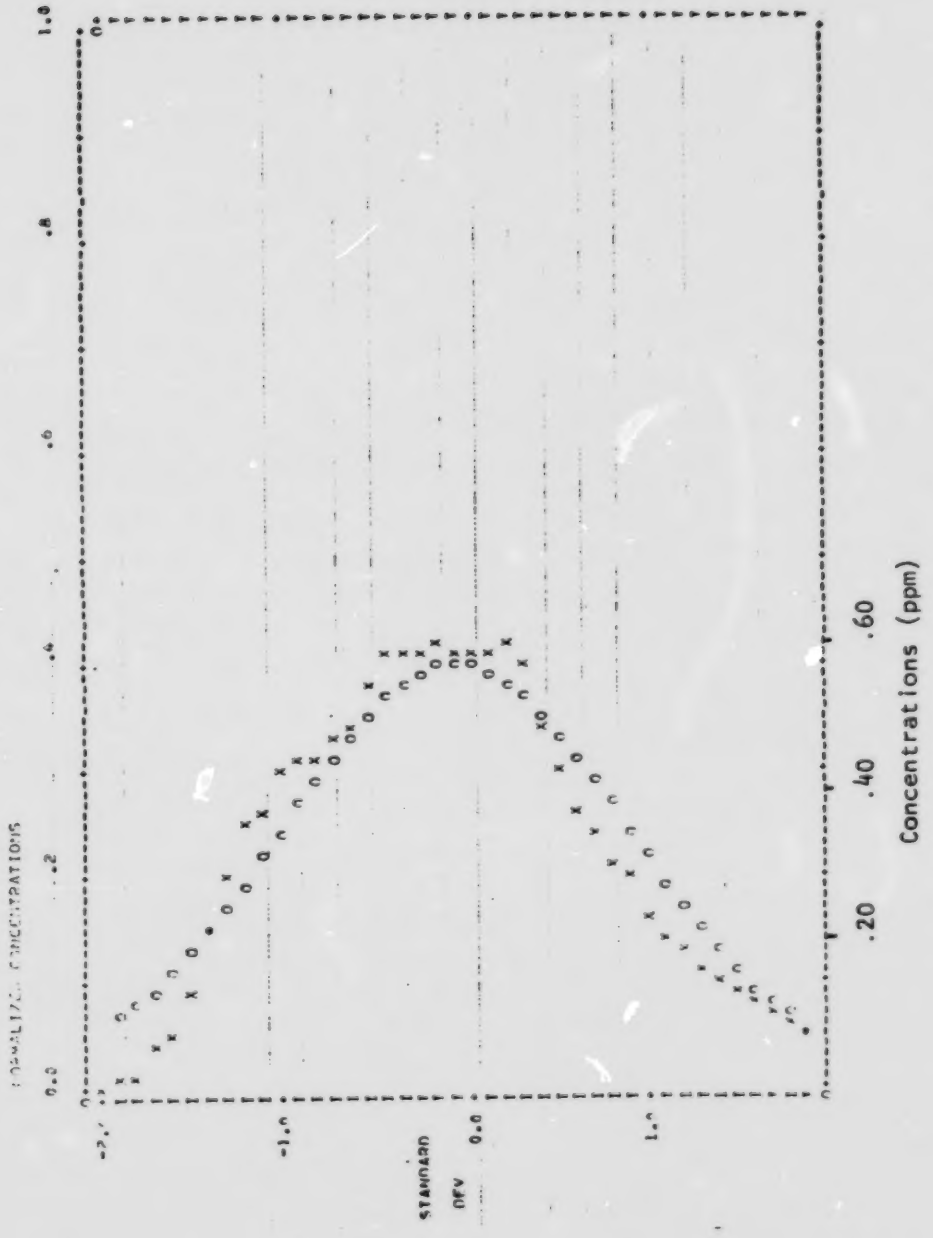

FIGURE 6 Normalized SO_2 concentrations for run 5 at an altitude of 910 m.^{2} (3000 ft.) MSL at a downwind distance of 1.6 km. (1 mile) on the flight of March 10, 1976 (1415-1705).

Figures 7 and 8 are similar normalized plots of SO_2 concentrations for runs 14 and 15 both at a height of 760 m MSL (2500 ft MSC) at 6.4 km (4 miles) downwind of GCOS. These runs were flown in opposite directions and indicate the repeatability of the minor peaks. Note how the minor peaks result in a much greater lateral standard deviation (σ_y) than would result with only the main plume. The multiple peaks are presumably from the multiple sources at GCOS and are visible to a greater or lesser extent on all the lower level traverses.

4.2.4 Plume geometry and mass flux

Table 2 summarizes the plume geometry and mass flux. Both mass flux estimates a . 40% too low. The wind speed used in the computation was 1.2 m/sec (2.7 mph); both the mass fluxes and the comparison of observed and theoretical plume rise estimates (discussed below) indicate that 1.8 m/sec is the correct wind speed. The tethersonde's maximum height on this day was 450 m AGL or approximately 700 m MSL (2300 ft MSL). Thus the wind speed estimate had to be extrapolated some 300 m (1000 ft) to plume center line.

Figures 9, 10, and 11 show the observed values of σ_y, σ_z, and normalized concentrations compared to the empirical curves derived by Pasquill and Gifford (see Turner 1969). The curves for the axial concentrations were computed using the Pasquill-Gifford formulation without a virtual source for reasons outlined in Appendix 7. The observed σ_y values are much larger than predicted but this effect may be due to the effect of multiple sources. Note that from 1.6 km to 6.4 km (1 mile to 4 miles) the slope of the change is parallel to the Pasquill-Gifford curves. By 16.4 km (9 miles) the observed σ_y is closer to the predicted values, indicating, perhaps, that at the GCOS site can be treated as a single source by that distance downwind.

The observed σ_y values agree much more closely to Pasquill-Gifford values and indicate a C or D stability. The larger value of σ_z at 1.6 km (1 mile) may reflect the efforts of lower level fugitive emissions.

The normalized axial center line concentrations suggest B or C stability. The departure of the observed values from the Pasquill-Gifford values will be discussed in the next chapter.

Also included in Table 2 are plume sigma values non-dimensionalized by turbulence values. These will be discussed below.

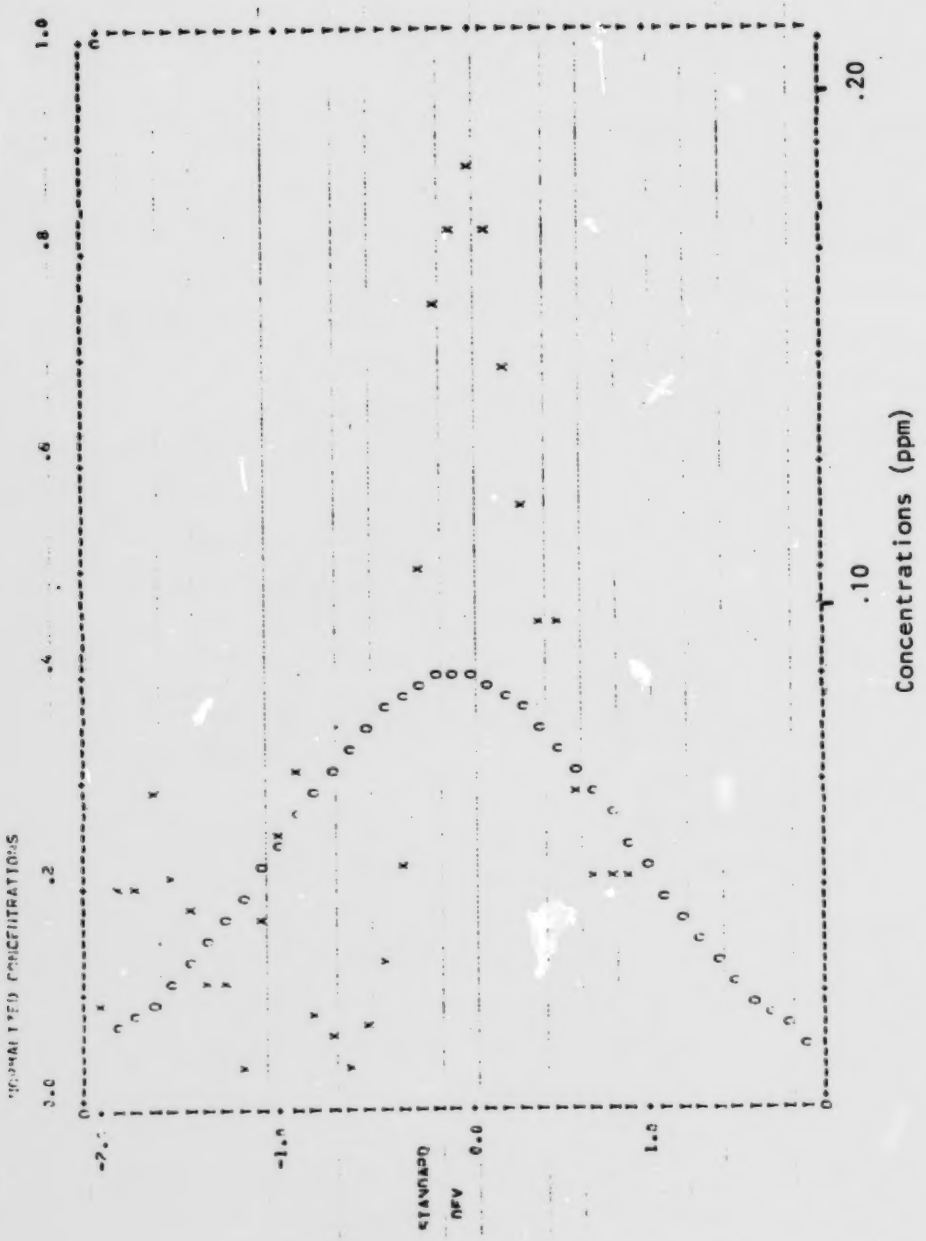

FIGURE 7 Normalized SO_2 concentrations for run 14 at an altitude of 760 m. (3000 ft.) MSL at a downwind distance of 6.4 km. (4 miles) on the flight of March 10, 1976 (1415-1705).

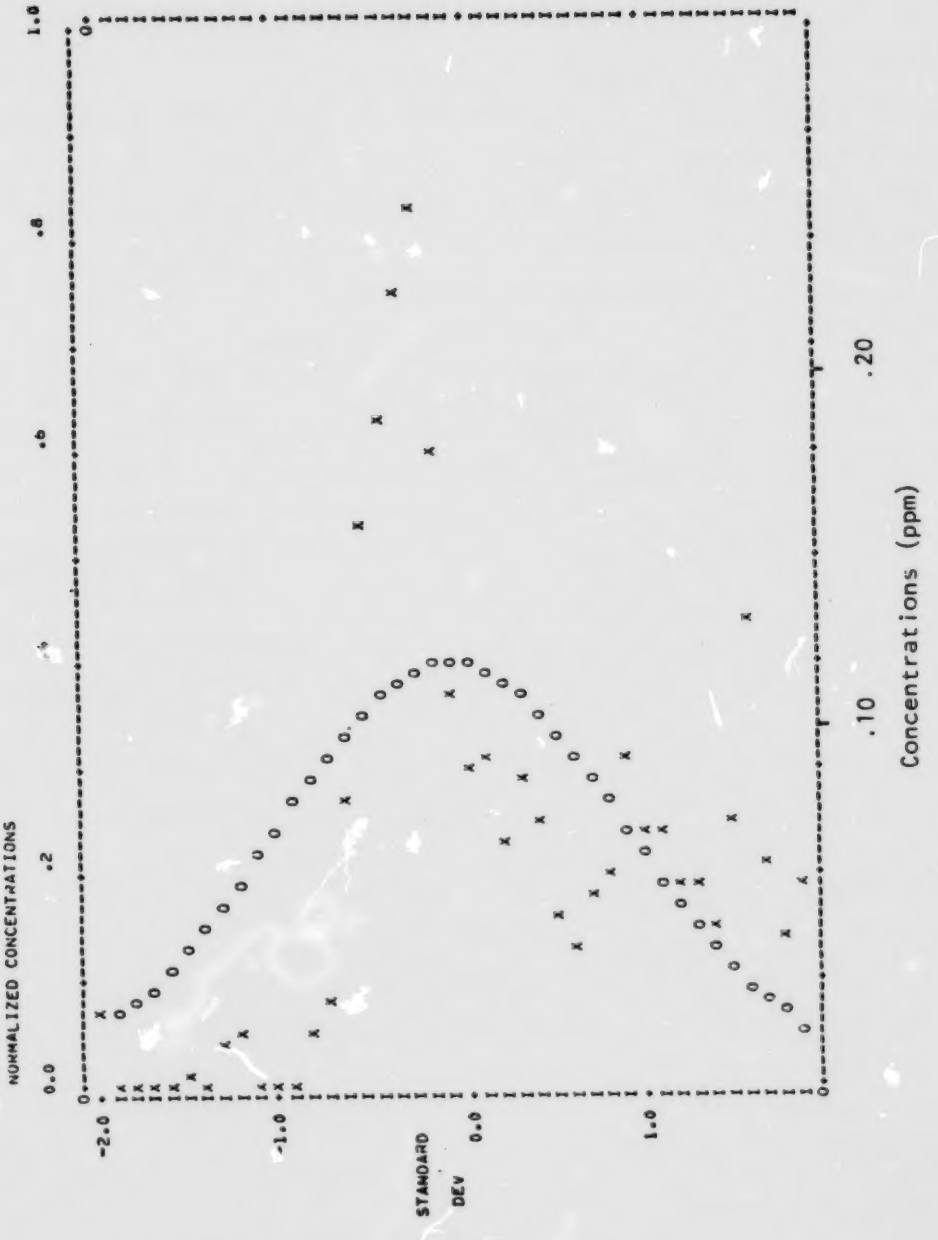

FIGURE 8 Normalized SO_2 concentrations for run 15 at an altitude of 760 m. (3000 ft.) MSL at a downwind distance of 6.4 km. (4 miles) on the flight of March 10, 1976 (1415-1705).

TABLE 2 Plume geometry and mass flux as function of downwind distance from source for flight of March 10, 1976

DOWNWIND DISTANCE X [km]	NORM. CL CONC $\chi\bar{U}Q^{-1}$ [$10^{-6}m^{-2}$]	σ_z [m] ± 20	σ_{ycl} [m] ± 100	SO_2 mass flux [metric tons per hour]	$\frac{\sigma_z \bar{U}}{\sigma_w} X$	$\frac{\sigma_{ycl} \bar{U}}{\sigma_{UH} X}$
1.6	0.91	170	1025	6.0	0.20	0.45
6.4	*	*	4010	*	*	0.44
14.5	0.29	290	2300	6.1	0.037	0.11

* insufficient data for reliable estimate

Q is the average output for the power house stack: 9.4 metric tons/hour (9.3 long tons/hour) (data are courtesy of GCOS)

$\bar{U}$ are estimated from the tethersonde data as 1.2 m/sec (2.7 mph) (data are courtesy of Dr. R. Mickle, AES, Downsview, Ontario); this value of wind speed is suspect since it must be extrapolated 300 m (1000 ft) to reach center line

χ is concentration in terms of mass of SO_2 per unit volume

SO_2 mass flux was calculated assuming the layer centered at 1220 m extended to 1280 m

σ_{ycl} σ_y value at center line

X downwind distance

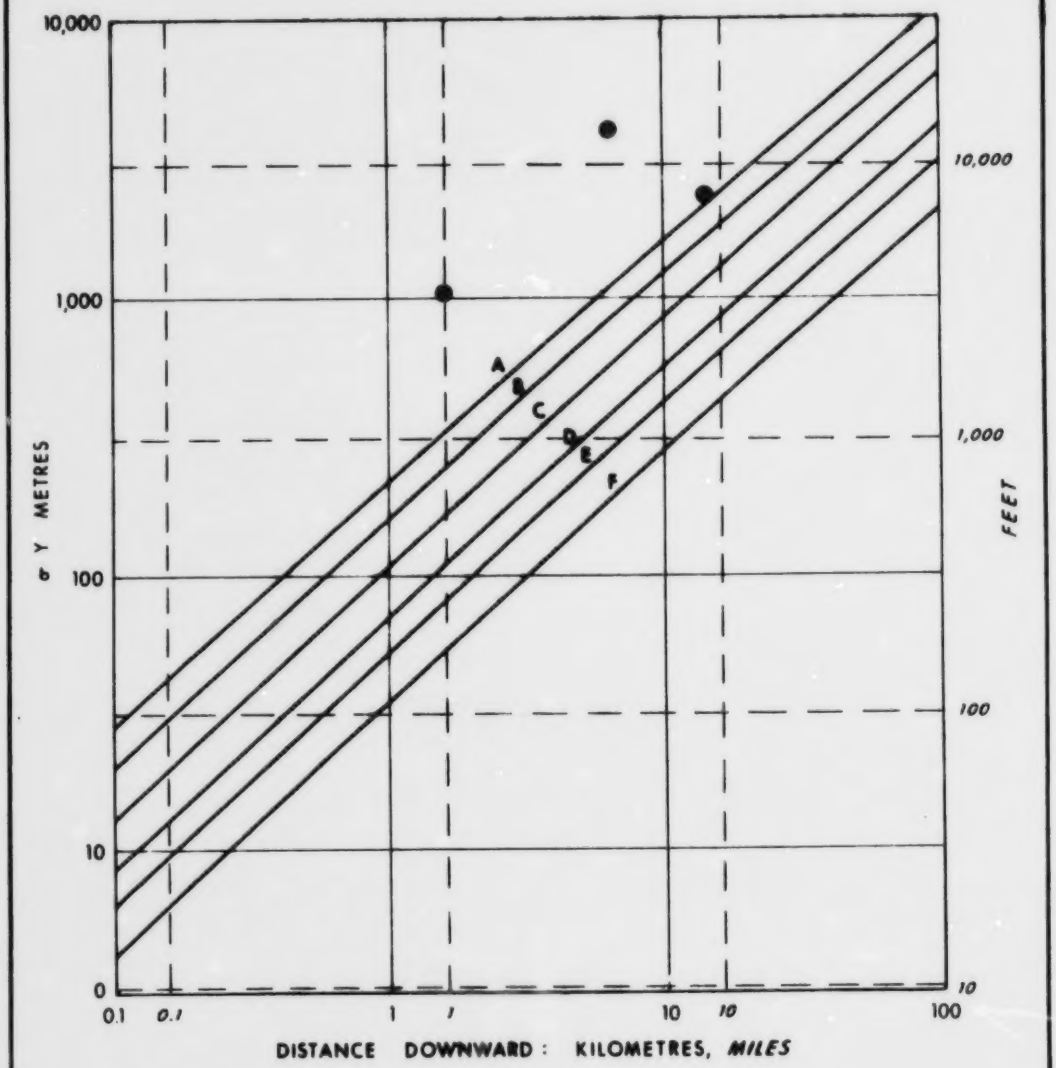

FIGURE 9 Observed lateral plume dispersion coefficients compared to Pasquill-Gifford curves for the flight of March 10, 1976 (1415-1705 MST).

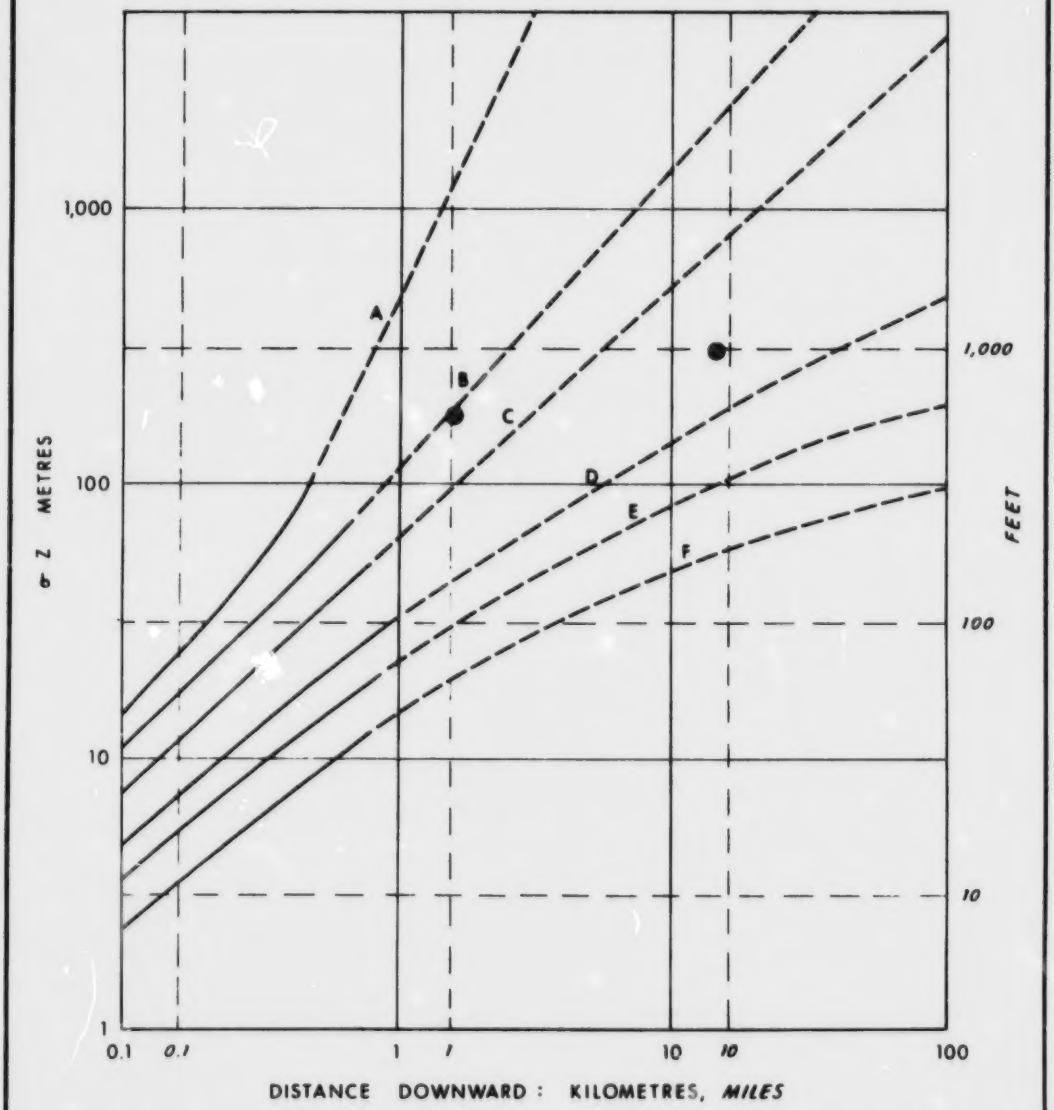

FIGURE 10 Observed vertical dispersion coefficient compared to Pasquill-Gifford curves for the flight of March 10, 1976 (1415-1705 MST).

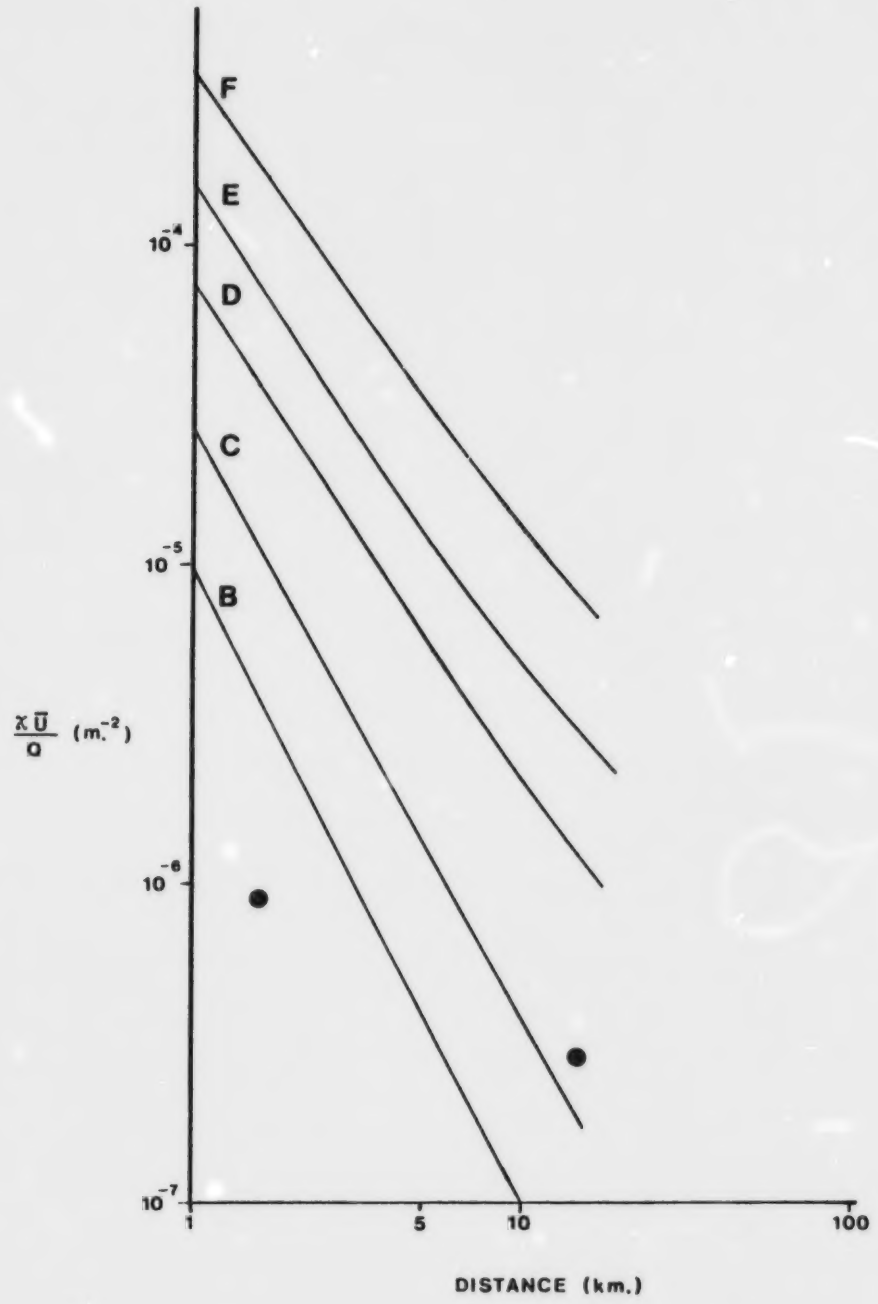

Figure 11. Comparison of observed normalized centerline concentrations with Pasquill-Gifford predictions for the flight of March 10, 1976 (1415-1705 MST).

4.2.5 A comparison of observed and calculated plume rise

The observed effective stack heights for three downwind distances are presented in Figure 12. It is evident from this figure that the plume attained its final rise of 610 m (2000 feet) at the first set of traverses located 1.6 km (1 mile) from the source.

Table 3 presents a comparison of observed and calculated plume rise. Because of doubt as to the wind speed two are presented in the table. In general all formulations give higher than observed plume rises. The predictions of the Bosanquet and Holland equations appear more correct than those estimated using Briggs and TVA (1972) for the conditions of March 10, 1976, (1415-1705). In all calculations it was necessary to assume a neutral atmosphere when in fact a neutral layer was capped by a lofted inversion at 1220 m MSL (4000 feet MSL). Preliminary calculations based on Briggs (1969) suggest the plume should not penetrate the inversion. Hence the Briggs and TVA (1972) plume rises are optimistic because of the deficiency common to all formulations of failing to recognize a changing temperature gradient while the apparent correctness of the other two formulas is coincidental.

4.2.6 Turbulence levels related to plume structure

Table 4 summarizes the turbulence data for the afternoon flight of March 10. As discussed in Section 4.1, the turbulence analysis was accomplished using 2-minute data segments a time over which the drift of the motion sensors was insignificant. Due to a malfunction of the pitot sensor, only the vertical and transverse wind components could be measured on each turbulence segment. Thus crosswind runs provided data for the vertical along wind components. The standard deviations of the wind components (σ_w, σ_u, and σ_v) represent the variation over all wavelengths whether strictly turbulent or not. The terms $\overline{W'U'}$, $\overline{W'V'}$, and $\overline{W'T'}$ generally represent actual turbulence-induced transport of momentum and heat.

From Table 4, it can be seen that there is very little vertical variation in the amount of energy in the vertical or horizontal wind field. However the vertical wind component has only about half as much energy as in the horizontal component. This measurement reflects the

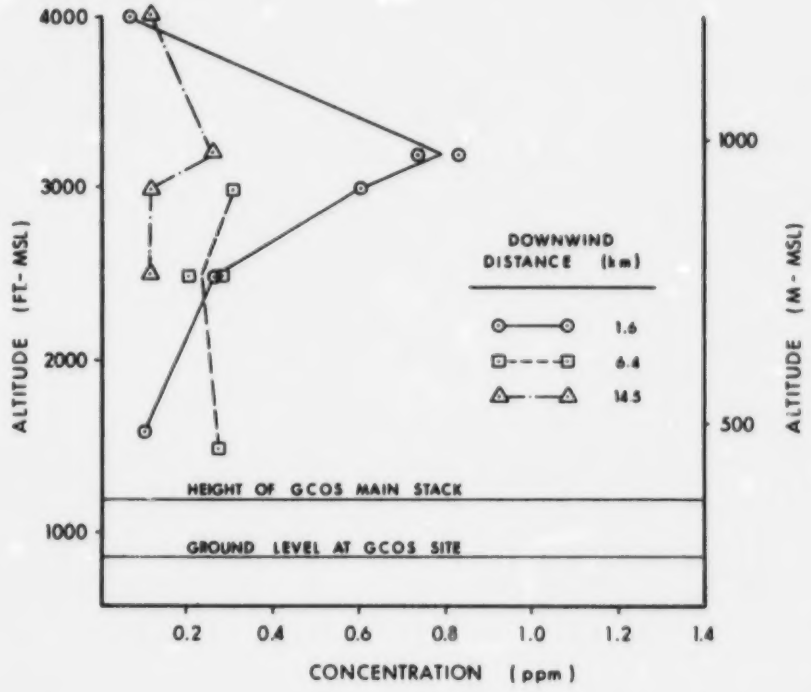

FIGURE 12 Maximum SO_2 concentrations along each traverse shown as a function of altitude for the flight of March 10, 1976 (1415-1705 MST).

TABLE 3 Observed and calculated plume rises for the powerhouse stack for the flight of March 10, 1976

DOWNWIND DISTANCE (km)	PLUME RISE OBSERVED (m) ±50	WINDSPEED (m/sec.)	RATIO CALCULATED TO OBSERVED VALUES OF uΔh BRIGGS TVA(1972) BOSANQUET HOLLAND FORMULATIONS 1	2	3	4
1.6	610	1.5	2.33	1.74	1.15	1.14
6.4	*					
14.5	610					
1.6	610	2.0	1.74	1.31	1.05	0.86
6.4	*					
14.5	610					

* reliable estimate not available

limitation on vertical size scale due both to stability effects and the presence of the ground. In the horizontal, large scale sizes can exist.

The heat flux $\overline{W'T'}$ shows a change with height. Although the statistics are rather weak, there is a strong indication that there is positive (upwards) heat flux at low levels becoming negative at upper levels. This behaviour would be expected for fumigation (unstable conditions) at lower levels, with a capping inversion at upper levels.

One commonly used measure of stability is the Monin-Obukhov length, L, relating mechanical to convective turbulence normalized by the height of the measurement, Z.

At 460 m MSL (1600 ft MSL), Z/L = -1.0 indicating slight instability. At 980 m MSL (3200 ft MSL), Z/L = +10 indicating very stable conditions. At intermediate levels near plume center line (760 m or 2500 ft), Z/L 0 indicating neutral stability. Clearly, the appropriate Pasquill-Gifford stability class will depend upon the effective stack height of the plume.

TABLE 4 Summary of turbulence data for the flight of March 10, 1976

HEIGHT [m MSL]	NUMBER OF RUNS		σ_w [m/sec]	σ_u [m/sec]	σ_v [m/sec]	$\overline{W'U'}$ $[m/sec]^2$	$\overline{W'V'}$ $[m/sec]^2$	$\overline{W'T'}$ [deg C-m/sec]
	1	//						
1220	4	0	0.71	1.5	*	0.21	*	-0.015
980	4	2	0.65	1.7	3.9	0.31	-0.37	-0.004
			(0.1)					(0.015)
910	5	1	0.87	2.1	2.4	-0.23	1.37	-0.015
			(0.10)	(0.4)		(0.15)		(0.02)
760	3	8	0.67	1.29	1.3	0.03	-0.06	-0.001
			(0.06)	(0.07)		(0.09)		(0.006)
490	3	0	0.72	2.5	*	-0.13	*	0.021

The bracketed values underneath some average quantities are standard deviations of those values

// number of runs parallel to the mean wind which yielded values for σ_v and $\overline{v'w'}$

1 number of crosswind runs giving values for σ_u and $\overline{U'W'}$

On a hot summer's day, a typical heat flux, $\overline{W'T'}$, is 0.2 [deg C -m/sec] (Davison (1973)); so that the heat flux observed here is only about 10% of a typical summer heat flux.

In Table 2, the plume sigma values σ_z and σ_y were non-dimensionalized by the corresponding standard deviations of the wind components and the time available for diffusion to take place $X/\overline{U}$, where X is downwind distance and $\overline{U}$ is the mean wind speed. The non-dimensionalized σ_z values decreased with distance. This effect may be due to the capping inversion limiting continued vertical diffusion. The non-dimensionalized σ_y values at 1.6 and 6.4 km (1 and 4 miles) are equal indicating a linear relationship between the turbulence and the diffusion. However at 14.5 km (8 miles) a drop-off has occurred indicating that the linear relationship does not continue indefinitely. These tentative suggestions will be amplified in the next chapter where the results of all the individual case studies can be brought together.

4.3 CASE STUDY FOR THE FLIGHT OF MARCH 11, 1976 (0750-1050)

4.3.1 General meteorology and visual plume description

When the plume was first approached at 0810, the plume was oriented directly to the east with very little vertical veering and not much rise; the plume center line was at approximately 2000' MSL; (see Figure 13 for the center line trajectory). Several miles downwind, (on the east side of the Athabasca River Valley) there was wide lateral dispersion with the visual plume filling-in creek valleys.

By 0930 the visual plume structure was changing with limited fumigation close to the stack. The upper boundary of the plume showed capping inversion effects with some layering.

The tethersonde profile at 0920 to 0944 showed a strong inversion up to 120 m (400 ft) AGL, then a neutral layer up to about 210 m (690 ft) AGL, then a weakly stable layer up to about 300 m (980 ft AGL). Since the tethersonde was operating in the river valley, the top of the strong surface inversion was at the height of the top of the stack. Thus the plume encountered a neutral layer topped by a weak stable layer. By the time of the tethersonde profile at 1054 to 1115, the surface-based inversion had disappeared.

The wind speed profile at 0920 had a strong shear with a 2 m/sec (6.4 ft/sec) wind near the surface becoming a 10 m/sec (32 ft/sec) wind at 200 m (640 ft) AGL. The wind speed was starting to decrease above 250 m (820 ft) AGL suggesting that there was a low level jet just above the inversion. The second profile starting at 1054 showed a mean wind speed gradually increasing with height to about 4 m/sec (13 ft/sec) near the center line height of 610 m MSL (2000 ft) or 365 m AGL (1200 ft) from the tethersonde site. This slower wind speed after some mixing had taken place suggests that the high winds detected earlier was indeed a thin low level jet.

4.3.2 Flight profiles

A race track pattern was flown with stacked crosswind traverses at 1.6 km (1 mile) and 6.4 km (4 miles) as shown in Figure 13 and Table . A series of stacked traverses were then flown at 3.2 km (2 miles) downwind; it was considered that would provide better repeatability

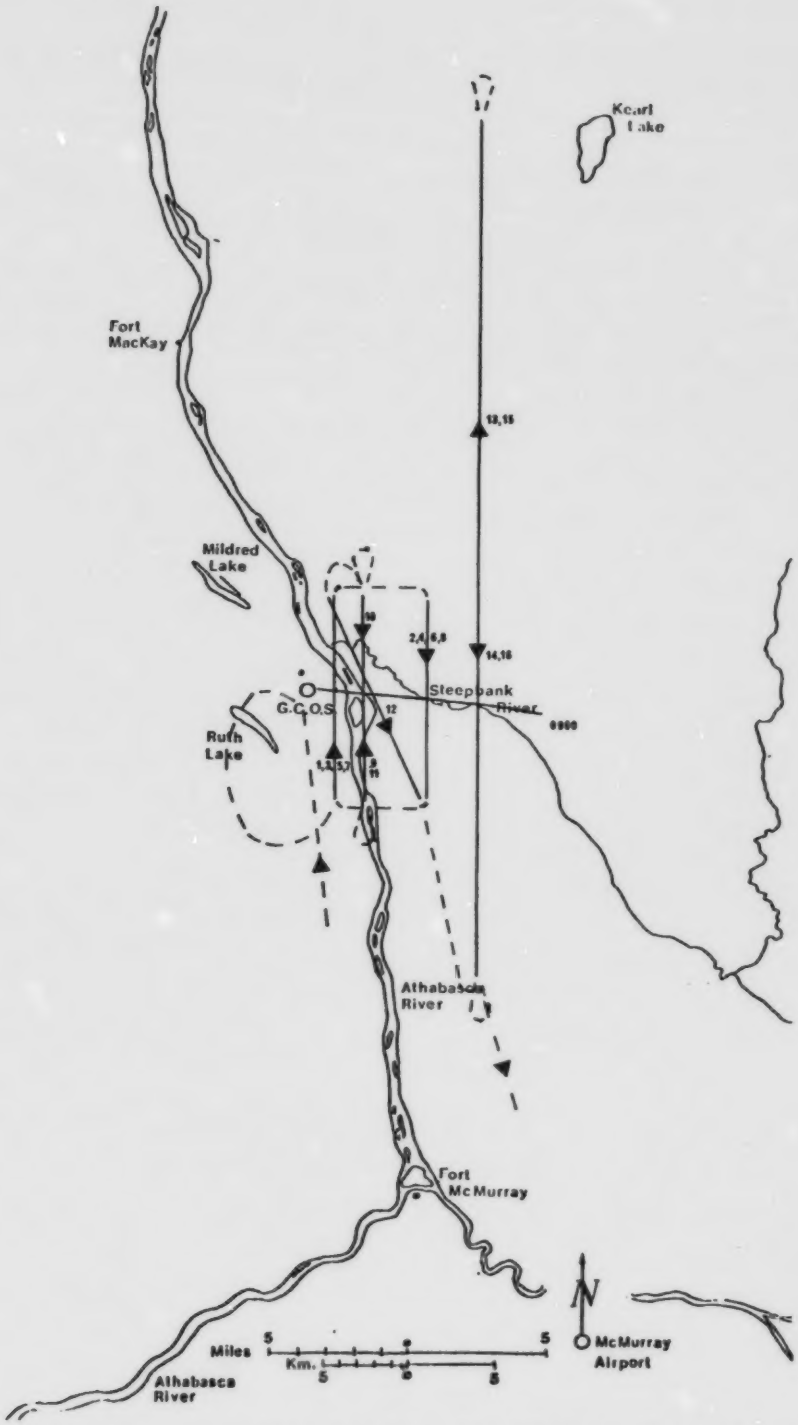

Figure 13 Flight profile for Mar. 11, 1976 (0750-1050). Solid lines denote numbered runs and dashed lines denote interconnecting legs. Plume centerline for 0900 is superimposed.

TABLE 5 Run information for flight of March 11, 1976 (0750-1050)

RUN NUMBER	TIME (MST)	ALTITUDE (m-MSL) ±20	DOWNWIND DISTANCE (km) ±0.3	σy (m) ±100	MAX CONC. (ppm) ±0.02	INTEGRATED CONC. (ppm-m) ±50	FLIGHT DIR. (From-to)
1	0817 - 0819	610	1.6	2310	0.220	333	S - N
2.	0821 - 0824	610	6.4	1175	0.418	714	N - S
3	0828 - 0832	910	1.6	2859 *	0.093 *	473 *	S - N
4	0834 - 0836	880	6.4	1686	0.058	127 +	N - S
5	0810 - 0843	460	1.6	1147	0.632	962	S - N
6	0845 - 0848	460	6.4	3283	0.082	280 +	N - S
7	0851 - 0854	670	1.6	3927	0.044	202	S - N
8	0858 - 0902	670	6.4	1639	0.403	868	N - S
9	0904 - 0907	670	3.2	1421	0.359	511	S - N
10	0910 - 0912	460	3.2	2110	0.218	434	N - S
11	0915 - 0918	610	3.2	892	1.069	1502	S - N
12	0924 - 0928	610	-	2006	0.469	1463	NW-SE
13	0931 - 0946	610	8.0	T	T	T	S - N
14	0948 - 1002	610	8.0	T	T	T	N - S
15	1007 - 1020	1220	8.0	T	T	T	S - N
16	1022 - 1034	1220	8.0	T	T	T	N - S

T Turbulence run
- Plume was traversed at an angle for an orientation check
* Incomplete traverse resulting in unreliable values for plume sigma and concentration values
+ Small part of plume was missed, so that integrated concentration values were increased by 10%

than 1.6 kms (1 mile) since there would be more time to smooth out longitudinal variation in the plume. Following an angular traverse (run 12), a series of turbulence runs were made at 610 m MSL and 1220 m MSL (2000 feet and 4000 feet).

By 0930, there appeared to be visually more fumigation than at the time of the beginning of the flight.

4.3.3 Isopleths and selected traverses

The isopleths of SO_2 concentrations for the traverses at 6.4 km (4 miles) and 3.2 km (2 miles) are shown in Figure 14. Although the response time of the Sign X SO_2 sampler was quite adequate to resolve the plume, there was an additional problem of purging the system after very large concentrations were encountered. The extension of the plume toward the north at 3.2 km (2 miles) at center line height is partially instrumental. Figure 15 is a normalized SO_2 concentration plot for run 11 at center line height at 3.2 km (2 miles), which had a maximum SO_2 count of over 1 ppm. A slow recovery of the sensor after the high concentrations is evident. Figure 16 is a similar plot for run 8 at 6.4 km (4 miles) downwind at 670 m (2200 ft). The wider plume (see Table 5) and the lower concentration (a maximum of 0.40 ppm) resulted in a more symmetric cross-section with an apparently real second peak. The sloping of the isopleths toward the north at low levels at 6.4 km (4 miles) was noted in the log sheets and can be attributed to the effects of wind veering with height. The complete set of normalized SO_2 concentration plots is included in the Appendix.

4.3.4 Plume geometry and mass flux

Table 6 summarizes the plume geometry and mass flux for the morning flight of March 11. The mass flux estimates were consistent at 3.2 and 6.4 kms (2 and 4 miles): the value at 1.6 km (1 mile) is suspect since the plume center line was missed.

Figures 17, 18, and 19 show the observed values of σ_y, σ_z and normalized concentrations compared to the Pasquill-Gifford curves. The observed σ_y values are again several times larger than predicted. The effect of multiple sources gives the plume much greater spread. The σ_z values indicate C to D stability (slightly unstable to neutral); whereas the normalized concentrations agree most closely with C stability (slightly unstable).

6.4 km. (4 mi.)

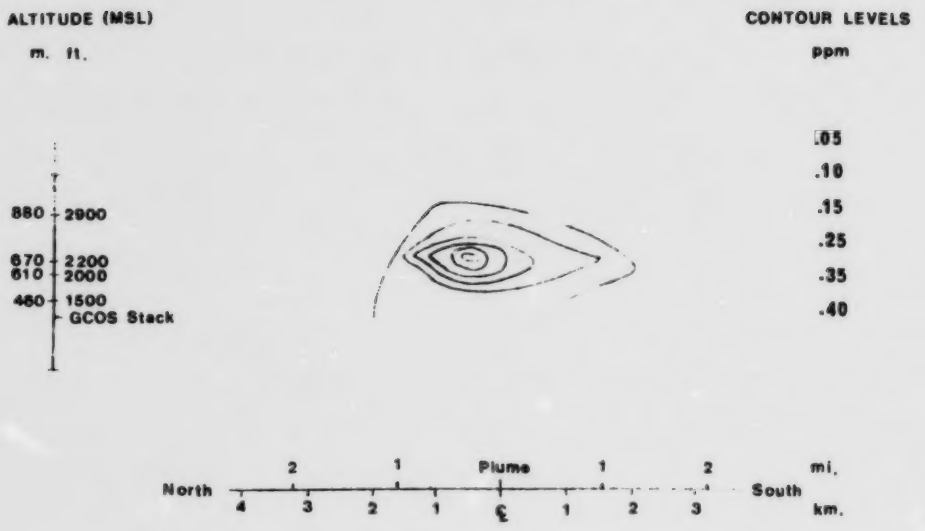

3.2 km. (2 mi.)

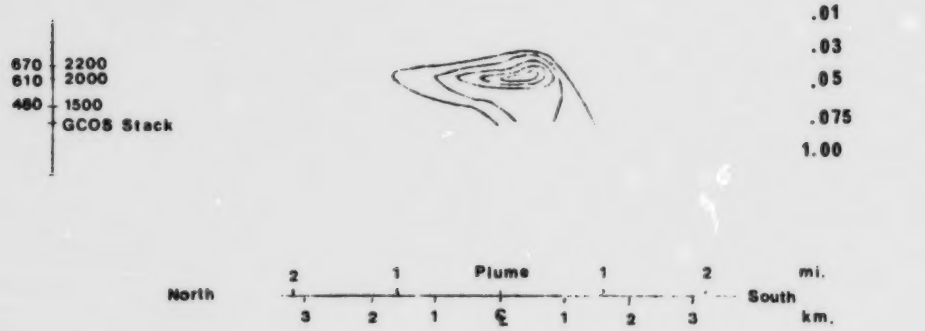

FIGURE 14 SO_2 Concentration Isopleths for March 11, 1976 (0745-1050 MST). Transects were flown downwind of GCOS stack at 3.2 km. (2 mi.) and 6.4 km. (4 mi.).

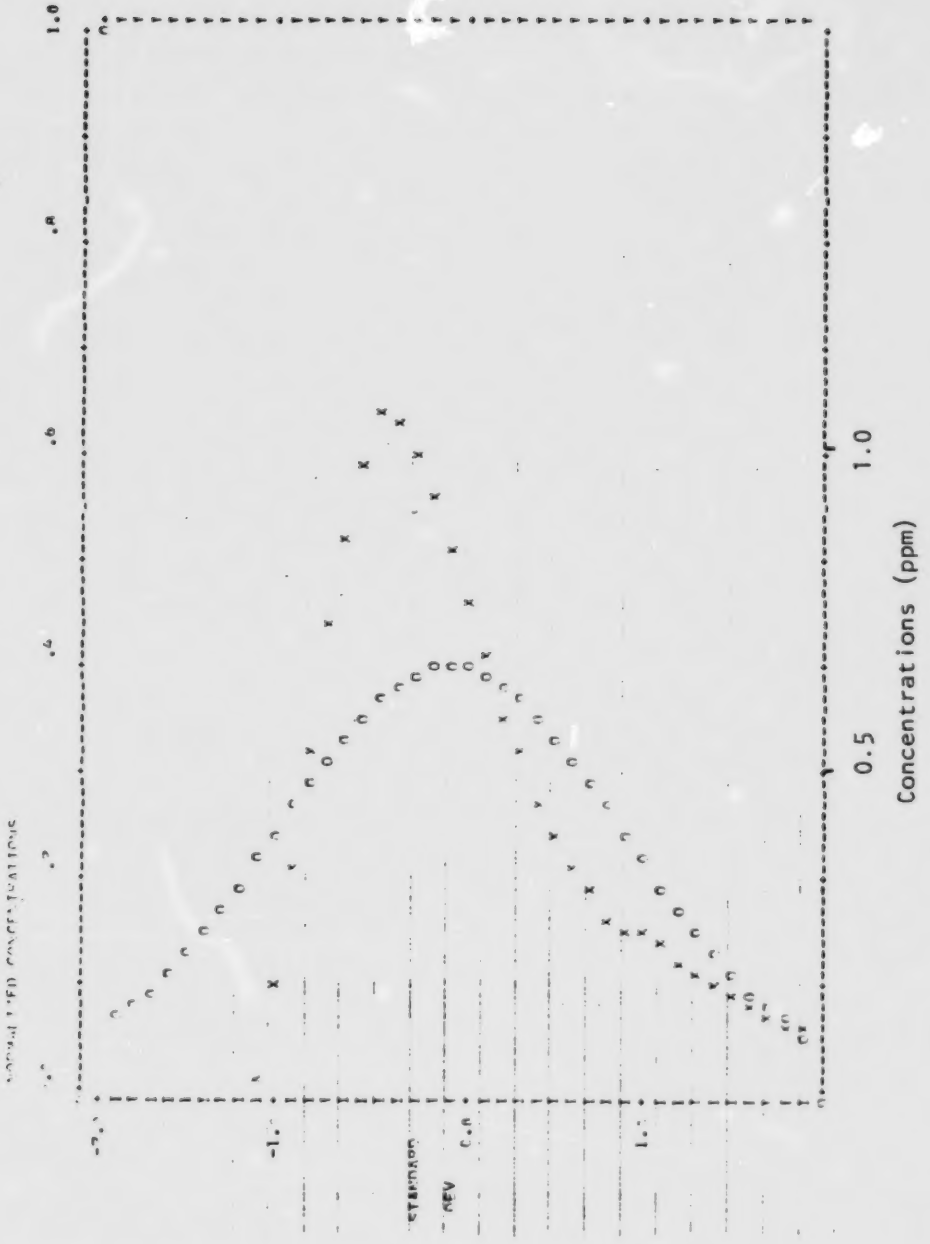

FIGURE 15 Normalized SO_2 concentrations for run 11 at an altitude of 610 m. (2000 ft.) MSL at a downwind distance of 3.2 km. (2 miles) on the flight of March 11, 1976 (0750-1050).

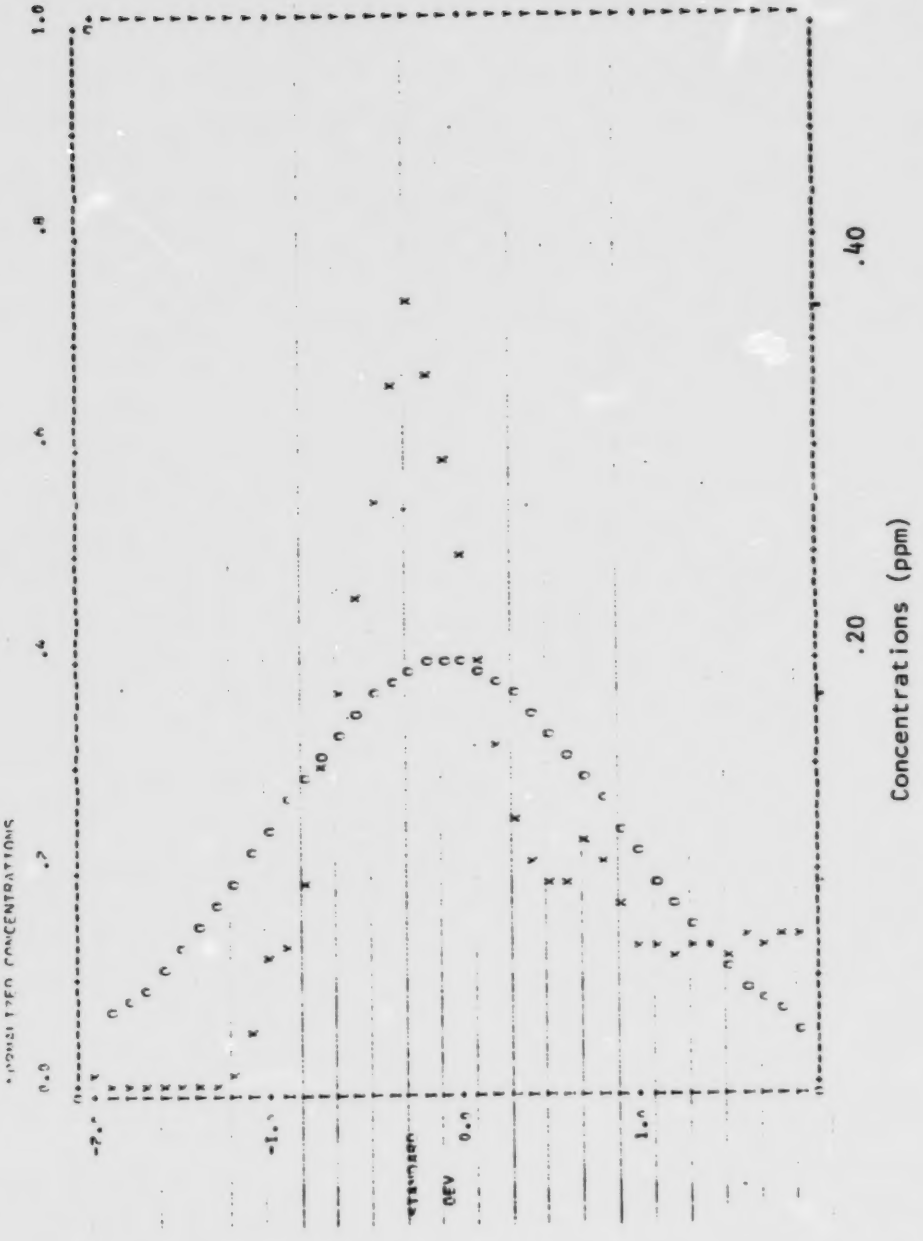

FIGURE 16 Normalized SO_2 concentrations for run 8 at an altitude of 670 m.(2200 ft.)MSL. at a downwind distance of 6.4 km. (4 miles) on the flight of March 11, 1976 (0750-1050).

TABLE 6 Plume geometry and mass flux as functions of downwind distance from the source for the flight of March 11, 1976 (0750-1050).

DOWNWIND DISTANCE X [km]	NORM. CL CONC $\chi \bar{U} Q^{-1}$ [$10^{-6} m^{-2}$] ± 0.1	σ_z [m] ± 20	σ_{ycl} [m] ± 100	SO_2 mass flux [metric tons per hour]	$\frac{\sigma_z \bar{U}}{\sigma_w X}$	$\frac{\sigma_y \bar{U}}{\sigma_{UH} X}$
* 1.6	2.03	77	1150	6.8	0.36	1.89
3.2	3.59	84	890	10.7	0.19	0.73
6.4	1.40	103	1180	9.7	0.12	0.49

$\bar{U}$ is the mean wind measured by the tethersonde (4.0 m/sec)
σ_w value used was the mean σ_w for all heights (0.54)
σ_{UH} value used was the weighted mean of σ_u and σ_v for all heights (1.52 m/sec)
Q is the mass flux of SO_2 being emitted; during this run Q = 10.9 metric tons per hour
* At 1.6 km probably missed CL which would be around 1800'. The result of this missing of the peak, is that the mean flux and the normalized centerline concentration are underestimated.

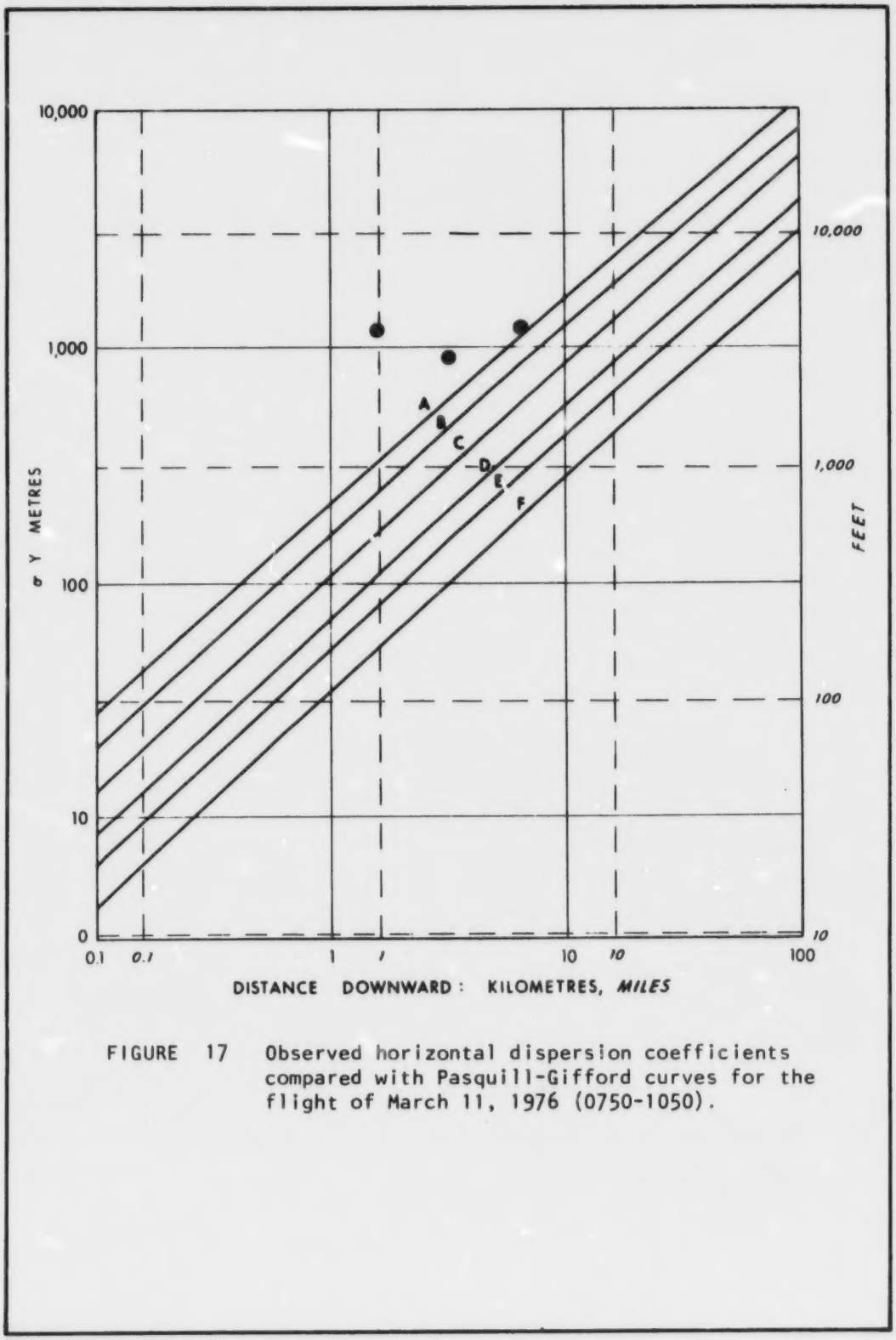

FIGURE 17 Observed horizontal dispersion coefficients compared with Pasquill-Gifford curves for the flight of March 11, 1976 (0750-1050).

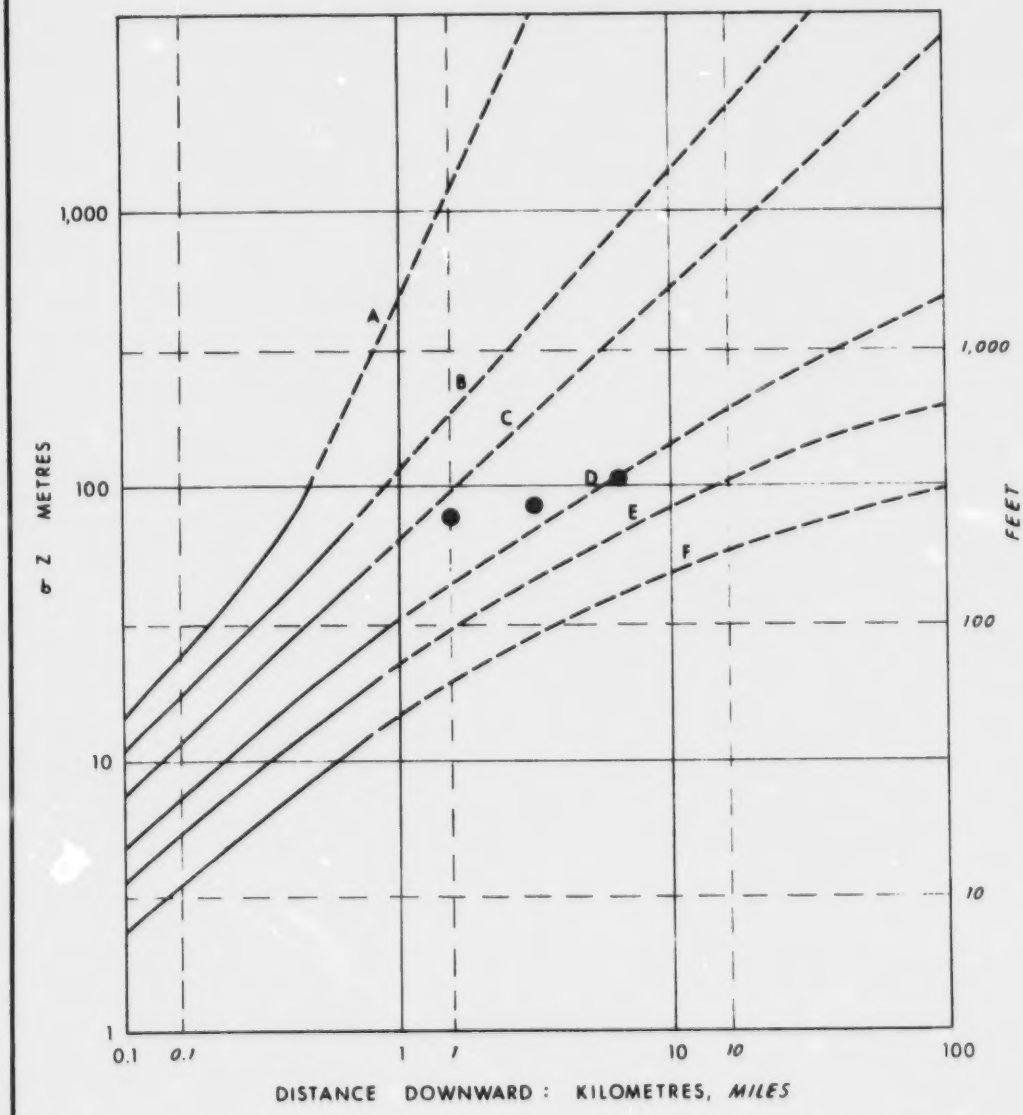

FIGURE 18 Observed vertical dispersion coefficient compared to Pasquill-Gifford for the flight of March 11, 1976 (0750-1050 MST).

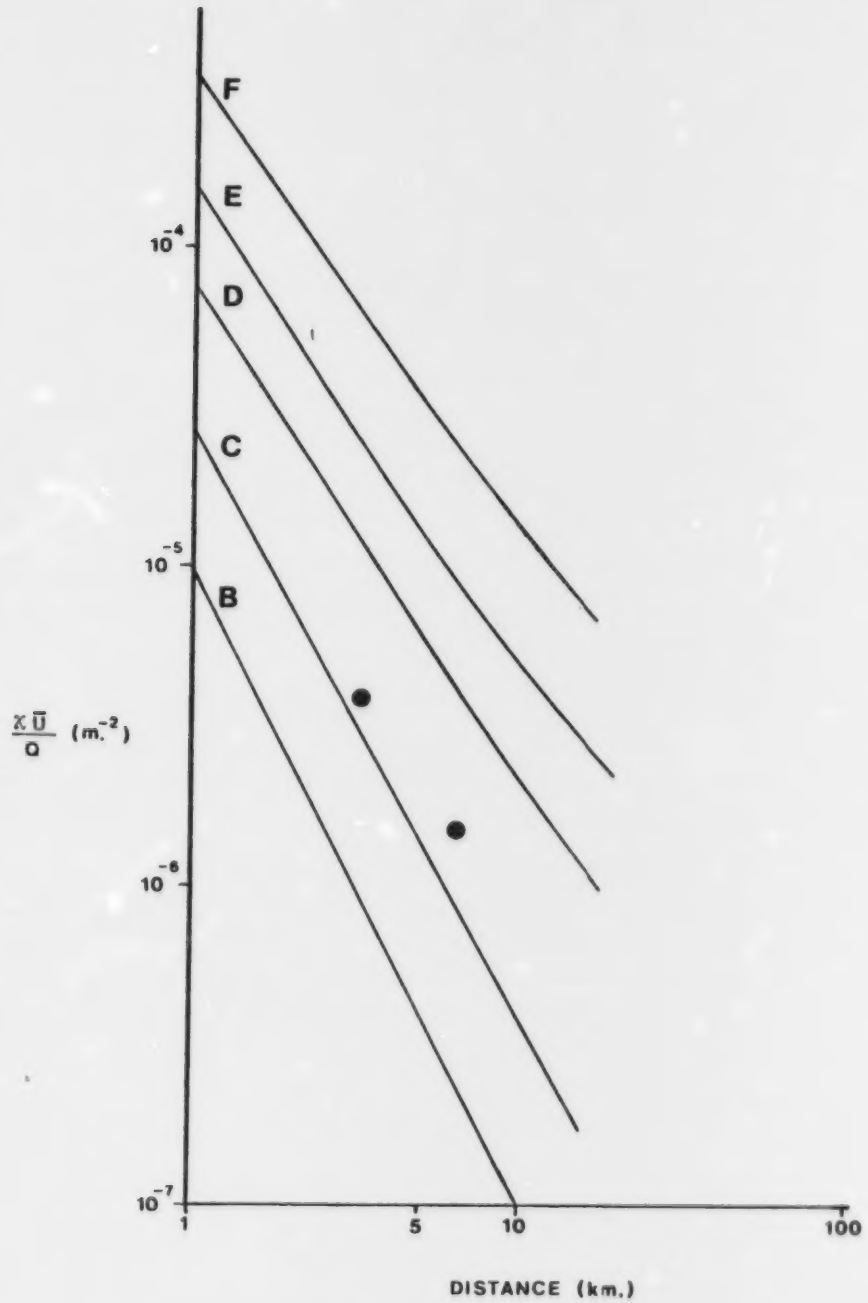

Figure 19. Comparison of observed normalized centerline concentrations with Pasquill-Gifford predictions for the flight of March 11, 1976 (0750-1050 MST).

The non-dimensionalized plume sigma values in Table 6 will be discussed below with the turbulence data.

4.3.5 A comparison of observed and calculated plume rise

Figure 20 depicts the effective stack height at three downwind distances. Unlike the first case, the plume still appears to be ascending at 1.6 km (5280 feet) downwind from the source reaching equilibrium by 3.2 km (10560 feet). Briggs suggests this should occur at 1.8 km (5900 feet) for a neutral atmosphere.

Table 7 compares calculated and observed plume rise using this product of plume rise and wind speed. This approach recognizes the inverse dependence of plume rise on wind speed. Because the wind velocity changed significantly during the survey two are presented. These wind velocities appear to bridge the observed rise for three of the formulas with only that of Holland departing significantly.

Guildberg (1975) observed that the TVA (1972) model performs best for high wind speeds which appears to be the case here. The underestimating by the Holland formulation seems to support observations attributed to Stiemke by Briggs (1969) that the formula works best when results are multiplied by a factor of 2.92.

The capping inversion at 300 m (980 feet AGL) may or may not have influenced the plume rise during the survey. If the wind speed were to be refined, the models seem to support (19 to 26 ft/sec).

4.3.6 Turbulence levels related to plume structure

Table 8 summarizes the turbulence data for the morning flight of March 11. Included in Table 8 are the standard deviations of the mean values wherever sufficient data were available for a meaningful error estimate.

Unlike the March 10 afternoon case, there is little change in the standard deviations of the velocities with height. However the vertical component is about 1/3 to 1/2 of the horizontal component.

The heat flux estimates are small and close to zero. The momentum flux is also very small. The positive value at 1220 m (4000 ft) may indicate an upward transport of momentum from a decaying low level jet. Because of the near-zero values for the turbulent fluxes reliable

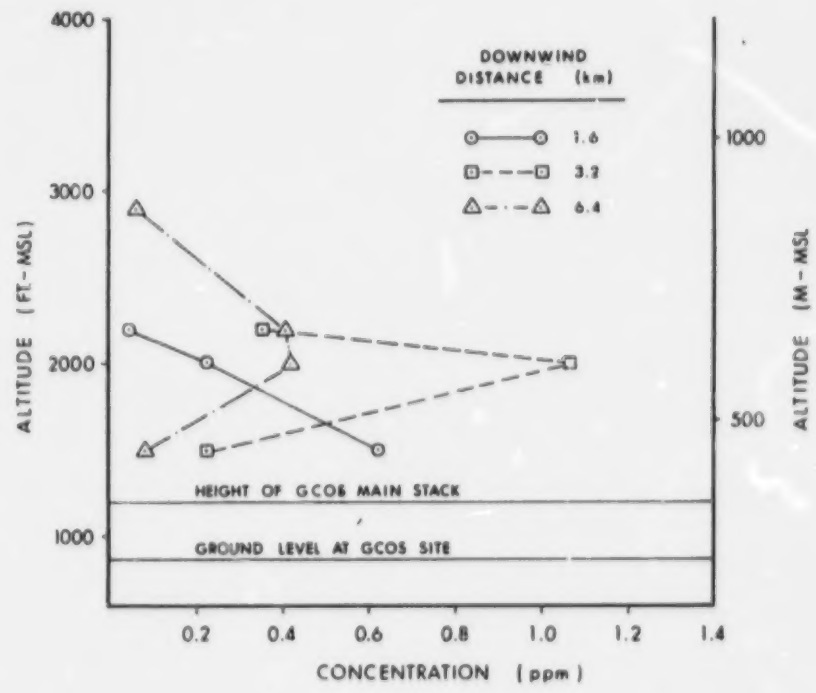

FIGURE 20 Maximum SO_2 concentrations along each traverse as a function of altitude for the flight of March 11, 1976 (0750-1050 MST).

TABLE 7 Observed and calculated plume rises for the powerhouse stack for the flight of March 11, 1976 (0750-1050).

DOWNWIND DISTANCE (km)	PLUME RISE OBSERVED (m) ±50	WINDSPEED (m/sec.)	RATIO CALCULATED TO OBSERVED VALUES OF ΔH BRIGGS IVA(1972) BOSANQUET HOLLAND FORMULATIONS 1	2	3	4
1.6	*	6.0	1.53	1.12	0.97	0.77
3.2	244					
6.4	244					
1.6	*	10.0	0.92	0.67	0.46	0.46
3.2	244					
6.4	244					

* reliable estimate not available

Monin-Obukhov stabilities cannot be calculated from their ratio. It is sufficient to say that regardless of the actual stability, the amount of energy in both mechanical and convective turbulence is very small.

In Table 6 the plume sigma values σ_z and σ_y were non-dimensionalized by the corresponding standard deviations of the wind components and the diffusion time. In both the horizontal and vertical directions, the non-dimensionalized plume spread decreased with increasing distance from the source. For the case of normalized σ_y, the presence of multiple sources may have had some effect but probably not much since the σ_y value used was the value at the center line height where there was no obvious evidence of secondary peaks. Also the delay in the purging of the instrument may have increased the σ_y values at the closer distances. A more detailed discussion of the non-dimensionalized plume sigmas appears in the next chapter.

TABLE 8 Summary of turbulence data for the flight of March 11, 1976 (0750-1050)

HEIGHT [m MSL]	NUMBER OF RUNS		σ_w [m/sec]	σ_u [m/sec]	σ_y [m/sec]	$\overline{w'u'}$ [m/sec]^2	$\overline{w'v'}$ [m/sec]^2	$\overline{w'T'}$ [deg C-sec]
	I	II						
1220	0	10	0.41 (0.08)	1.58 (0.3)	*	0.26 (0.18)	*	0.006 (0.01)
910	1	2	0.54	0.96	3	0.04	-0.1	0.054
670	0	3	0.45	0.90	*	0.07	*	0.027
610	1	14	0.57 (0.06)	1.68 (0.2)	1	-0.03 (0.15)	0.1	-0.009 (0.015)
460	0	3	0.50	1.24	*	-0.08	*	-0.004

II / I

* insufficient data for reliable estimate

4.4 CASE STUDY FOR FLIGHT OF MARCH 11, 1976 (1250-1655)

4.4.1 General meteorology and visual plume description

In the afternoon the plume was much higher than in the morning flight, 1200 m MSL (4000 ft) compared to 600 m (2000 ft). The plume was still directed basically toward the east as shown in Figure 21. The sky was almost cloudless near the start of the flight except for a bank of stratiform cloud on the western horizon. Although there were no visual capping effects, there was not a rapid vertical dispersion and the flights were generally fairly smooth except at lower levels. By 1400, high clouds were beginning to move in along with some strato-cumulus.

The tethersonde profile, which began at 1242, indicated a slightly stable temperature profile to 500 m (1650 ft) AGL or 744 m (2440 ft) MSL. The average wind speed at 400 to 500 m AGL was 2.8 m/sec (9.2 ft/sec).

4.4.2 Flight profiles

At first a series of turbulence runs were made on the east side of the Athabasca River at 1220 m and 610 m (4000 ft and 2000 ft) MSL. Then a series of stacked traverses in a race track pattern were flown at 3.2 km (2 miles) and 8 km (5 miles) downwind from GCOS. A third set of traverses were then made at 16.1 km (10 miles) followed by a series of turbulence runs on both sides of the river valley at 610 m (2000 ft).

4.4.3 Isopleths and selected traverses

Figure 22 shows the isopleths of SO_2 concentration at the three downwind distances flown.

The secondary peaks at 8 km (5 miles) downwind are presumably due to secondary sources at GCOS. Perhaps these sources had not yet mixed high enough to be detected on the lowest run at 3.2 km (2 miles).

The shifting of the maximum concentration toward the north at 3.2 km (2 miles) is an effect which was noted by the airborne observer and can be attributed to the wind veering with height. The anvil-shaped top of the isopleth contours at 3.2 km (2 miles) suggests an elevated inversion limiting vertical mixing.

The maximum SO_2 concentration detected was in run 11 at 910 m (3000 ft) MSL at 3.2 km (2 miles). The normalized concentrations for

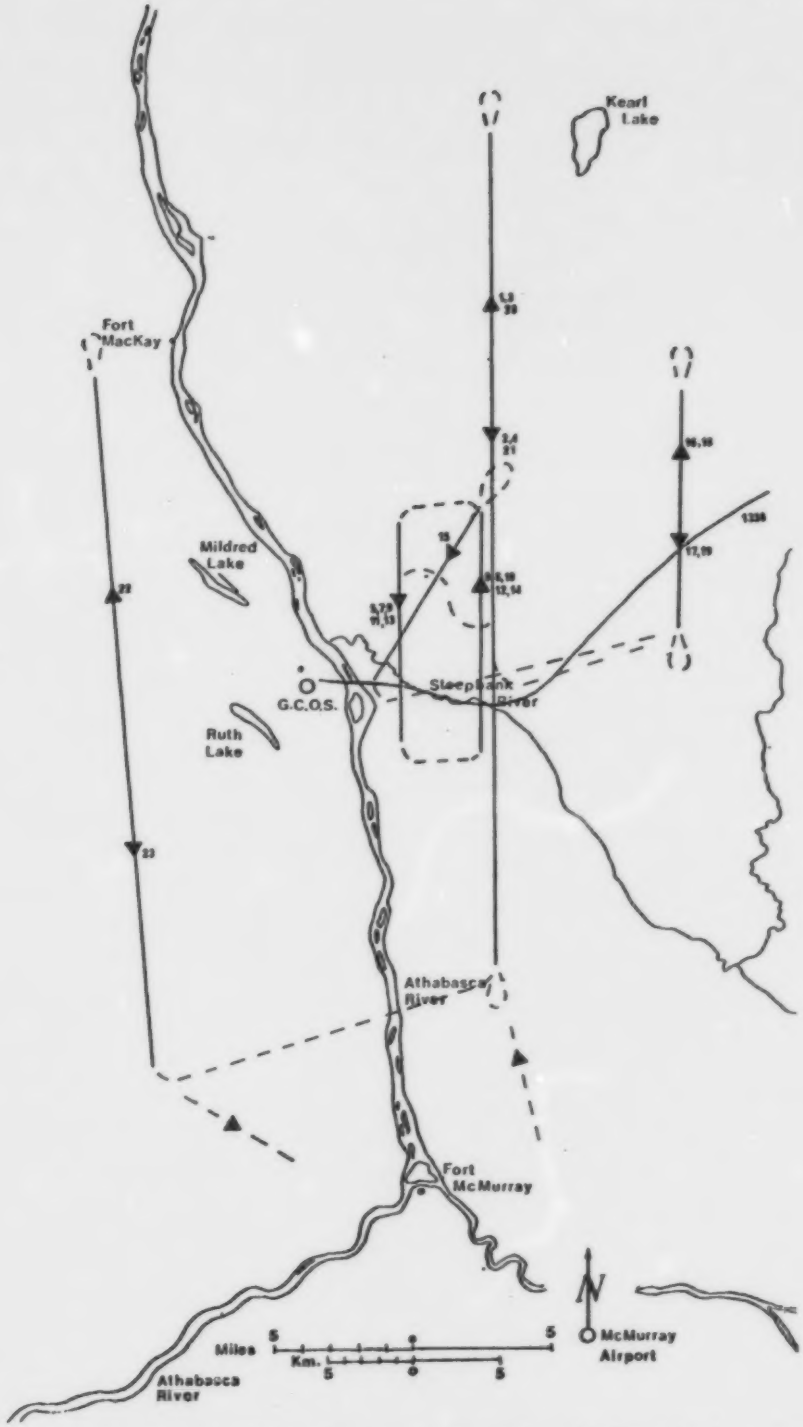

Figure 21 Flight profile for Mar 11, 1976 (1250-1655). Solid lines denote numbered runs and dashed lines denote interconnecting legs. Plume centerline for 1330 is superimposed.

TABLE 9 Run information for flight of Mar. 11, 1976 (1250 - 1655).

RUN NUMBER	TIME (MST)	ALTITUDE (m-MSL) ±20	DOWNWIND DISTANCE (km) ±0.3	σ$_y$ (m) ±100	MAX CONC. (ppm) ±0.02	INTEGRATED CONC. (ppm-m) ±50	FLIGHT DIR. (From-to)
1	1306 - 1318	1220	8.0	T	T	T	S - N
2	1319 - 1331	1220	8.0	T	T	T	N - S
3	1334 - 1346	610	8.0	T	T	T	S - N
4	1348 - 1355	610	8.0	T	T	T	N - S
5	1359 - 1401	610	3.2	1820	0.19	580 +	N - S
6	1404 - 1407	610	8.0	2230	0.20	770 +	S - N
7	1412 - 1415	1070	3.2	2920	0.14	190	N - S
8	1417 - 1420	1070	8.0	2250	0.08	310	S - N
9	1424 - 1426	1370	3.2	3430	0.08	120	N - S
10	1428 - 1430	1370	8.0	2480	0.06	220	S - N
11	1433 - 1436	910	3.2	1540	0.26	430	N - S
12	1438 - 1441	910	8.0	1900	0.14	460	S - N
13	1445 - 1448	460	3.2	2230	0.09	230	N - S
14	1450 - 1453	460	8.0	2010	0.16	560	S - N
15	1457 - 1501	610	-	3210	0.08	400	NE-SW
16	1512 - 1516	760	16.1	*	0.25	*	S - N
17	1518 - 1522	550	16.1	3140	0.11	410	N - S
18	1524 - 1527	910	16.1		0.12		S - N
19	1529 - 1533	910	16.1	3720 **	0.12	600 **	N - S
20	1543 - 1556	610	8.0	T	T	T	S - N
21	1557 - 1612	610	8.0	T	T	T	N - S
22	1618 - 1627	610	8.0	T	T	T	S - N
23	1628 - 1640	610	8.0	T	T	T	N - S

T turbulence run
- plume was traversed at an angle for a check on orientation of traverses with respect to plume axis
* incomplete traverse resulted in unreliable values for plume sigma and integrated concentration
** run 18 was incomplete at the northern end; run 19, at the southern end; sigma values and integrated concentration were estimated from a composite of runs 18 and 19.
+ small part of plume was missed; so that integrated concentration values were increased by 10%

16 km. (10 mi.)

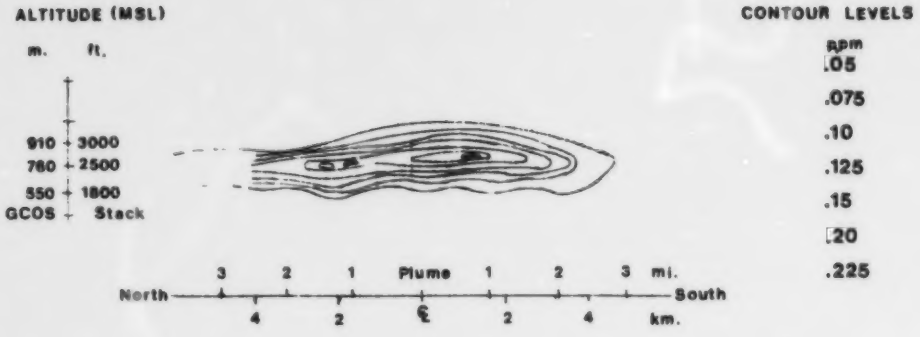

8 km. (5 mi.)

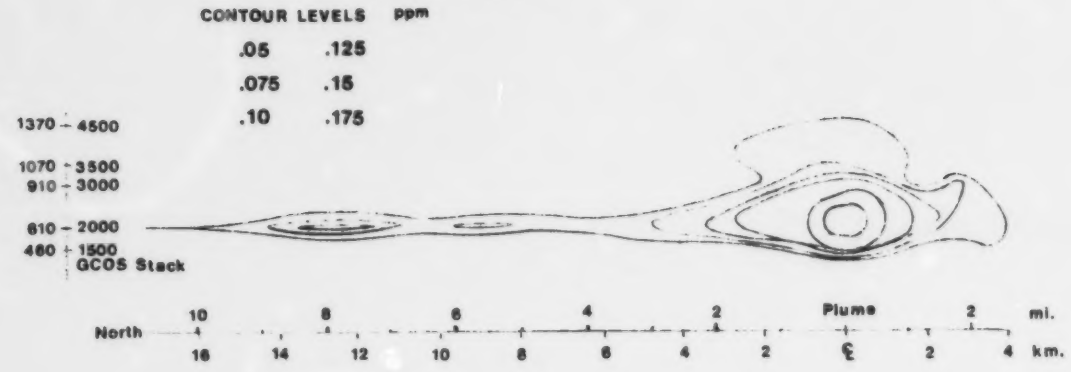

3.2 km. (2 mi.)

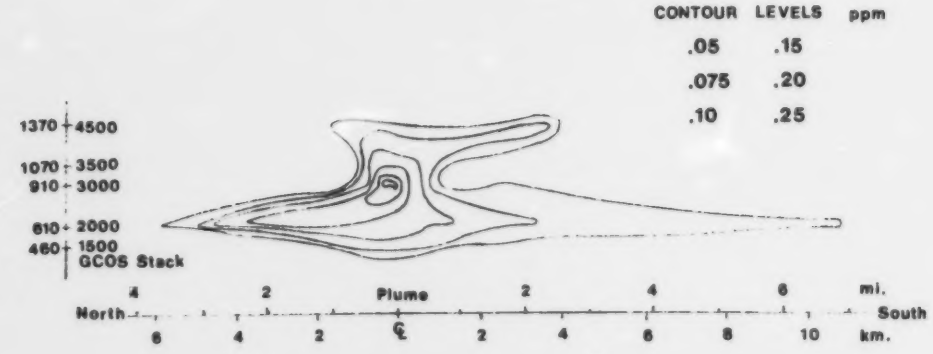

FIGURE 22 SO_2 Concentration Isopleths for March 11, 1976 (1250-1655 MST). Transects were flown downwind of GCOS stack at 3.2 km. (2 mi.), 8 km. (5 mi.) and 16 km. (10 mi.).

run 11 are shown in Figure 23. The plume appears to be more peaked than the Gaussian of the same area; a minor secondary peak is visible near the end of the run (south end). Note that there are no obvious instrumental purging problems such as encountered in the morning flight discussed previously.

Figure 24 shows the normalized concentrations for run 6 at 8 km (5 miles) at a height of 610 m (2000 ft) MSL. The secondary peaks are evident and contribute to a much greater lateral standard deviation than would be generated by the main plume itself.

4.4.4 Plume geometry and mass flux

Table 10 summarizes the plume geometry and mass flux for the afternoon flight of March 11. The mass fluxes agreed to within about 25% with the source strength as provided by GCOS. The wide spacing of the flight levels needed to capture the limits of the plume meant that vertical resolution within the plume was fairly limited; hence the mass flux estimates are not as reliable as the estimates for the morning case.

Figures 25, 26, and 27 show the observed values of σ_y, σ_z and normalized concentrations compared to the Pasquill-Gifford curves. As with the other case studies, the σ_y values are consistently larger than predicted. However, the σ_z values fall about the slightly unstable (C) curve. The normalized concentrations do not decrease with distance as expected. Presumably this result is due to a fairly narrow high concentration core which was missed at the closer distances. Figure 28 of the maximum concentrations as a function of height suggests that the center line may be close to 750 m (2500 ft) MSL.

The non-dimensionalized plume sigma values will be discussed below with the turbulence data.

4.4.5 A comparison of observed and predicted plume rise

The observed effective stack heights for the afternoon survey of March 11, 1976, are presented in Figure 28. Because of the vertical spread of the plume and attempts to make measurements at three downwind distances the plume center line depicted by the maximum concentration was not captured at two of the three locations. This explains the apparent descent of the plume with distance from the source.

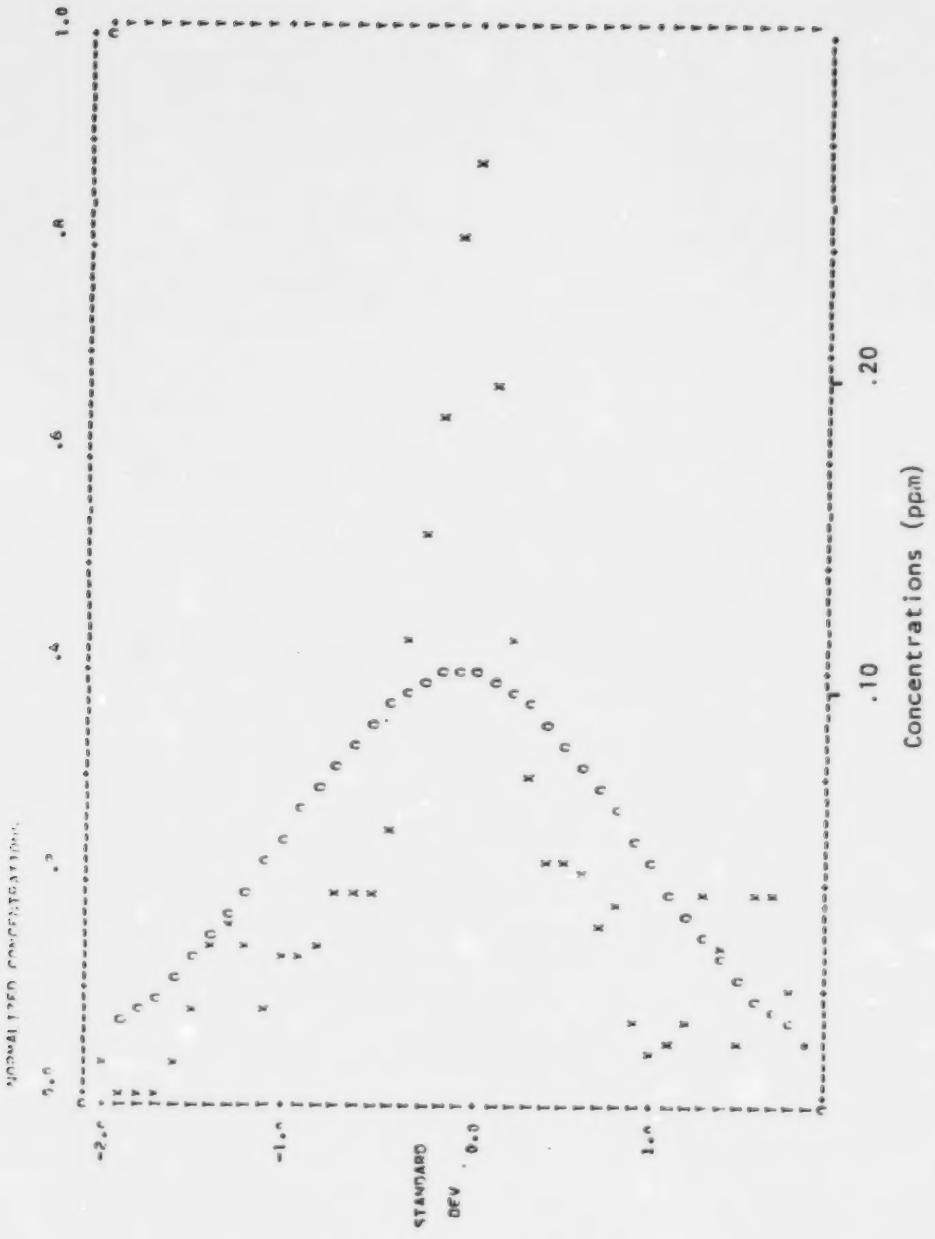

FIGURE 23 Normalized SO_2 concentrations for run 11 at an altitude of 910 m. (3000 ft.) MSL at a downwind distance of 3.2 km. (2 miles) on the flight of March 11, 1976 (1250-1655).

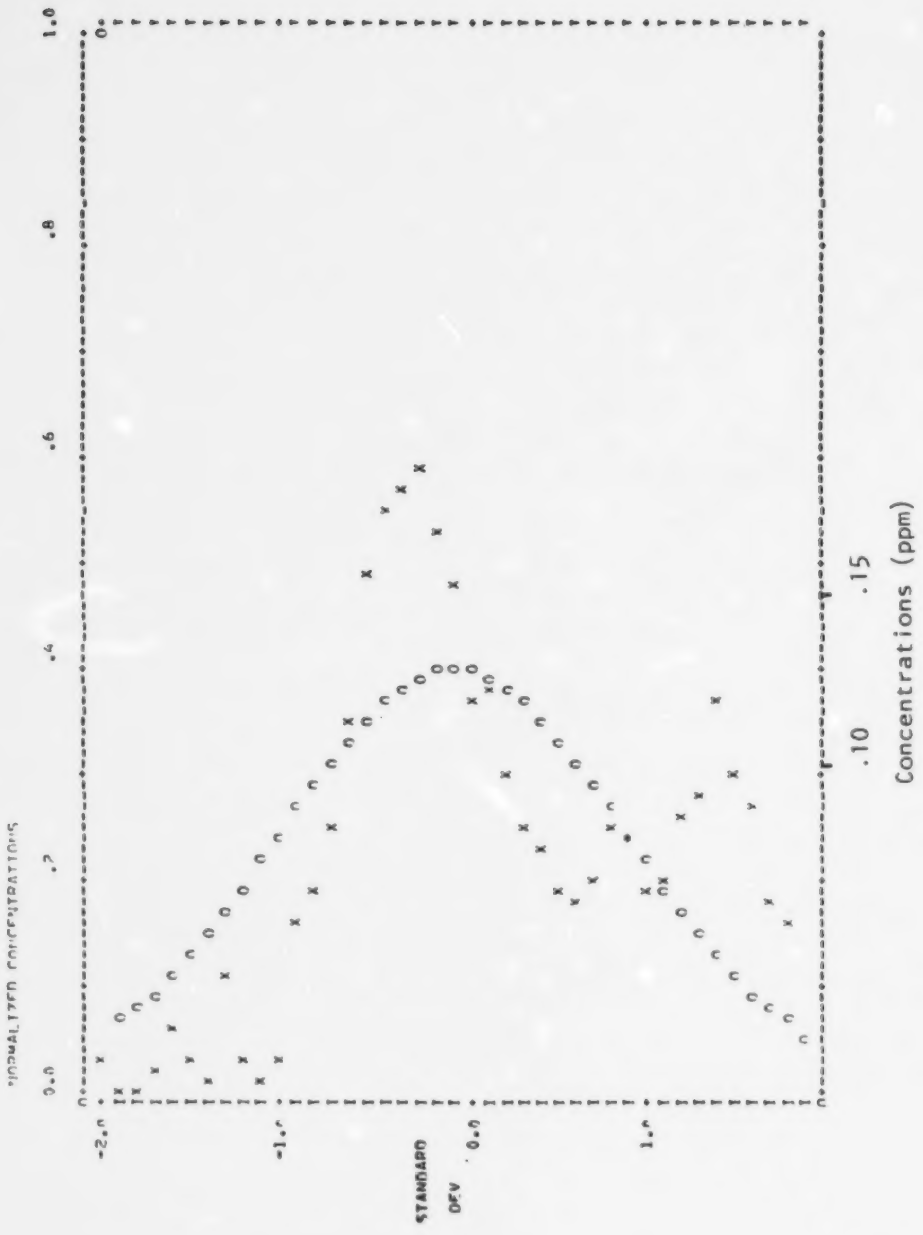

FIGURE 24 Normalized SO_2 concentrations for run 6 at an altitude of 610 m. (2000 ft.) MSL at a downwind distance of 8.0 km. (5 miles) on the flight of March 11, 1976 (1250-1655).

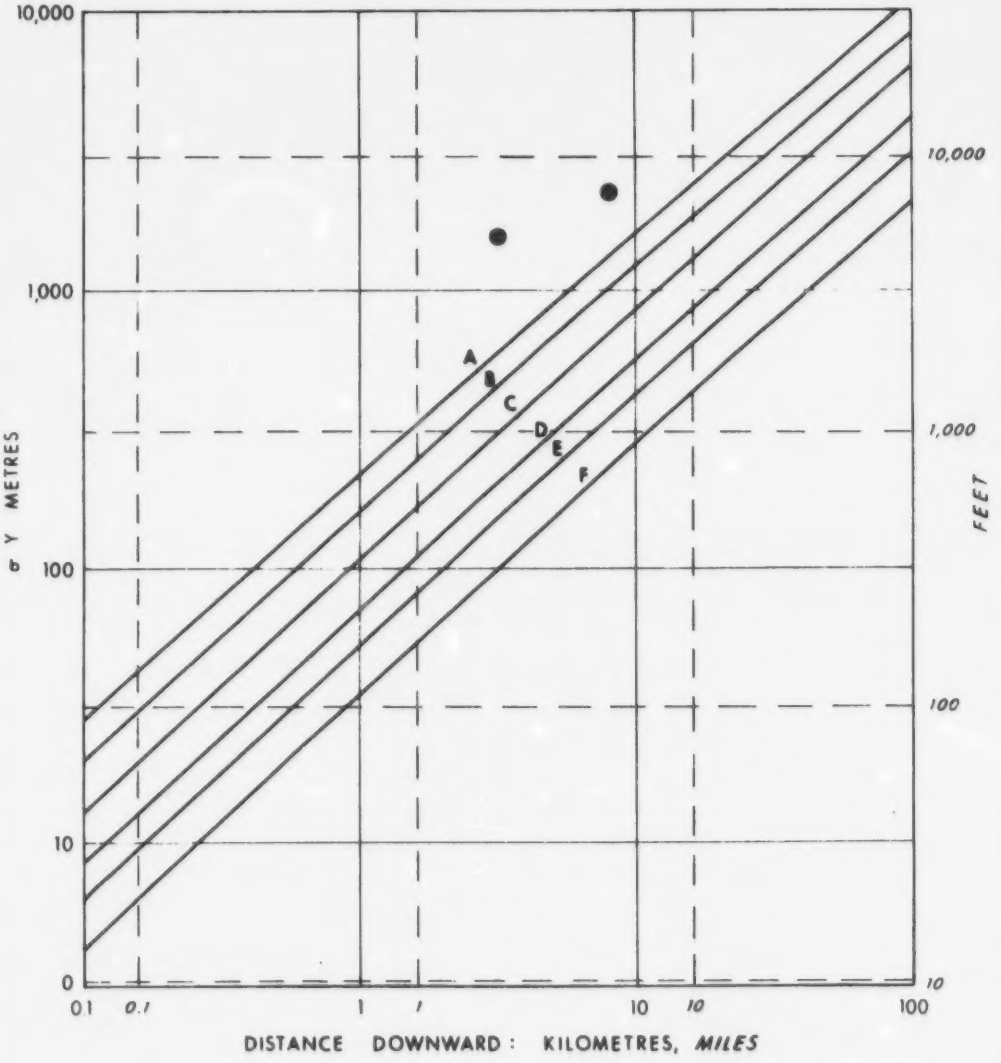

FIGURE 25 Observed horizontal dispersion coefficient compared to Pasquill-Gifford curves for the flight of March 11, 1976 (1250-1655 MST).

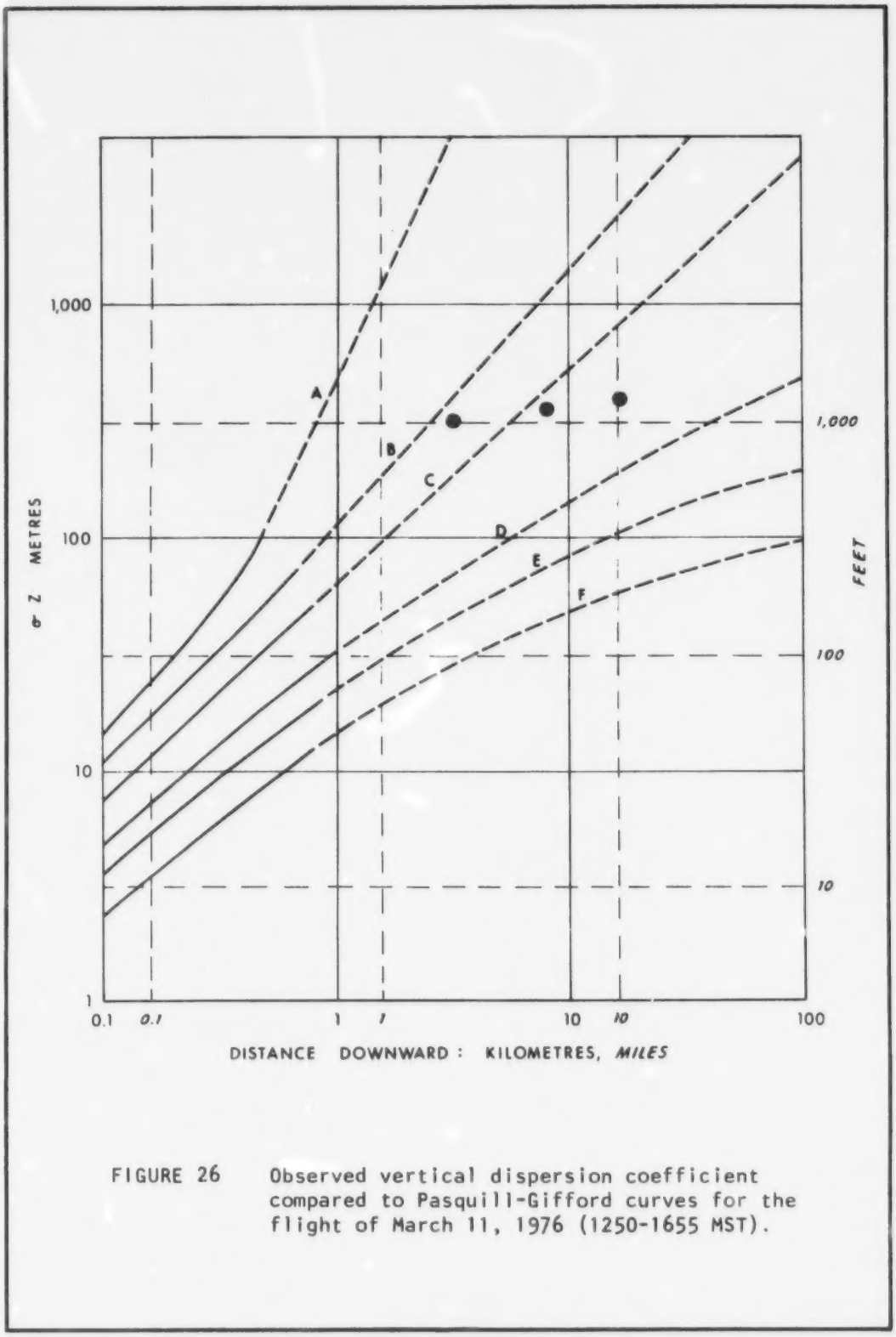

FIGURE 26 Observed vertical dispersion coefficient compared to Pasquill-Gifford curves for the flight of March 11, 1976 (1250-1655 MST).

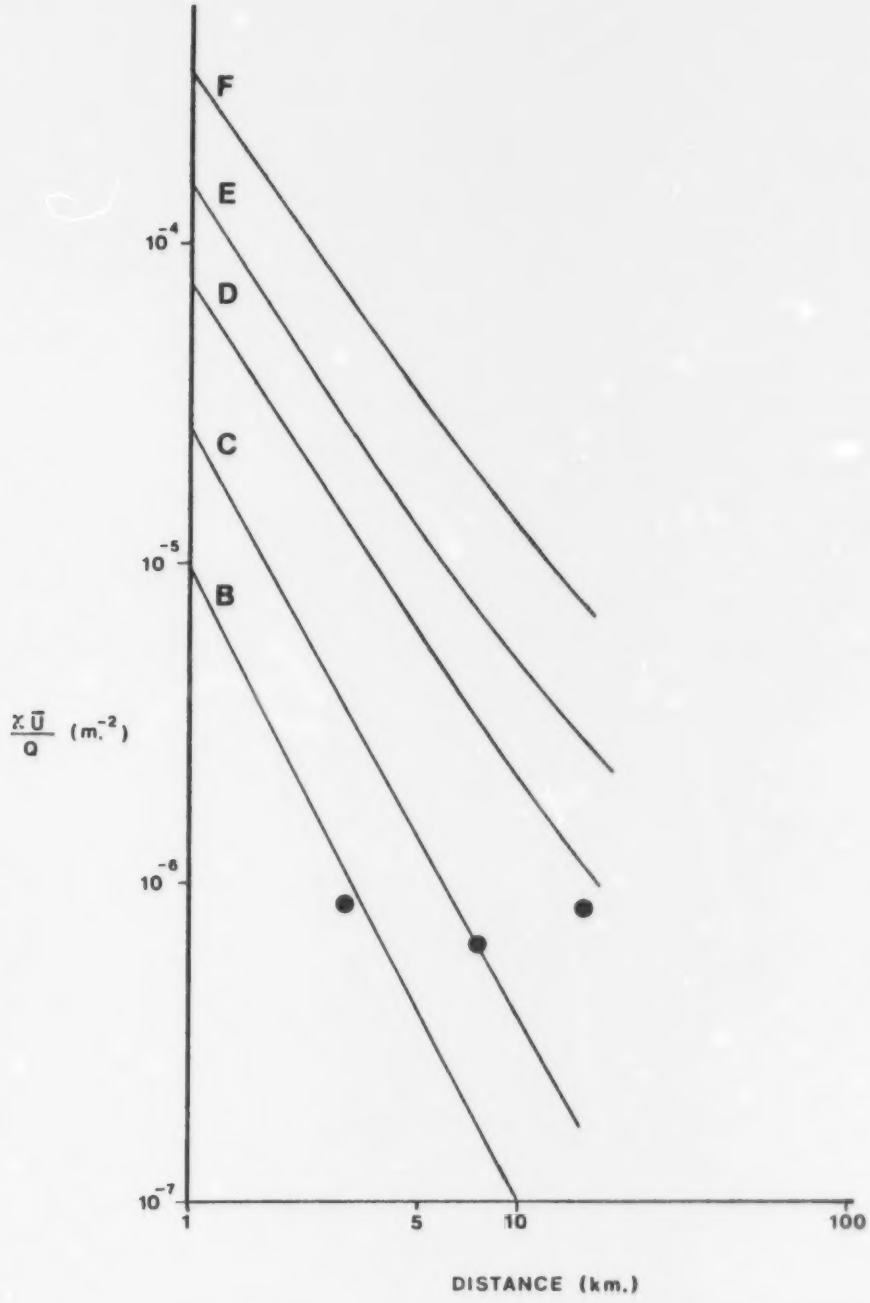

Figure 27. Comparison of observed normalized centerline concentrations with Pasquill-Gifford predictions for the flight of March 11, 1976 (1250-1655 MST).

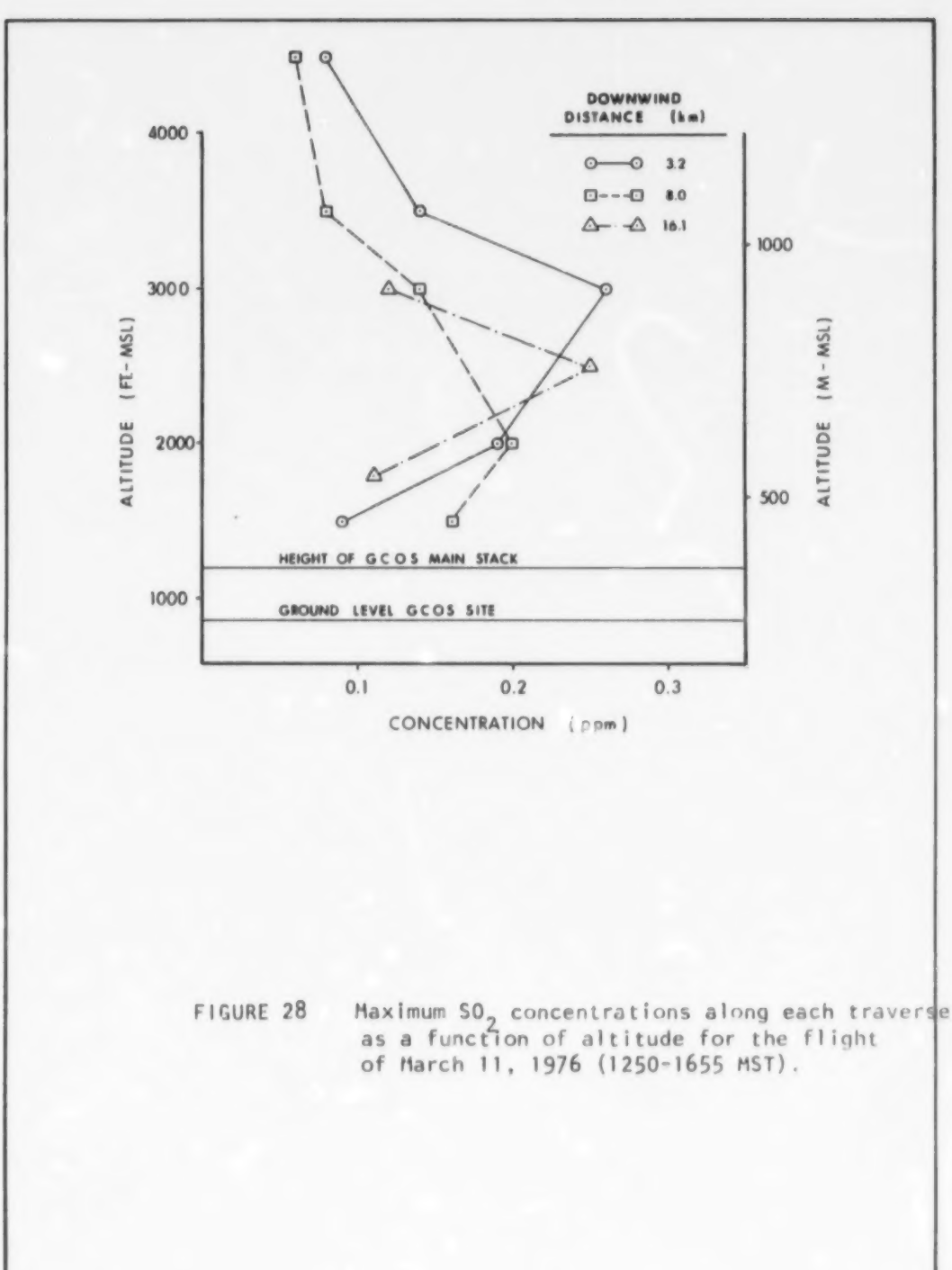

FIGURE 28 Maximum SO_2 concentrations along each traverse as a function of altitude for the flight of March 11, 1976 (1250-1655 MST).

TABLE 10 Plume geometry and mass flux as functions of downwind distance from the source for the flight of March 11, 1976 (1250-1655)

DOWNWIND DISTANCE X [km]	NORM. CL CONC $\frac{\bar{X}\bar{U}}{Q}^{-1}$ [10^{-6} m^{-2}] ±0.1	σ_z [m] ±20	σ_{ycl} [m] ±100	SO_2 mass flux [metric tons per hour]	$\frac{\sigma_z \bar{U}}{\sigma_{wcl} X}$	$\frac{\sigma_y \bar{U}}{\sigma_{UH} X}$
3.2	0.77	306	1540	8.8	0.24	0.81
8.0	0.59	339	2230	12.9	0.11	0.47
16.1	0.74	383	*	*	0.06	*

* reliable estimate not available
$\bar{Q}$= sum of SO_2 emmissions as supplied by GCOS = 10.2 metric tons per hour
$\bar{U}$= mean wind speed as measured by the AES tethersonde at 400 to 500 m (1300 to 1650 ft.) AGL : 2.8 m/sec (9.2 ft./sec.)

Table 11 summarizes a comparison of calculated and observed plume rises for a wind speed of 2.0 m/sec. Two stability classifications were investigated because of the near neutral conditions and the dramatic effect stability has on some of the plume rise models. Agreement with the observed value is improved substantially by assuming a slightly stable condition (0.2°C/100m). The Briggs method overestimates slightly whereas the others are substantially higher.

4.4.6 Turbulence levels related to plume structure

Table 12 summarizes the turbulence data for the afternoon flight of March 11. Included in Table 12 are the standard deviations of the mean values wherever sufficient data were available for a meaningful error estimate.

Of special interest is the decrease in the values of σ_w and σ_u with increasing height. Above about 1000 m (3300 ft) MSL, the standard deviation of the vertical velocity is very similar to the values found at all heights in the morning height. Below this level the standard deviation, σ_w, is about twice as large. Thus the amount of energy in the vertical wind component is about four times larger below 1000 m (3300 ft) MSL than above. A similar change although not quite as sharp appears for horizontal wind standard deviation.

TABLE 11 Observed and calculated plume rise for the powerhouse stack for the flight of March 11, 1976 (1250 - 1655).

DOWNWIND DISTANCE (km)	PLUME RISE OBSERVED (m) ±50	WINDSPEED (m/sec.)	RATIO CALCULATED TO OBSERVED VALUES OF uΔh BRIGGS TVA(1972) BOSANQUET HOLLAND FORMULATIONS 1	2	3	4
Slightly Stable						
3.2	*	2.0	1.10	1.84	1.55	1.50
8.0	*					
16.1	400					
Neutral						
3.2	*	2.0	3.80	2.80	1.70	2.00
8.0	*					
16.1	400					

* reliable estimate not available

The momentum fluxes at 610 and 1220 m (2000 and 4000 ft) MSL also show change with height. At the lower level, there is a clear negative momentum flux indicating that the wind at this level is influenced by the surface drag. However at 1220 m (4000 ft) MSL, the momentum flux is near zero.

The heat flux does not show such strong changes with height. However a near-zero heat flux at 610 m becomes a negative heat flux at 1220 m indicating stable conditions at the higher level.

Thus, the standard deviation of the wind components and the turbulent fluxes all indicate a weakly mixed layer up to an altitude of about 1000 m (3000 ft) MSL which was topped by a stable layer.

Turbulence runs were made at 610 m (2000 ft) MSL on the east side of the Athbasca River before and after the plume traverses and on the west side of the river after the plume traverses. The turbulent statistics for these three groups are compared in Table 12.

TABLE 12 Summary of turbulence data for the flight of March 11, 1976 (1250-1655)

	HEIGHT [m MSL]	NUMBER OF RUNS I	NUMBER OF RUNS //	σ_w [m/sec]	σ_u [m/sec]	σ_v [m/sec]	$\overline{w'u'}$ [m/sec]^2	$\overline{w'v'}$ [m/sec]^2	$\overline{w'T'}$ [deg C-m sec]
	1370	2	0	0.54	0.9	*	0.11	*	0.018
+	1220	10	0	0.65	1.32	*	0.05	*	-0.040
				(0.10)	(0.13)		(0.09)		(0.03)
	1070	2	0	0.57	1.4	*	0.43	*	0.012
	910	2	2	1.21	1.8	2.1	-0.27	0.10	0.030
	760	1	0	1.26	2.2	*	-1.28	*	0.033
+	610	28	3	1.10	1.66	2.8	-0.36	-0.85	0.000
				(0.03)	(0.20)		(0.07)		(0.006)
	550	1	0	1.17	2.3	*	-0.21	*	-0.033
	460	2	0	1.07	2.8	*	0.24	*	0.030
+	A	7		1.01	1.24	*	-0.30	*	0.034
				(0.08)	(0.1)		(0.07)		(0.01)
+	B	11		1.12	1.83	*	-0.32	*	-0.002
				(0.05)	(0.3)		(0.13)		(0.01)
+	C	8		1.07	1.74	*	-0.55	*	-0.017
				(0.06)	(0.10)		(0.1)		(0.013)

* reliable estimate not available
\+ standard deviations of the mean values are shown underneath in brackets
A runs 3 and 4 at 610 m (2000 ft.) MSL near start of flight on the east (downwind) side of river valley
B runs 20 and 21 at 610 m (2000 ft.) MSL near end of flight on the east (downwind) side of river valley
C runs 22 and 23 at 610 m (2000 ft.) MSL near end of flight on the west (upwind) side of river valley
I number of crosswind runs
// number of along-wind runs

A comparison of groups A and B, in Table 12 represents a stationarity check. There appears to be an increase of the standard deviations of the wind components by 10 or 20 per cent with a decrease in heat flux. The increase in cloudiness through the flight can account for the decreased heat flux.

A comparison of groups B and C, in Table 12, is a check on the effect of the river valley on the turbulence. Since the downwind runs of Group B were about 8 km (5 miles) from the river and the flight level was about 300 m (1000 ft) above the ground, there was sufficient distance for the boundary layer at the flight level to become at least partially modified by the river valley effects(see, for example, Blom and Wartena (1969)). For this case study there are no changes in the averaged turbulent quantities which can be considered statistically significant. It is quite possible that changes in the averaged turbulent quantities existed at lower levels and perhaps further downwind. However, the river valley effects were not important for the mixing of the main plume effluent within 8 km (5 miles) of the source.

In Table 10 the plume sigma values were non-dimensionalized by the corresponding standard deviations of the wind and the diffusion time. As with the previous case studies examined the non-dimensional plume spread decreased with distance. Further discussion with the results of all the case studies is included in Chapter 5.

4.5 CASE STUDY FOR THE FLIGHT OF MARCH 12, 1976 (1420-1650)

4.5.1 General meteorology and visual plume description

When the GCOS site was approached at 1430, the plume was seen to be heading southeast over the Steepbank River with obvious garden-hoising or meandering, (see Figure 29). There was a heavy altocumulus cloud cover over about 9/10 of the sky with a scattered cumulus layer having bases of 1680 m (5500 ft) MSL. A cumulus cloud was noted directly over the maximum plume rise about 1 km (0.6 mile) downwind from the stack. On a run at 1580 m (5200 ft) MSL, 4.8 km (3 miles) downwind from the stack, the aircraft was just below cloud base and the main plume was clearly seen to feed directly into the cloud.

The tethersonde profile to 500 m (1640 ft) AGL indicated a slightly stable layer. The wind profiles showed considerable differences for profiles commencing at 1431 and at 1623. The mean wind speed over 100 minutes from 1440 to 1620 was 2.6 m/sec (8.5 ft/sec). The standard deviation of the 10-minute average wind speeds was 0.8 m/sec (2.6 ft/sec).

4.5.2 Flight profiles

A turbulence run was flown on the way to GCOS from McMurray at a height of 910 m (3000 ft) MSL. Then a race track pattern was set up at downwind distances of 4.8 km (3 miles) and 11.3 km (7 miles). After runs 2 and 3 were flown, the orientation of the race track was shifted to be more nearly perpendicular to the plume. A final set of turbulence runs at 1220 m (4000 ft) MSL completed the flight profiles. Figure 29 and Table 13 show the layout and details of the flight profiles.

4.5.3 Isopleths and selected traverses

The isopleths of the SO_2 concentrations for the traverses at 4.8 km (3 miles) and 11.3 km (7 miles) are shown in Figure 30. As can be seen from the isopleths, there were isolated areas of SO_2 which could not be reliably interpolated to other altitudes. Of particular interest was run 6 at 760 m (2500 ft) at 4.8 km (3 miles) along which there was no area of high SO_2 concentrations. A similar flight level with very low SO_2 concentrations was run 5 at 1220 m (4000 ft) MSL at 11.3 km (7 miles) downwind.

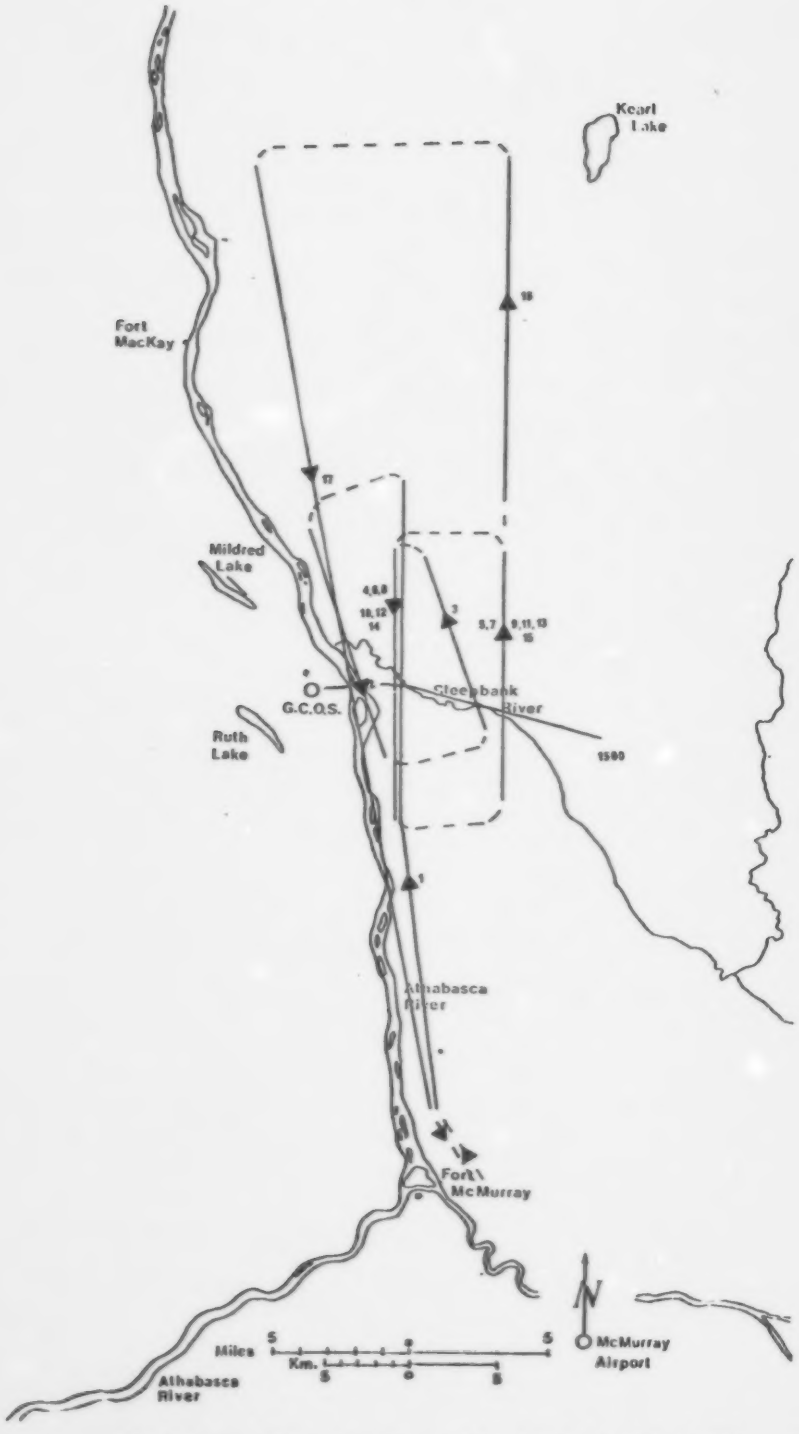

Figure 29 Flight profile for Mar. 12, 1976 (1420-1650). Solid lines denote numbered runs and dashed lines denote interconnecting legs. Plume centerline for 1500 is superimposed.

TABLE 13 Run information for flight of March 12, 1976 PM (1420-1650)

RUN NUMBER	TIME (MST)	ALTITUDE (m-MSL) ±20	DOWNWIND DISTANCE (km) ±0.3	σ_y (m) ±100	MAX CONC. (ppm) ±0.02	INTEGRATED CONC. (ppm-m) ±30	FLIGHT DIR. (From-to)
1	1430 - 1440	910	4.8	T	T	T	S - N
2	1442 - 1445	1220	3.2	2490	0.155	458	NW-SE
3	1446 - 1450	220	8.9	3430	0.077	234	SE-NW
4	1452 - 1455	1220	4.8	3160	0.149	360	N - S
5	1457 - 1500	1220	11.3	3660	0.058	196	S - N
6	1503 - 1507	760	4.8	*	0.094	*	N - S
7	1509 - 1511	760	11.3	3330	0.099	333 +	S - N
8	1515 - 1519	1070	4.8	*	0.160	*	N - S
9	1521 - 1524	1070	11.3	3840	0.093	407	S - N
10	1528 - 1531	910	4.8	2130	0.194	528	N - S
11	1533 - 1537	910	11.3	M	M	M	S - N
12	1541 - 1544	670	4.8	2820	0.133	514 +	N - S
13	1546 - 1550	670	11.3	4010	0.122	367	S - N
14	1533 - 1559	1580	4.8	1470	0.098	191	N - S
15	1601 - 1603	1580	11.3	2370	0.101	200	S - N
16	1605 - 1614	1220	11.3	T	T	T	S - N
17	1616 - 1633	1220	2.4	T	T	T	NW-SE

* incomplete traverse resulted in unreliable value
T Turbulence run
\+ integrated concentration was increased by 10% due to the missing of the edge of the plume
M data missing due to system malfunction

11.3 km (7 mi.)

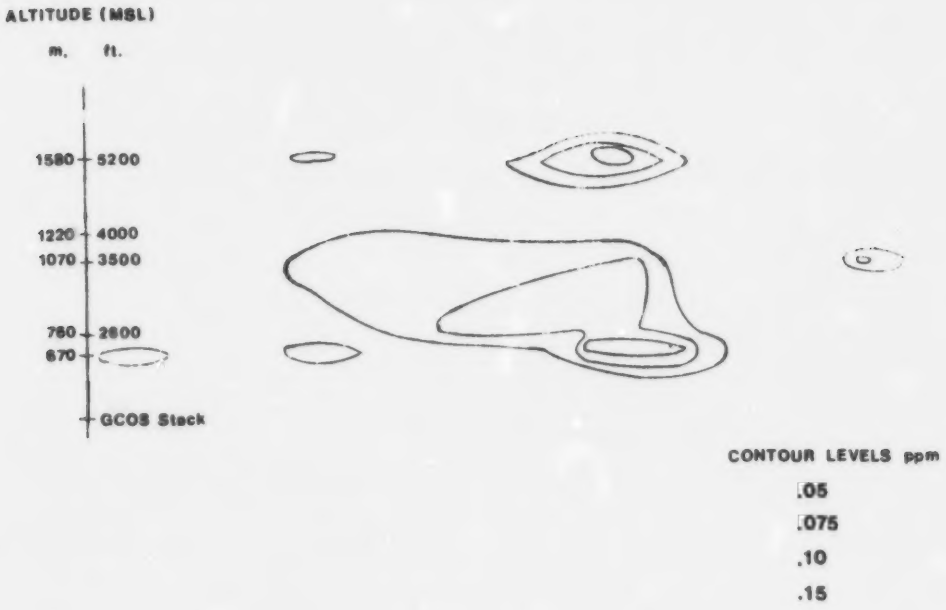

4.8 km. (3 mi.)

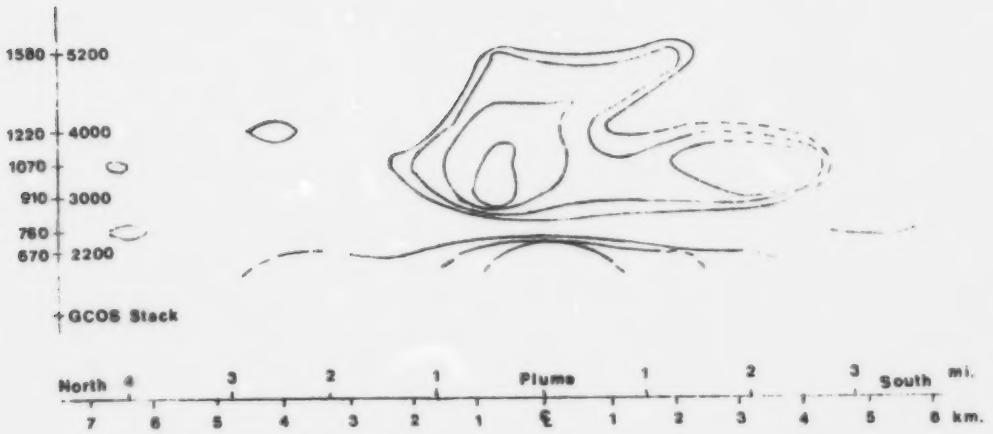

FIGURE 30 SO_2 Concentration Isopleths for March 12, 1976 (1420-1650). Transects were flown downwind of GCOS stack at 11.3 km. (7 mi.) and 4.8 km. (3 mi.).

Figure 31 shows the normalized SO_2 concentration on run 10 at a height of 910 m (3000 feet) at 4.8 km (3 miles) downwind. The multiple peak structure is clear. The large variability in the wind field mentioned earlier may account for the large instantaneous fluctuation detected by the airborne sensor.

The normalized SO_2 concentrations for run 15 at 1580 m (5200 ft) MSL at 11.3 km (7 miles) downwind from the source are shown in Figure 32. It is clear that the high concentration represents a real peak and not a noise spike. The four points on Figure 32 above 0.075 ppm represent a distance of 0.4 standard deviations or 950 m (3100 ft.).

4.5.4 Plume geometry and mass flux

Table 14 summarizes the plume geometry and mass flux for the afternoon flight of March 12. In spite of uncertainty as to the representativeness of individual traverses to the long term average concentrations, the mass fluxes agree quite closely with the emission data.

The observed σ_y, σ_z and normalized concentration values in Table 14 were compared with the Pasquill-Gifford curves in Figure 33, 34, and 35. The σ_y values are three or four times larger than predicted. The σ_z values are close to the slightly unstable (C) curves; whereas the normalized concentrations at the axial center line fall between B and C stabilities. The above differences between the observed values and the Pasquill-Gifford values are similar to those in the previous case studies examined above.

4.5.5 A comparison of observed and calculated plume rise

Figure 36 illustrates the vertical concentration profiles at two downwind distances as taken from a series of stacked traverses. Only those traverses pertaining to the downwind distance of 4.8 km indicate a possible center line at 915 m (3000 feet) MSL. However field notes and photographs of the plume on this day suggest the plume rise (ie. center line) was in the order of 1677 m (5500 feet) MSL. This discrepancy has not been resolved to date.

Table 15 compares the calculated and observed plume rises for the measurements taken on this day. An average wind of 2.6 m/sec accompanying neutral conditions was utilized in the analysis. Because of the

TABLE 14 Plume geometry and mass flux for the flight of March 12, 1976 (1420 - 1650)

DOWNWIND DISTANCE X [km]	NORM. CL CONC $X\bar{U}\,Q^{-1}$ [$10^{-6}m^{-2}$] ±0.1	σ_z [m] ±20	σ_{ycl} [m] ±100	SO_2 mass flux [metric tons per hour]	$\frac{\sigma_z \bar{U}}{\sigma_w X}$	$\frac{\sigma_y \bar{U}}{\sigma_{UH} X}$
4.8	0.47	246	2130	12.3	0.19	0.73
11.3	0.30	488	3840	9.7	0.16	0.56

Q = sum of SO_2 emissions = 10.1 metric tons per hour (courtesy of GCOS)

$\bar{U}$ = mean wind speed at plume center line height = 2.6 m/sec (8.9 ft/sec) (courtesy of AES)

σ_{UH} = the standard deviation of the horizontal wind component = $(\sigma_u + \sigma_v)/Z$

unresolved nature of the observed plume rise two possible values are tabulated. Although the wind speed and the stability classification are reasonably defined which of the plume rise models best fits the data is indeterminable.

4.5.6 Turbulence levels related to plume structure

The turbulence data are summarized in Table 16. Only at 1220 m (4000 feet) MSL were there sufficient runs for meaningful estimates of the standard deviations of the mean turbulent quantities. On this day, the pitot system functioned properly permitting simultaneous three-dimensional turbulence measurements and so there was no need to classify the runs according to whether they were crosswind or alongwind. There is no significant difference between σ_u and σ_v indicating that the energy distribution between the horizontal wind components was roughly equal, validating approximations made on other case days.

The heat flux estimates showed considerable variations between the two-minute data segments at 1220 m (4000 feet). Even the sign of the heat flux is not certain.

TABLE 15 Observed and calculated plume rise for the powerhouse stack for the flight March 12, 1976 (1420-1650)

DOWNWIND DISTANCE (km)	PLUME RISE OBSERVED (m) ±50	WINDSPEED (m/sec.)	RATIO CALCULATED TO OBSERVED VALUES OF uΔh BRIGGS TVA(1972) BOSANQUET HOLLAND FORMULATIONS 1	2	3	4
3.2	*	2.6	1.63	1.23	0.93	0.80
4.8	550					
8.9	*					
11.3	-					
3.2	*	2.6	0.68	0.52	0.39	0.34
4.8	-					
8.9	*					
11.3	1310					

* reliable estimate not available

The momentum flux at 1220 m (4000 feet) was negative indicating that the effect of surface drag was being felt at 1220 m (4000 feet) MSL, and thus that the mixed boundary layer extended to at least that altitude. This result is in agreement with the irregular nature of the SO_2 concentration which suggested considerable mixing.

The very small heat flux means that the turbulence was mechanical and not convective. This conclusion is supported by the presence of a fairly heavy overcast which would suppress surface heating and hence the convective energy supply. The stability would be close to neutral (C stability) which is what the σ_z values indicated on the Pasquill-Gifford curves. The Pasquill-Gifford curves for the normalized concentrations at center line, shown in Figure 35, tended to overestimate the actual concentrations.

The non-dimensionalized plume spreads in both the lateral and vertical directions were presented in Table 14. There was a decrease with distance similar to previous case studies.

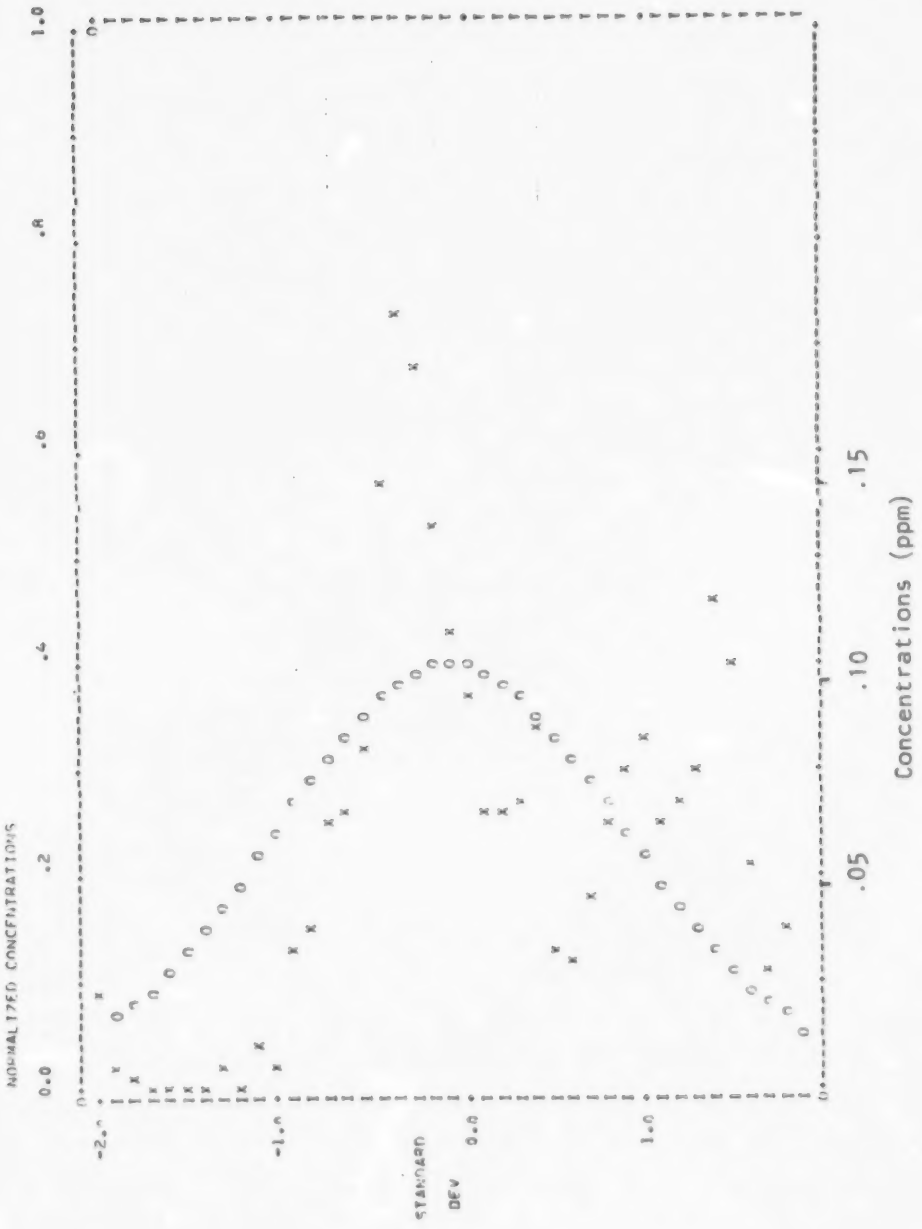

FIGURE 31 Normalized SO_2 concentrations for run 10 at an altitude of 910 m. (3000 ft.) MSL at a downwind distance of 4.8 km. (3 miles) on the flight of March 12, 1976 (1420-1650).

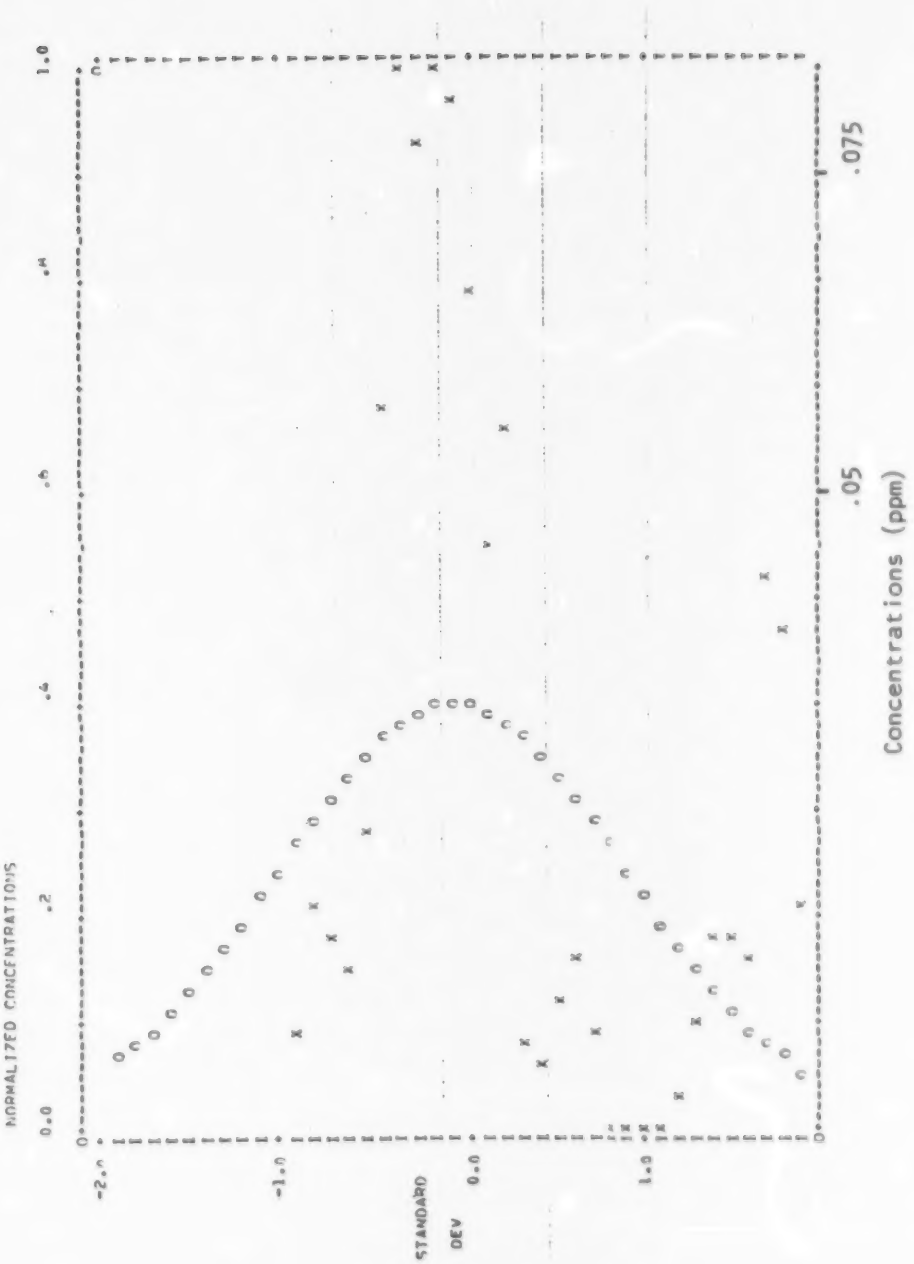

FIGURE 32 Normalized SO_2 concentrations for run 15 at an altitude of 1580 m. (6000 ft.) MSL at a downwind distance of 11.3 km. (7 miles) on the flight of March 12, 1976 (1420-1650)

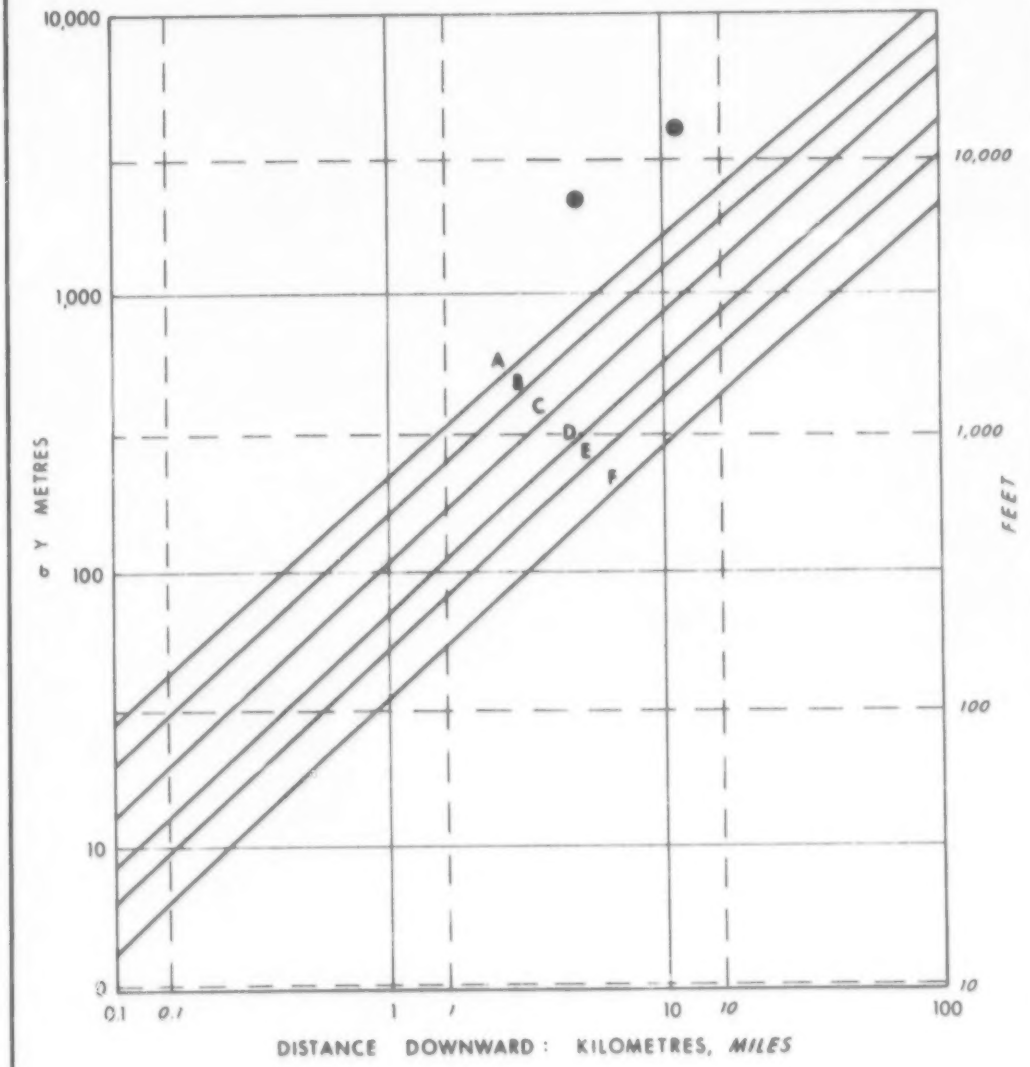

FIGURE 33 Observed horizontal dispersion coefficients compared to Pasquill-Gifford curves for the flight of March 12, 1976 (1420-1650 MST).

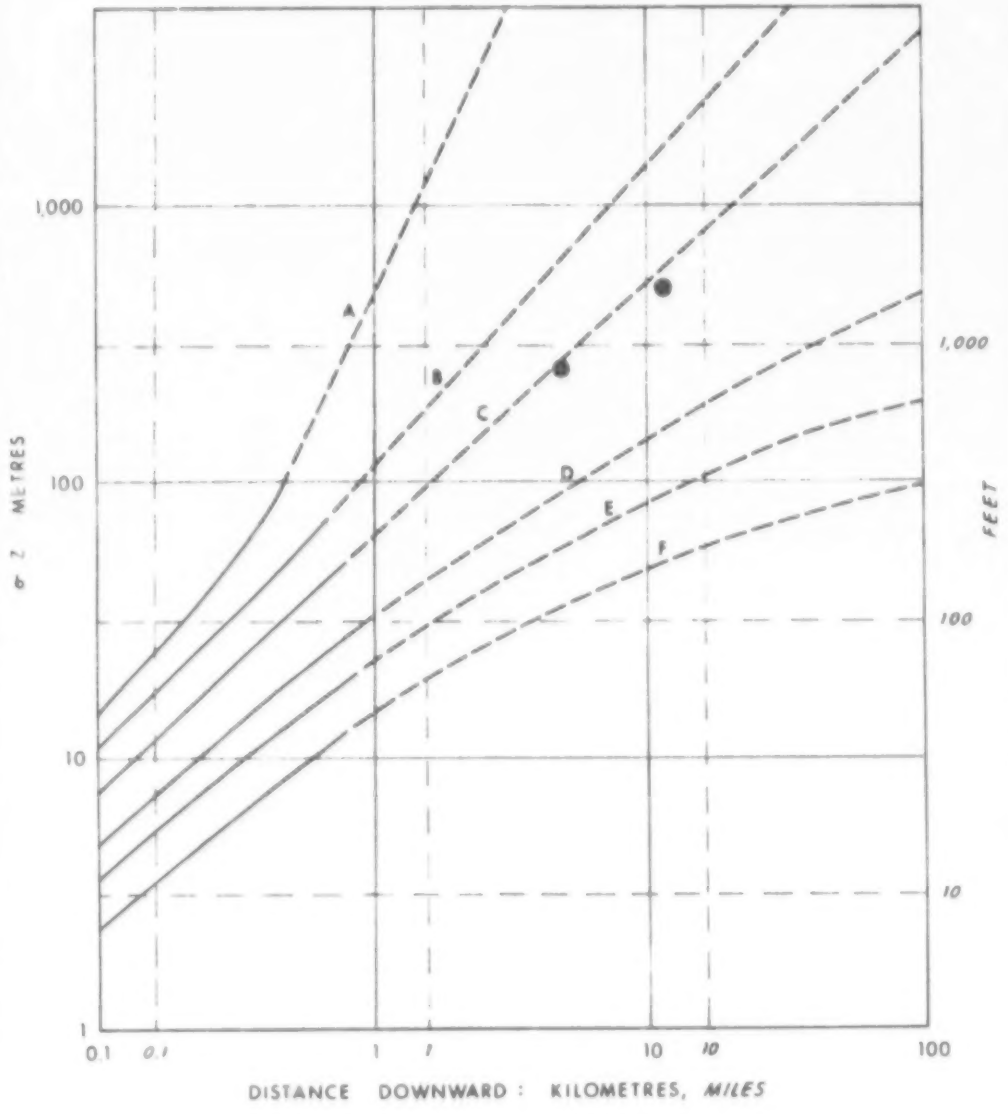

FIGURE 34 Observed vertical dispersion coefficient compared with Pasquill-Gifford curves for the flight of March 12, 1976 (1420-1650 MST).

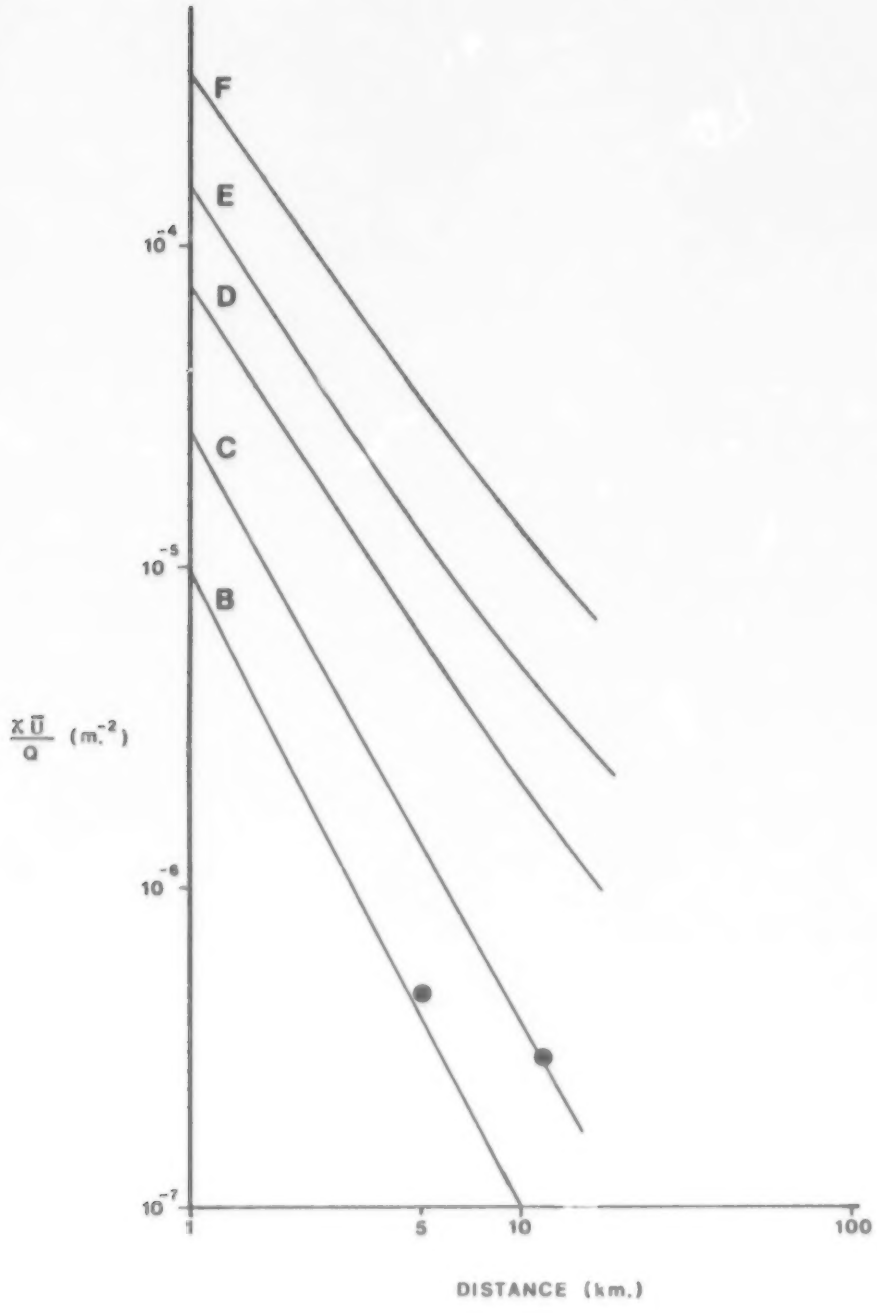

Figure 35. Comparison of observed normalized centerline concentrations with Pasquill-Gifford predictions for the flight of March 12, 1976 (1420-1650 MST).

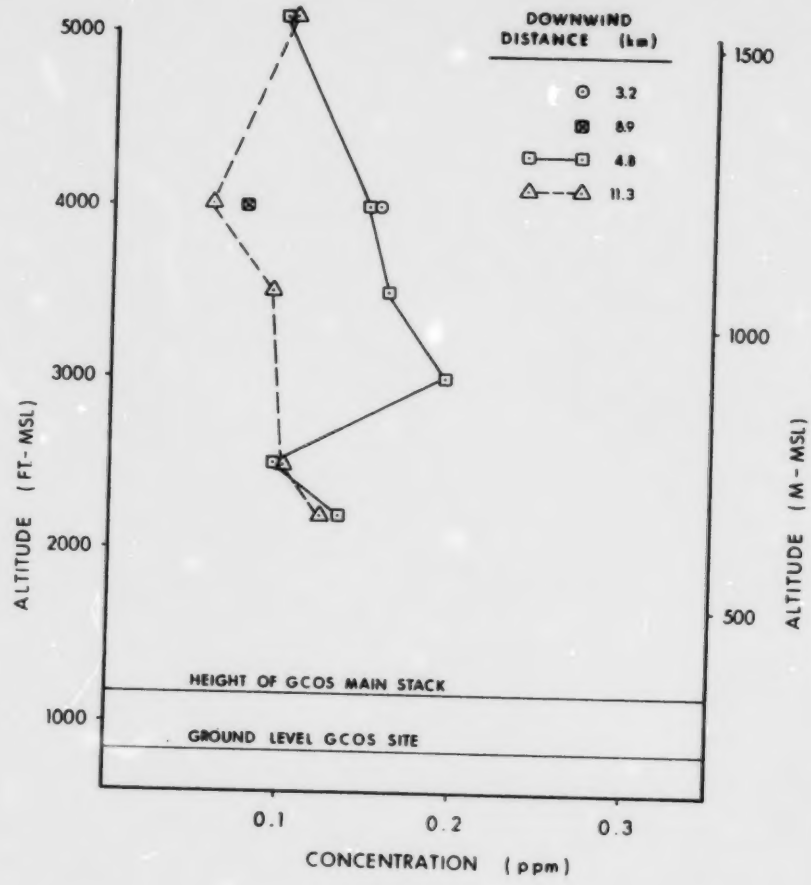

FIGURE 36 Maximum SO_2 concentrations along each traverse shown as a function of altitude for the flight of March 12, 1976 (1420-1650 MST).

TABLE 16 Summary of turbulence data for March 12, 1976 (1420-1650)

HEIGHT [m]	NUMBER OF RUNS	σ_w [m/sec]	σ_v [m/sec]	σ_u [m/sec]	$\overline{w'u'}$ $[m/sec]^2$	$\overline{w'v'}$ $[m/sec]^2$	$\overline{w'T'}$ [deg C- m/sec]
1580	3	0.95	1.01	1.62	-0.236	0.758	0.082
* 1220	12	0.71	1.88	1.42	-0.26	0.03	0.006
		(0.07)	(0.5)	(0.1)	(0.2)	(0.1)	(0.015)
1070	3	0.85	0.88	1.85	-0.01	-0.257	-0.001
910	1	1.13	1.81	1.37	1.37	-0.402	0.133
760	2	0.92	1.39	1.53	-0.06	-0.183	0.000
670	3	1.02	1.19	1.52	-0.012	-0.472	0.038

* The standard deviations of the mean values at 1220 m (4000 feet) MSL are shown beneath the corresponding mean value. The other altitudes do not have sufficient data to define similar meaningful standard deviations.

4.6 CASE STUDY FOR THE FLIGHT OF MARCH 15, 1976 (0740-0940)

4.6.1 General meteorology and visual plume description

In this early morning case, there were clear skies with fairly steady winds from the northeast. The plume was very narrow horizontally and very thin in the vertical at the beginning of the flight. The center line trajectory is shown in Figure 37. By about 0830 the plume showed a definite spreading towards the south; the northern side of the plume boundary was much sharper. At 0840, the plume showed a definite layering effect with clear air between the layers. The main plume effluent was now below and further to the south than a residual layer.

The tethersonde was profiling throughout the time of the flight with two complete profiles showing little difference. The temperature profiles indicated several hard inversions up to 500 m (1640 feet) AGL or 745 m (2440 feet) MSL. The wind profiles showed light variable winds to a height of about 300 m (980 feet) AGL topped by a layer of increasing wind speed to a speed of 5 m/sec (16 ft/sec) at 450 m (1480 feet) and then a slight decrease. The plume center line was close to 350 m (1150 feet) AGL, and so was in the layer of strong vertical shear of the wind speed.

4.6.2 Flight profiles

A race track pattern was set up at 3.2 km (2 miles) and 8.0 km (5 miles) as shown in Figure 37 and Table 17. Since the plume had a very limited vertical extent, the vertical resolution of the profiles was good. Runs 8 and 9 were flown at the same altitude and distance downwind but in opposite directions to check for repeatability and any instrumental response problems. Following the plume traverses, turbulence runs were made at 610 m (2000 feet) MSL parallel to the river valley on the west side and then crosswind.

4.6.3 Isopleths and selected traverses

The isopleths of SO_2 concentration are shown in Figure 38. The concentrations measured in this case study were much larger than any of the other case studies and correspondingly the lateral plume standard deviations σ_y were much smaller than any others.

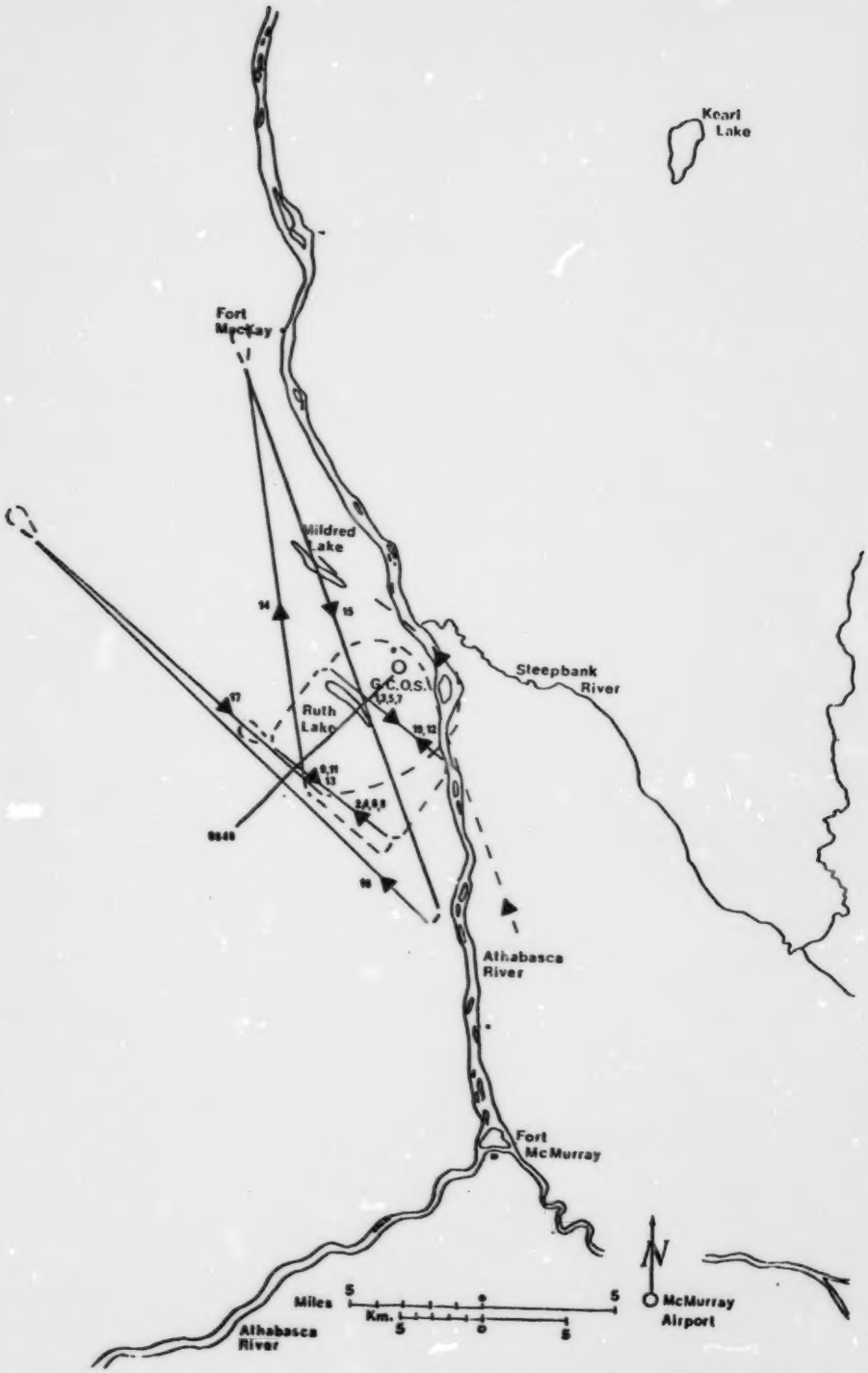

Figure 37 Flight profile for Mar. 15, 1976 (0740-0940). Solid lines denote numbered runs and dashed lines denote interconnecting legs. Plume centerline for 0840 is superimposed.

TABLE 17 Run information for flight of March 15, 1976 AM (0740-0940)

RUN NUMBER	TIME (MST)	ALTITUDE (m-MSL) ±20	DOWNWIND DISTANCE (km) ±0.3	σ_y (m) ±100	MAX CONC. (ppm) ±0.02	INTEGRATED CONC. (ppm-m) ±50	FLIGHT DIR. (From-to)
1	0800 - 0802	610	3.2	302	5.43	3730	NW-SE
2	0803 - 0805	610	8.0	405	4.08	3580	SE-NW
3	0807 - 0809	460	3.2	+	+	+	NW-SE
4	0811 - 0813	460	8.0	+	+	+	SE-NW
5	0815 - 0816	760	3.2	+	+	+	NW-SE
6	0820 - 0821	760	8.0	M	M	M	SE-NW
7	0823 - 0825	550	3.2	387	2.26	1550	NW-SE
8	0828 - 0830	550	8.0	473	6.12	6350	SE-NW
9	0831 - 0833	550	8.0	500	6.01	6030	NW-SE
10	0836 - 0838	520	3.2	2041	2.62	2890	SE-NW
11	0840 - 0842	520	8.0	1184	2.04	4740	NW-SE
12	0844 - 0846	670	3.2	518	2.34	1860	SE-NW
13	0848 - 0850	670	8.0	1514	0.24	270	NW-SE
14	0854 - 0901	610	-	T	T	T	S - N
15	0902 - 0912	610	-	T	T	T	N - S
16	0914 - 0920	610	9.7	T	T	T	SE-NW
17	0925 - 0929	610	8.0	T	T	T	NW-SE

T Turbulence run
\+ NO SO_2 detected on these traverses
M data lost due to system malfunction
\- run not crosswind

8 km. (5 mi.)

3.2 km. (2 mi.)

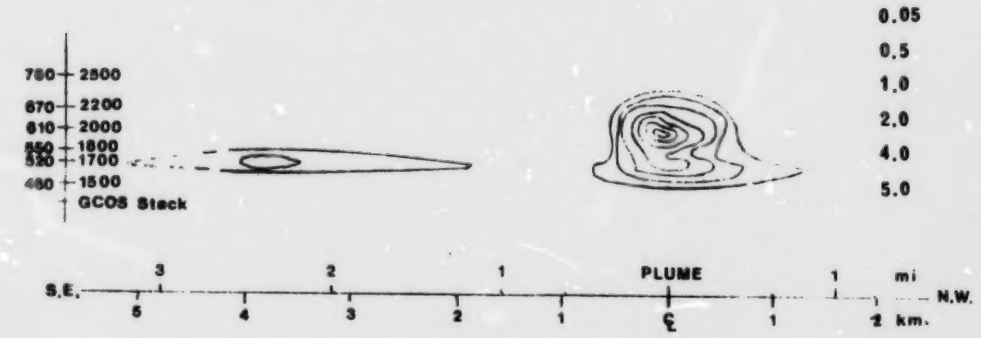

FIGURE 38 SO_2 Concentration Isopleths for March 15, 1976 (0740-0940). Transects were flown downwind of GCOS stack at 3.2 km. (2 mi.) and 8 km. (5 mi.).

There was evidence of multiple sources at 460 m (1500 feet) MSL. The effluent from all the stacks could be visually seen to rise almost straight up before reaching the layer with strong wind shear. Figure 39 shows the normalized SO_2 concentrations for run 11 at 520 m (1700 feet) MSL at 8 km (5 miles) downwind. The presence of the secondary sources can be seen on this run even though considerable mixing has taken place.

Runs 8 and 9 shown in Figures 40 and 41 are of particular interest for repeatability and instrumental checks. Some instrumental response problem due to purging after the very high concentrations (6 ppm) is evident. Nevertheless, the concentrations appear to have a slightly more peaked distribution than Gaussian. The σ_y values, the maximum concentrations and the integrated concentrations for runs 8 and 9 as shown in Table 17 are in excellent agreement; the repeatability of the above traverse statistics is 95% or better.

4.6.4 Plume geometry and mass flux

Table 18 summarizes plume geometry and mass flux data. Figure 42 shows the maximum concentrations along each traverse as a function of height. The plume center line can be seen to be about 610 m (2000 feet) MSL at 3.2 km (2 miles) and then dropping to about 550 m (1800 feet) MSL by 8.0 km (5 miles). As mentioned above this altitude is in a layer of high wind shear in the vertical. From the tethersonde profiles the mean wind speed at 550 m (1800 feet) MSL is 1.7 m/sec and at 610 m (2000 ft) MSL is 2.9 m/sec. The question then arises as to whether the wind speed at a given altitude over the river valley is a representative wind speed for the same MSL altitude some 11 km (8 miles) further downwind where the ground elevation is about 100 m (330 feet) higher. Furthermore the height of the center line is not known accurately enough to obtain a good wind speed estimate for accurate mass flux computation. A wind speed of 2.3 m/sec (7.4 ft/sec) (the average of the wind speeds at 550 and 610 m (1800 and 2000 ft) MSL gives SO_2 mass fluxes of 11.9 and 11.3 metric tons per hour at 3.2 and 8.0 km (2 and 5 miles) respectively in excellent agreement with the emission value of 11.6 metric tons per hour. Such close agreement is somewhat fortuitous considering the very large vertical wind shear and the uncertainty in the exact plume center line height.

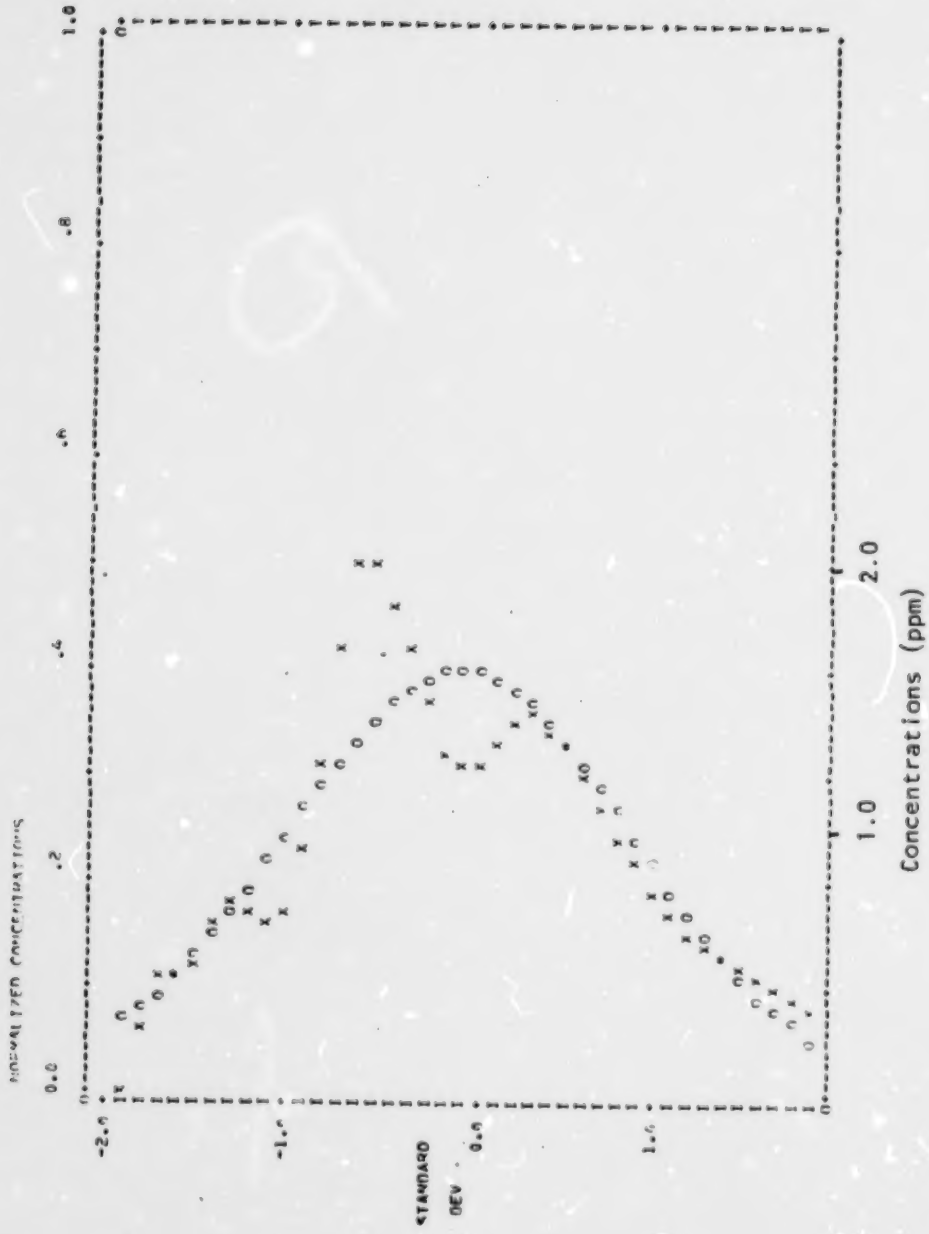

FIGURE 39 Normalized SO_2 concentrations for run 1 at an altitude of 520 m. (1700 ft.) MSL at a downwind distance of 8.0 km. (5 mi.) on the flight of March 15, 1976 (0740-0940).

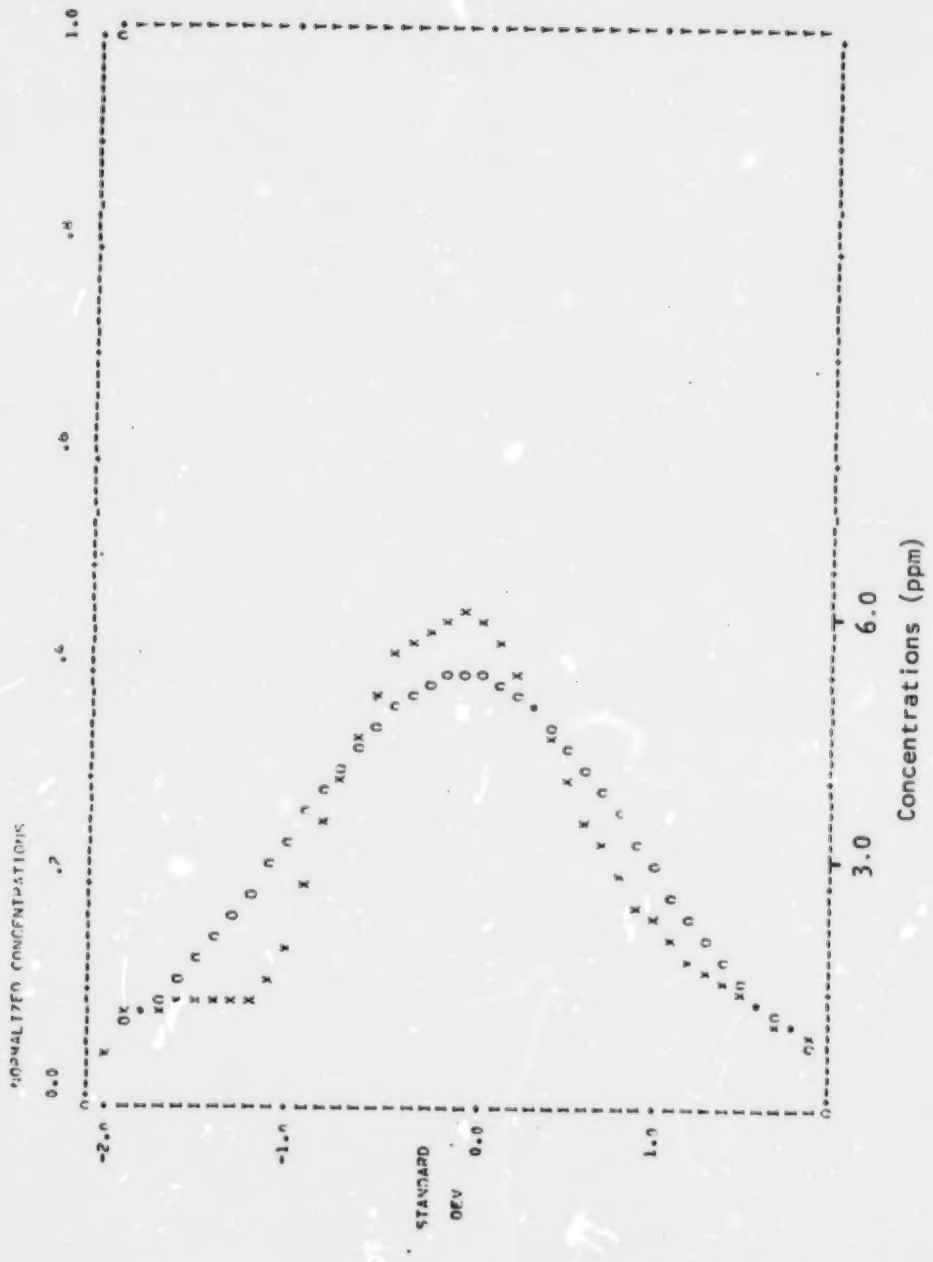

FIGURE 40 Normalized SO_2 concentrations for run 8 at an altitude of 550 m. (1800 ft.) MSL at a downwind distance of 8.0 km. (5 mi.) on the flight of March 15, 1976 (0740-0940).

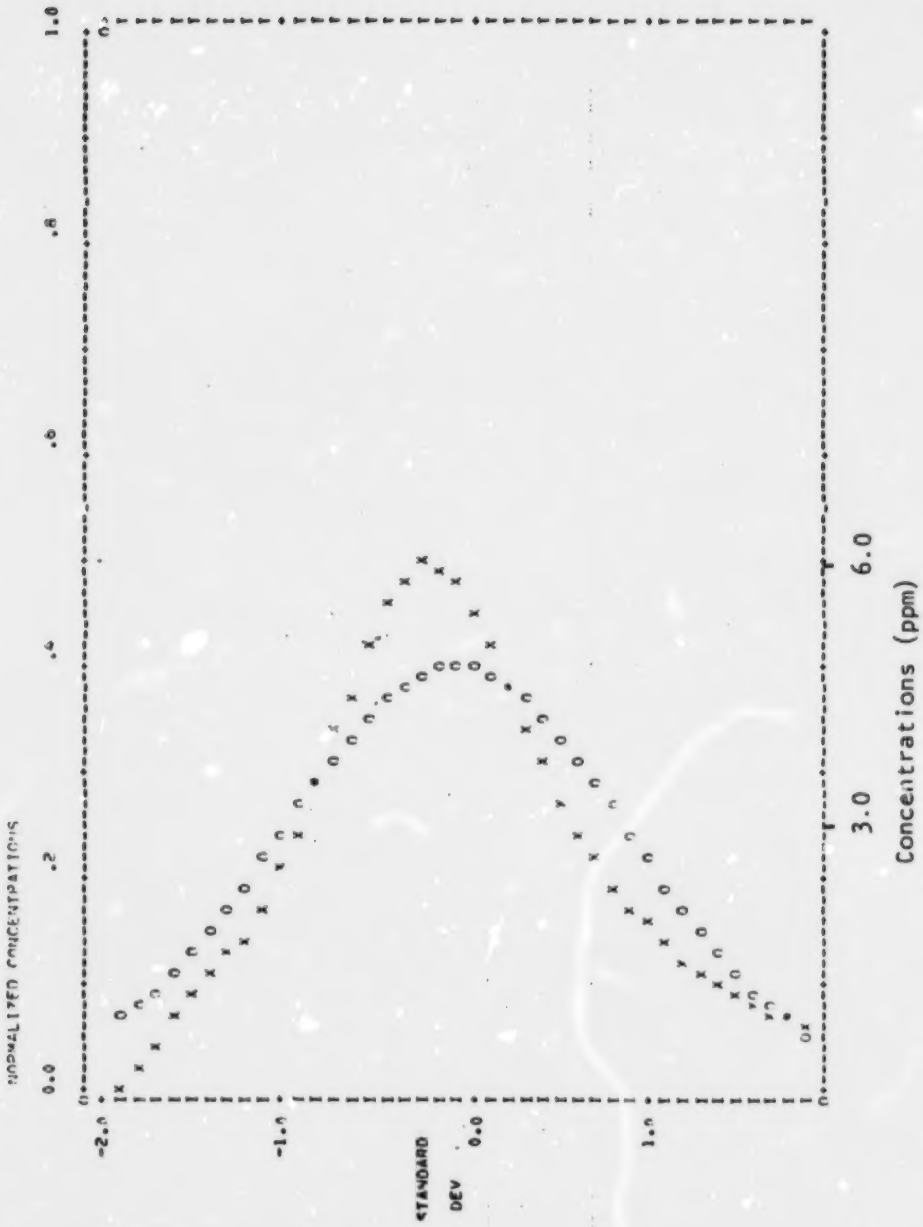

FIGURE 41 Normalized SO_2 concentrations for run 9 at an altitude of 550 m. (1800 ft.) MSL at a downwind distance of 8.0 km. (5 mi.) on the flight of March 15, 1976 (0740-0940).

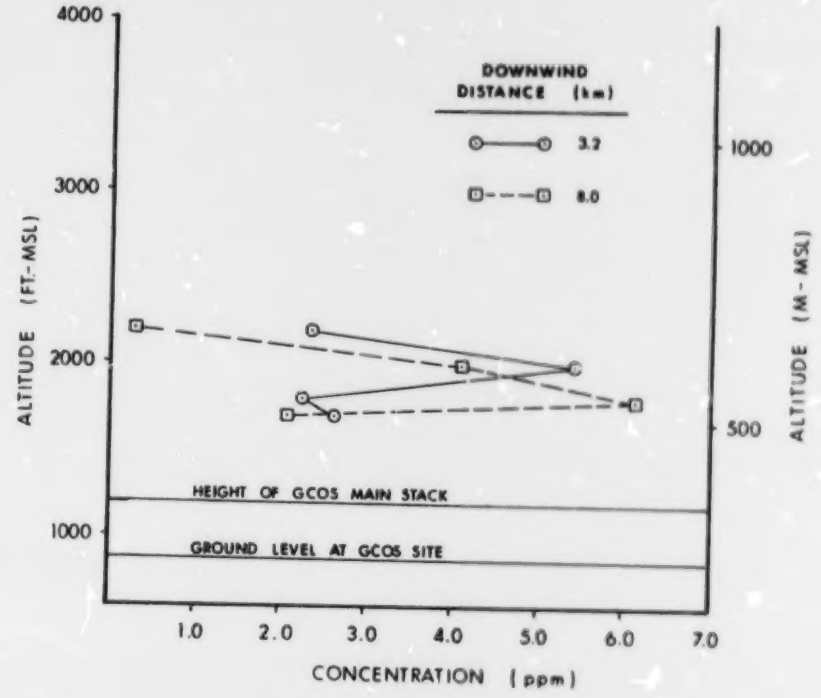

FIGURE 42 Maximum SO_2 concentrations along each traverse shown as a function of altitude for the flight of March 15, 1976 (0740-0940).

TABLE 18 Plume geometry and mass flux as functions of downwind distance from the source for the flight of March 15, 1976 (0740 - 0940)

DOWNWIND DISTANCE X [km]	NORM. CL CONC $\chi\bar{U}\,Q^{-1}$ [$10^{-6}\,m^{-2}$] ± 0.1	σ_z [m] ± 20	σ_{ycl} [m] ± 100	SO_2 mass flux [metric tons per hour]	$\frac{\sigma_z \bar{U}}{\sigma_w X}$	$\frac{\sigma_y \bar{U}}{\sigma_{UH} X}$
3.2	10.7	116	302	13.2	0.26	0.20
8.0	12.0	100	472	12.6	0.09	0.12

$\bar{U}$ is the mean wind speed at plume center line height as measured by the tethersonde ($\bar{U}$ = 2.5 m/sec (8.2 ft/sec))
Q is the sum of SO_2 emissions as supplied by GCOS = 11.6 metric tons /hr.
X downwind distance
χ centre line concentration of SO_2 (mass volume)

The comparisons of the observed values of σ_y, σ_z and normalized center line concentrations with the Pasquill-Gifford curves are shown in Figures 43, 44, and 45. Unlike all the previous case studies the values of σ_y fall along the curves. Presumably the combination of the very weak winds at low levels, the lack of directional shear in the vertical and the very limited vertical mixing gave rise to a plume geometry at center line which resembled a single-source plume. The center line concentrations suggest D or E stability. Note that the center line concentration was highest at 8 km (5 miles) suggesting that the plume center line was very narrow and was probably missed at 3.2 km (2 miles).

4.6.5 A comparison of observed and calculated plume rise

Vertical concentration profiles based on surveys of March 15, 1976, (0740 - 0940) are presented in Figure 42. The profile at 3.2 km downwind suggests an initial over-shoot to 610 m (2000 feet) MSL while the profile at 8.0 km indicates a levelling off at 550 m (1800 feet) MSL. As alluded to earlier in the discussion of this case, the layer of high shear between these altitudes probably contributed to the effective stack height attained.

TABLE 19 Observed and calculated plume rise for the powerhouse stack for the flight of March 15, 1976 (0740-0940)

DOWNWIND DISTANCE (km)	PLUME RISE OBSERVED (m) ±50	WINDSPEED (m/sec.)	RATIO CALCULATED TO OBSERVED VALUES OF $u\Delta h$ BRIGGS TVA(1972) BOSANQUET HOLLAND FORMULATIONS			
			1	2	3	4
3.2	240	1.8	0.81	0.79	1.56	2.70
8.0	180		1.08	1.03	2.09	3.60

Table 19 summarizes a comparison of observed and calculated plume rises for this day. The average wind speed and temperature gradient between the top of the stack and the effective stack height used in plume rise calculations were 1.8 m/sec and 2.5 °C/100 meters respectively. These data were abstracted from the tethered balloon measurements. Over the lower half of the plume rise a very strong inversion was evident approaching 10°C/100 meters.

The March 15, 1976, case was the only moderately stable case ($\Delta\theta/\Delta Z$ = 0.025°C/m) of the five analyzed. It is evident that the Briggs and TVA (1972) formulations give very satisfactory estimates whereas the other two overestimate significantly. The overestimating of the Holland models for stable conditions is consistent with observations made by Turner (1970) and attributed to Holland by Briggs (1969). However Briggs' (1971) subsequently showed that the Holland model underestimates during these conditions. In this latter study Briggs found the Bosanquet model to overestimate plume rise.

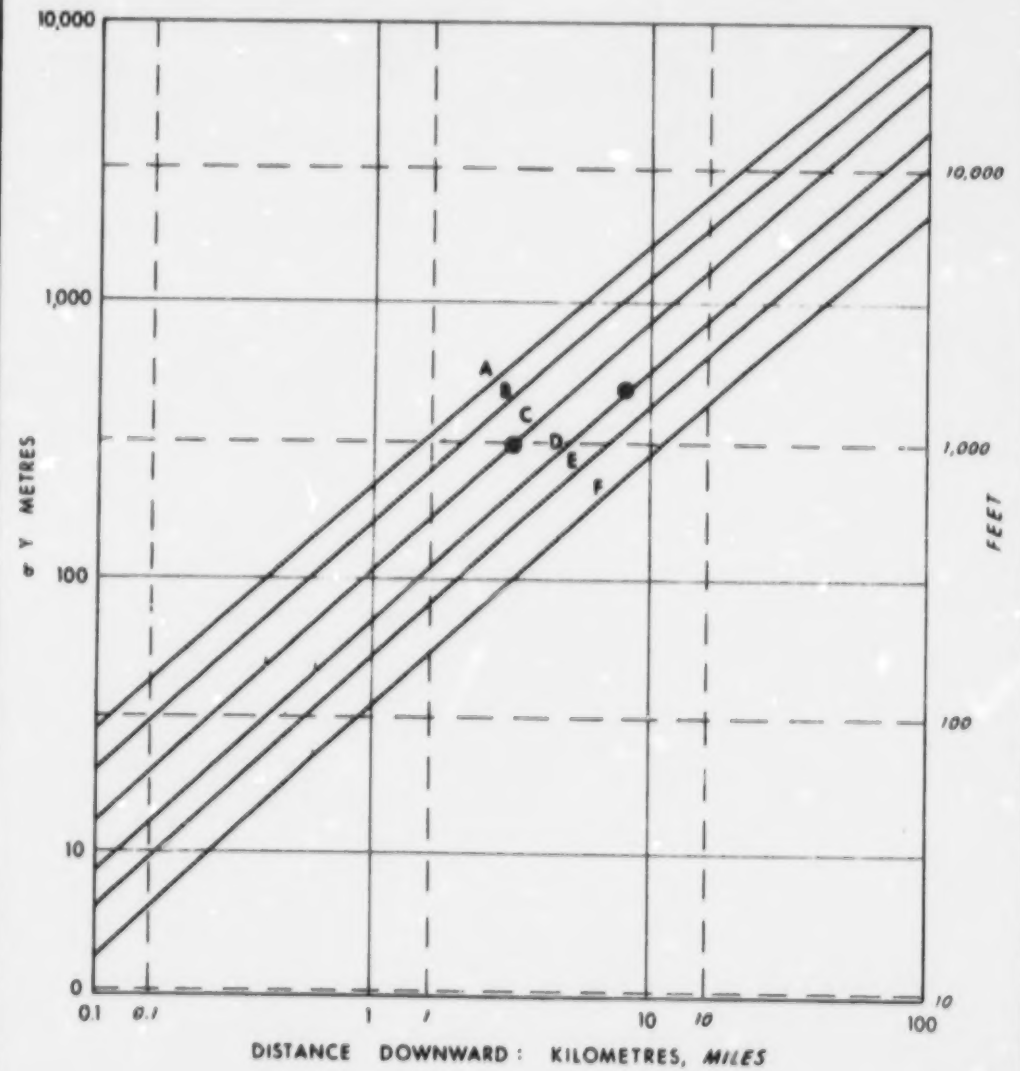

FIGURE 43 Observed horizontal dispersion coefficients compared to Pasquill-Gifford curves for the flight of March 15 (0740-0940 MST).

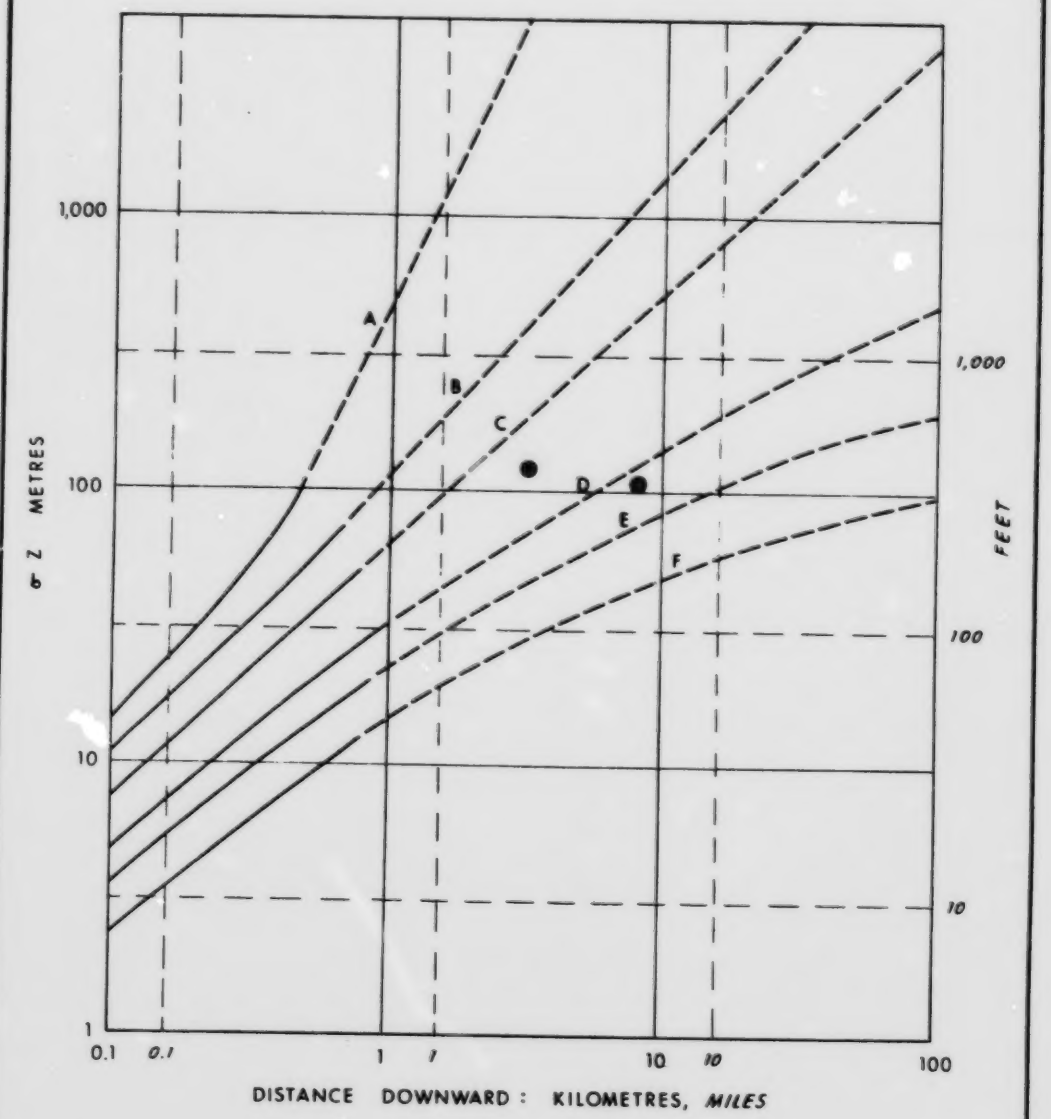

FIGURE 44 Observed vertical dispersion coefficient compared to Pasquill-Gifford curves for the flight of March 15, 1976 (0740-0940 MST).

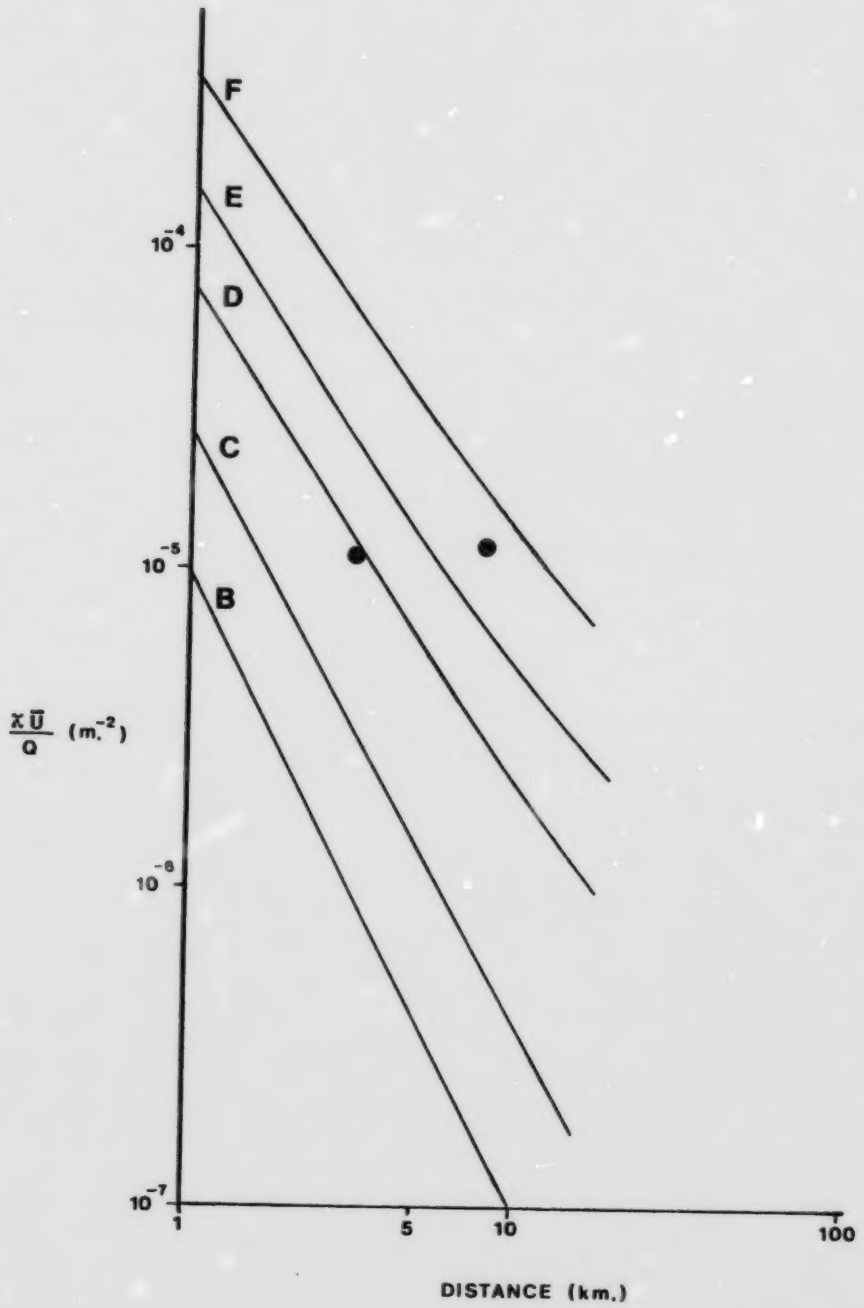

Figure 45. Comparison of observed normalized centerline concentrations with Pasquill-Gifford predictions for the flight of March 15, 1976 (0700-0940 MST).

4.6.6 Turbulence levels related to plume structure

The summary of turbulence data is presented in Table 20. The horizontal wind standard deviations are all of comparable size and have a mean of 1.2 m/sec; the vertical wind standard deviation is about 30% as large.

The momentum flux $\overline{U'W'}$ has a net positive value if all runs are averaged. However two large positive values at 460 and 550 m (1500 feet and 1800 feet) MSL dominate the contributions. Both tethersonde profiles showed a low level jet with a maximum speed of 2.2 m/sec (7.2 feet/sec) centered at 445 m (1460 feet) MSL which might explain the presence of occasional, large positive momentum flux values at these altitudes. Within the strong wind shear layer above 550 m (1800 feet) MSL, the momentum flux was very small indicating virtually no mechanical turbulence. The visual observations of layering near the top of the visual plume confirms that very little vertical mixing was taking place.

The heat flux is close to zero particularly at the higher levels indicating virtually no convective turbulence.

Because of the lack of turbulent fluxes, the σ_w values are very likely due to laminar wave flow which would induce very little if any mixing but which would cause an apparent spreading of the time-averaged plume for an Eulerian observor.

The non-dimensionalized plume spreads presented earlier in Table 18 can now be interpreted. σ_z does not have a linear spread, but rather is approximately constant with increasing diffusion time. The use of σ_w as a non-dimensionalizing parameter may not be appropriate unless laminar and turbulent contributions to σ_w can be separated. The increase of σ_y is less than linear with diffusion time. The magnitudes of these non-dimensionalized plume sigma values will be compared with other case studies in the following chapter.

TABLE 20 Summary of turbulence data for flight of March 15, 1976 (0740-0940)

HEIGHT [m MSL]	NUMBER OF RUNS		σ_w	σ_u	σ_v	$\overline{W'U'}$	$\overline{W'V'}$	$\overline{W'T'}$
	I	//	[m/sec]	[m/sec]	[m/sec]	[m/sec]^2	[m/sec]^2	[deg C- m/sec]
460	2	1	0.45	2.27	2.91	0.29	0.53	0.03
520	2	0	0.15	0.72	*	0.00	*	0.00
550	3	1	0.35	0.88	2.45	0.13	-0.65	0.02
+610	5	1	0.35	1.22	0.25	0.00		0.00
670	2	0	0.50	0.53	*	0.02	*	-0.01
all	14	3	0.35	1.29	1.87	0.072	-0.04	0.006

* insufficient data for reliable estimate
I number of crosswind runs
// number along-wind runs
\+ the seven two-minute segments from runs 14 and 15 were included for σ_w W'T'; these seven segments had σ_{UH} of 0.95 and a $\overline{W'U'}$ of -0.001

5. DISCUSSION OF THE CASE STUDY RESULTS

5.1 A COMPARISON OF PLUME GEOMETRY WITH PASQUILL-GIFFORD RESULTS

For each of the case studies examined in the previous chapter, the observed values of σ_y, σ_z and normalized center line concentrations were compared to the Pasquill-Gifford curves as presented by Turner. In Table 21 each case study is briefly described and a Pasquill-Gifford stability class assigned is shown. In Figures 46, 47, and 48 all of the case study values are compared with the Pasquill-Gifford curves.

The σ_y values can be seen to be significantly larger than predicted. The presence of multiple sources can partly explain the discrepancy, since the multiple peaks result in much larger σ_y values than would result from just the main plume. Note that if second order moments had been used for the plume standard deviation calculation rather than the adopted method which kept the area constant, the discrepancy would have been much larger. The case of the morning of March 15 is of particular interest. The lack of low level directional shear may have been very important in keeping the σ_y values small. If that interpretation is correct, then the characteristics of the wind profile may be very important. Note that the slope of the observed points for each stability class is close to the slopes of the Pasquill-Gifford curves.

The σ_z values also separate fairly well according to stability class. However the observed σ_z values do not increase with distance as quickly as predicted. Undoubtedly this result is due to the presence of elevated inversions. The assignment of a single stability class for a boundary layer comprising of several different stabilities in the vertical is not appropriate.

The normalized center line concentrations tend to be lower than predicted. This result is consistent with the σ_y values since the σ_y values are larger than predicted. The concentrations scatter fairly widely along the predicted curve. This scatter can probably be attributed to the difficulty in obtaining a reliable maximum concentration particularly for stable conditions when the concentration gradients in the vertical are large. The concentrations do not decrease with increasing distance as quickly as predicted; again, this result is consistent, since the σ_z values did not increase with distance as quickly as predicted.

TABLE 21 The assigned Pasquill-Gifford stability classes for each of the case studies.

FLIGHT	METEOROLOGICAL DESCRIPTION	ASSIGNED STABILITY
March 10 (1415-1705)	neutral at centerline height, stable above and unstable below	D
March 11 (0750-1050)	very little turbulence with stable near-surface layer	E
March 11 (1250-1655)	mixed up to center line height, stable above	D
March 12 (1470-1650)	well mixed boundary layer with mechanical turbulence and no heat flux	D
March 15 (0740-0940)	very stable layers with strong wind shear at 300 m. AGL; very little turbulence	F

The observed discrepancies between the Pasquill-Gifford curves for σ_z and the observed values are not inconsistent with other experimental results. A summary of experimental results presented by Slade (1968, pg. 131) indicates that especially under stable conditions the Pasquill-Gifford curves tend to overestimate the measure of σ_z with distance. The occurrence of a similar suppression of vertical dispersion for the neutral case for these AOSERP results probably is a result of elevated stable layers occurring for winter conditions at high latitudes. Similar elevated stable layers are probably less frequent at lower latitudes or during warmer seasons of the year.

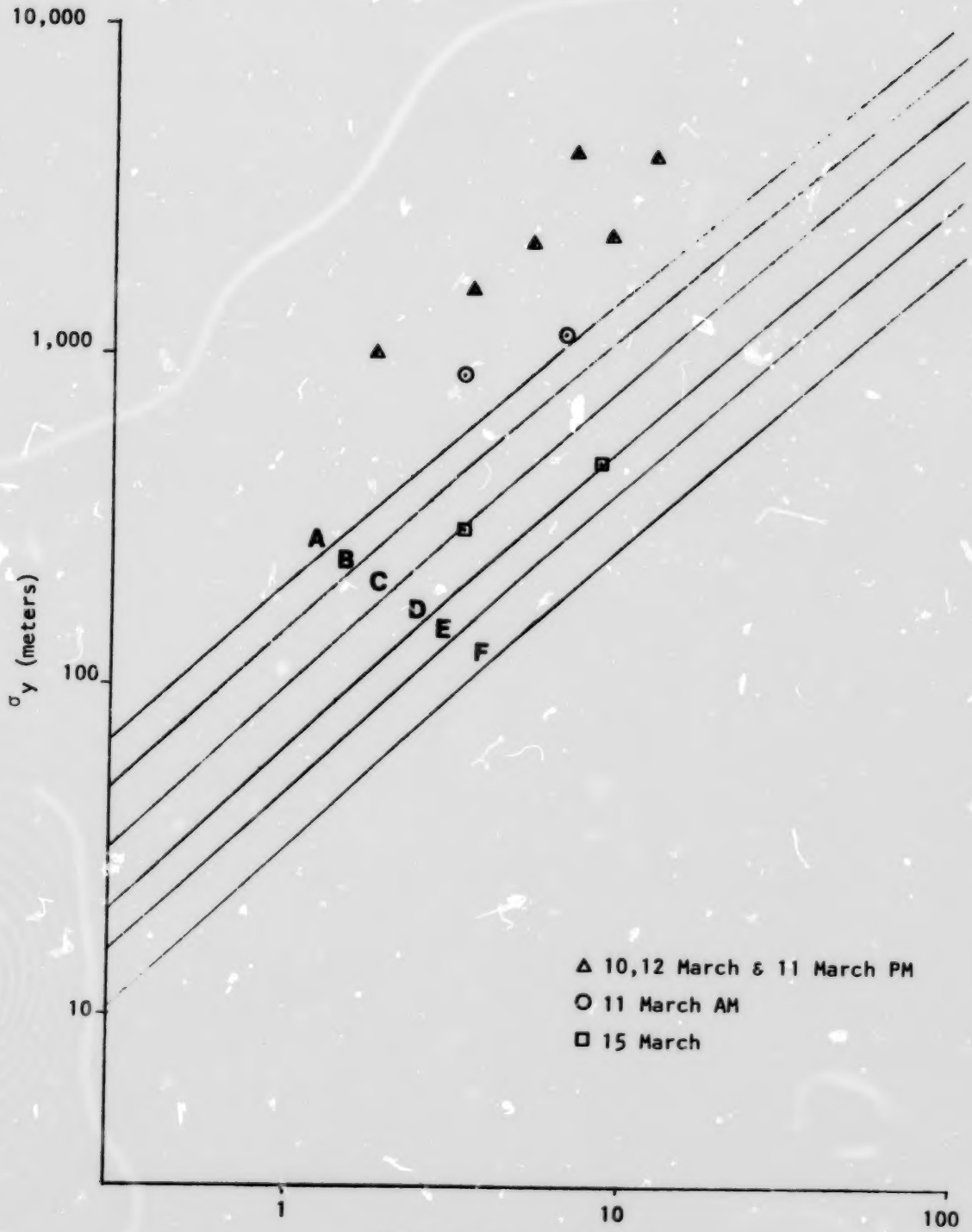

FIGURE 46 Comparison of observed σ_y values with Pasquill-Gifford

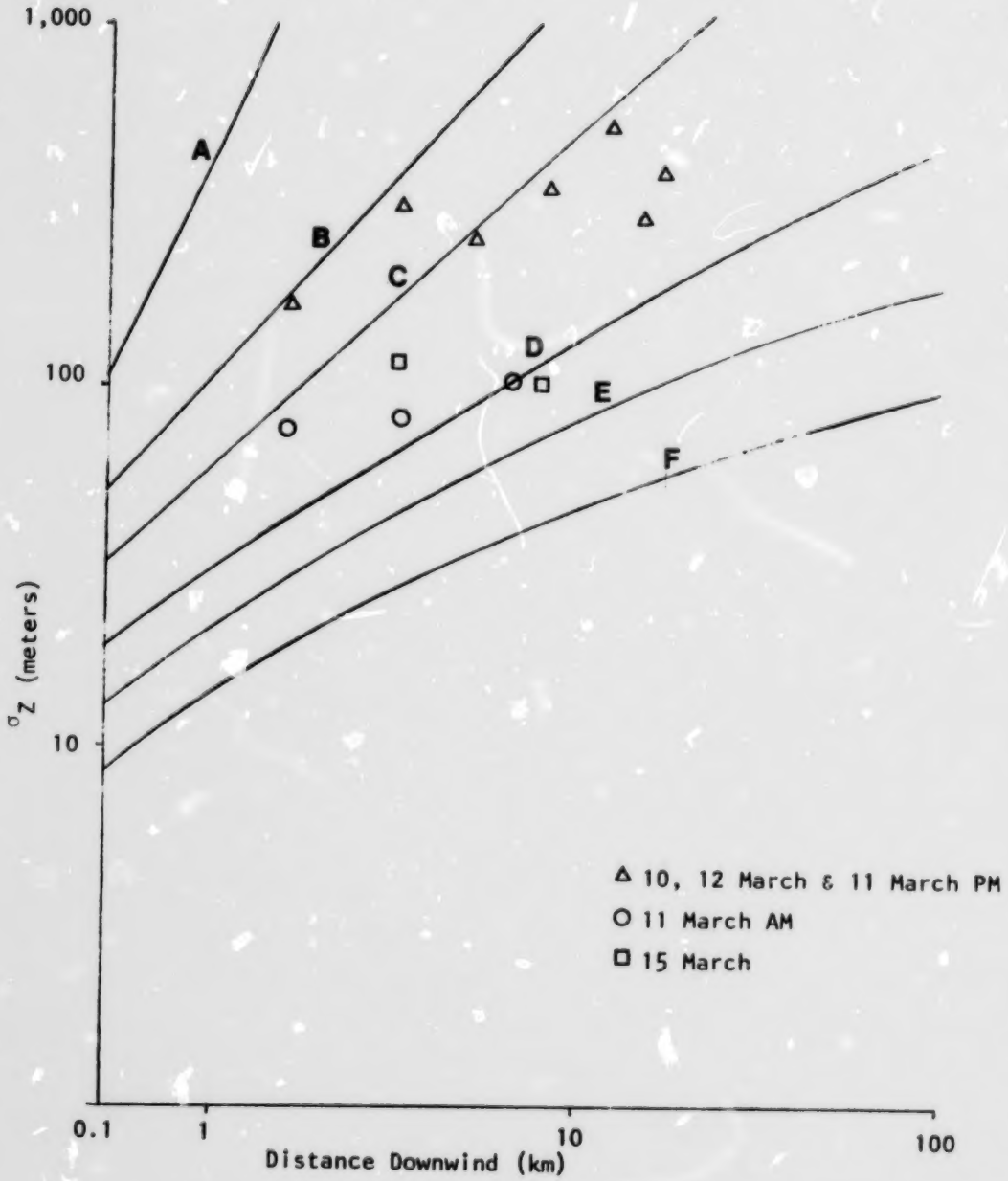

FIGURE 47 Vertical dispersion coefficient as a function of downwind distance from the source as compared with Pasquill-Gifford values.

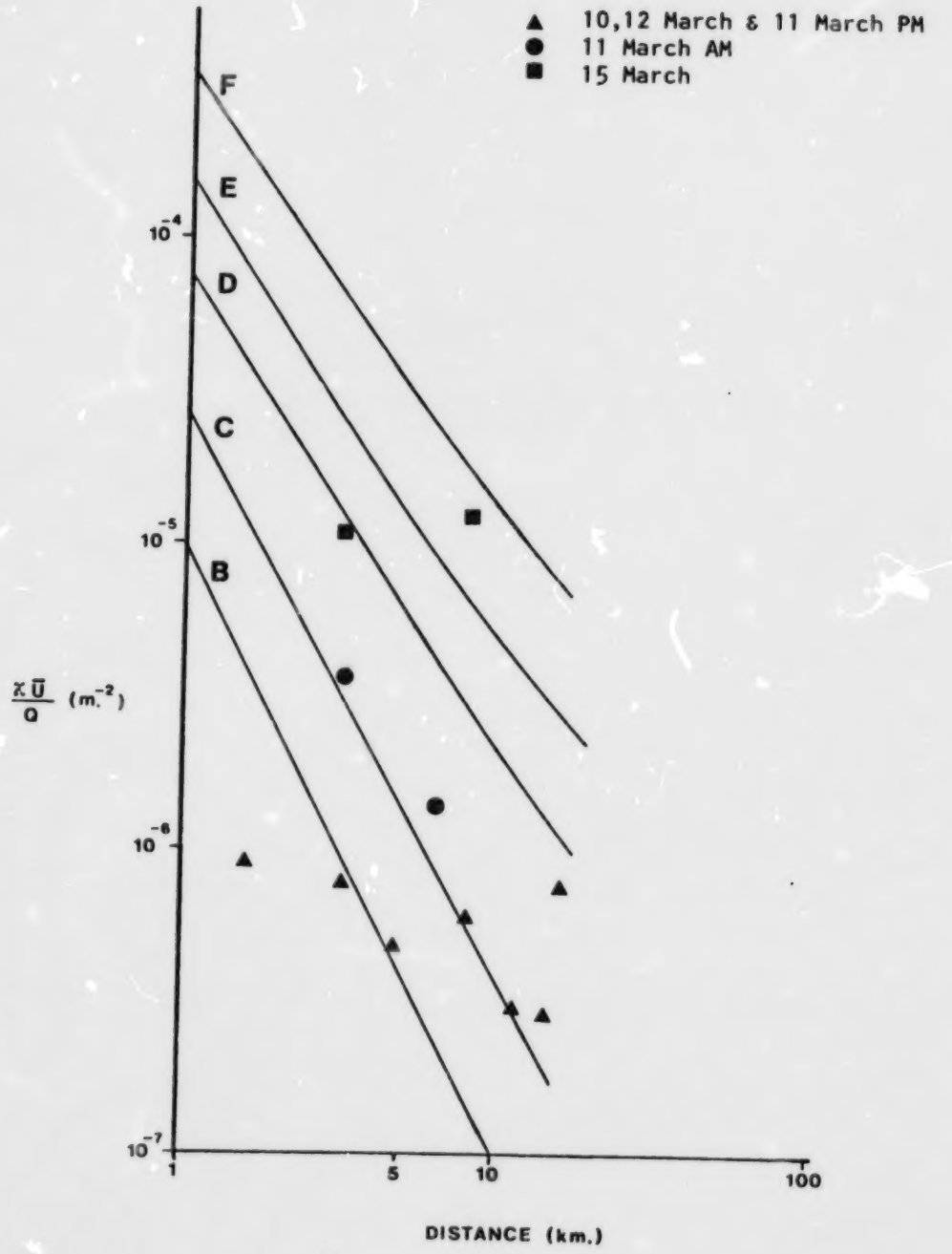

Figure 48. Comparison of observed normalized centerline concentrations with Pasquill-Gifford predictions for the various stability classes.

5.2 THE EFFECTS OF TOPOGRAPHY ON DISPERSION

Enhancement of turbulence production by topography would be expected to appear in increased vertical and horizontal dispersion, since turbulence is inherently three-dimensional.

The increased σ_y values were very much larger than predicted by the Pasquill-Gifford curves but much of this discrepancy may be due to the effects of multiple sources.

The σ_z values, however, should be largely independent of this multiple source effect. The fact that the observed σ_z values did not increase with distance as quickly as predicted was attributed to the effects of elevated inversions. However, in addition, the σ_z values are consistently larger than the Pasquill-Gifford values for the appropriate stability classes. At downwind distances of less than 5 km, the limiting effects on the growth of σ_z due to elevated inversions can probably be considered to be small. Thus much of the enhanced vertical mixing at these closer distances (typically a factor of two to three) can be attributed to enhanced turbulence production due to topography. For the very stable case of March 15, there was very little turbulence at plume height and so topographical effects were probably small. However, the lack of a directional wind shear from near the surface to plume height meant that, for this case study alone, there was no horizontal separation of the plumes from different sources; so that the observed σ_z values may not be appropriate for comparison with the Pasquill-Gifford values.

The normalized axial center-line concentrations (see again Figure 48) also indicate a much lower concentration than predicted. At less than 5 km any question regarding the suitability of the assumption of no virtual source in the computation of the theoretical curves is unimportant. The observed center-line concentrationsat less than 5 km are typically 5 to 10 times less than predicted. This discrepancy combined with the σ_z discrepancy and mass continuity requirements suggests that a factor of 2 or 3 in the σ_y discrepancies can be attributed to enhanced mixing due to turbulence. The fact that the σ_z and σ_y discrepancies attributable to turbulent mixing are approximately equal gives further support to the idea of enhanced three-dimensional turbulent mixing.

A distinction between effective and actual values of σ_y and σ_z needs to be emphasized. The computation of the amount of the σ_y discrepancy attributable to enhanced turbulence by the method in the previous paragraph assumes that the Gaussian model is appropriate. The effective values of σ_y and σ_z are the values needed to match the Gaussian prediction to the observed SO_2 concentration. The difference between the effective and observed σ_y values has been attributed principally to the effects of multiple sources; although the non - Gaussian behaviour of the plume may also have a significant effect in the discrepancies.

The Athabasca River Valley itself is probably not responsible for the enhanced mixing of the plume within the first 5 or 10 km downwind from the stack. As discussed in detail in the case study of March 11 (1250 - 1655) (Section 4.4), there were no statistically significant differences in the various averaged turbulence quantities upwind and downwind (about 8 km (5 miles)) of the river at typical plume heights (300 m or 1000 ft. AGL). Presumably the flow separates at the edges of the valley; so that the effect of the valley topography is not large compared to background turbulence levels as far as the main plume is concerned. The valley has very great effects, however, on the low level wind field and low level emmissions as visually noted almost every morning.

5.3 SUMMARY OF PLUME RISE DATA

Figure 49 summarizes the ratios of calculated to observed plume rise for the five cases analyzed. An initial assessment of these data suggests the methods of Briggs, TVA (1972) and Bosanquet et al give a similar range of results whereas Holland is considerably more inconsistent. Eliminating those cases where the rise was through a non-uniform temperature gradient or considerable doubt of the observed values exists, tends to improve the consistency of the predictions by Briggs and TVA (1972). In contrast the results of the other two techniques is noted to deteriorate. The Briggs model appears to best predict low wind speed cases particularly if accompanied by stable atmospheric conditions. For the one moderately high wind speed case the TVA (1972) model performs best. The Bosanquet et al and Holland formulations severely overestimated the plume rise for the stable case. In general these observations are consistent with those found in the literature (Briggs (1971), Guldberg (1975) and Moses and Kraimer (1972)).

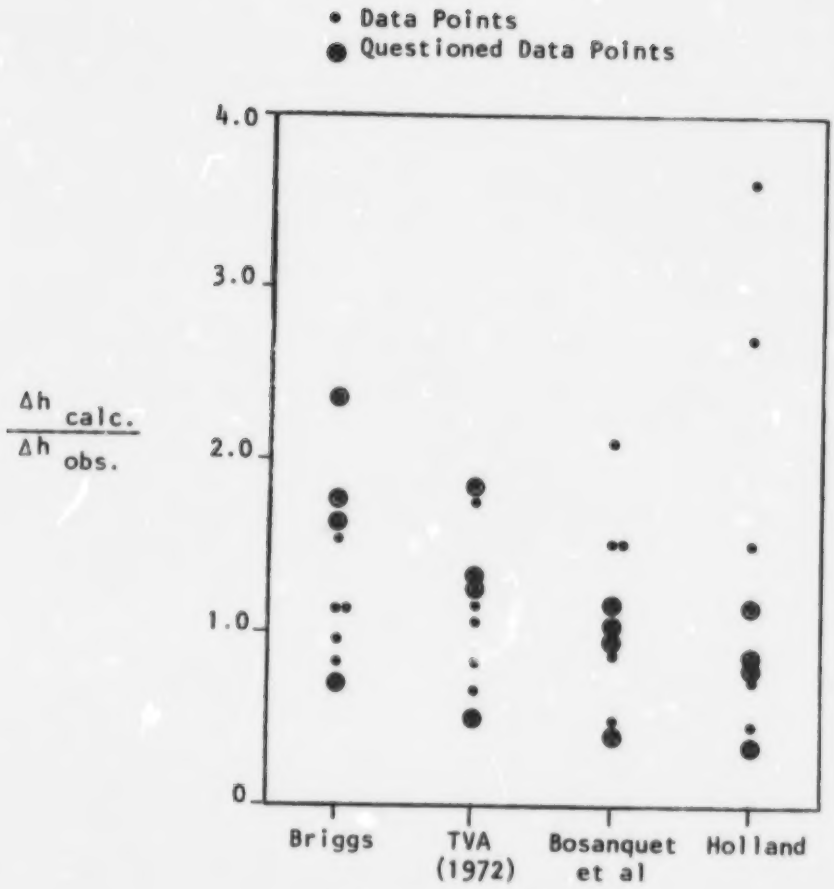

FIGURE 49 Summary of ratios of calculated to observed plume rises.

5.4 The relationship between the standard deviation of the plume dispersion and the turbulent statistics

The Pasquill-Gifford curves relating plume dispersion to stability are empirical curves designed for gently rolling countryside. No account is made for non-homogeneous and non-stationary conditions or for the effects of topography and meso-scale meteorology. Although the Pasquill-Gifford curves are often very useful it is desirable to relate the plume dispersion to the turbulence actually causing the dispersion. Then if the turbulence can be properly parameterized in terms of readily available meteorological data, plume dispersion formulations will be more accurate and less site specific.

The theory of turbulent diffusion was largely developed by Taylor who developed an expression relating particle displacements to the auto correlation function for homogeneous, stationary turbulence

$$\sigma_y^2 = 2\sigma_v^2 \int_0^T \int_0^\tau R(\xi)\, d\xi\, d\tau \qquad (5.1)$$

where T is the diffusion time and where R is the Lagrangian auto-correlation function of the appropriate velocity component. A similar equation relates σ_z to σ_w. For large dispersion times, T, equation (5.1) reduces to

$$\sigma_y^2 = 2\sigma_v^2 t_L T \qquad (5.2)$$

where t_L is the Lagrangian integral time scale given by

$$t_L = \int_0^\infty R(\xi)\, d\xi \qquad (5.3)$$

According to Taylor's theory (and to Pasquill's formulation if we take $f_1 = 1$), a plot of σ_y / σ_v versus $T^{\frac{1}{2}}$ should yield straight lines with a slope $(2\, t_{Ly})^{\frac{1}{2}}$ where t_{Ly} is the horizontal lateral integral time scale. Figure 50 shows that the data supports Taylor's theory. If the curves are forced to go through the origin, then the power law dependence of the form

$$\sigma_y / \sigma_v = \alpha T^n \qquad (5.4)$$

where α and n are constants, yields an average value of $n = 0.46$. This observed value is clearly very close to Taylor's prediction of 0.5. The

maximum value of n is 0.69 for the March 12 case; the minimum is 0.36 for the March 10 case. Note that to compensate for the effect of a more rapid spread of the plume at short dispersion times, the origin in Figure 50 should be shifted up the ordinate scale. The computed power law constants, n, would then be slightly smaller.

The average lateral integral time scale computed from equation (5.2) and the observed data is about 130 seconds. However, because of the complications of multiple sources and the effects of wind shear on the vertical, the calculation of the integral time scales from (5.2) may not be valid. Although the curves on Figure 50 generally indicate an increasing time scale for more turbulent situations as expected, the increased slope and hence longer time scale for March 11 AM compared to March 10 is puzzling. A comparison with directly measured integral time scales would resolve the uncertainty and perhaps determine the other controlling parameters.

A similar analysis can be done for the vertical plume spread (see Figure 51). Some care is necessary in interpreting Figure 51. Taylor's theory is applicable only for homogeneous turbulence and is not applicable where there are limits to the vertical growth either in the form of elevated inversions or the surface. Referring to Table 21, we can see that most of the case studies are under meteorological conditions which limit the applicability of Taylor's theory. The effects of the initial plume interaction with the environmental air and the more rapid initial spread is more obvious in Figure 51 than in Figure 50. The actual shift of the effective origin up the ordinate is roughly the same but represents a much larger fraction of the vertical spread. The data for March 15 is associated with large experimental errors due to a very thin plume and very low turbulence levels. The March 12 data suggests a more rapid vertical spread than $T^{\frac{1}{2}}$; however this effect may be due to the presence of multiple plumes (see again the isopleths for the March 12 case). The other case studies are not inconsistent with a $T^{\frac{1}{2}}$ diffusion rate. However, a more complex expression with allowances for stable layers aloft is desirable.

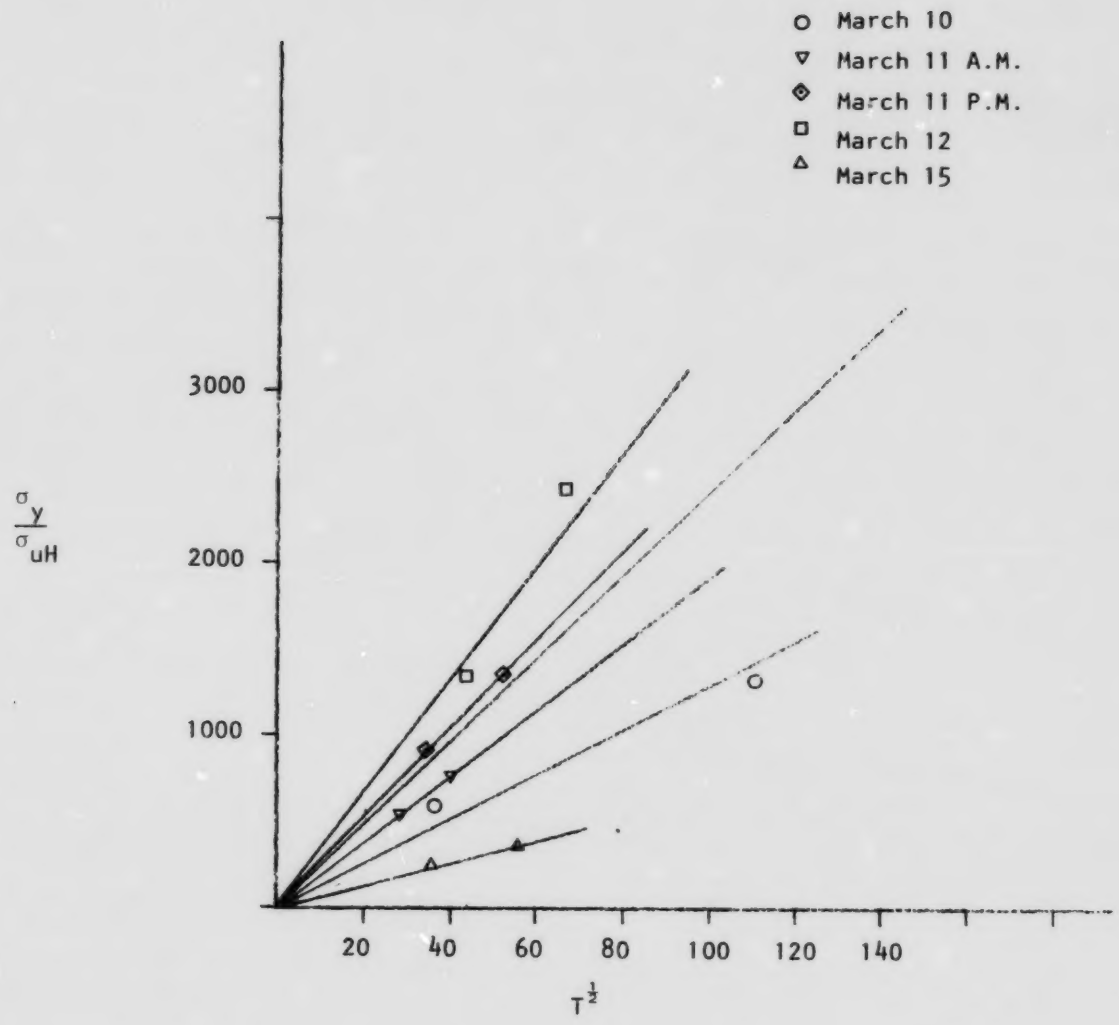

Figure 50. Horizontal plume spread versus the root of the dispersion time.

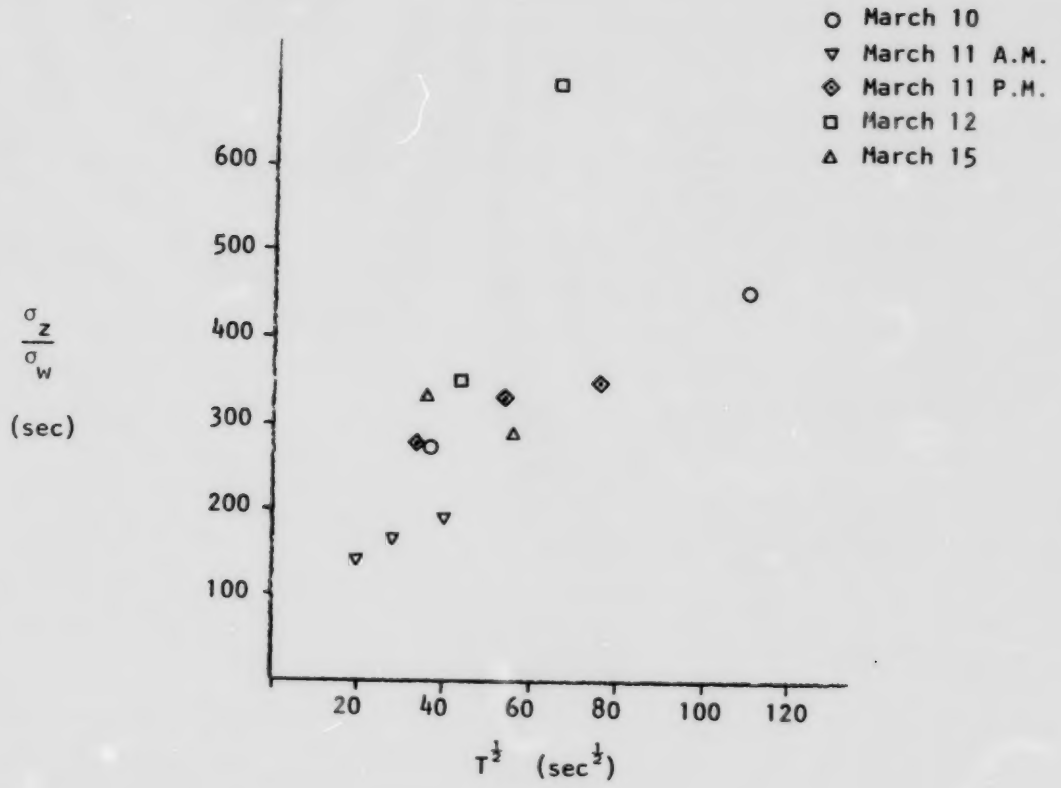

Figure 51. Vertical plume spread versus the root of dispersion time.

An approach to the problem of relating turbulence to observed plume sigma values has recently been developed by Draxler (1976). Draxler did not calculate or estimate integral time scales, t_L; rather he defined a time T_1 corresponding to the diffusion time required for f_1 to drop to 0.5. This approach forced all his data sets to cross at $f_1 = 0.5$ as well as at the origin: $f_1 = 1$ at $T = 0$. Draxler then determined the values of f_1 and f_2 using his values of T_1. Basically Draxler had an equation with two unmeasured quantities and he proceeded to arbitrarily define one of them. He determined an empirical relationship between σ_y and σ_v valid for his data set but not necessarily related to either Lagrangian integral time scales or Pasquill's universal functions, f_1 and f_2.

It is instructive to consider the form of the Lagrangian integral time scales from the known characteristics of turbulent spectra. Since the autocorrelation function and the power spectral density are Fourier transforms of one another, the extensive literature on spectral shapes can be utilized. If a spectral gap exists between the turbulence and the larger scale eddies, then the integral time scale is well defined. At a lag of $1/n_1$ seconds, the autocorrelation coefficient will be approximately equal to the integral from n_1 to the low frequency limit, n_2 normalized by the total area (see Figure 52). It is well known that the Eulerian spectral shape near the surface scales along the frequency axis according to $n\bar{z}/\bar{U}$, where $\bar{z}$ is height and $\bar{U}$ is the mean wind speed. For the Lagrangian spectral shape a scaling with $\bar{z}$ in the mixed boundary layer is expected. Hence in a mixed boundary layer, the Lagrangian integral time scale will certainly vary with height. Under stable conditions the small scale turbulence near the surface still scales along the frequency axis as $n\bar{z}/\bar{U}$ but the total area under the curves is greatly decreased due to a lack of low frequency contributions (see for example Kaimal et. al. (1972). Thus the Lagrangian integral time scale can be expected to vary both with height and stability. Attempts to develop relationships between the plume dispersion coefficients and turbulence levels should consider the variations of the integral time scales within the plume environment.

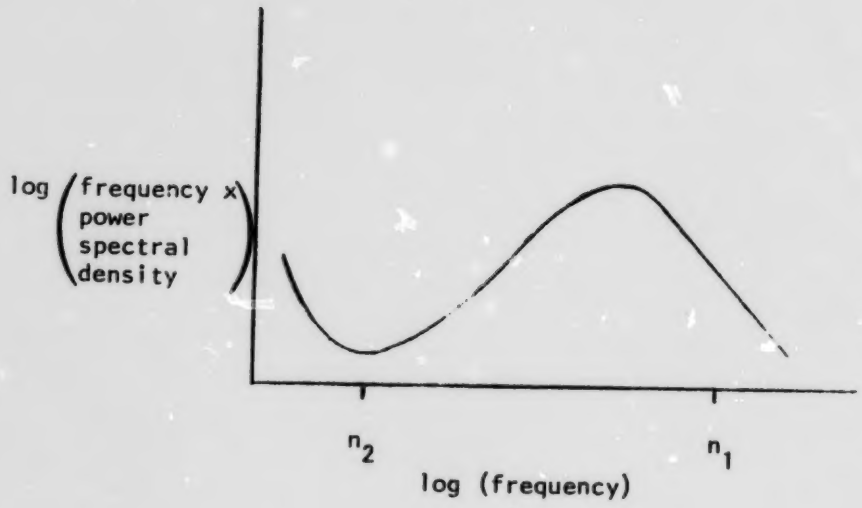

FIGURE 52 Schematic velocity spectral shape. Integration from n_1 to n_2 approximates the integral time scale.

5.5 A recommended procedure for relating turbulence and plume dispersion

There is a very promising approach to the problem of relating turbulence and plume dispersion, an approach which is possible using the type of data available from this study.

The main requirement is to be able to measure the integral time scale. Although the Lagrangian time scale is virtually impossible to measure at the Athabasca oil sands site, the Eulerian time scale could be measured and then related to the Lagrangian with confidence.

The turbulence data from the aircraft could provide the auto-correlations and spectral analysis could give confidence as to the reliability of the values and whether or not spectral gaps exist. Even if spectral gaps do not exist and the definition of the wind standard deviations becomes arbitrary, a low frequency cut-off could be set by the size scale which can influence the plume within about 10 km of the source.

With the measurement of the wind component standard deviations, the plume sigma values and the integral time scales as functions of height, the forms of Pasquill's universal functions could be determined.

There would still be the problems of differentiating laminar and fully turbulent contributions to the standard deviations of the wind components and of how to properly analyse cases in which the plume encounters very different stabilities with height or in which conditions are non-homogeneous or non-stationary. However the data set available would be more complete than any other large-scale diffusion studies at an industrial site.

6. CONCLUSIONS

The experimental design and the equipment used in this study were fully adequate to provide the data necessary for the accomplishment of the goals of the plume survey program. From the analysis and interpretation of the data, several specific conclusions can be made.

The observed values of the lateral plume dispersion coefficent, σ_y, were several times larger than the Pasquill-Gifford values largely due to the presence of multiple sources.

The observed values of the vertical plume dispersion coefficient, σ_z, were of similar magnitude to the Pasquill-Gifford values but increased more slowly with increasing downwind distance. This behavior was attributed to increasingly stable conditions aloft which are not accounted for in the predicted values.

The normalized center line concentrations, $\chi\bar{U}\ Q^{-1}$ were consistent with the σ_y and σ_z values; they were smaller than the Pasquill-Gifford values and decreased more slowly with increasing downwind distances.

The SO_2 mass flux could be calculated by transverse and then vertical integration of the SO_2 plume traverse data to a typical accuracy of 10 to 20%. There were two major sources of error: uncertainty of the appropriate wind speed whenever the tethersonde did not reach effective stack height, and lack of good vertical resolution by the stacked traverses.

The center line trajectory can be determined reasonably well from observer field notes and photographs.

The center line height is difficult to obtain reliably, unless there is good vertical resolution by the stacked traverses or else good photography conditions (usually only for stable conditions). On days in which there is a well mixed boundary layer, the vertical distance over which traverses are required is quite large. Thus only two downwind distances can usually be flown before stationarity problems develop.

The observed values of plume rise were compared with the values from the following formulations: Briggs, TVA (1972), Bosanquet et al and Holland. The ratios of observed to theoretical are consistent with those found in the literature. The Briggs model is best for low wind speeds especially in stable conditions. The TVA model is best for the moderate wind speed case.

A single stability class is seldom adequate to describe the boundary layers observed.

All of the case studies showed that the transverse plume spread σ_y / σ_{uH}, varied with $T^{\frac{1}{2}}$ where T is the dispersion time. This behaviour is predicted by Taylor's classical mixing theory for homogeneous turbulence. However the implied values of the Lagrangian integral time scales do not scale with stability as expected. Careful autocorrelation and spectral analysis is needed to obtain independent estimates of the time scales to resolve the problem.

The vertical plume spread σ_z / σ_w showed much scatter. Although much of the data was not inconsistent with a diffusion rate of $T^{\frac{1}{2}}$, a more complex formulation than Taylor's theory is clearly required.

As predicted by several theoretical studies, the averaging time required for stable turbulent estimates is quite large. Even though the aircraft provides about twenty times as much data as a stationary platform, turbulence runs in addition to the plume traverses are necessary.

Under neutral, mixed conditions and light-to-moderate winds from the west (the case study of March 11, 1976 (1250-1655)), there was little effect by the Athabasca River valley topography on the turbulent statistics at typical plume heights. The effects at lower levels and under other meteorological conditions is not yet known.

The results of this study were derived from the five case studies available from the March 1976 field study which met the meteorological and data quality criteria set out earlier. Although the results are considered accurate, they should not be interpreted as being representative of the whole range of meteorological conditions. These results are considered to be a late winter case, not a spring case.

7. RECOMMENDATIONS

Based upon the experience gained during the March 1976 field study and the results of the subsequent data analysis, specific recommendations are presented below. These are meant for consideration for possible future field programs.

7.1 POSITION RECOVERY

Accurate navigation using visual flight positioning is very difficult, particularly on the east side of the Athabasca River. It is recommended that position recovery instrumentation be used on subsequent field trips. Such a positioning system should be highly reliable without the need for frequent technical maintenance.

7.2 STATIONARITY PROBLEMS

The main plume from GCOS generally has a high effective stack height and so the vertical depth over which stacked traverses are required is large. It is recommended that in order to avoid significant changes in the plume structure, the number of downwind distance for the stacked traverses be kept to two. It is better to have increased vertical resolution than another downwind distance.

7.3 COORDINATION BETWEEN THE TETHERSONDE AND AIRCRAFT OPERATIONS

There is a need for better communication and coordination between the tethered balloon and aircraft operations. Specifically it is recommended that a tethersonde profile be made immediately before and after the aerial survey. During the actual survey the tethersonde should be kept at effective stack height as radioed to the tethersonde ground site by the airborne observors. Depending upon meteorological conditions additional tethersonde profiles might be advantageous.

It is recognized that the tethersonde may have other research objectives which may conflict with the above operational suggestions. If such is the case then better real-time communication is even more desirable.

7.4 AIRCRAFT OPERATIONAL BASE

It is recommended that the McMurray airport be used as the operational base for the aircraft for subsequent field programs. Although the Mildred Lake air strip is more convenient to AOSERP field camp, there

are operational requirements which make McMurray a much superior base. Whenever there is frost on the wings or control surfaces, this frost must be removed prior to take-off. This requirement could result in long delays for a plane that is left unhangered at Mildred Lake especially if wet snow has fallen and subsequently frozen.

Fuel is only available at McMurray and so the aircraft must fly to McMurray every day in any case. A heated hangar is of real value to enable preflight and post-flight instrumentation validation checks. The availability of an aircraft mechanic is a definite advantage to staying at McMurray. The above logistical and operational advantages are partially offset by increased costs and isolation from the rest of the investigators at the AOSERP field camp. However, in balance, it is recommended that the aircraft be stationed at McMurray except possibly during a warm-weather field trip. Major project review meetings could be held every second or third evening at the AOSERP camp. The airborne scientist could commute to these meetings by vehicle.

7.5 TIMING OF SUBSEQUENT FIELD TRIPS

An expanded data base is needed to ensure representative results. A careful review of the pollution climatology is necessary for the selection of the critical time periods but some comments now are appropriate. Field studies during very cold weather in mid-winter are feasible but there are serious operational problems which require a reasonable lead time for adequate preparation. It is suggested that mid-spring be considered a priority time since vegetation is no longer dormant and yet the sun angle is still low enough to generate extended limited-mixing cases.

7.6 RECOMMENDED APPLICATION OF THE DATA BANK

It is recommended that the objective of the plume dispersion field studies be to relate the observed dispersion to the turbulence structure and secondly to relate the observed turbulence to the mean meteorological conditions. Such a formulation should be the basis of a numerical simulation of the plume dispersion for the AOSERP study area. The observed dispersion cannot be well represented by simple Gaussian-type models.

8. LIST OF REFERENCES

Blom, J. and L. Wartena. 1969. The influence of changes in surface roughness on the development of the turbulent boundary layer in the lower layers of the atmosphere. J. of Atm. Sciences, 26: 255-265.

Briggs, G.A. 1969. Plume rise. AEC Critical Review Series,TID-25075.

————————. 1971. Some recent analyses of plume rise observations. Proc. Second Int. Clean Air Congress. Academic Press,1029-1032.

Davison, D.S. 1973. The structure of convection in the planetary boundary layer. PhD Thesis, University of British Columbia, 152p.

Donelan, M. and M. Miyake. 1973. Spectra and fluxes in the boundary layer of the trade wind zone. J. of Atm. Sciences, 30: 444-464.

Draxler, R.R. 1976. Determination of atmospheric diffusion parameters. Atm. Env., 10: 99-105.

Guldberg, P.H. 1975. A comparison study of plume rise formulas applied to tall stack data. J. Applied Met., 14: 1402-1405.

Kaimal, J.C., J.C.Wyngaard, Y.Izumi and O.R.Cote. 1972. Spectral characteristics of surface layer turbulence. Quart. J. Roy. Met. Soc., 98: 563-589.

McBean, G.A., and J.I.MacPherson. 1976. Turbulence above Lake Ontario: velocity and scalar statistics. Submitted for publication.

Montgomery, T.L., S.B.Carpenter, W.C.Colbaugh, and F.W.Thomas. 1972. Results of recent TVA investigations of plume rise. J. Air Pollution Control Assoc., 22: 779-784.

Moses, H., and M.R.Kraimer. 1972. Plume rise determination - a new technique without equations. J. Air Pollution Control Assoc. 22: 621-630.

Pasquill, F. 1971. Atmospheric dispersion of pollution. Quart. J. Roy. Met. Soc., 97: 369-395.

Slade, D.H., (ed). 1968. Meteorology and atomic energy 1968. U.S. Atomic Energy Commission, TID-24190.

Turner, B.D. 1969. Workbook of atmospheric dispersion estimates. U.S. Dept. of Health, Ed. and Welfare, Public Health Service Pub., 999-AP-26.

Wyngaard, J.C. 1973. On surface-layer turbulence. In D.A. Haugen(ed), Workshop on micrometeorology. Amer. Met. Soc., Science Press, Ephrata, Pa. 392p.

APPENDICES

SO_2 Traverses for March 10, 1976 (1415 - 1705)	119
SO_2 Traverses for March 11, 1976 (0750 - 1050)	137
SO_2 Traverses for March 11, 1976 (1250 - 1655)	150
SO_2 Traverses for March 12, 1976 (1420 - 1650)	167
SO_2 Traverses for March 15, 1976 (0740 - 0940)	182
Emission Characteristics from GCOS Plant	193
The Appropriate Gaussian Equation for Normalized Axial Centre Line Concentrations	194

APPENDIX 1 SO_2 TRAVERSES FOR MARCH 10 (1415-1705)

This appendix contains the normalized SO_2 traverses for the flight of March 10, 1976 (1415-1705). The run information table for this flight is reproduced for convenience in interpreting each traverse.

TABLE Run information for flight of March 10, 1976 (1415-1705)

RUN NUMBER	TIME (MST)	ALTITUDE (m-MSL) ±20	DOWNWIND DISTANCE (km) ±0.3	σ_y (m) ±100	MAX CONC. (ppm) ±0.02	INTEGRATED CONC. (ppm-m) ±50	FLIGHT DIR. (From-to)
1	1431 - 1435	1220	1.6	3350	0.06	210	W - E
2	1441 - 1448	1220	14.5	5640	0.11	700	E - W
3	1453 - 1457	760	1.6	3420	0.26	510	W - E
4	1500 - 1505	760	14.5	3710	0.11	610	E - W
5	1508 - 1512	910	1.6	790	0.60	1100	W - E
6	1516 - 1521	910	14.5	*	0.11	*	E - W
7	1525 - 1528	490	1.6	*	0.10	*	W - E
8	1533 - 1537	490	9.7	*	0.08	*	E - W
9	1540 - 1544	980	1.6	920	0.83	1440	W - E
10	1548 - 1553	980	14.5	2300	0.25	480	E - W
11	1555 - 1600	980	-	2030	0.32	890	SW-NE
12	1602 - 1606	980	1.6	1130	0.73	1300	E - W
13	1610 - 1616	910	6.4	4010	0.30	1130	W - E
14	1618 - 1622	760	6.4	3580	0.20	770	E - W
15	1624 - 1628	760	6.4	2840	0.27	840	W - E
16	1630 - 1633	460	6.4	*	0.27	*	E - W
17	1638 - 1644	760	-	T	T	T	N - S
18	1645 - 1651	760	-	T	T	T	S - N
19	1652 - 1658	760	-	T	T	T	N - S

- flight not perpendicular to plume (i.e. not crosswind)
* imcomplete sectioning of plume so that reliable values not available
T turbulence run

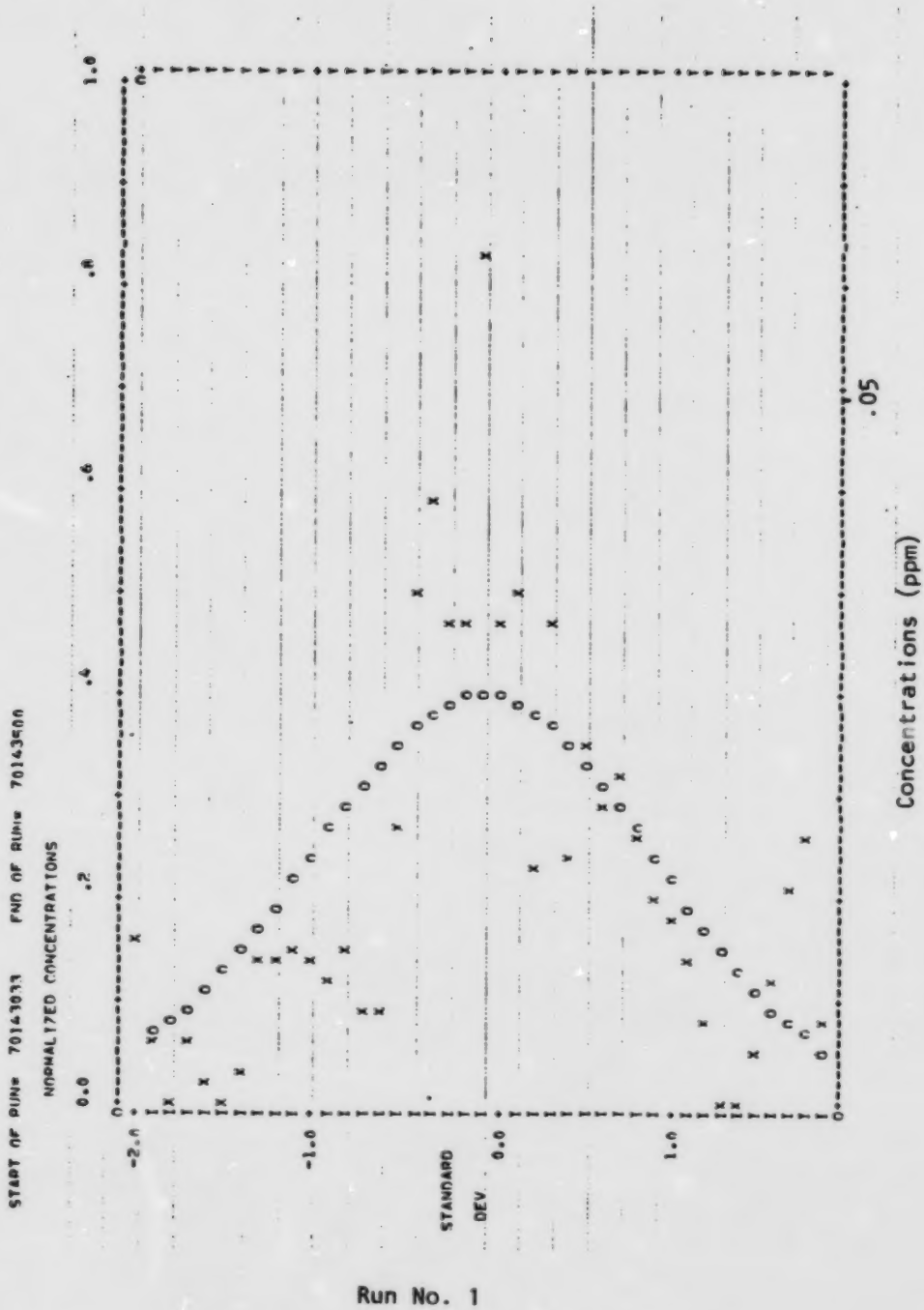
START OF RUN= 70143033 END OF RUN= 70143500
NORMALIZED CONCENTRATIONS
0.0
.2
.4
.6
.8
1.0
-2.0
-1.0
STANDARD
DEV
0.0
1.0
.05
Concentrations (ppm)

Run No. 1

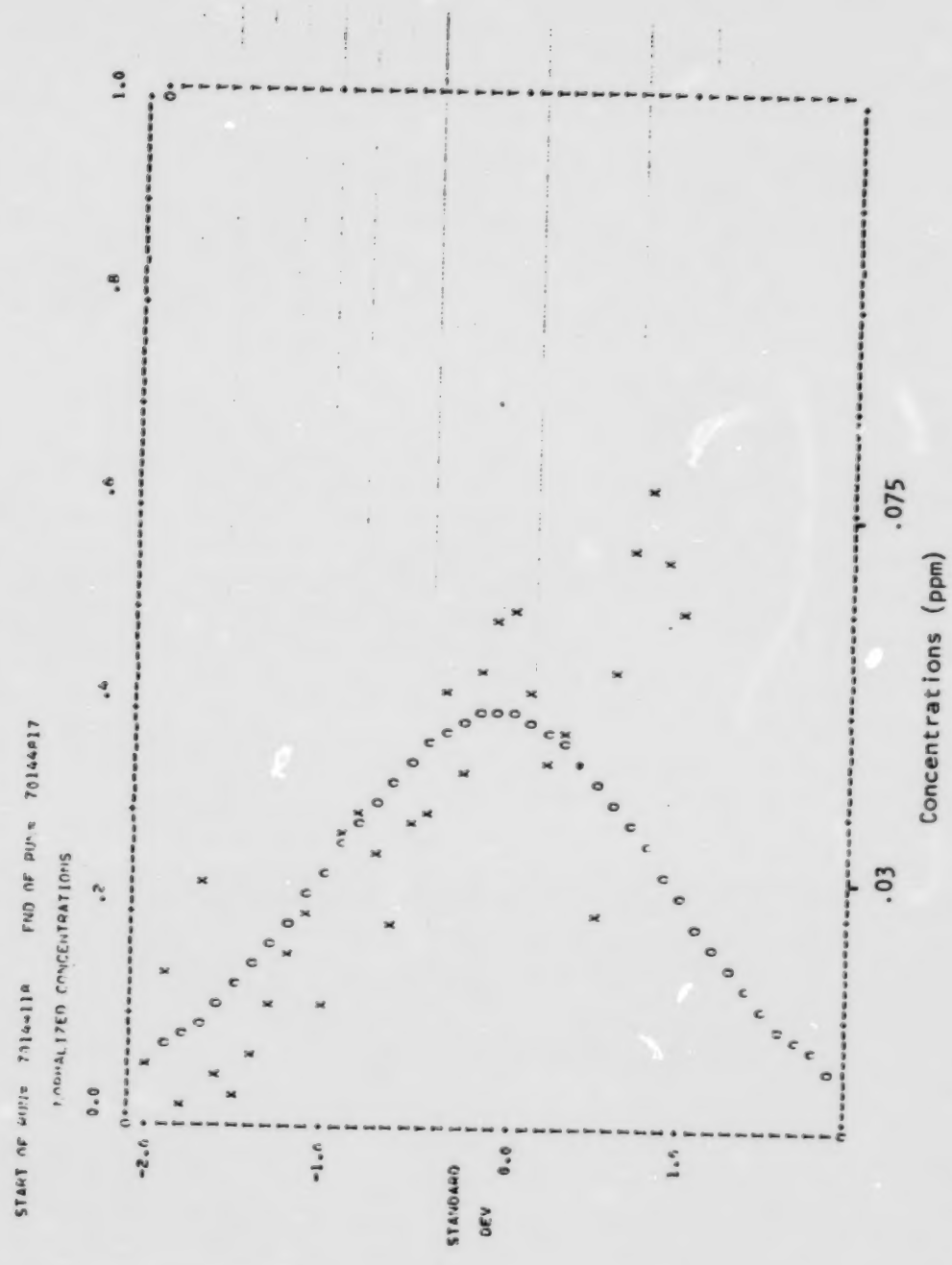
START OF RUN: 70144118 END OF RUN: 70144817
NORMALIZED CONCENTRATIONS
0.0
.2
.4
.6
.8
1.0
-2.0
-1.0
STANDARD DEV
0.0
1.0
.03
.075
Concentrations (ppm)

Run No. 2

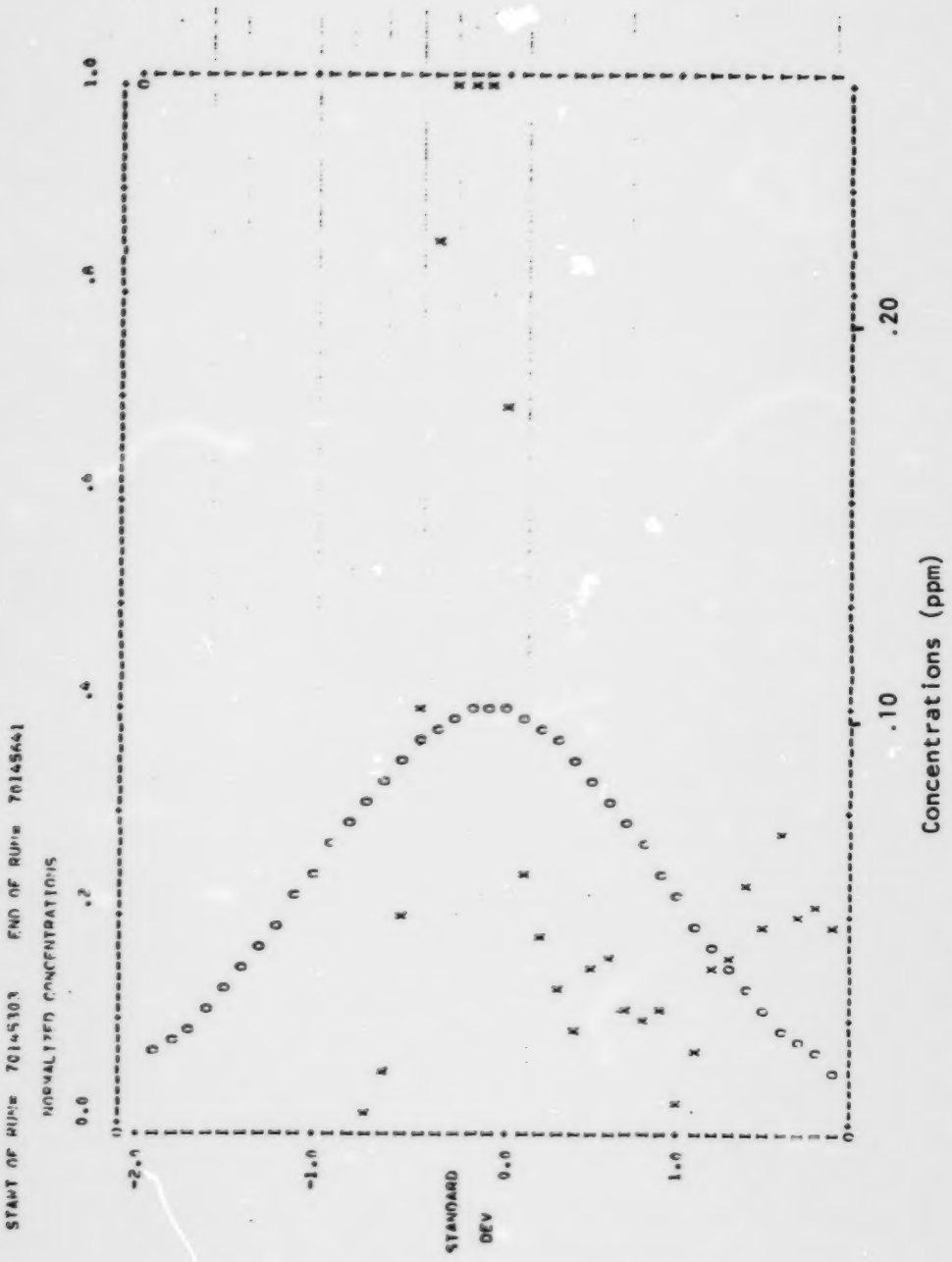
START OF RUN= 70145303 END OF RUN= 70145641
NORMALIZED CONCENTRATIONS
0.0
.2
.4
.6
.8
1.0
-2.0
-1.0
0.0
1.0
STANDARD DEV
.10
.20
Concentrations (ppm)

Run No. 3

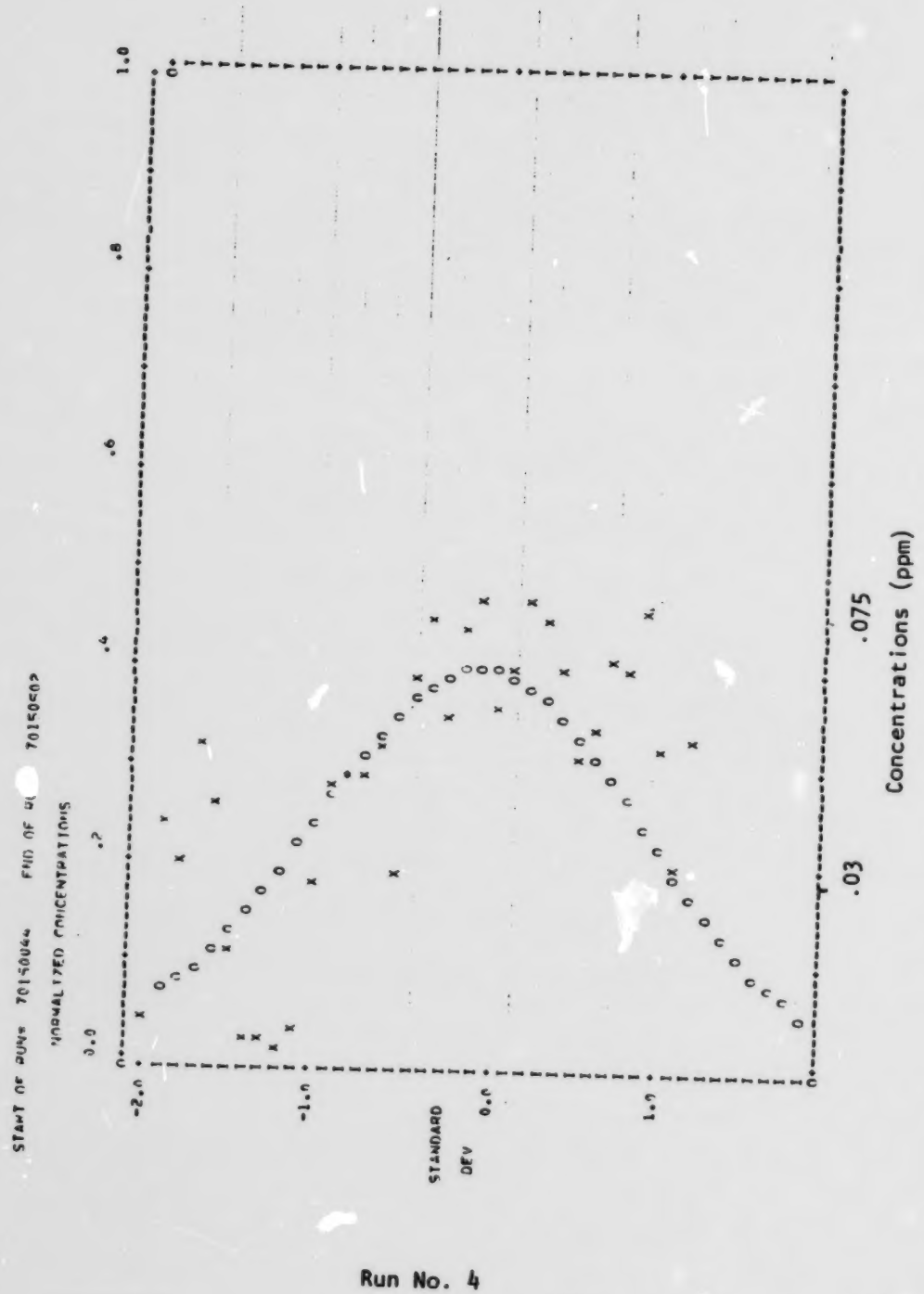
START OF RUN= 70150044 END OF RU 70150603
NORMALIZED CONCENTRATIONS
0.0
.2
.4
.6
.8
1.0
-2.0
-1.0
0.0
1.0
STANDARD DEV
.03
.075
Concentrations (ppm)

Run No. 4

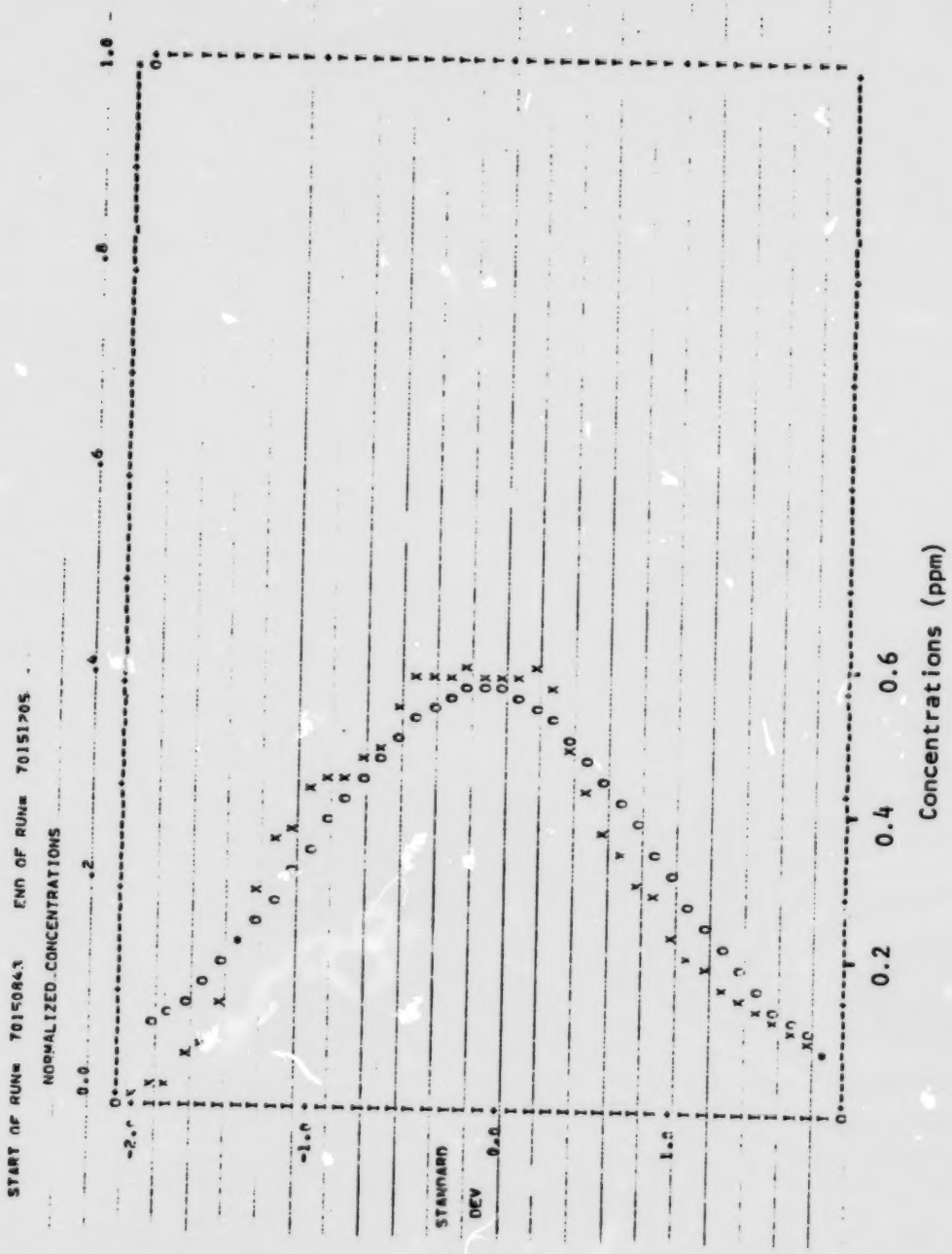
START OF RUN= 70150843 END OF RUN= 70151705
NORMALIZED CONCENTRATIONS
STANDARD DEV 0.0
0.2
0.4
0.6
Concentrations (ppm)

Run No. 5

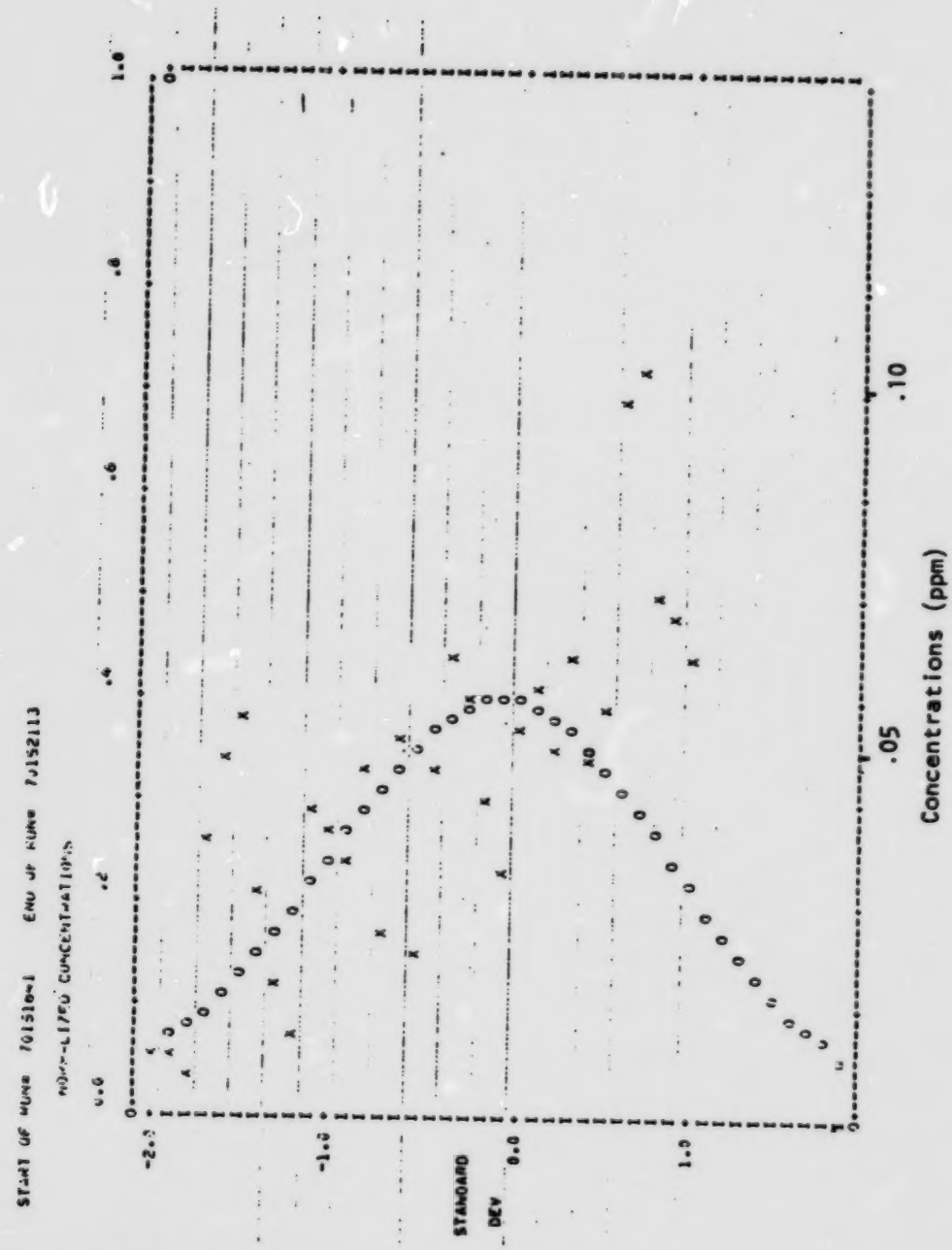
START OF RUNS 7015104 END OF RUNS 7015211
NON-LIFED CONCENTRATIONS
0.0
.2
.4
.6
.8
1.0
-2.0
-1.0
0.0
1.0
STANDARD DEV
.05
.10
Concentrations (ppm)

Run No. 6

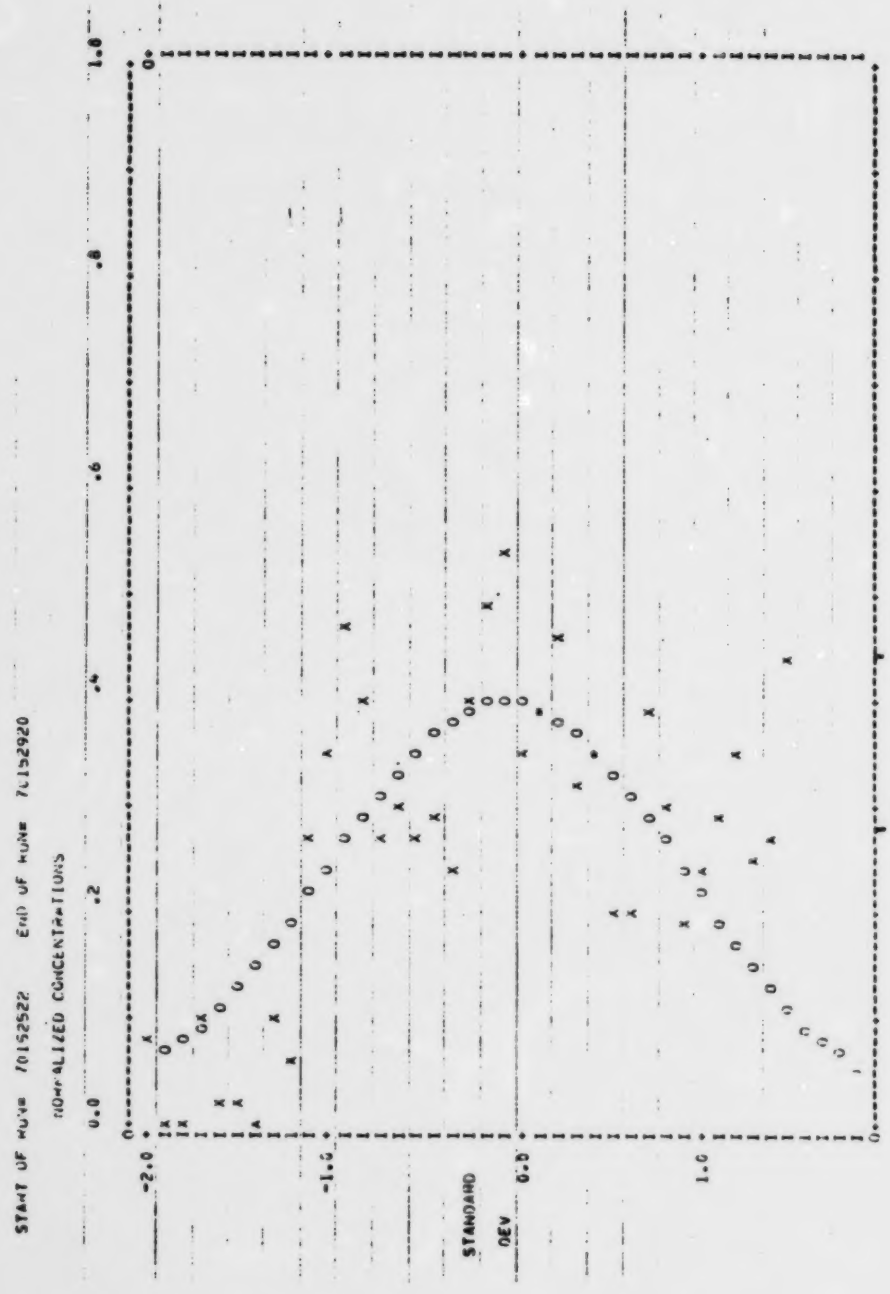
START OF RUN= 70152522 END OF RUN= 70152920
NORMALIZED CONCENTRATIONS
0.0
.2
.4
.6
.8
1.0
-2.0
-1.0
STANDARD
DEV 0.0
1.0
.05
.075
Concentrations (ppm)

Run No. 7

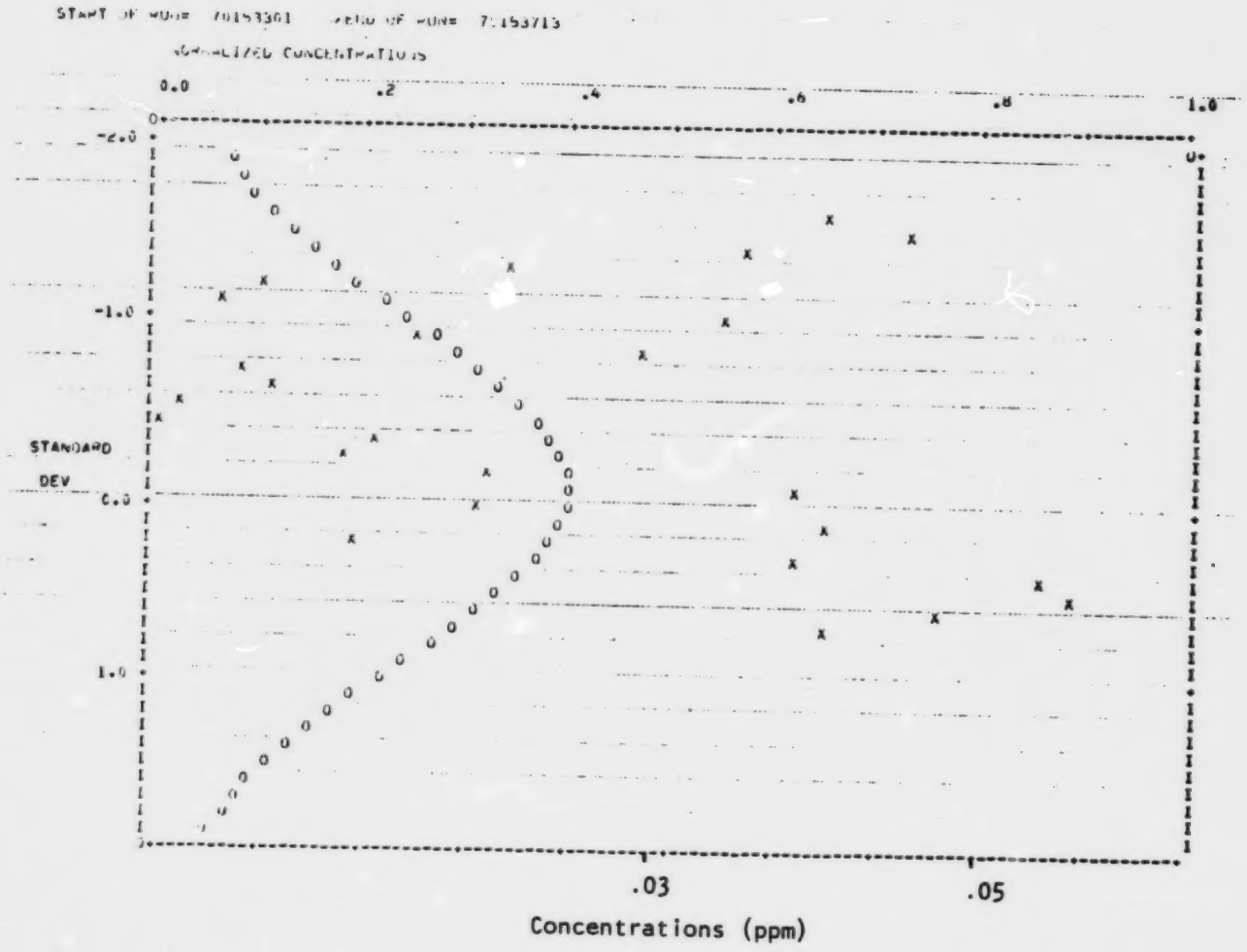
START OF RUN= 7:153301
END OF RUN= 7:153713
NORMALIZED CONCENTRATIONS
0.0
.2
.4
.6
.8
1.0
-2.0
-1.0
0.0
1.0
STANDARD
DEV
.03
.05
Concentrations (ppm)

Run No. 8

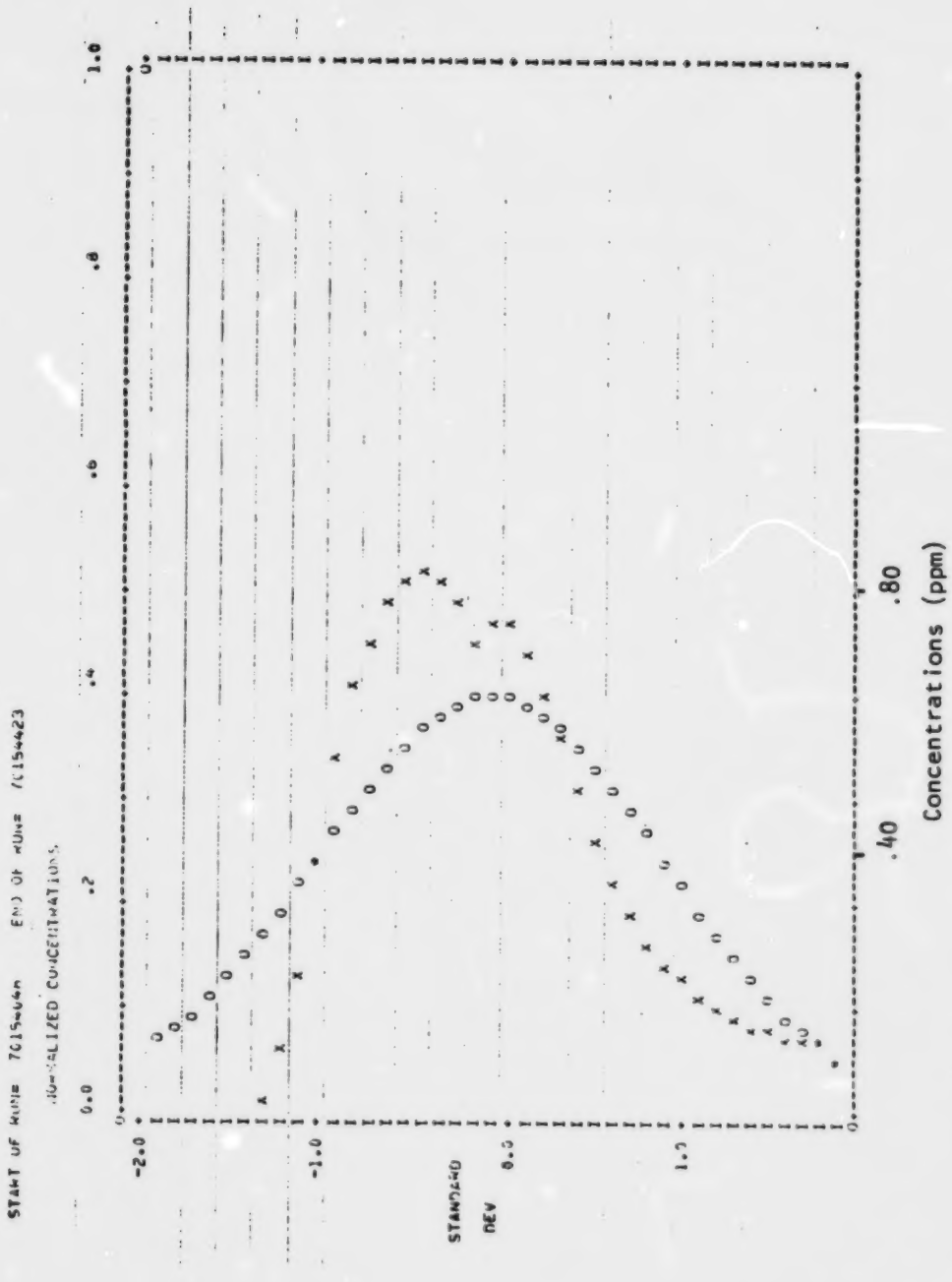
START OF RUN: 761540N END OF RUN: 761544Z3
NORMALIZED CONCENTRATIONS
0.0
.2
.4
.6
.8
1.0
-2.0
-1.0
STANDARD DEV
0.0
1.0
.40
.80
Concentrations (ppm)

Run No. 9

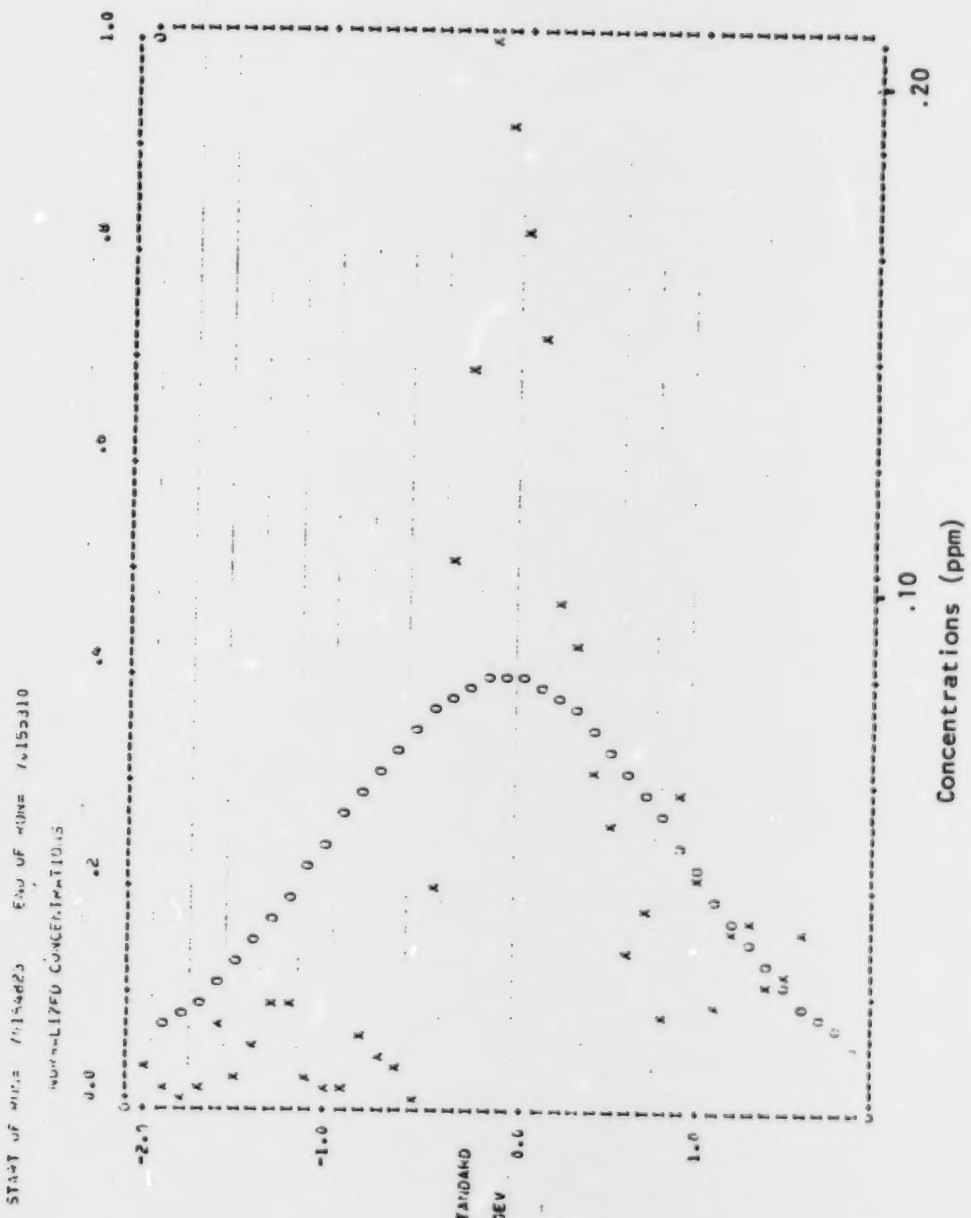

Run No. 10

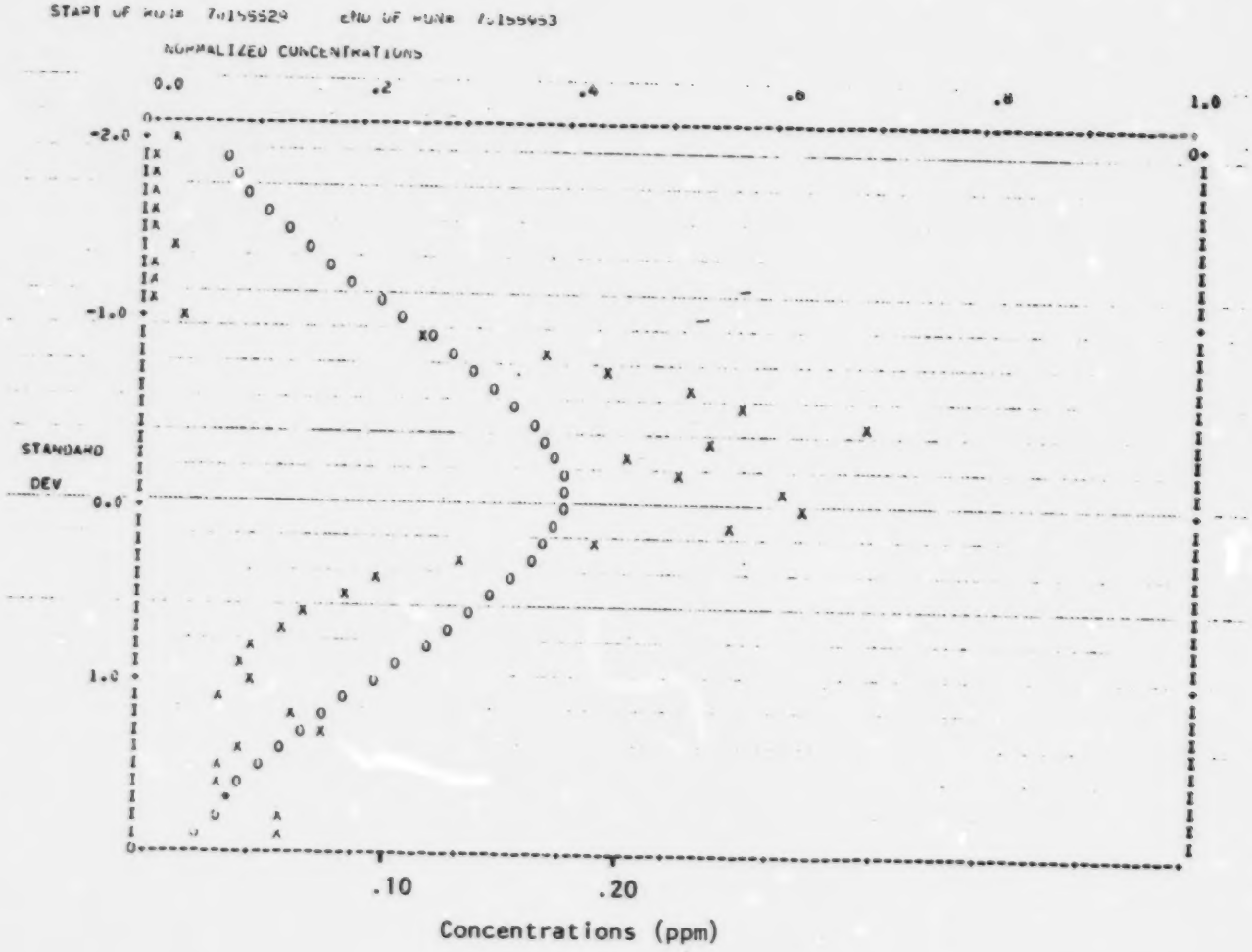
START OF RUN 7d155529
END OF RUN 7d155953
NORMALIZED CONCENTRATIONS
0.0
.2
.4
.6
.8
1.0
-2.0
-1.0
STANDARD
DEV
0.0
1.0
.10
.20
Concentrations (ppm)

Run No. 11

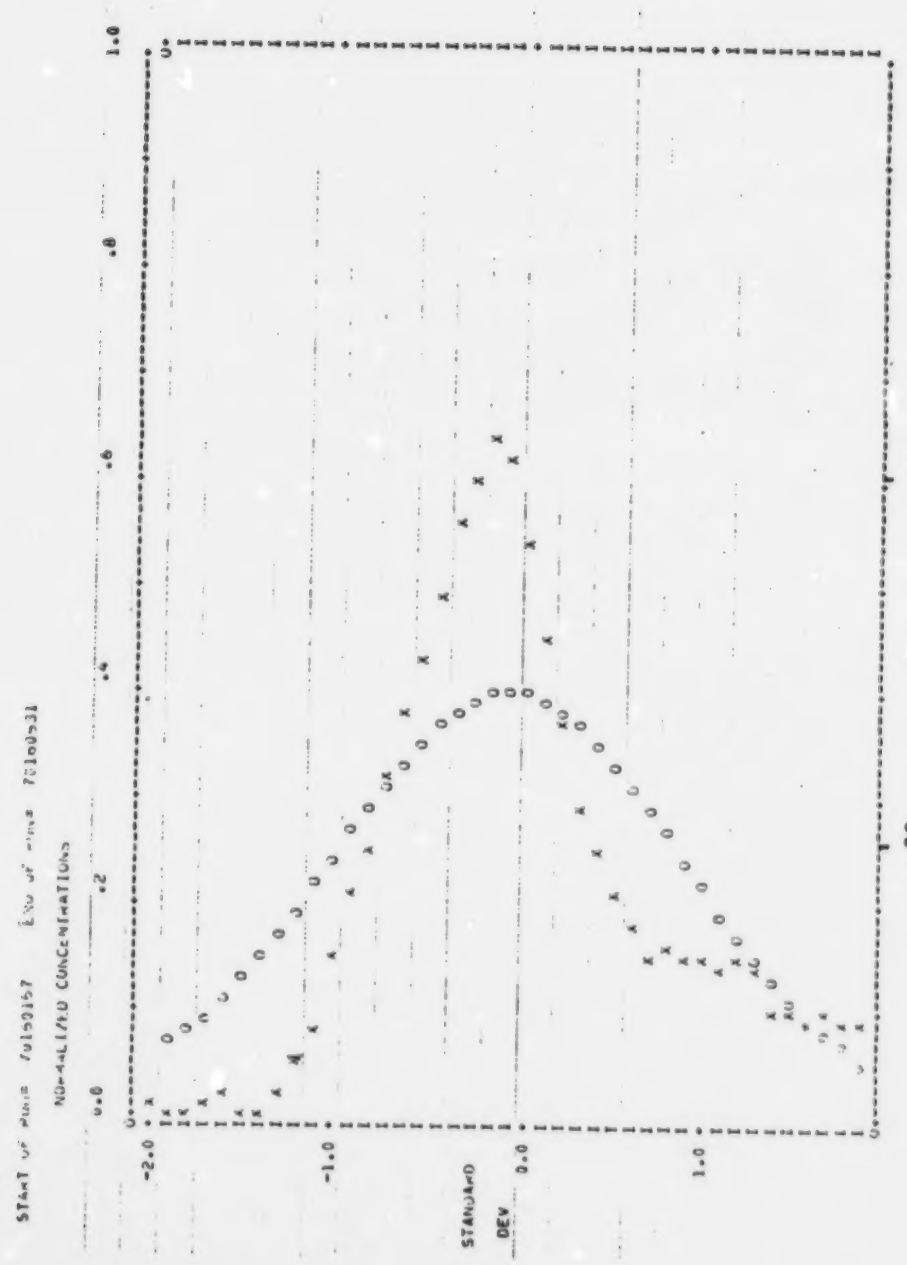
NORMALIZED CONCENTRATIONS
1.0
.8
.6
.4
.2
0.0
-2.0
-1.0
1.0
STANDARD
DEV
0.0
.30
.70
Concentrations (ppm)

Run No. 12

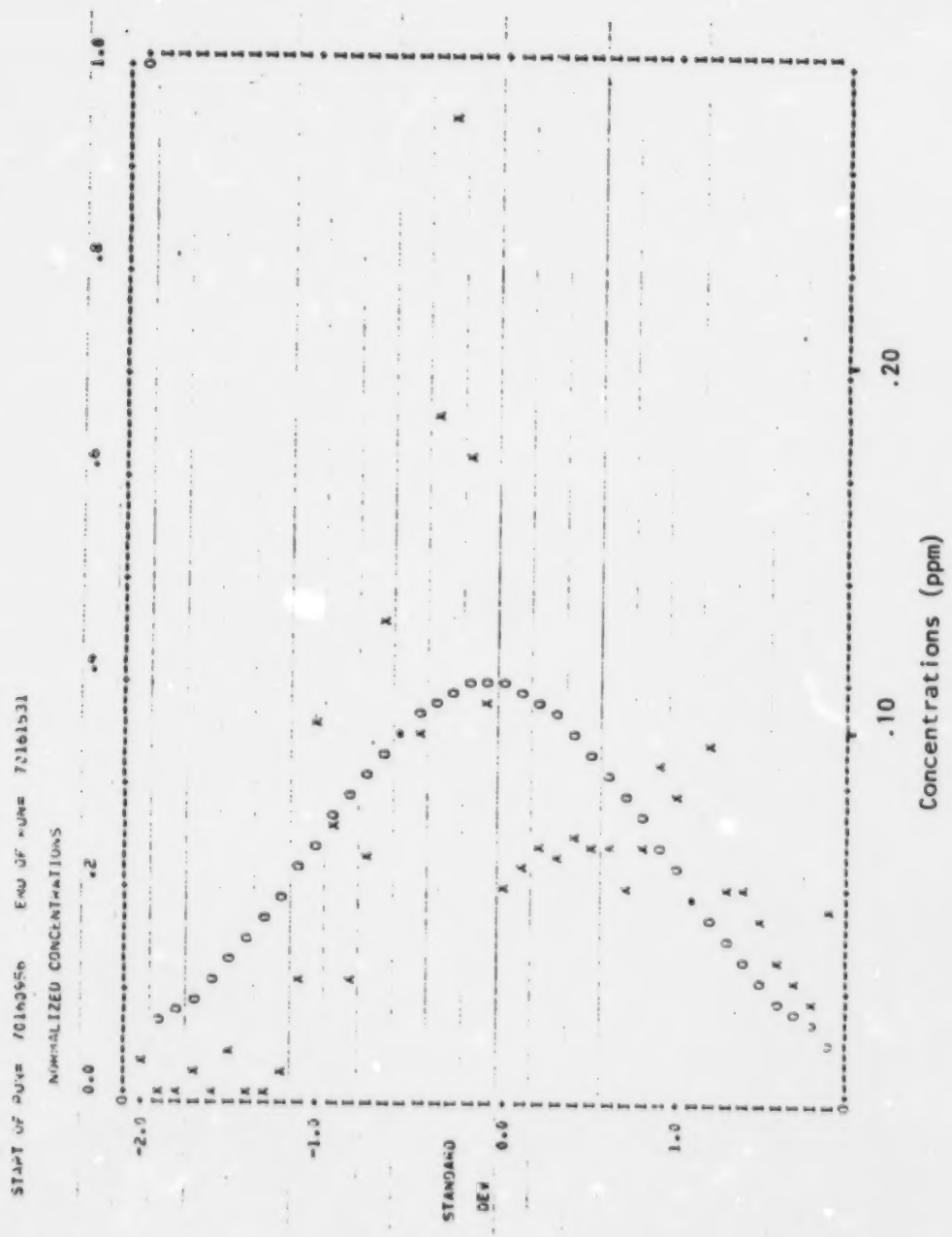
START OF RUN= 7010956 END OF RUN= 7016131
NORMALIZED CONCENTRATIONS
0.0
.2
.4
.6
.8
1.0
-2.0
-1.0
1.0
STANDARD
DEV 0.0
.10
.20
Concentrations (ppm)

Run No. 13

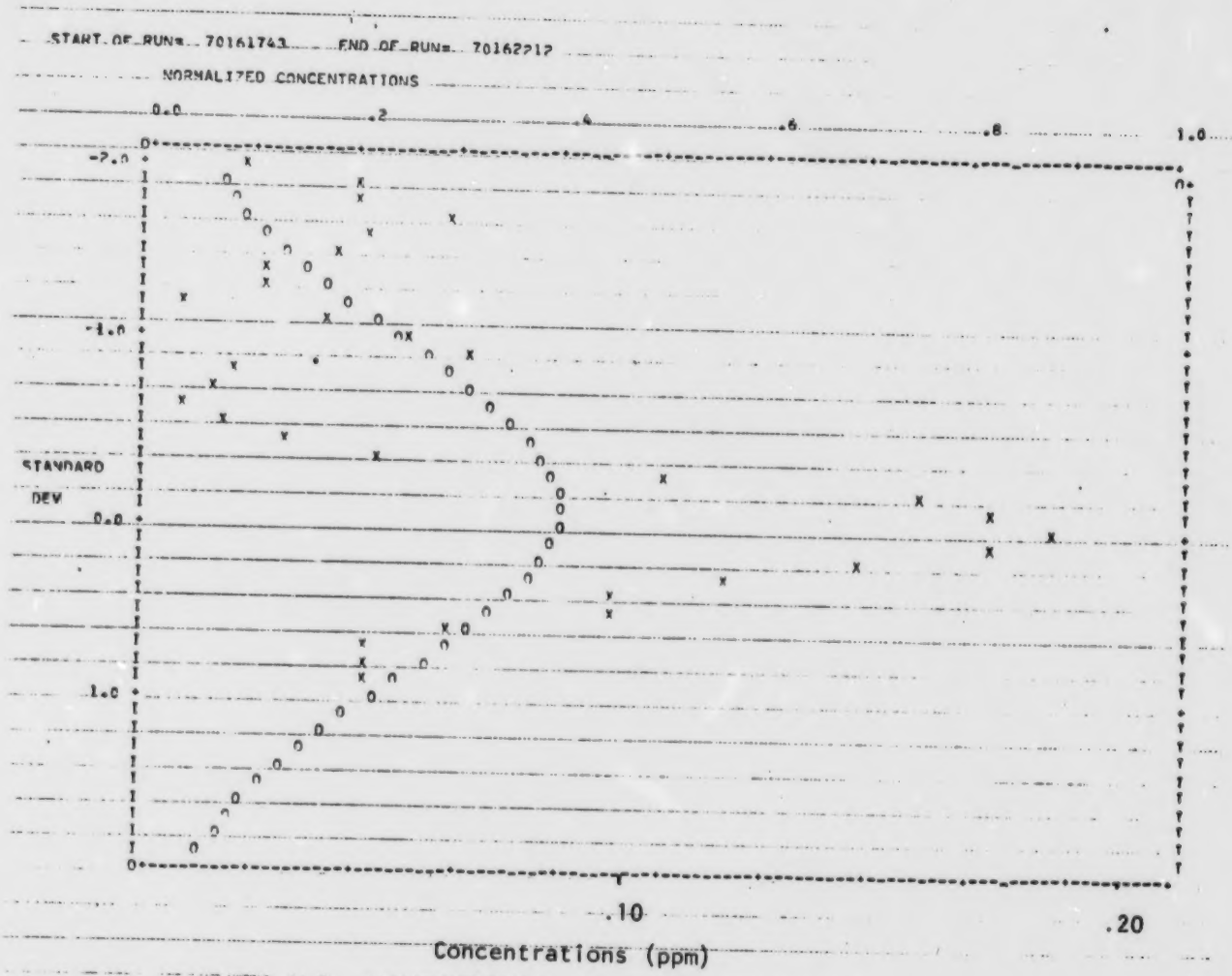
START OF RUN= 70161743 END OF RUN= 70162217
NORMALIZED CONCENTRATIONS
0.0
.2
.4
.6
.8
1.0
-2.0
-1.0
STANDARD
DEV
0.0
1.0
.10
.20
Concentrations (ppm)

Run No. 14

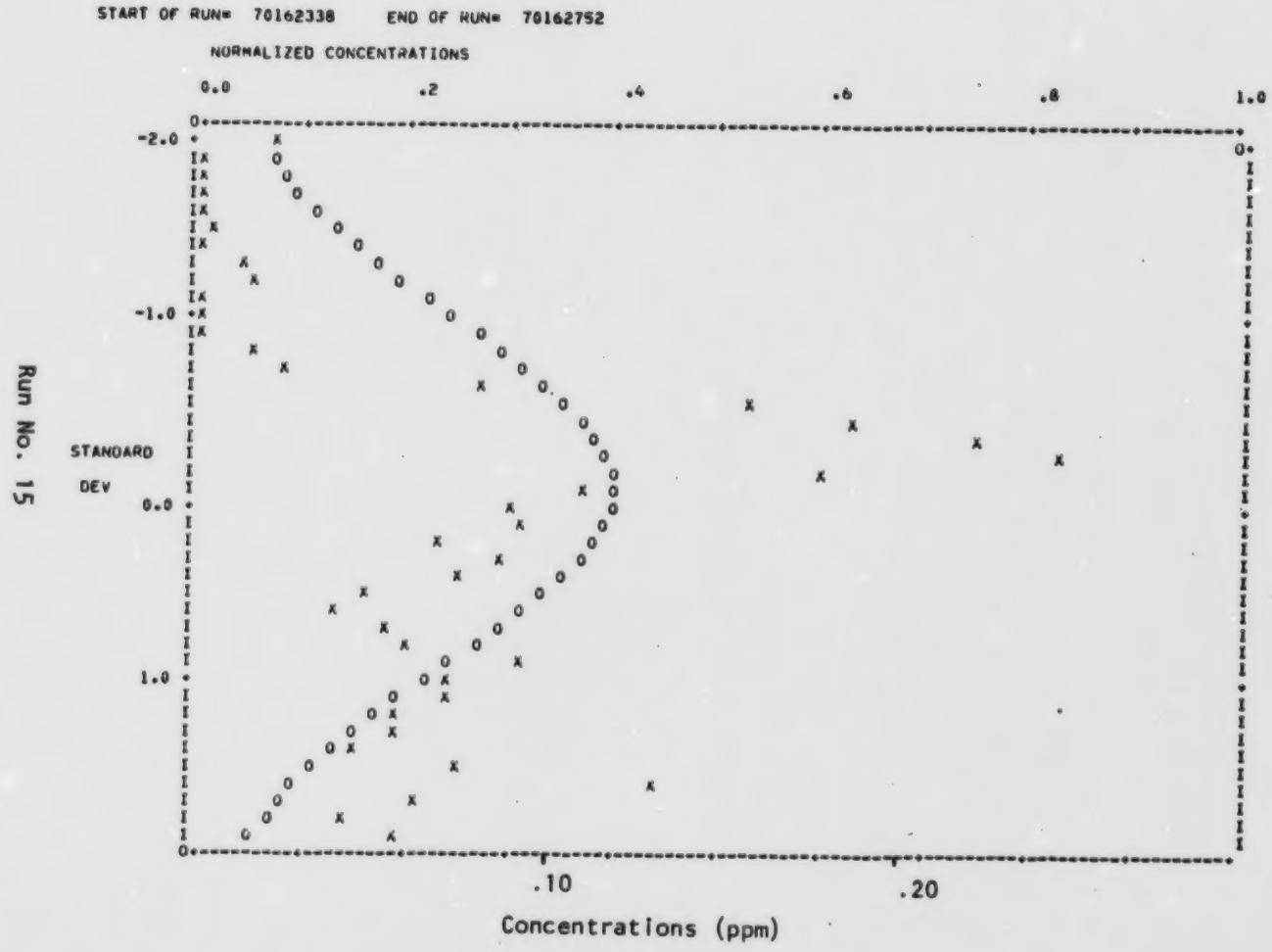
START OF RUN= 70162338 END OF RUN= 70162752
NORMALIZED CONCENTRATIONS
0.0
.2
.4
.6
.8
1.0
-2.0
-1.0
0.0
1.0
STANDARD
DEV
.10
.20
Concentrations (ppm)
Run No. 15

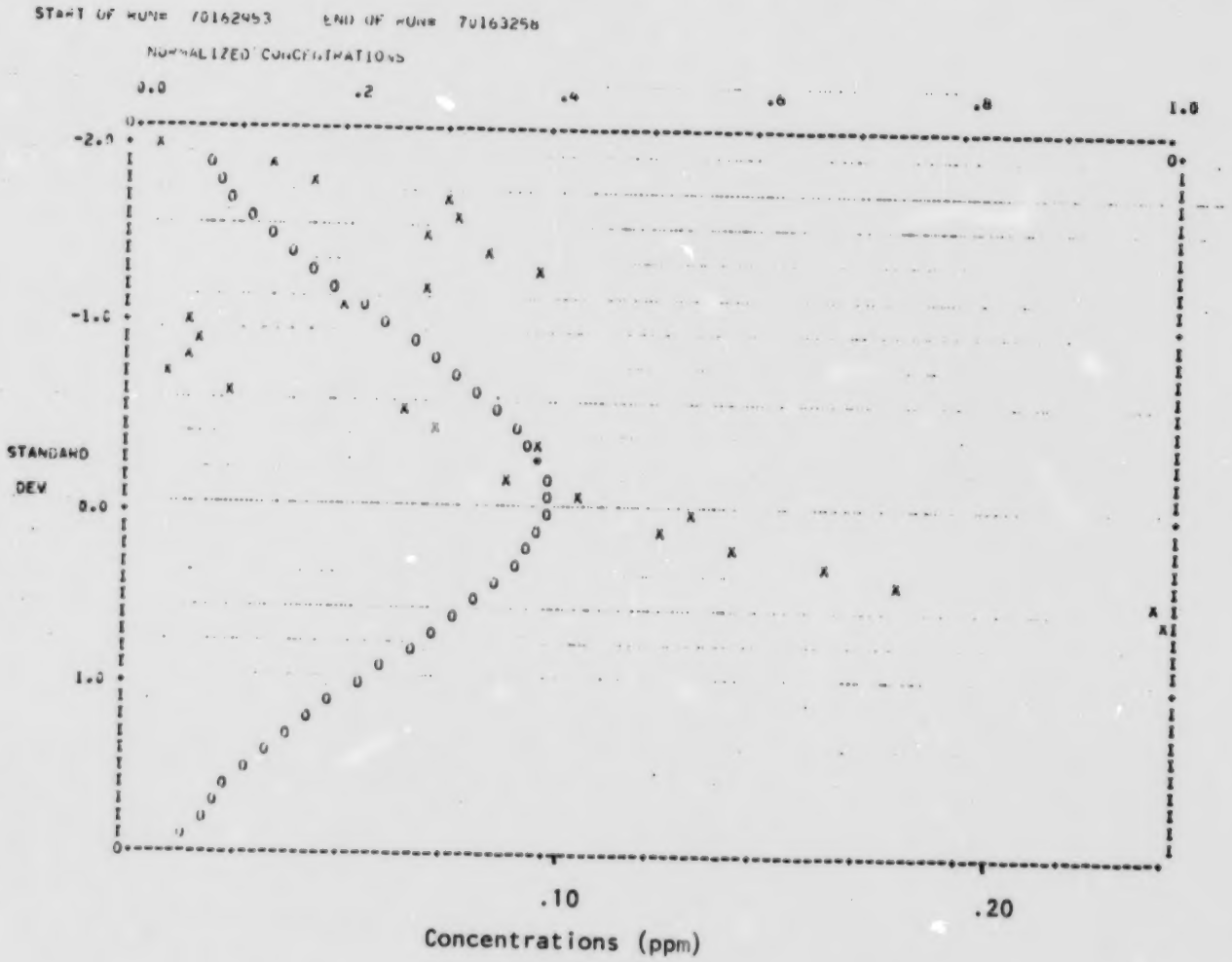
START OF RUN= 70162453 END OF RUN= 70163258
NORMALIZED CONCENTRATIONS
0.0
.2
.4
.6
.8
1.0
-2.0
-1.0
0.0
1.0
STANDARD
DEV
.10
.20
Concentrations (ppm)

Run No. 16

APPENDIX 2 SO_2 TRAVERSES FOR MARCH 11, 1976 AM (0750-1050)

This appendix contains the normalized SO_2 traverses for the flight of March 11 AM, 1976 (0750-1050). The run information table for this flight is reproduced for convenience in interpreting each traverse.

TABLE Run information for flight of March 11, 1976 (0750-1050)

RUN NUMBER	TIME (MST)	ALTITUDE (m-MSL) ±20	DOWNWIND DISTANCE (km) ±0.3	σ_y (m) ±100	MAX CONC. (ppm) ±0.02	INTEGRATED CONC. (ppm-m) ±50	FLIGHT DIR. (From-to)
1	0817 - 0819	610	1.6	2310	0.220	333	S - N
2.	0821 - 0824	610	6.4	1175	0.418	714	N - S
3	0828 - 0832	910	1.6	2859 *	0.093 *	473 *	S - N
4	0834 - 0836	880	6.4	1686	0.058	127 +	N - S
5	0810 - 0843	460	1.6	1147	0.632	962	S - N
6	0845 - 0848	460	6.4	3283	0.082	280 +	N - S
7	0851 - 0854	670	1.6	3927	0.044	202	S - N
8	0858 - 0902	670	6.4	1639	0.403	868	N - S
9	0904 - 0907	670	3.2	1421	0.359	511	S - N
10	0910 - 0912	460	3.2	2110	0.218	434	N - S
11	0915 - 0918	610	3.2	892	1.069	1502	S - N
12	0924 - 0928	610	-	2006	0.469	1463	NW-SE
13	0931 - 0946	610	8.0	T	T	T	S - N
14	0948 - 1002	610	8.0	T	T	T	N - S
15	1007 - 1020	1220	8.0	T	T	T	S - N
16	1022 - 1034	1220	8.0	T	T	T	N - S

T Turbulence run
- Plume was traversed at an angle for an orientation check
* Incomplete traverse resulting in unreliable values for plume sigma and concentration values
+ Small part of plume was missed, so that integrated concentration values were increased by 10%

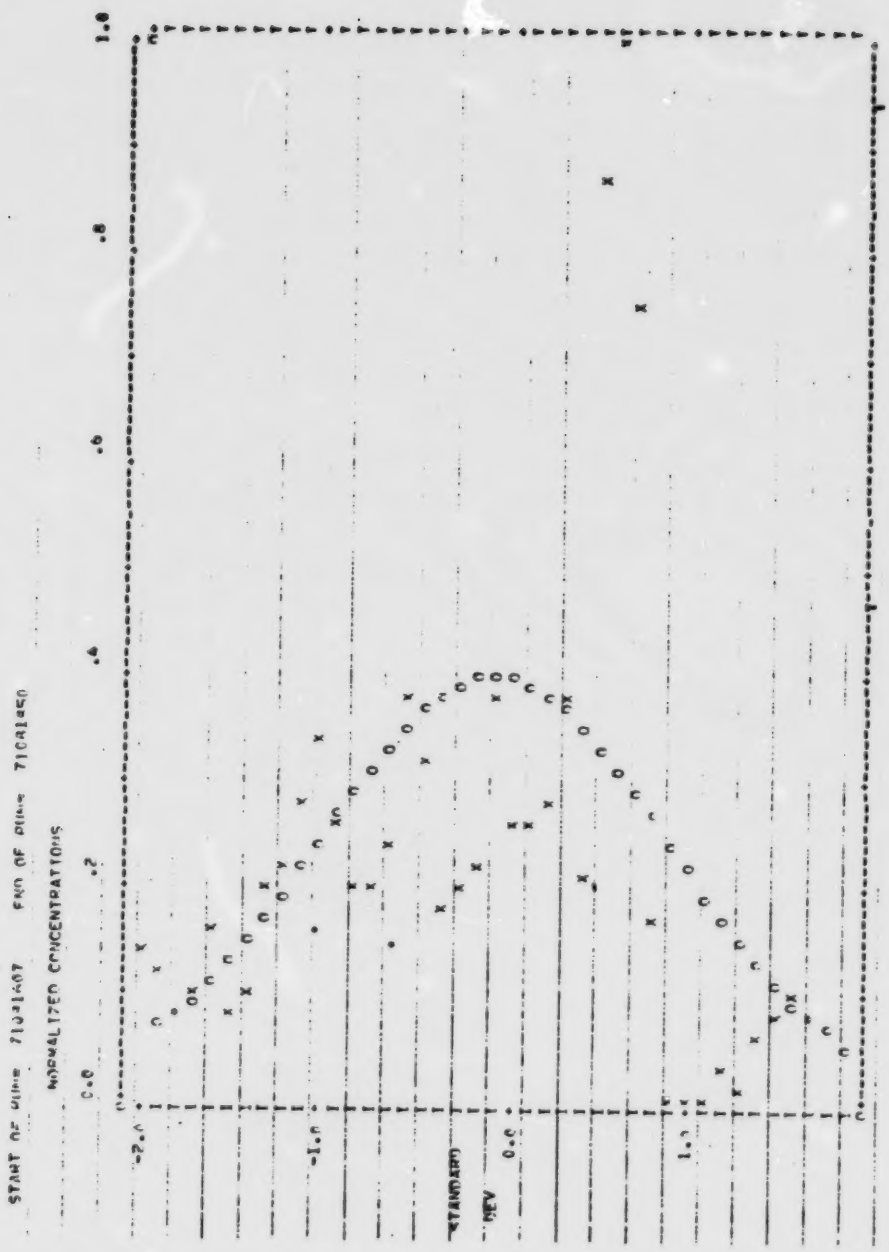
START OF RUN 71031607 END OF RUN 71031650
NORMALIZED CONCENTRATIONS
0.0
.2
.4
.6
.8
1.0
-2.0
-1.0
STANDARD
DEV
0.0
1.0
0.1
0.2
Concentrations (ppm)

Run No. 1

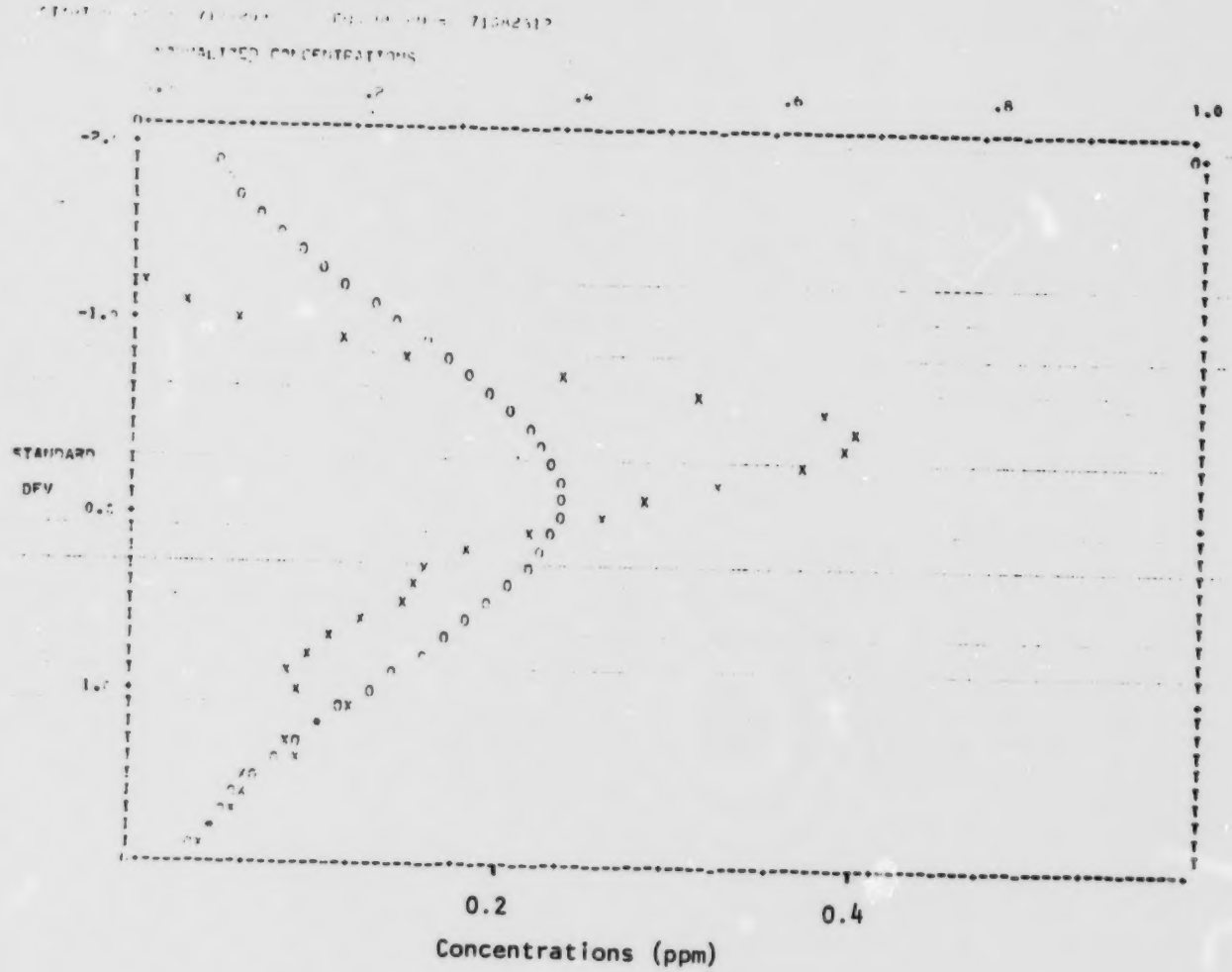

Run No. 2

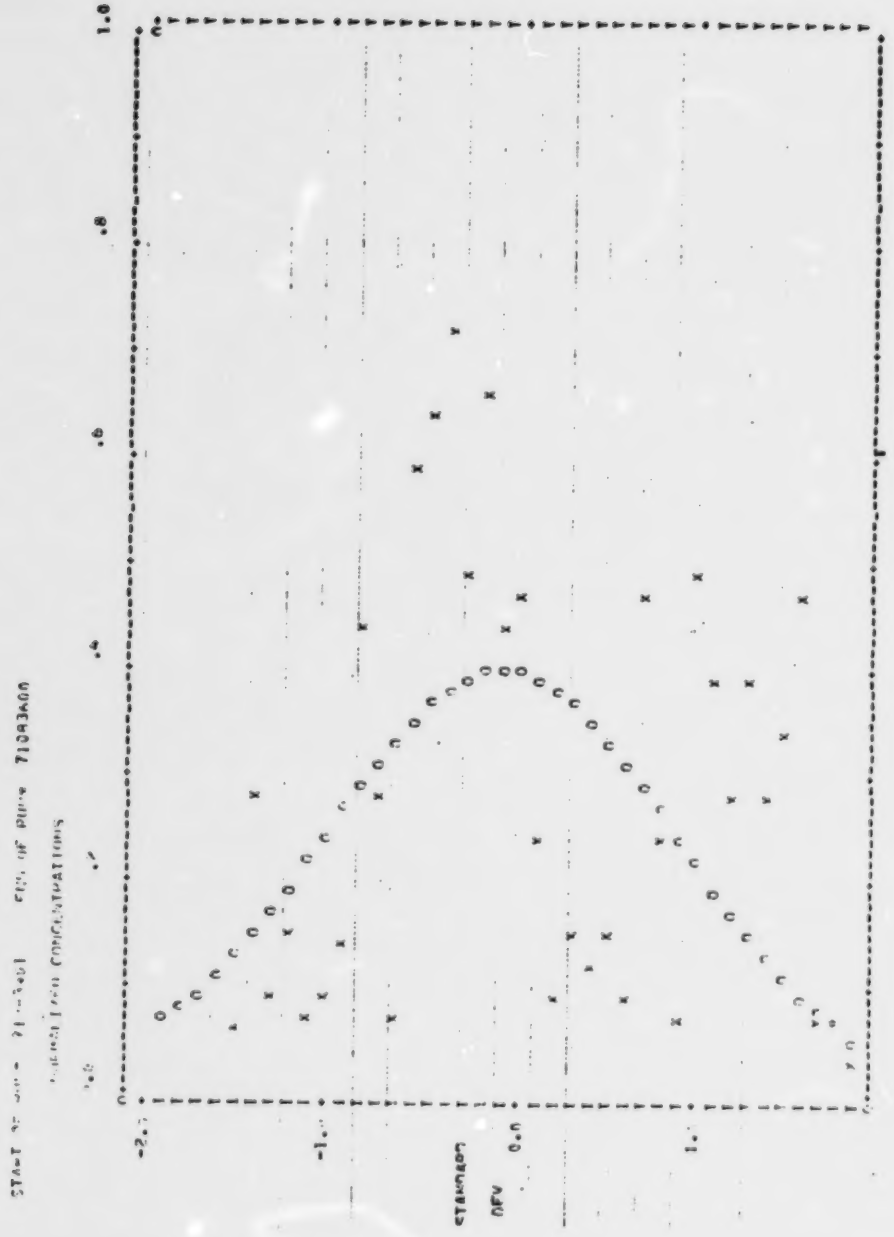

Run No. 4

Run No. 5

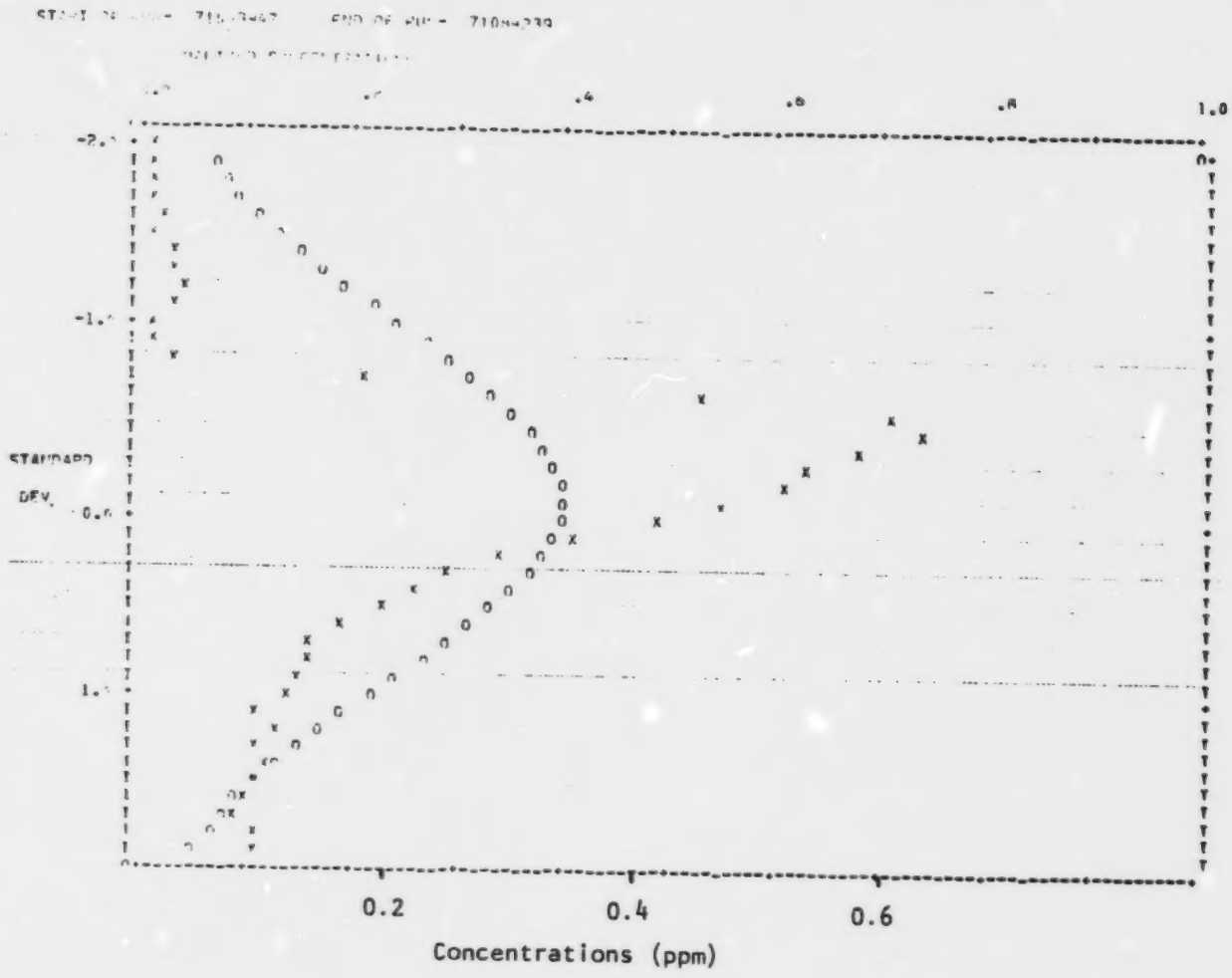

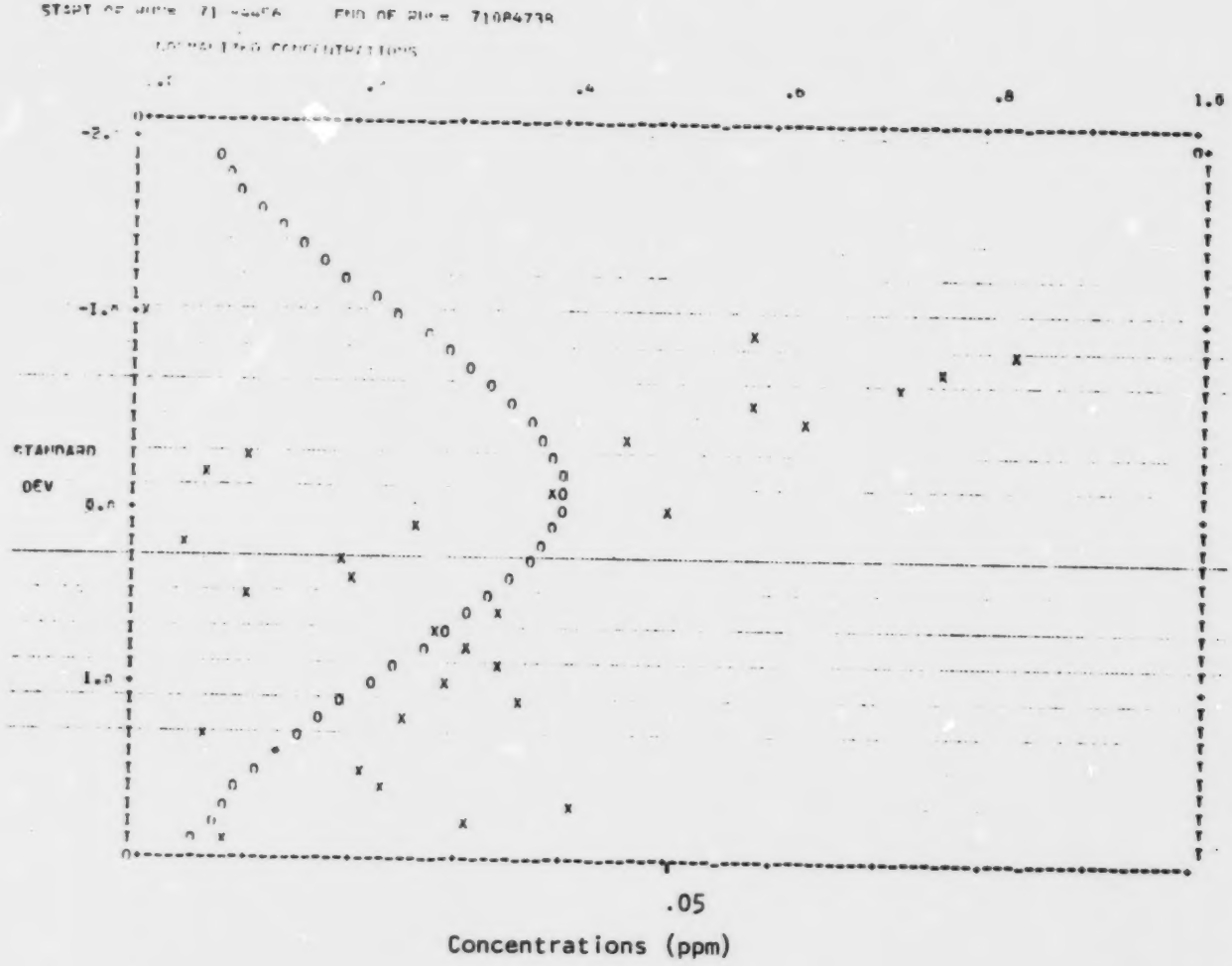
END OF RUN = 71084738
.4
.6
.8
1.0
-2.
-1.
STANDARD
DEV
0.0
1.0
.05
Concentrations (ppm)

Run No. 6

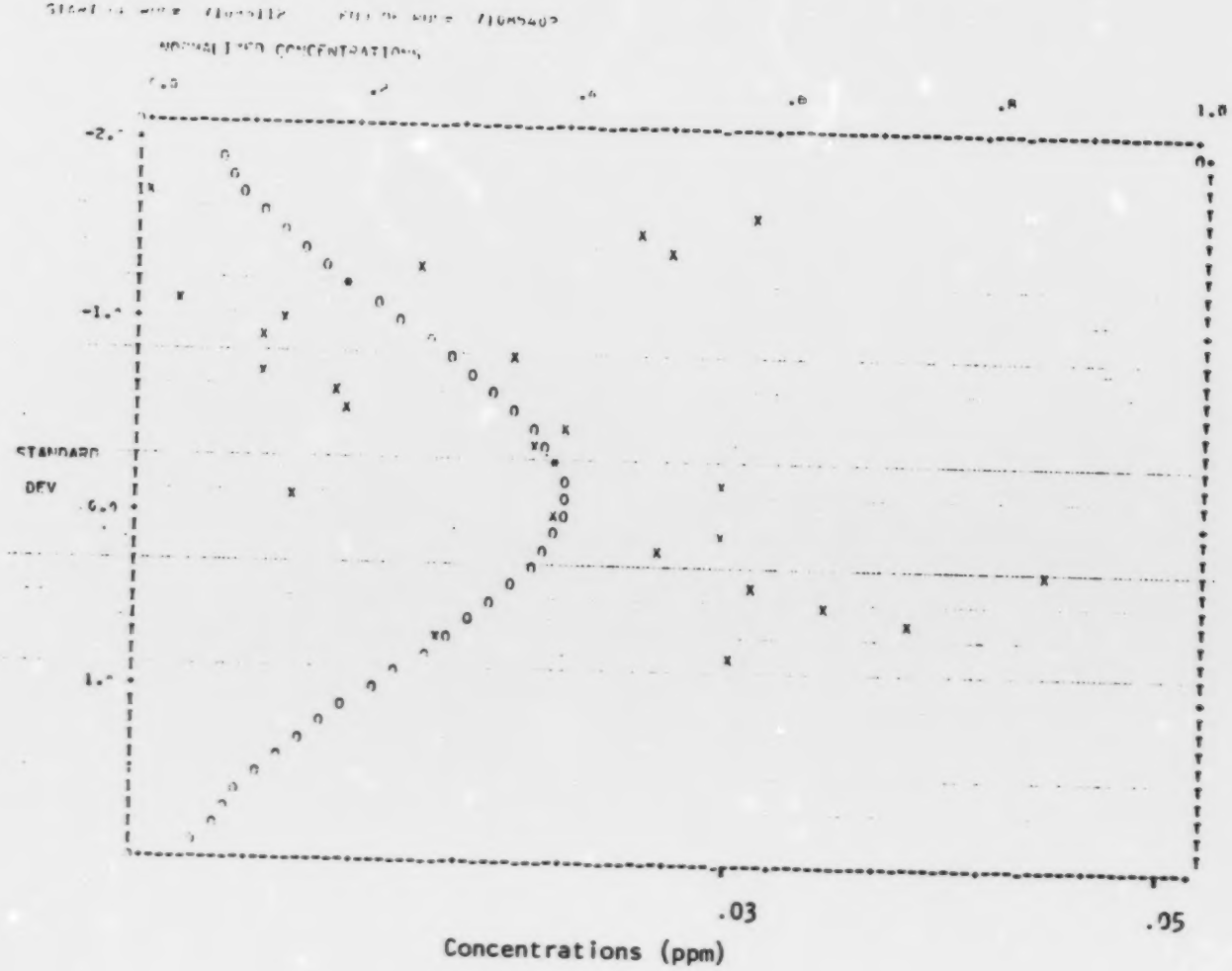
NORMALIZED CONCENTRATIONS
1.0
-2.
-1.
STANDARD
DEV
0.0
1.
.03
.05
Concentrations (ppm)

Run No. 7

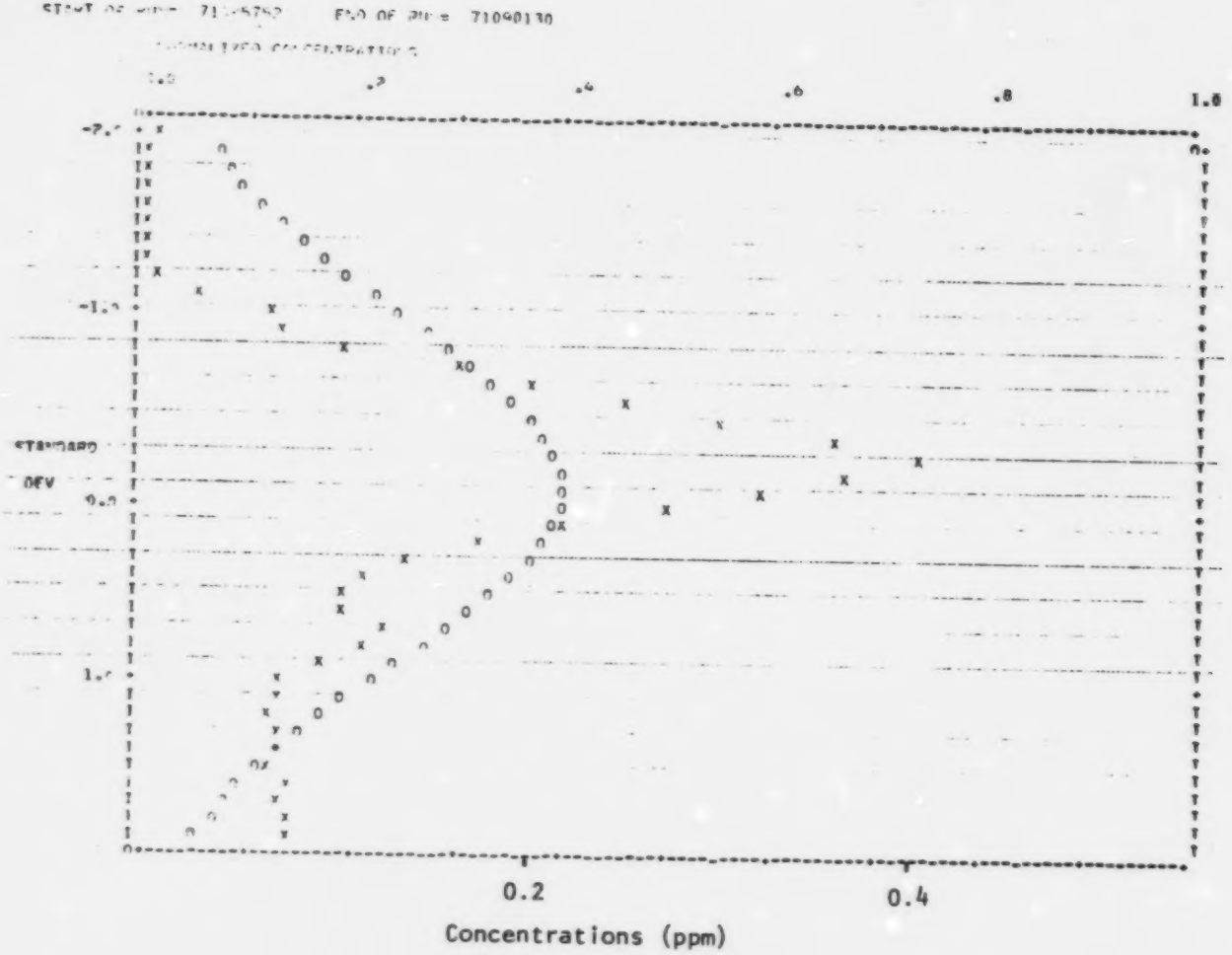

Run No. 8

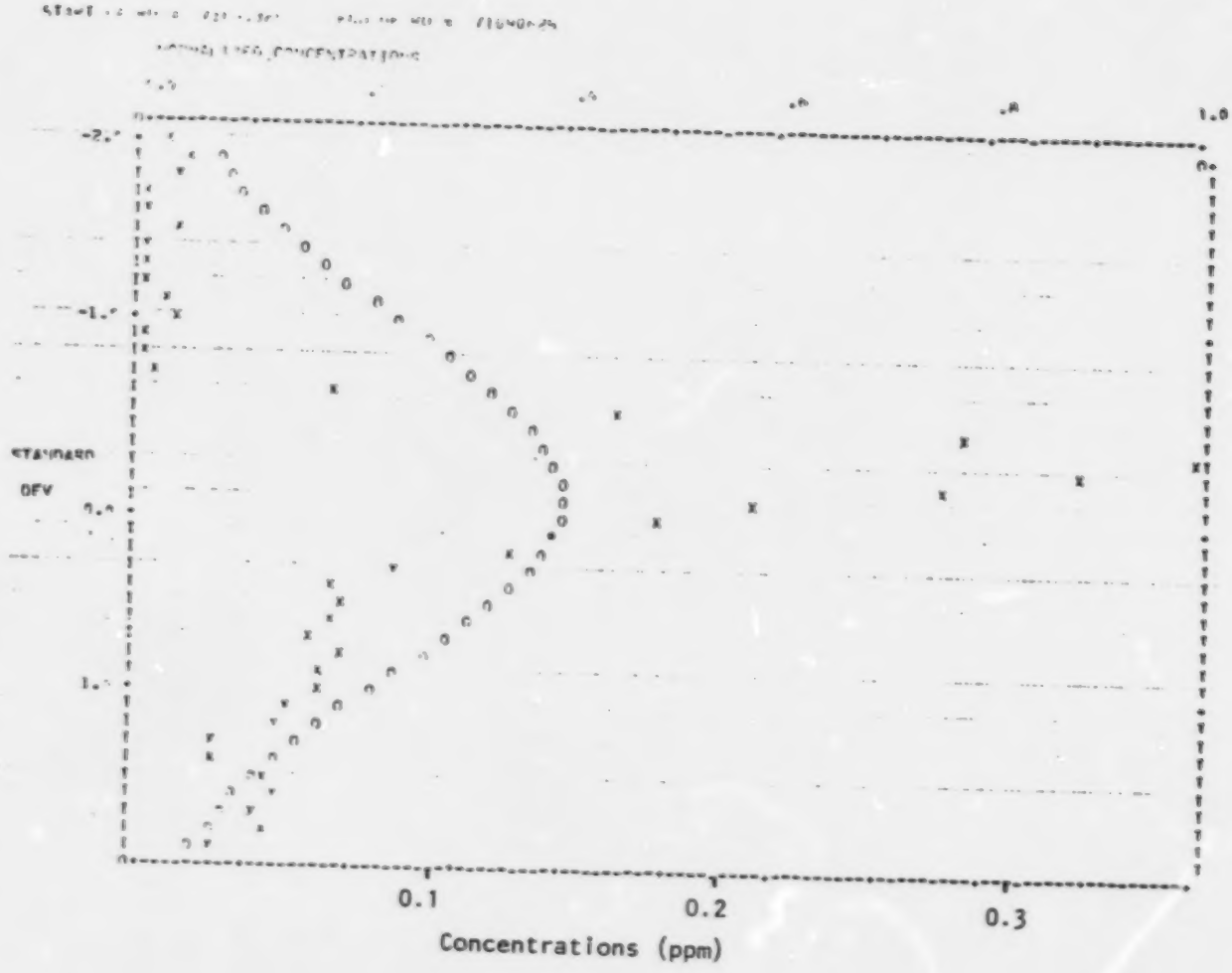

Run No. 9

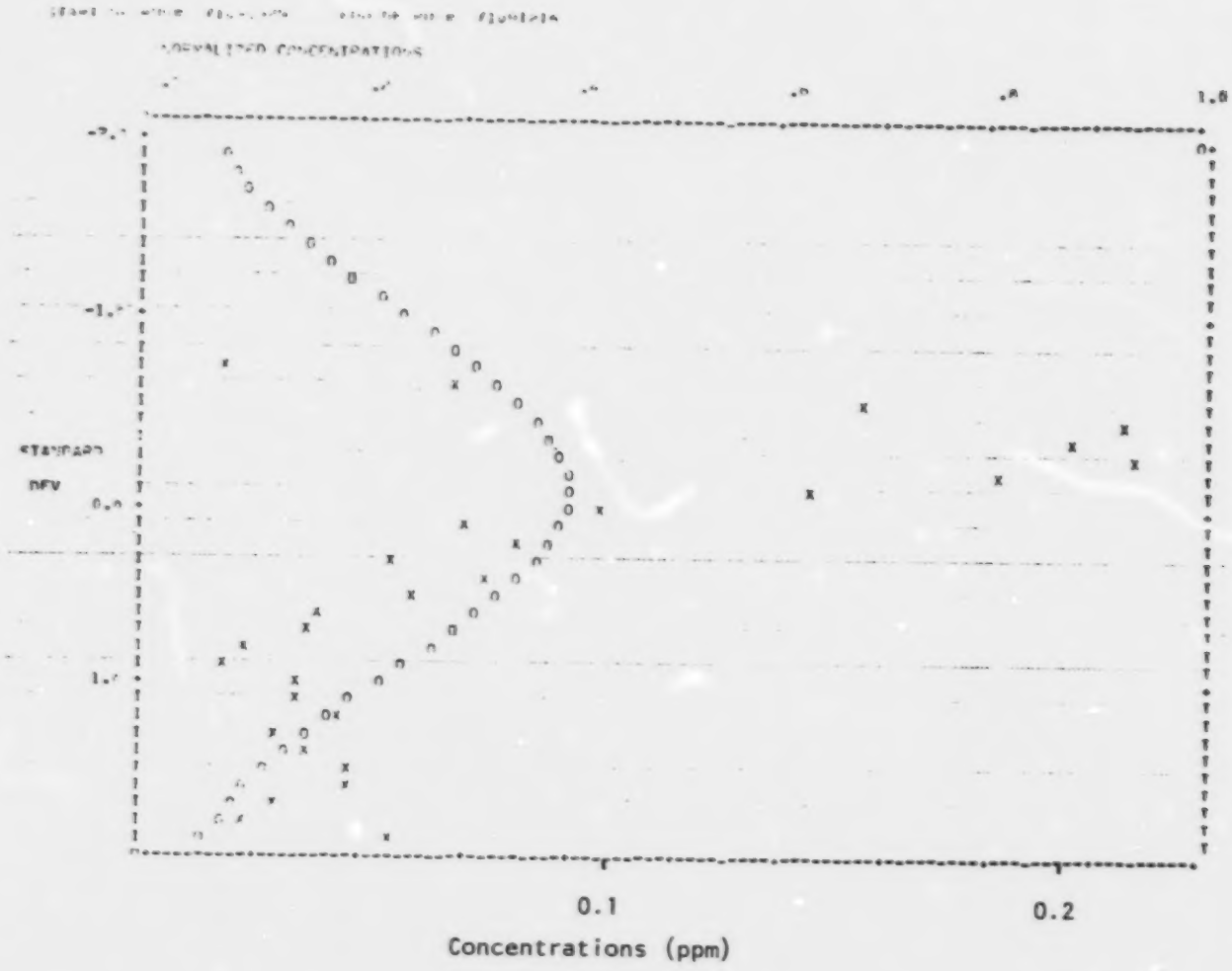
Run No. 10
0.1
0.2
Concentrations (ppm)

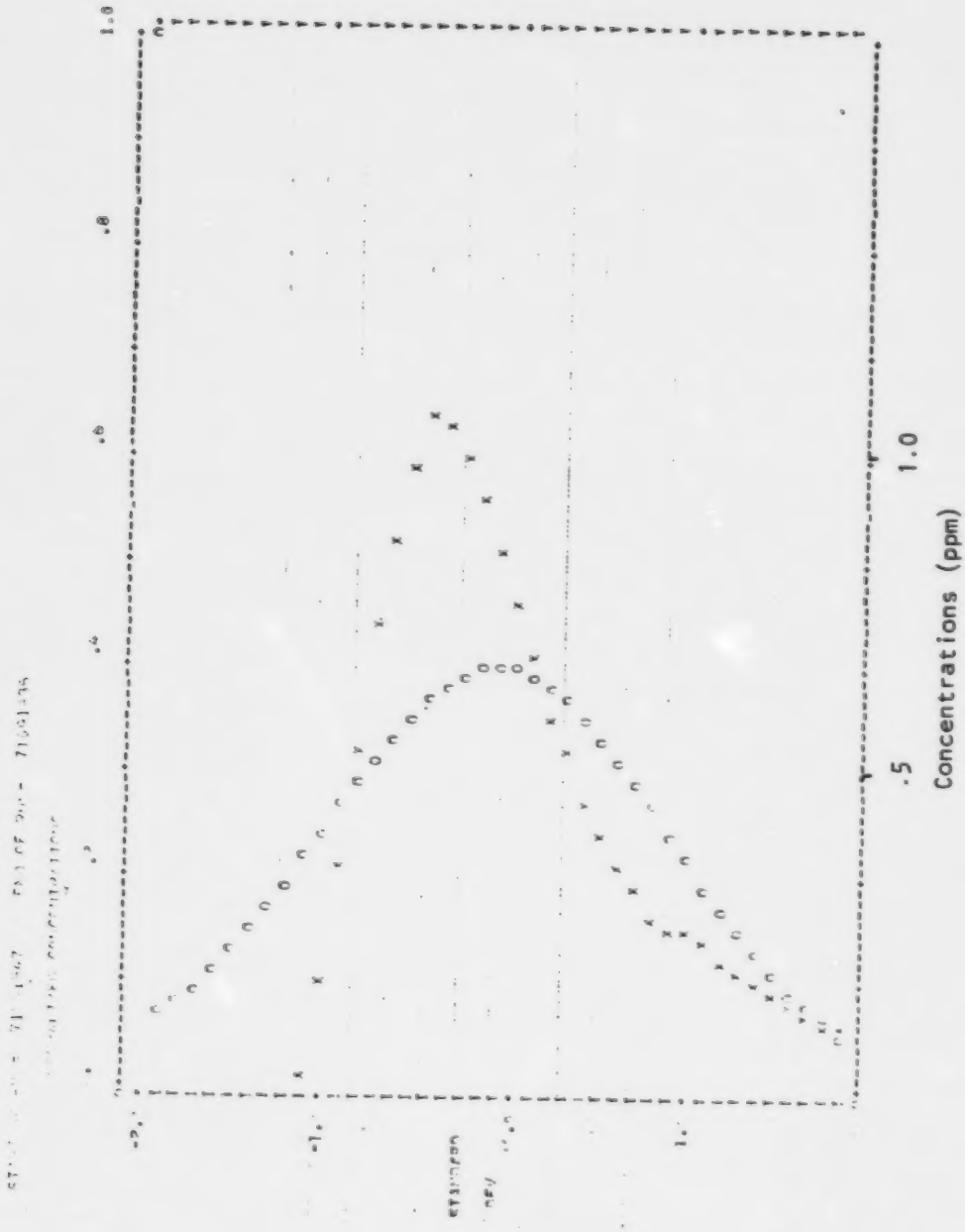

Run No. 11

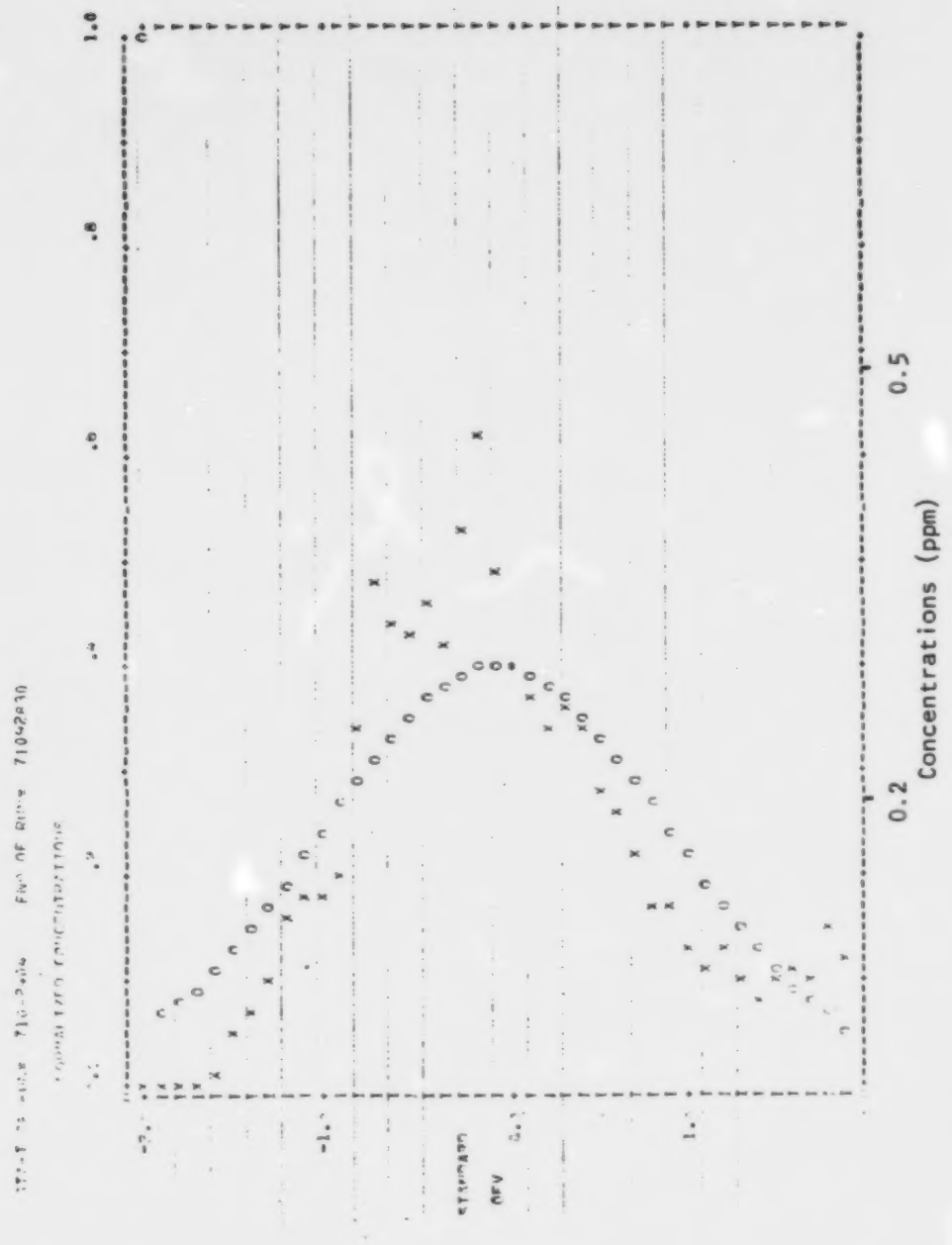

Run No. 12

APPENDIX 3 SO_2 TRAVERSES FOR MARCH 11 PM, 1976 (1250-1655)

This appendix contains the normalized SO_2 traverses for the flight of March 11 PM, 1976 (1250-1655). The run information table for this flight is reproduced for convenience in interpreting each traverse.

TABLE Run information for flight of March 11, 1976 (1250 - 1655).

RUN NUMBER	TIME (MST)	ALTITUDE (m-MSL) ±20	DOWNWIND DISTANCE (km) ±0.3	σ (m) ±100	MAX CONC. (ppm) ±0.02	INTEGRATED CONC. (ppm-m) ±50	FLIGHT DIR. (From-to)
1	1306 - 1318	1220	8.0	T	T	T	S - N
2	1319 - 1331	1220	8.0	T	T	T	N - S
3	1334 - 1346	610	8.0	T	T	T	S - N
4	1348 - 1355	610	8.0	T	T	T	N - S
5	1359 - 1401	610	3.2	1820	0.19	580 +	N - S
6	1404 - 1407	610	8.0	2230	0.20	770 +	S - N
7	1412 - 1415	1070	3.2	2920	0.14	190	N - S
8	1417 - 1420	1070	8.0	2250	0.08	310	S - N
9	1424 - 1426	1370	3.2	3430	0.08	120	N - S
10	1428 - 1430	1370	8 0	2480	0.06	220	S - N
11	1433 - 1436	910	3.2	1540	0.26	430	N - S
12	1438 - 1441	910	8.0	1900	0.14	460	S - N
13	1445 - 1448	460	3.2	2230	0.09	230	N - S
14	1450 - 1453	460	8.0	2010	0.16	560	S - N
15	1457 - 1501	610	-	3210	0.08	400	NE-SW
16	1512 - 1516	760	16.1	*	0.25	*	S - N
17	1518 - 1522	550	16.1	3140	0.11	410	N - S
18	1524 - 1527	910	16.1		0.12		S - N
19	1529 - 1533	910	16.1	3720 **	0.12	600 **	N - S
20	1543 - 1556	610	8.0	T	T	T	S - N
21	1557 - 1612	610	8.0	T	T	T	N - S
22	1618 - 1627	610	8.0	T	T	T	S - N
23	1628 - 1640	610	8.0	T	T	T	N - S

T turbulence run
- plume was traversed at an agle for a check on orientation of traverses with respect to plume axis
* incomplete traverse resulted in unreliable values for plume sigma and integrated concentration
** run 18 was incomplete at the northern end; run 19, at the southern end sigma values and integrated concentration were estimated from a composite of runs 18 and 19.
+ small part of plume was missed; so that integrated concentration values were increased by 10%

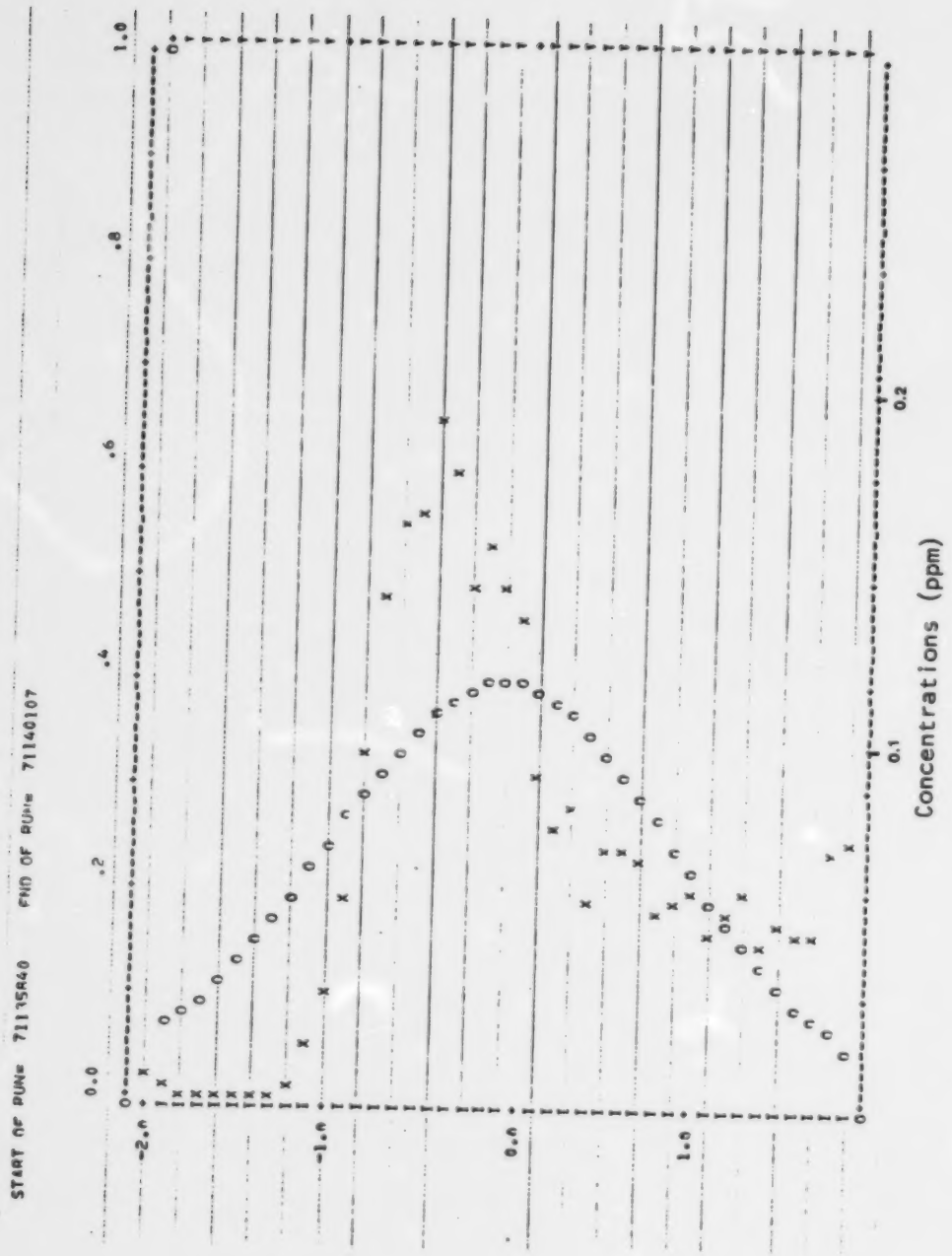
START OF RUN= 71115R40 END OF RUN= 71140107
0.0
.2
.4
.6
.8
1.0
-2.0
-1.0
0.0
1.0
0.2
0.1
Concentrations (ppm)

Run No. 5

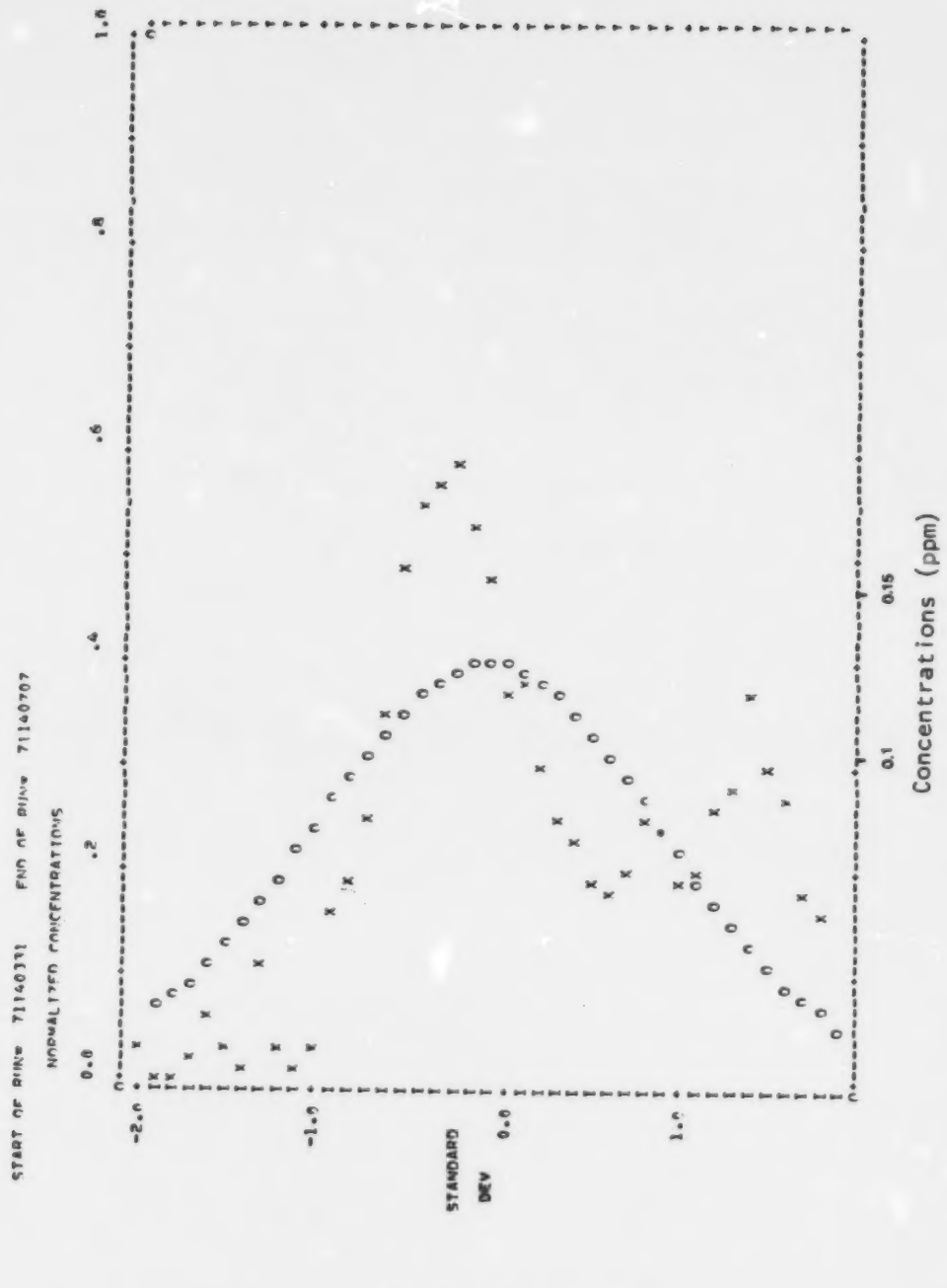
START OF RUN= 71140331 END OF RUN= 71140707
NORMALIZED CONCENTRATIONS
0.0
.2
.4
.6
.8
1.0
-2.0
-1.0
0.0
1.0
STANDARD DEV
0.1
0.15
Concentrations (ppm)

Run No. 6

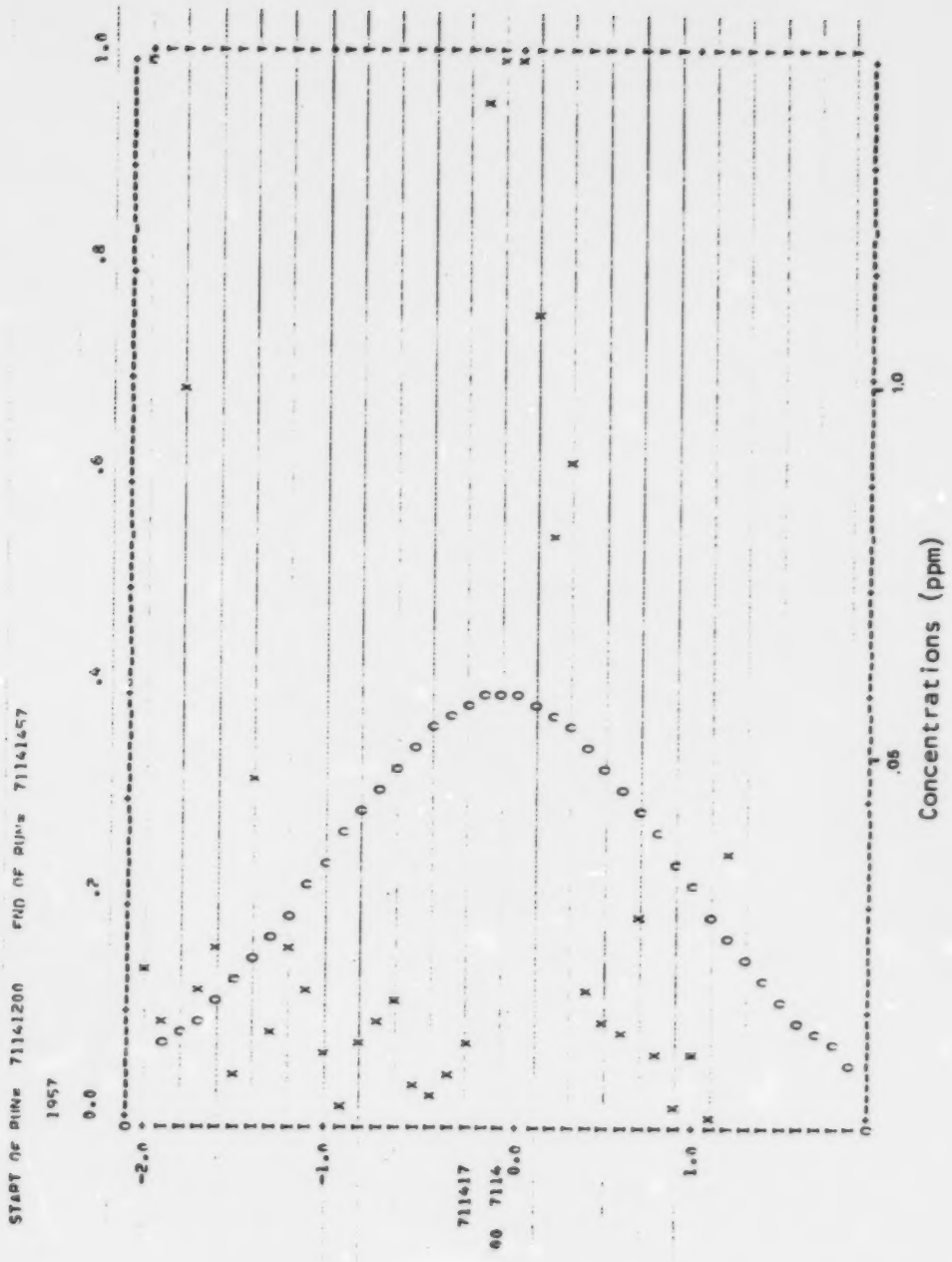
START OF RUN= 71141200
END OF RUN= 71141657
1957
0.0
.2
.4
.6
.8
1.0
-2.0
-1.0
1.0
711417
00 7114
0.0
.05
1.0
Concentrations (ppm)

Run No. 7

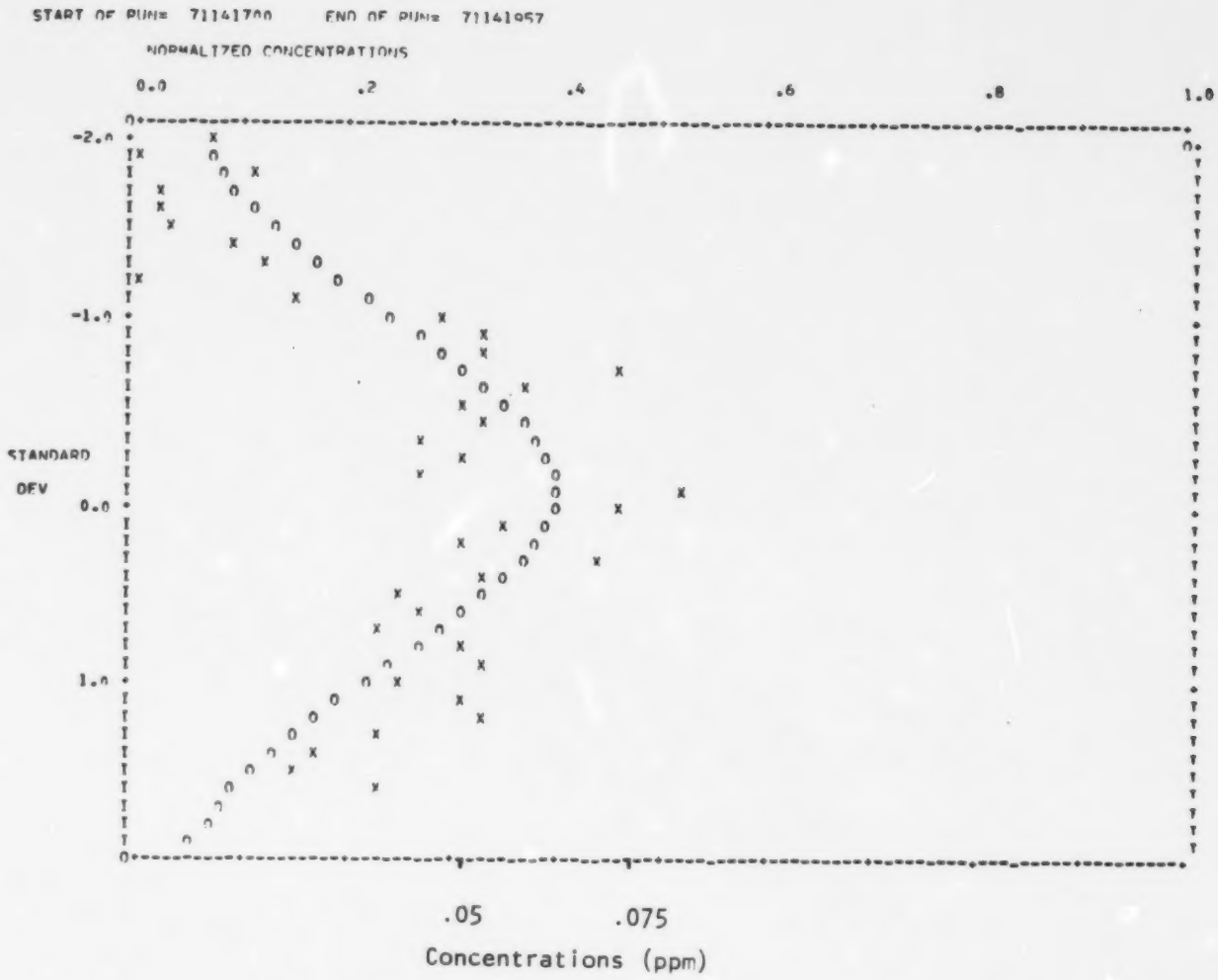
START OF RUN= 71141700 END OF RUN= 71141957
NORMALIZED CONCENTRATIONS
0.0
.2
.4
.6
.8
1.0
-2.0
-1.0
STANDARD
DEV
0.0
1.0
.05
.075
Concentrations (ppm)

Run No. 8

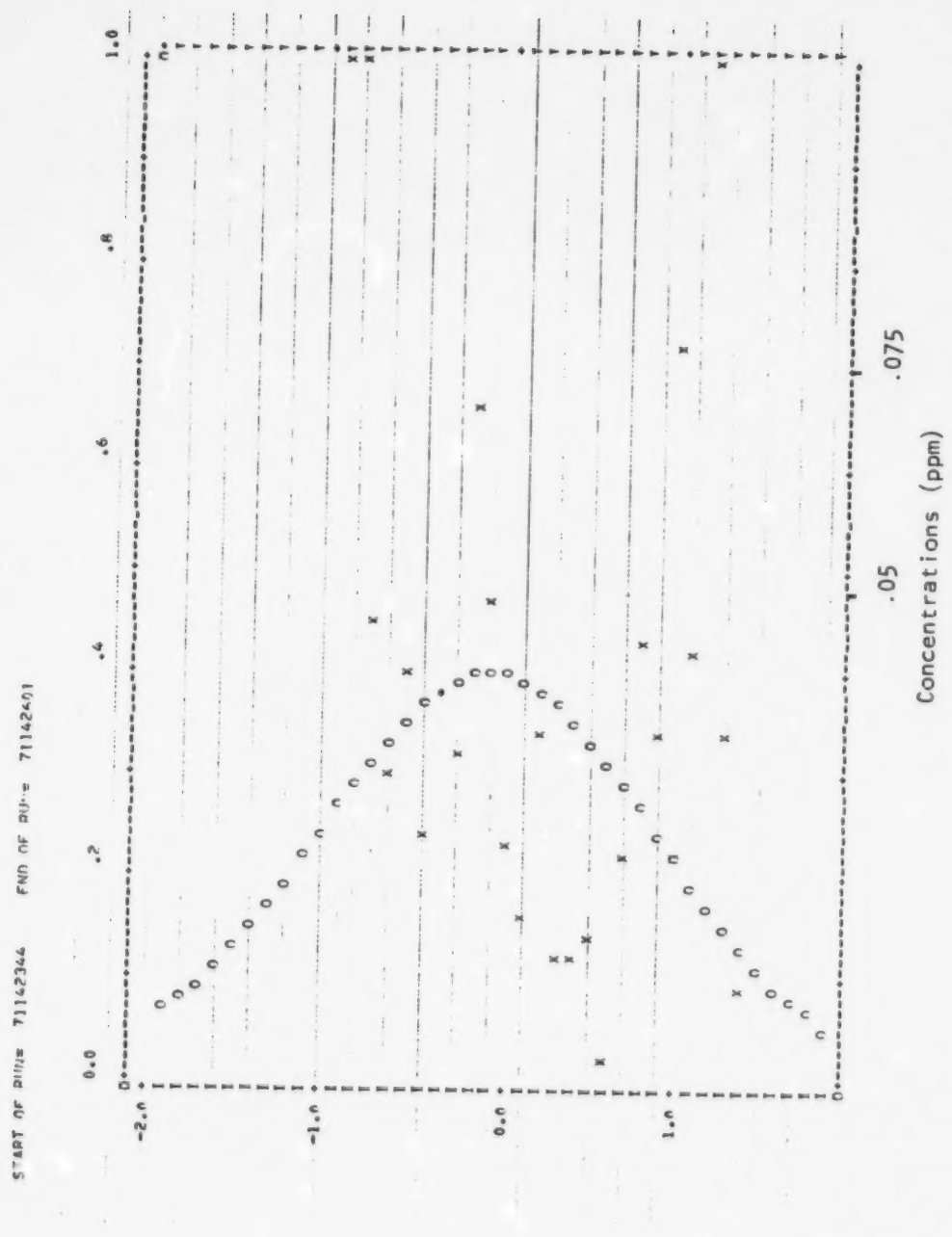
START OF RUN= 71142344 END OF RUN= 71142401
0.0
.2
.4
.6
.8
1.0
-2.0
-1.0
0.0
1.0
.05
.075
Concentrations (ppm)

Run No. 9

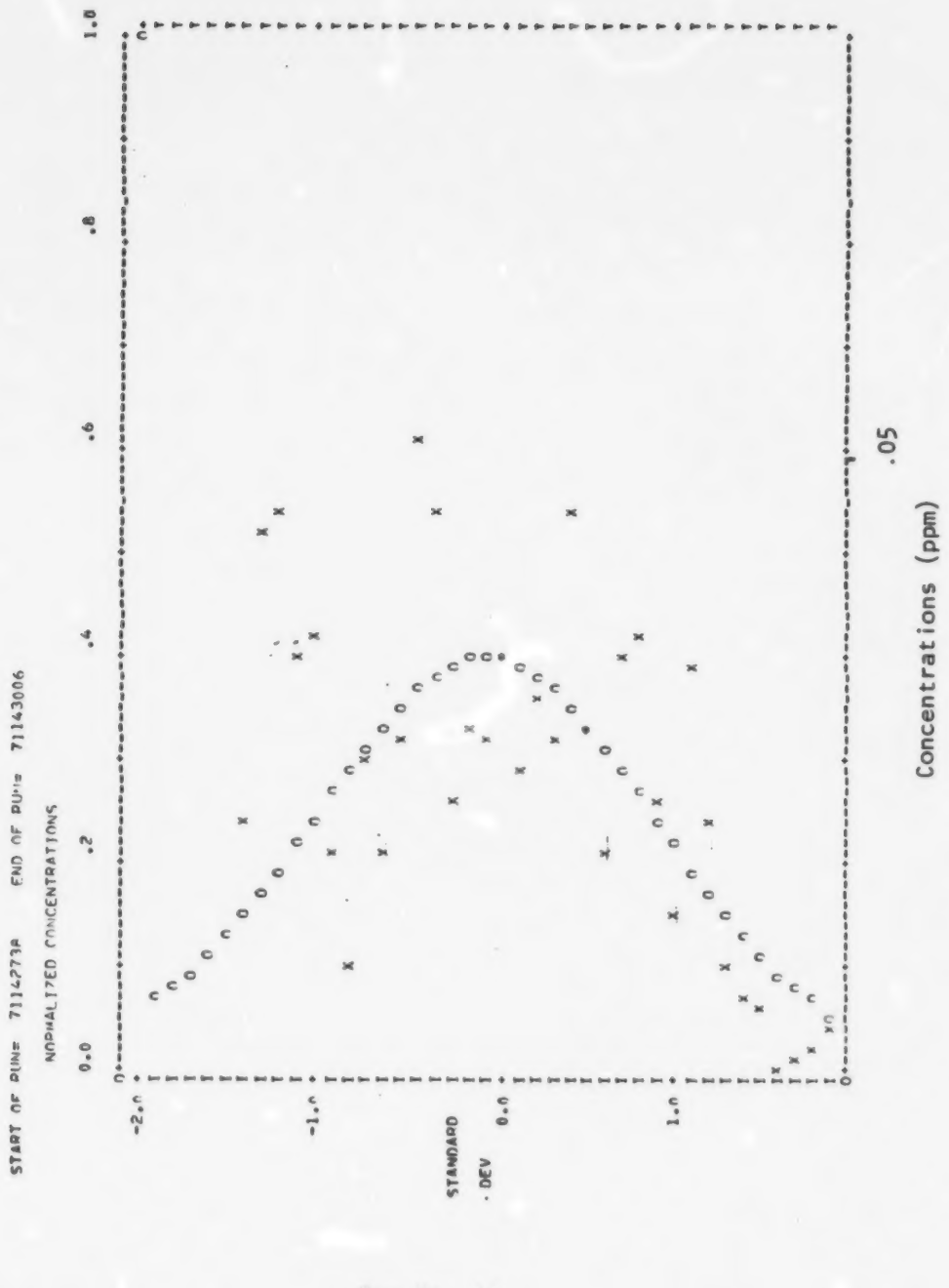
START OF RUN= 71142738 END OF RUN= 71143006
NORMALIZED CONCENTRATIONS
0.0
.2
.4
.6
.8
1.0
-2.0
-1.0
STANDARD
DEV
0.0
1.0
.05
Concentrations (ppm)

Run No. 10

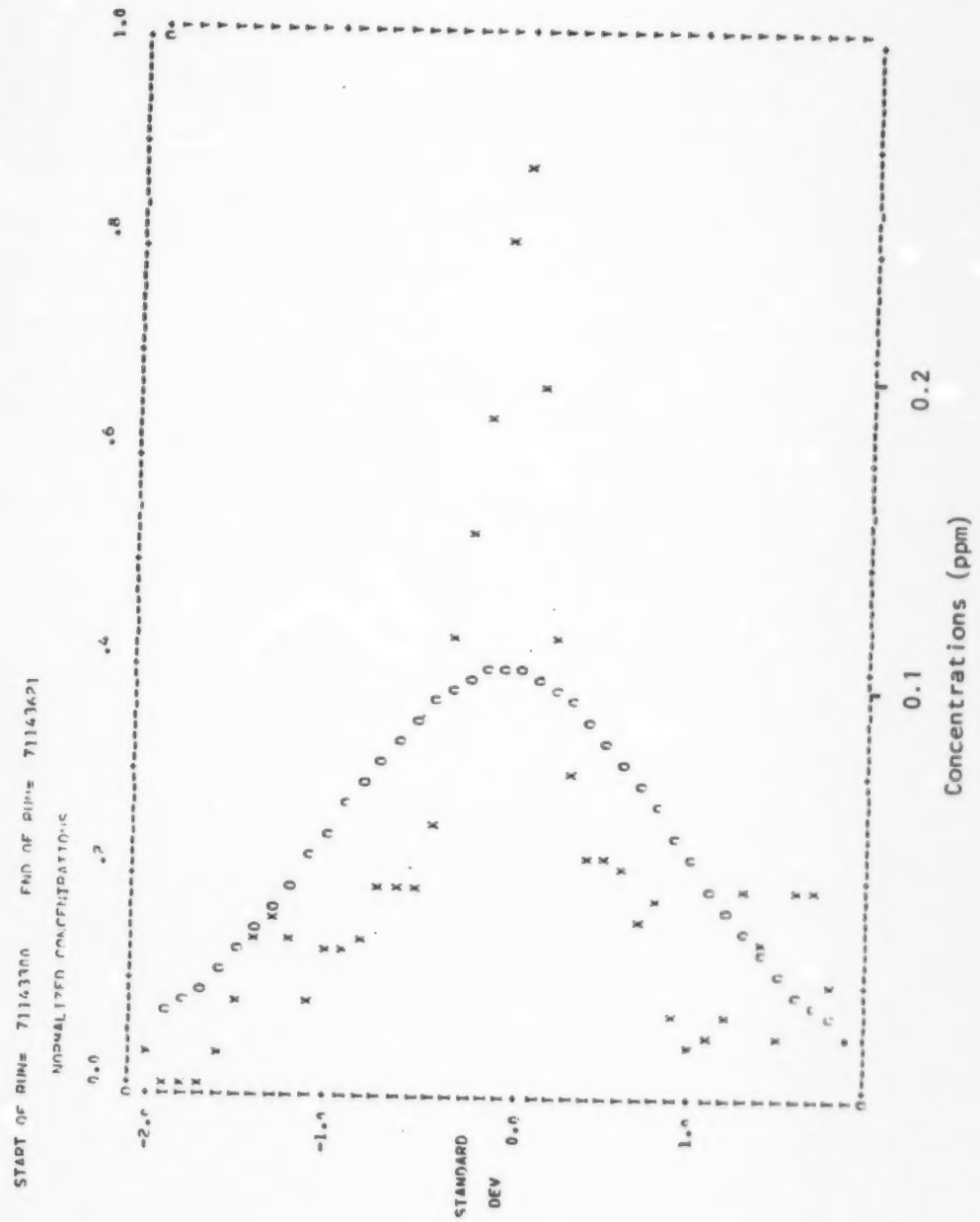
START OF RUN= 71143000 END OF RUN= 71143021
NORMALIZED CONCENTRATIONS
0.0
.2
.4
.6
.8
1.0
-2.0
-1.0
1.0
STANDARD
DEV
0.0
0.1
0.2
Concentrations (ppm)

Run No. 11

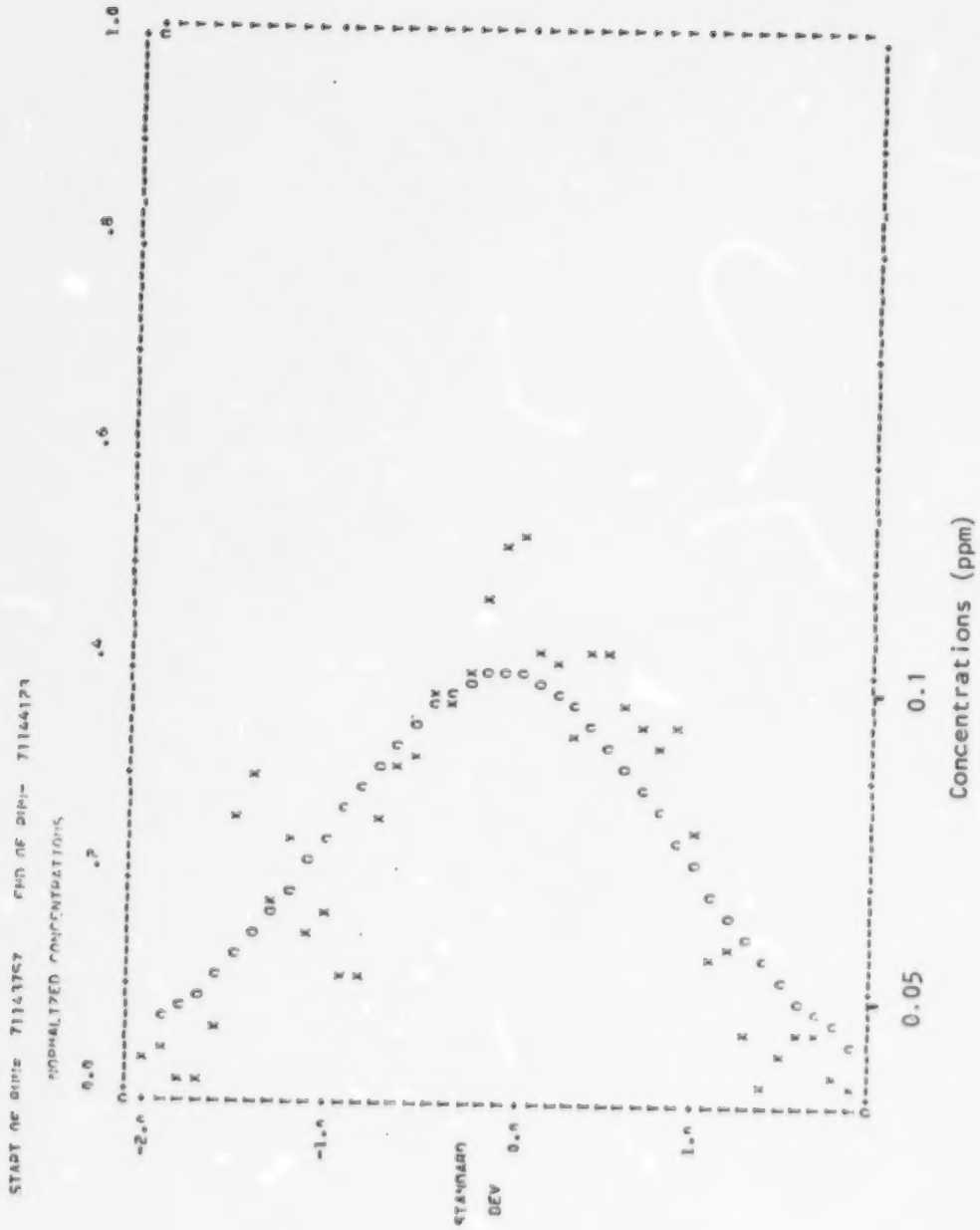

Run No. 12

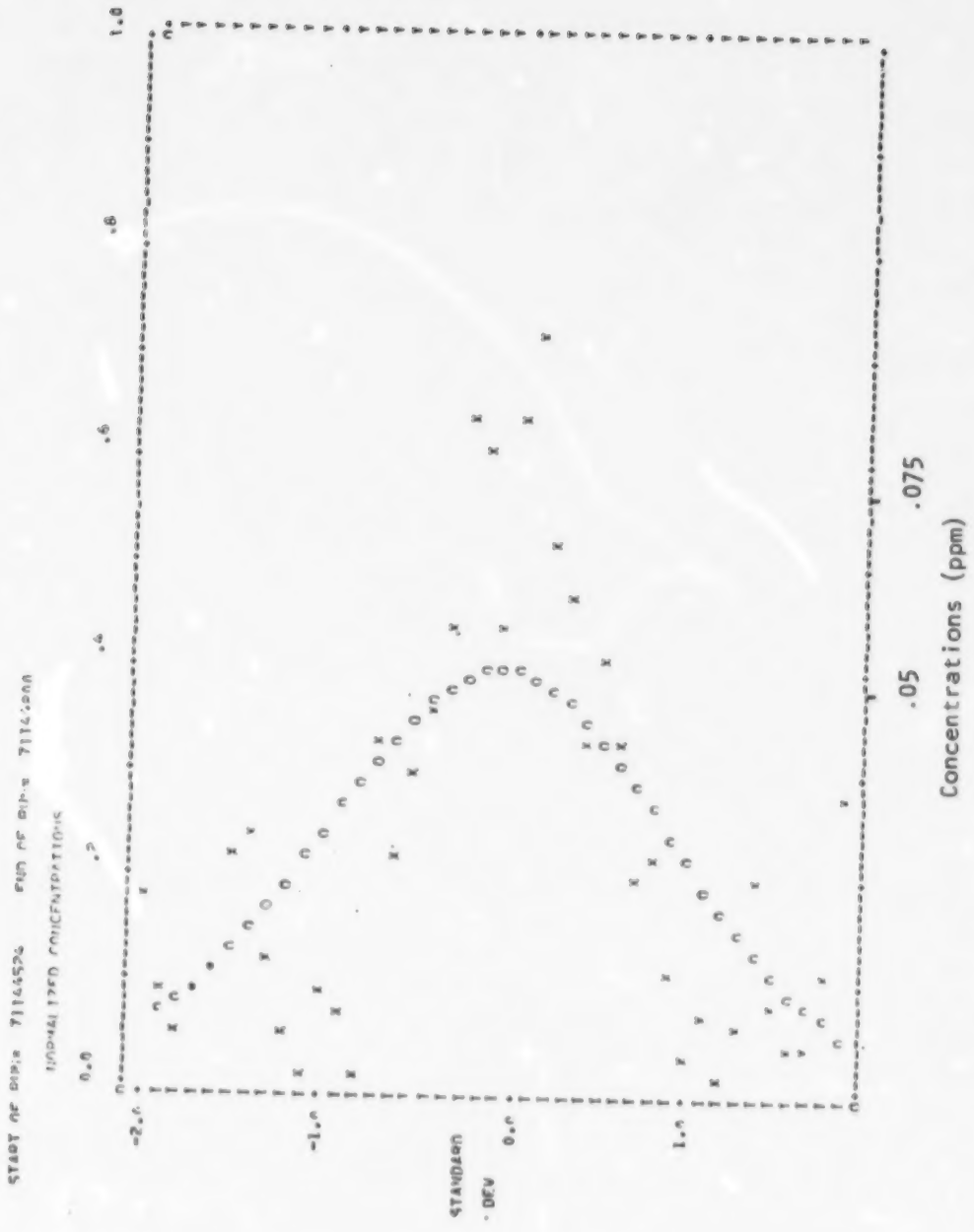

Run No. 13

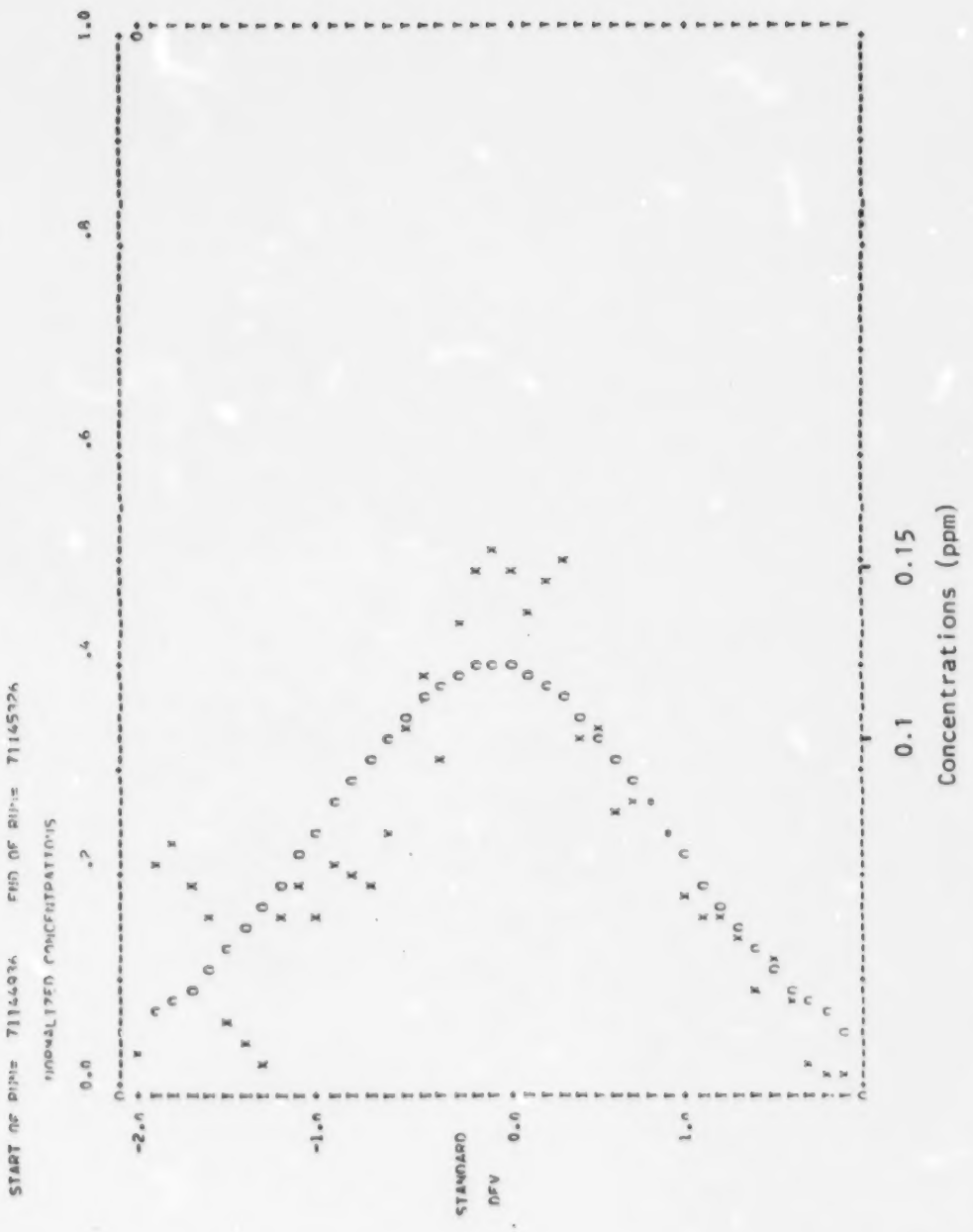
START OF RUN= 71146936 END OF RUN= 71146936
NORMALIZED CONCENTRATIONS
0.0
.2
.4
.6
.8
1.0
-2.0
-1.0
STANDARD
DEV
0.0
1.0
0.1
0.15
Concentrations (ppm)

Run No. 14

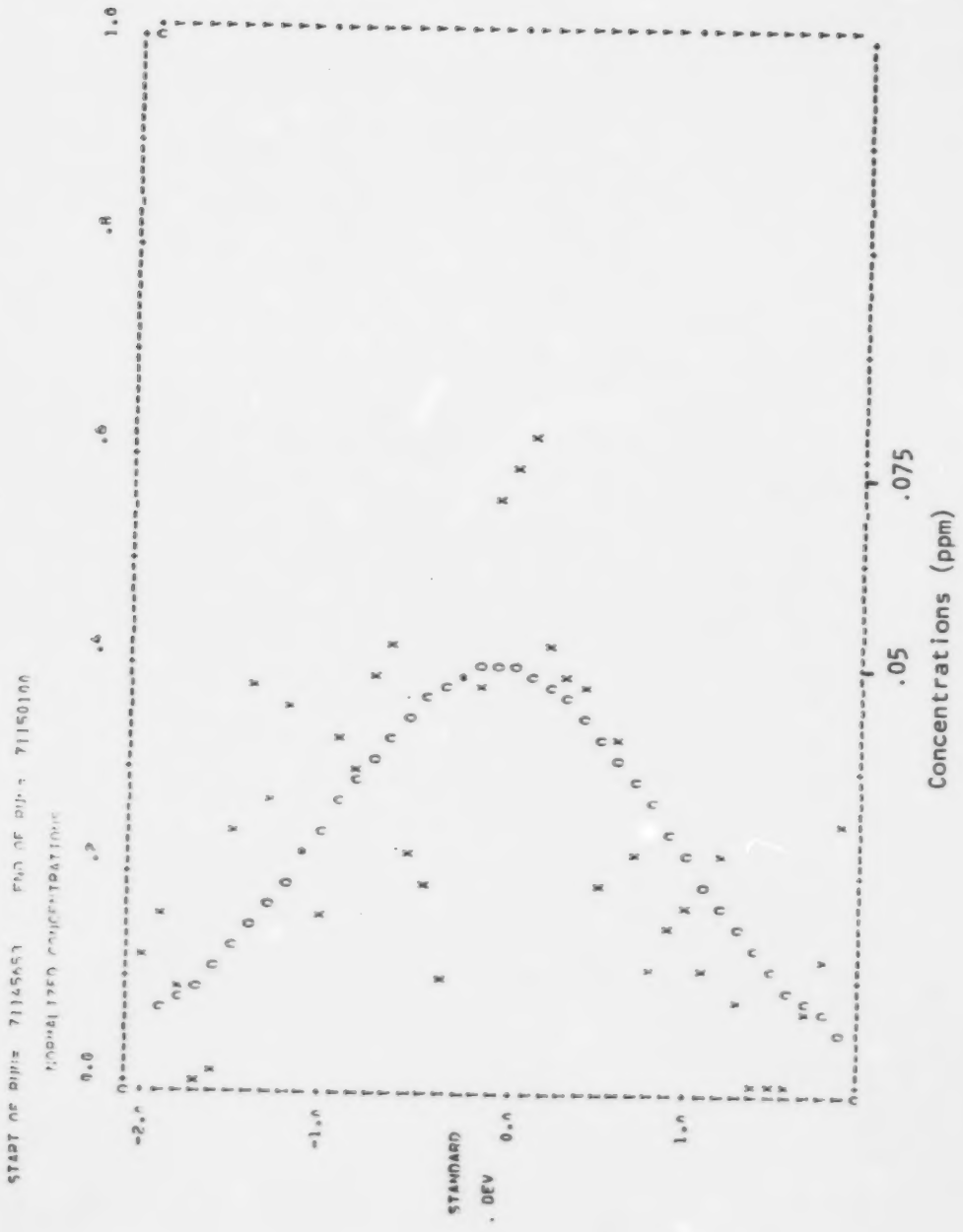
START OF RUN: 71145057 END OF RUN: 71150100
NORMALIZED CONCENTRATIONS
0.0
.2
.4
.6
.8
1.0
-2.0
-1.0
0.0
1.0
STANDARD DEV
.05
.075
Concentrations (ppm)

Run No. 15

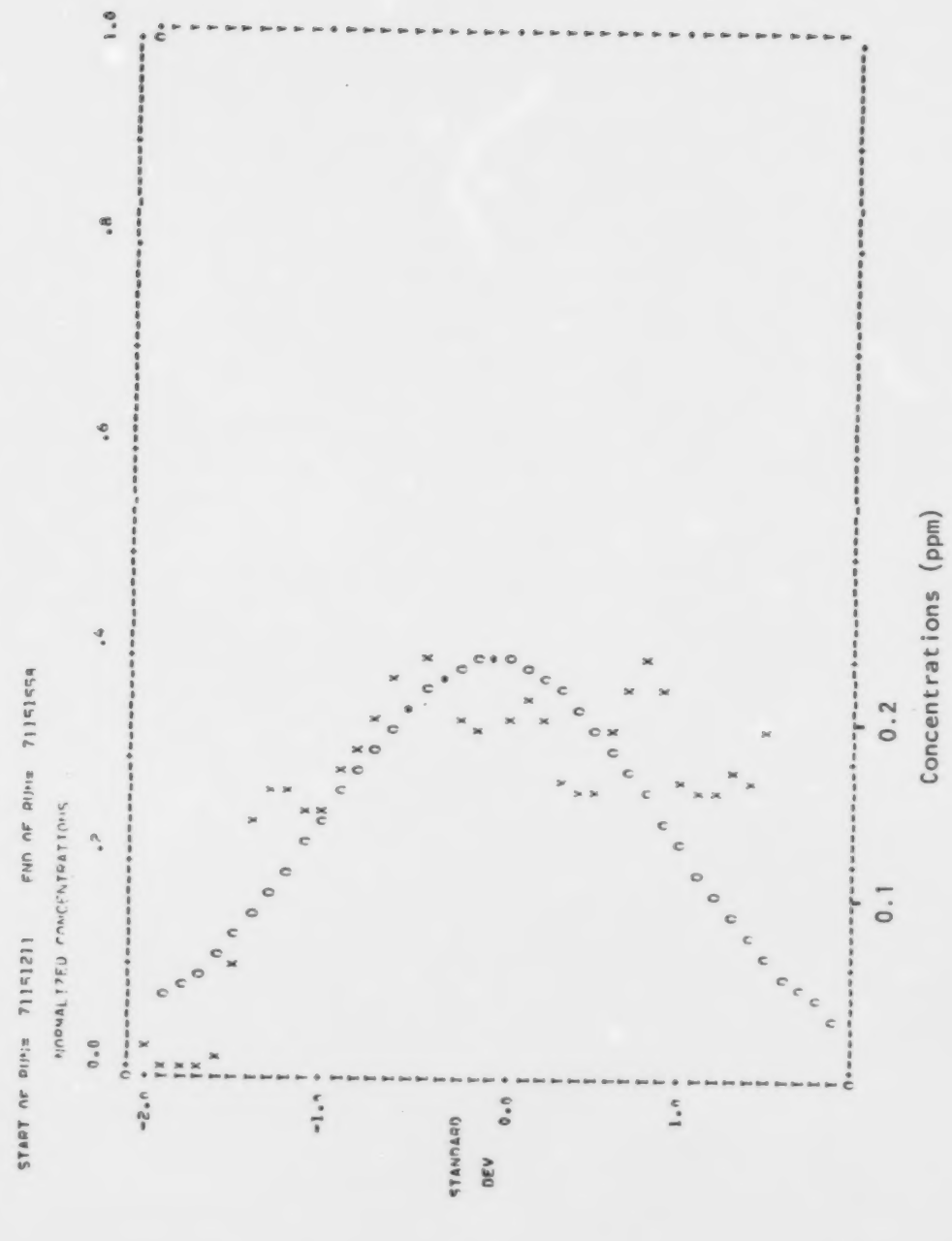
START OF RUN= 71151211 END OF RUN= 71151559
NORMALIZED CONCENTRATIONS
0.0
.2
.4
.6
.8
1.0
-2.0
-1.0
0.0
1.0
STANDARD
DEV
0.1
0.2
Concentrations (ppm)

Run No. 16

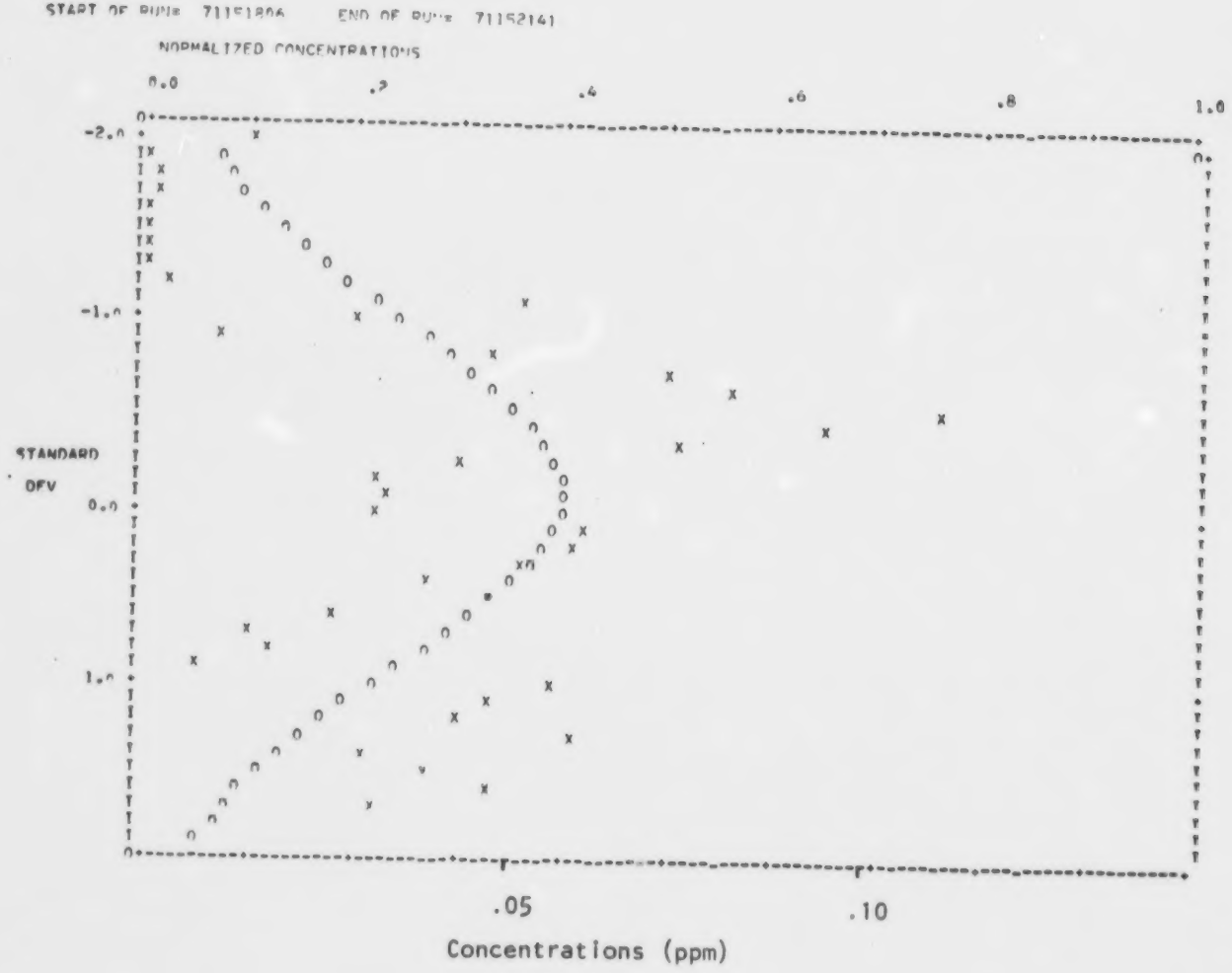
START OF RUN: 71151806
END OF RUN: 71152141
NORMALIZED CONCENTRATIONS
0.0
.2
.4
.6
.8
1.0
-2.0
-1.0
0.0
1.0
STANDARD
DEV
.05
.10
Concentrations (ppm)

Run No. 17

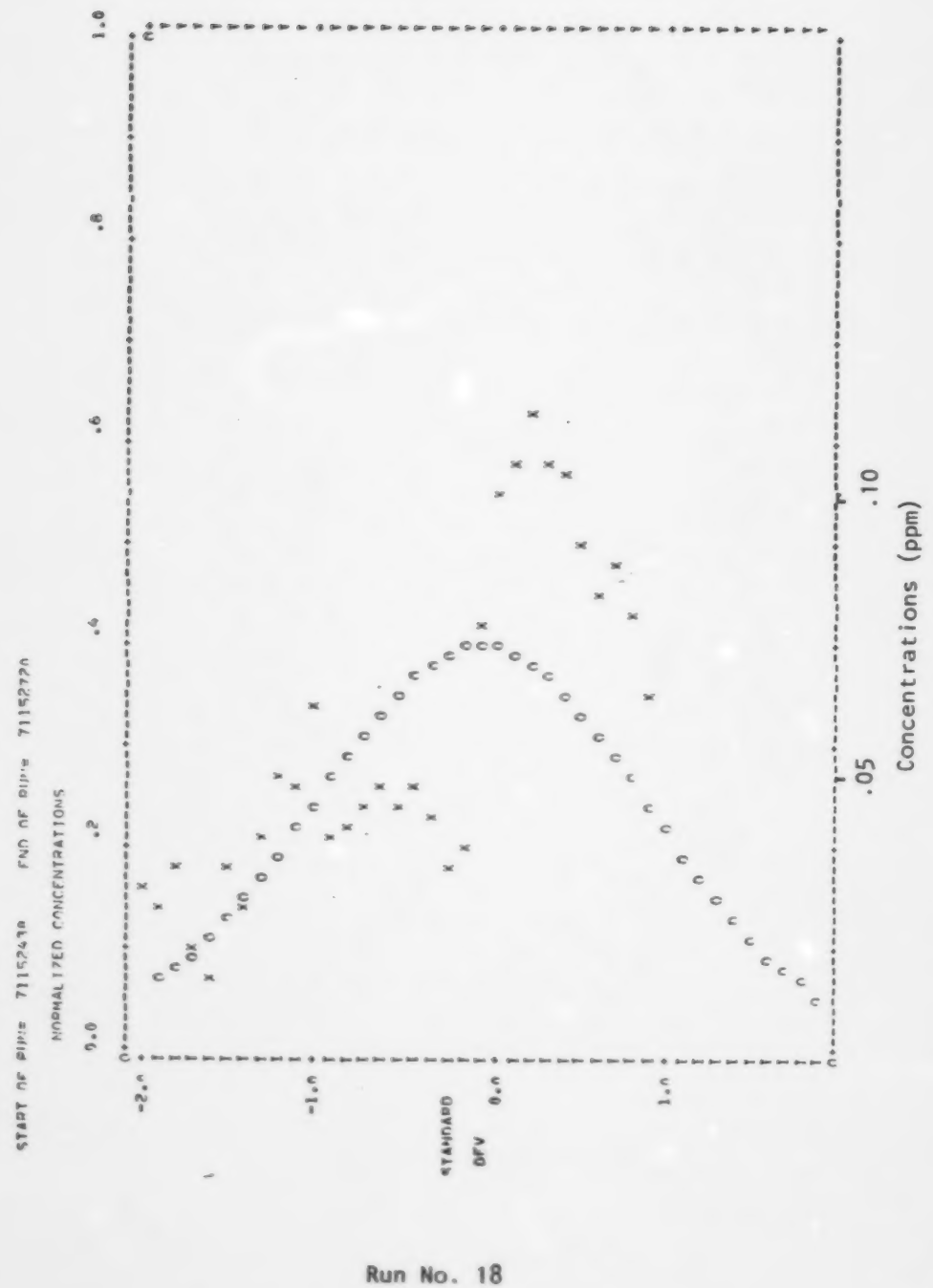
START OF PIPE 7115247A END OF PIPE 7115272A
NORMALIZED CONCENTRATIONS
0.0
.2
.4
.6
.8
1.0
-2.0
-1.0
STANDARD
DEV 0.0
1.0
.05
.10
Concentrations (ppm)

Run No. 18

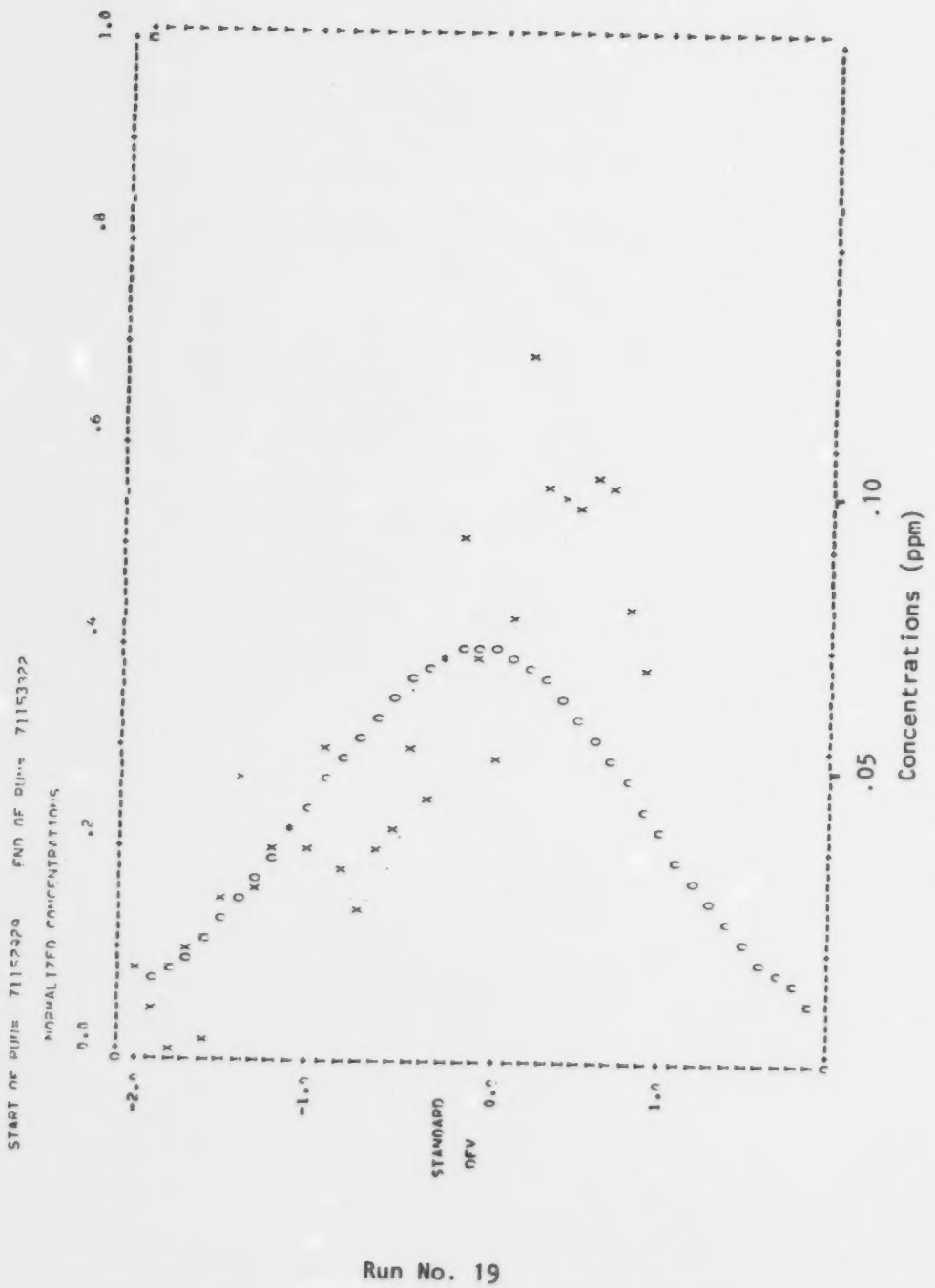
START OF PIPE 71152929 END OF PIPE 71153222
NORMALIZED CONCENTRATIONS
0.0
.2
.4
.6
.8
1.0
-2.0
-1.0
0.0
1.0
STANDARD
DEV
.05
.10
Concentrations (ppm)

Run No. 19

APPENDIX 4 SO_2 TRAVERSES FOR MARCH 12, 1976 PM (1420-1650)

This appendix contains the normalized SO_2 traverses for the flight of March 12, 1976 PM (1420-1650). The run information table for this flight is reproduced for convenience in interpreting each traverse.

TABLE Run information for flight of March 12, 1976 PM (1420-1650)

RUN NUMBER	TIME (MST)	ALTITUDE (m MSL) ±20	DOWNWIND DISTANCE (km) ±0.3	σ_y (m) ±100	MAX CONC. (ppm) ±0.02	INTEGRATED CONC. (ppm-m) ±30	FLIGHT DIR. (From-to)
1	1430 - 1440	910	4.8	T	T	T	S - N
2	1442 - 1445	1220	3.2	2490	0.155	458	NW-SE
3	1446 - 1450	1220	8.9	3430	0.077	234	SE-NW
4	1452 - 1455	1220	4.8	3160	0.149	360	N - S
5	1457 - 1500	1220	11.3	3660	0.058	196	S - N
6	1503 - 1507	760	4.8	*	0.094	*	N - S
7	1509 - 1511	760	11.3	3330	0.099	333 +	S - N
8	1515 - 1519	1070	4.8	*	0.160	*	N - S
9	1521 - 1524	1070	11.3	3840	0.093	407	S - N
10	1528 - 1531	910	4.8	2130	0.194	528	N - S
11	1533 - 1537	910	11.3	M	M	M	S - N
12	1541 - 1544	670	4.8	2820	0.133	514 +	N - S
13	1546 - 1550	670	11.3	4010	0.122	367	S - N
14	1533 - 1559	1580	4.8	1470	0.098	191	N - S
15	1601 - 1603	1580	11.3	2370	0.101	200	S - N
16	1605 - 1614	1220	11.3	T	T	T	S - N
17	1616 - 1633	1220	2.4	T	T	T	NW-SE

* incomplete traverse resulted in unreliable value
T Turbulence run
\+ integrated concentration was increased by 10% due to the missing of the edge of the plume
M data missing due to system malfunction

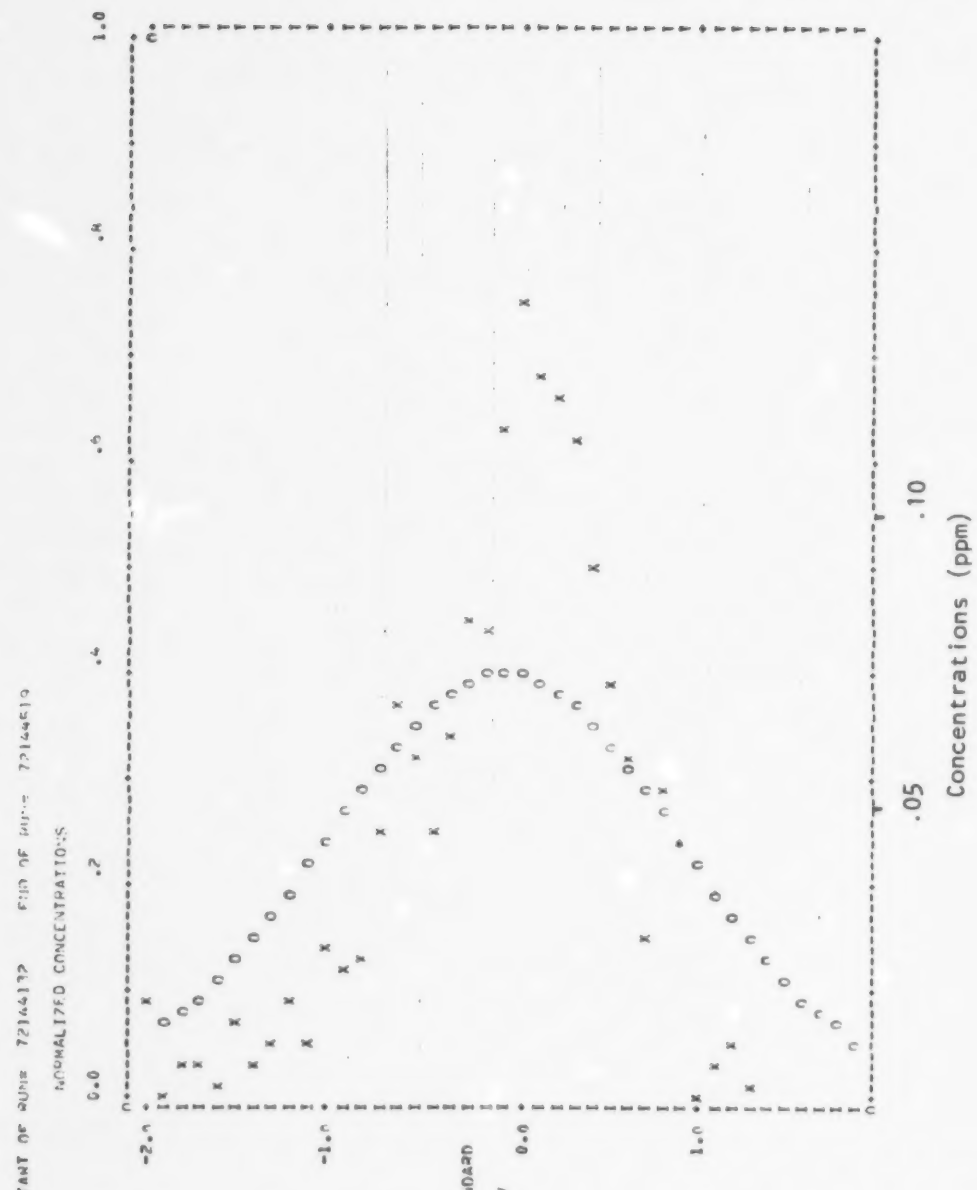
START OF RUN= 72144132 END OF RUN= 72144619
NORMALIZED CONCENTRATIONS
0.0
.2
.4
.6
.8
1.0
-2.0
-1.0
STANDARD DEV
0.0
1.0
.05
.10
Concentrations (ppm)

Run No. 2

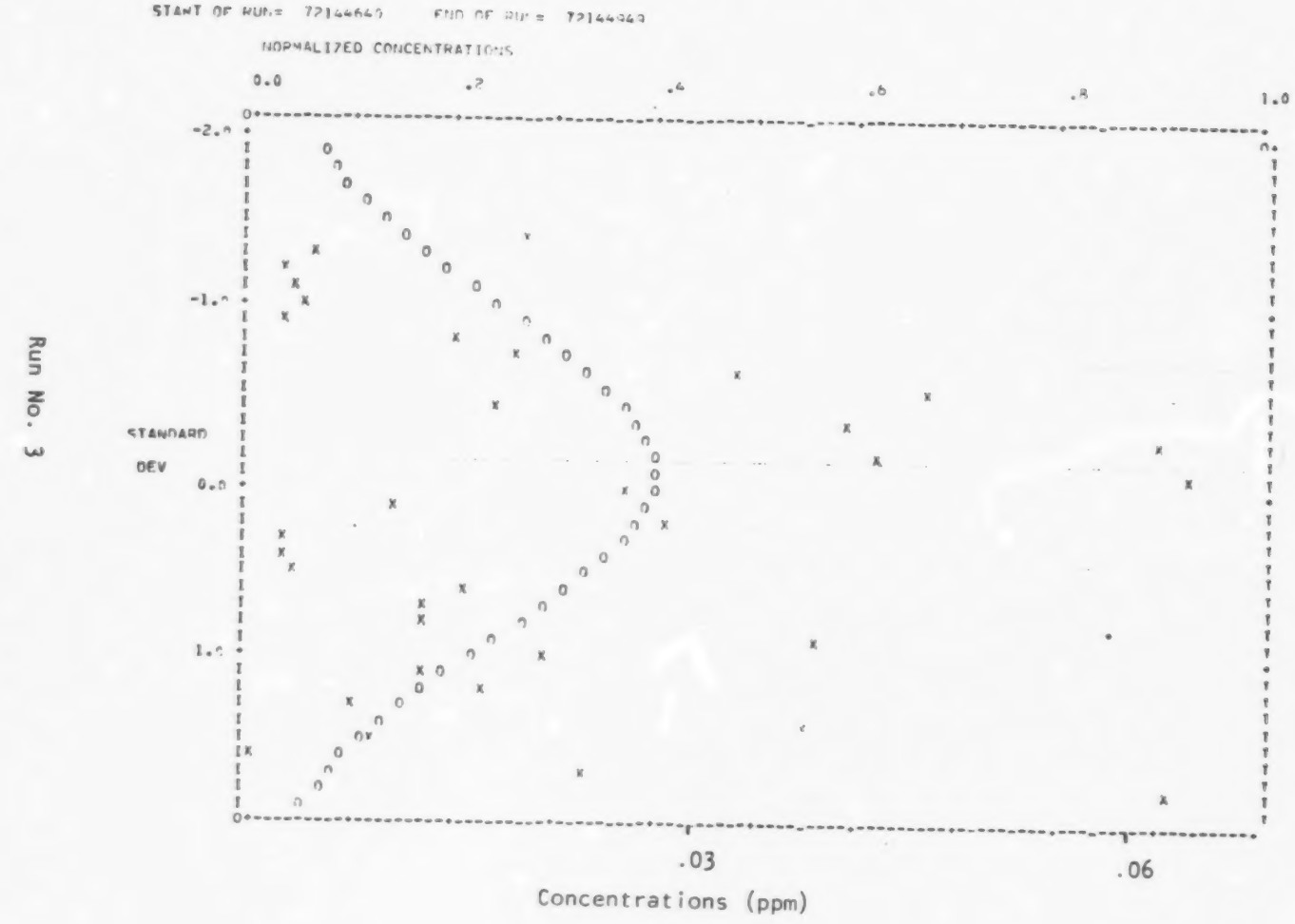
START OF RUN= 72144640
END OF RUN = 72144949
NORMALIZED CONCENTRATIONS
0.0
.2
.4
.6
.8
1.0
-2.0
-1.0
0.0
1.0
STANDARD
DEV
.03
.06
Concentrations (ppm)

Run No. 3

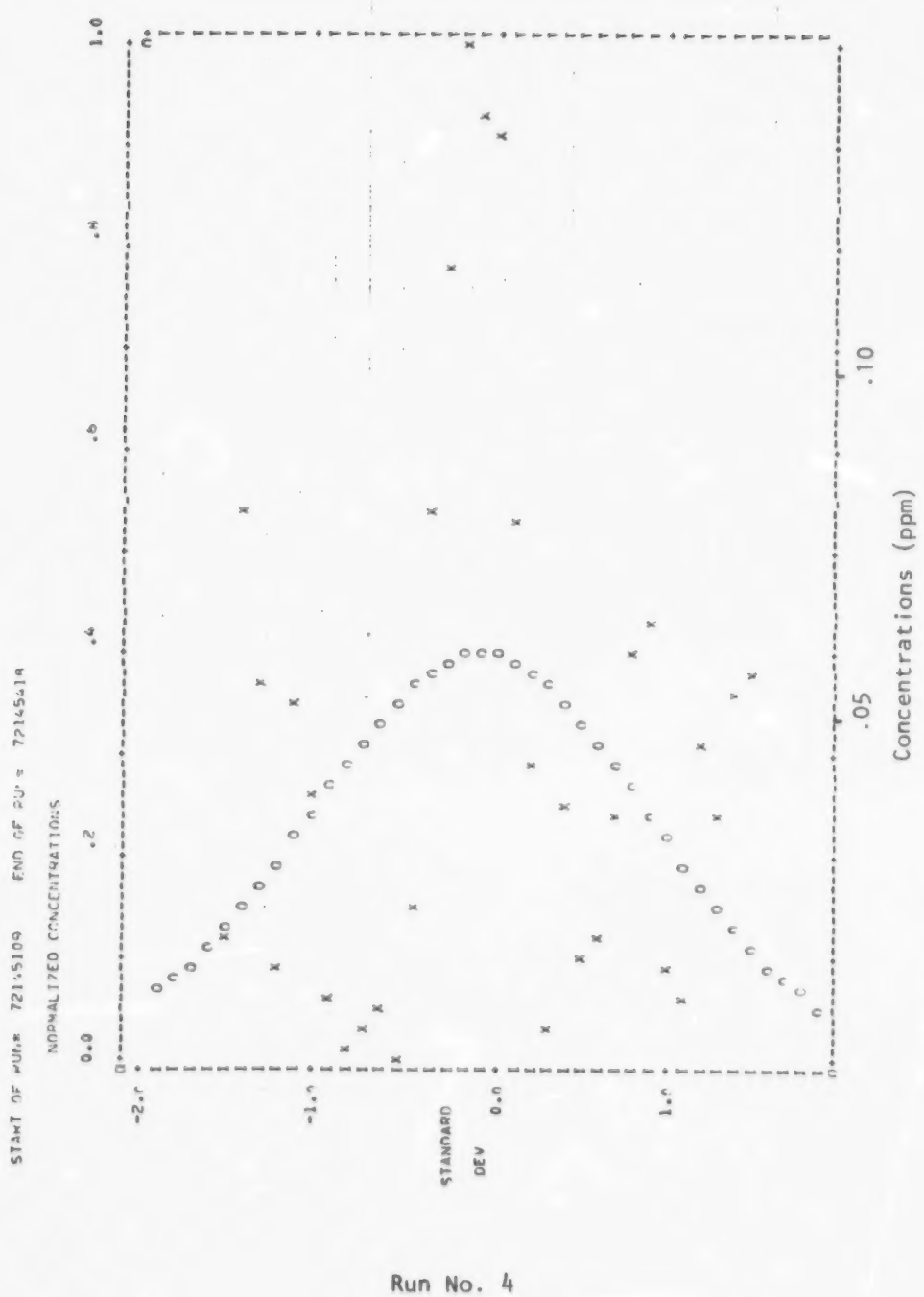
START OF RUN= 7214.5109 END OF RU = 7214.5419
NORMALIZED CONCENTRATIONS
0.0
.2
.4
.6
.8
1.0
-2.0
-1.0
0.0
1.0
STANDARD DEV
.05
.10
Concentrations (ppm)

Run No. 4

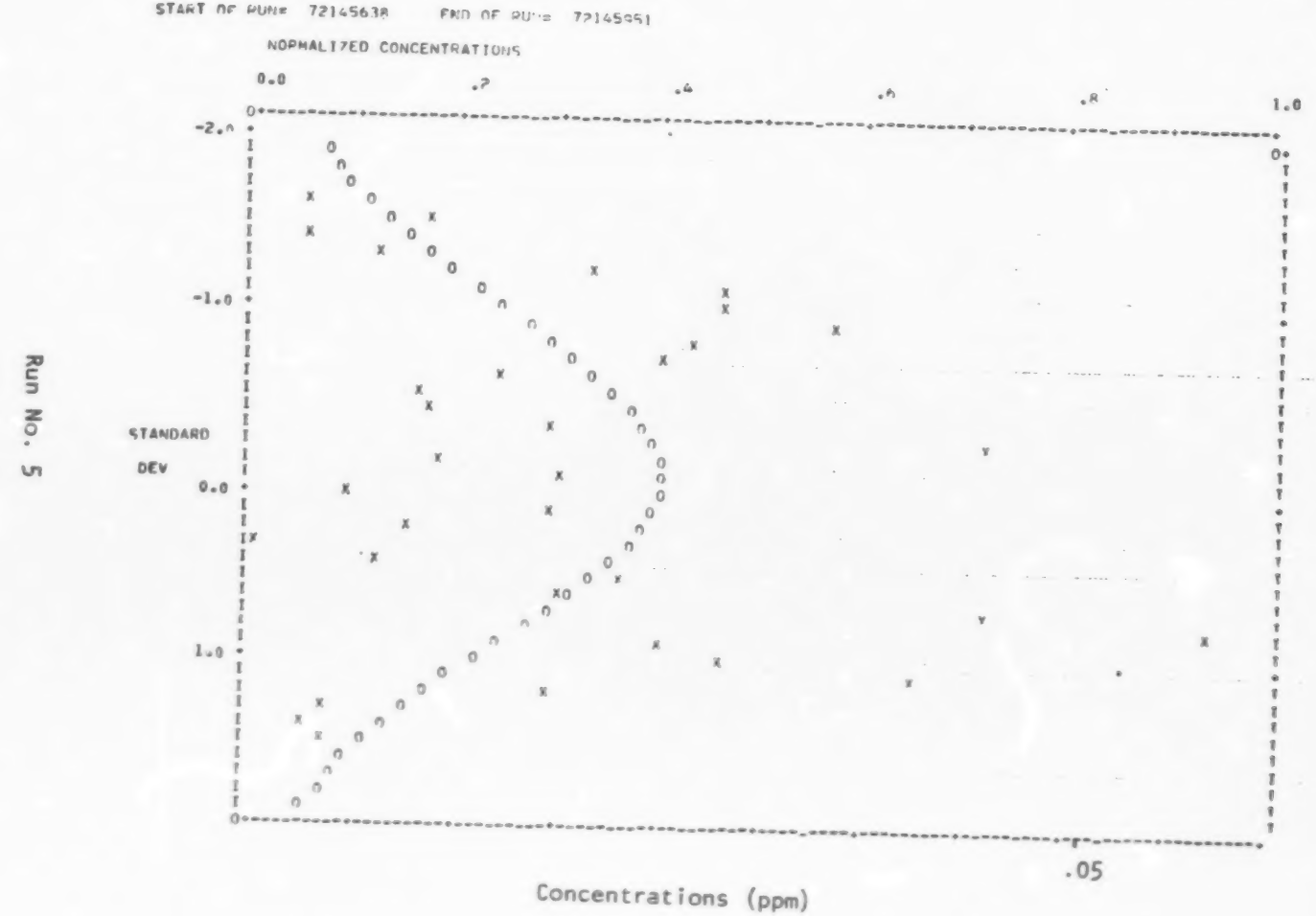
START OF RUN= 7214563R
END OF RUN= 7214595I
NORMALIZED CONCENTRATIONS
0.0
.2
.4
.6
.8
1.0
-2.0
-1.0
0.0
1.0
STANDARD
DEV
.05
Concentrations (ppm)
Run No. 5

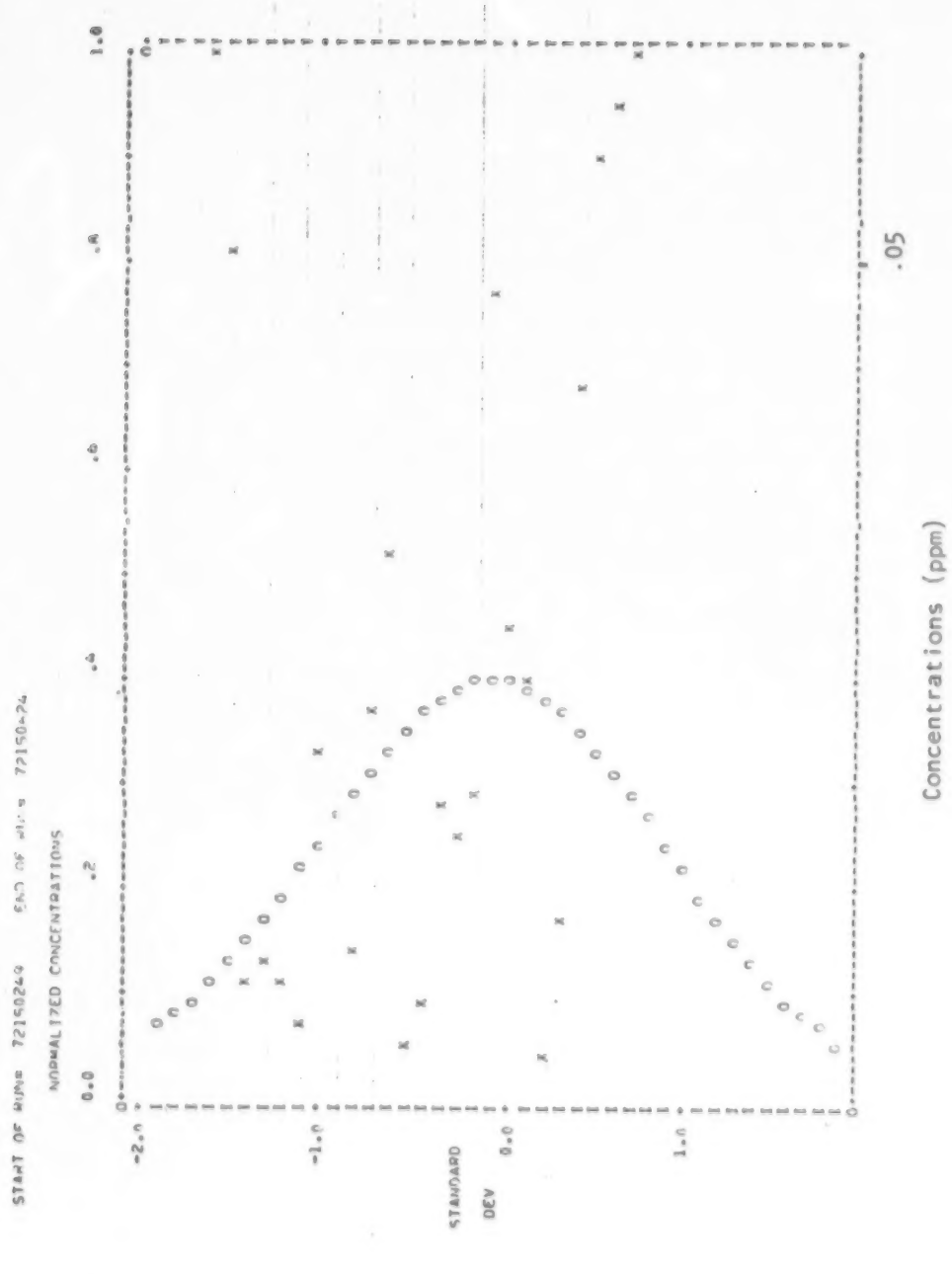
START OF RUN= 72150249 END OF RUN= 72150424
NORMALIZED CONCENTRATIONS
0.0
.2
.4
.6
.8
1.0
-2.0
-1.0
0.0
1.0
STANDARD DEV
.05
Concentrations (ppm)

Run No. 6

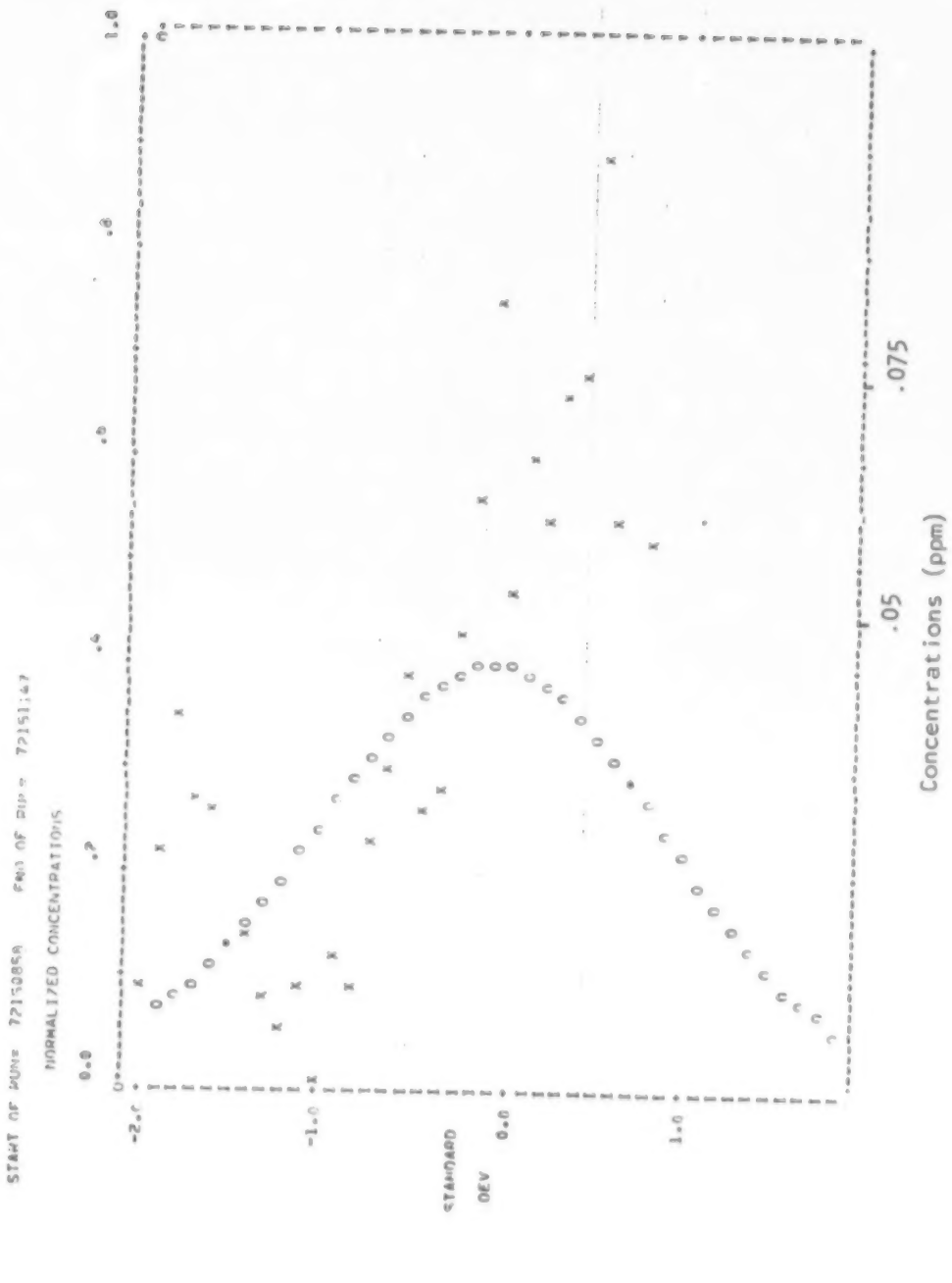
START OF RUN= 7215085A
NORMALIZED CONCENTRATIONS
-2.0
-1.0
0.0
1.0
STANDARD
DEV
.05
.075
Concentrations (ppm)

Run No. 7

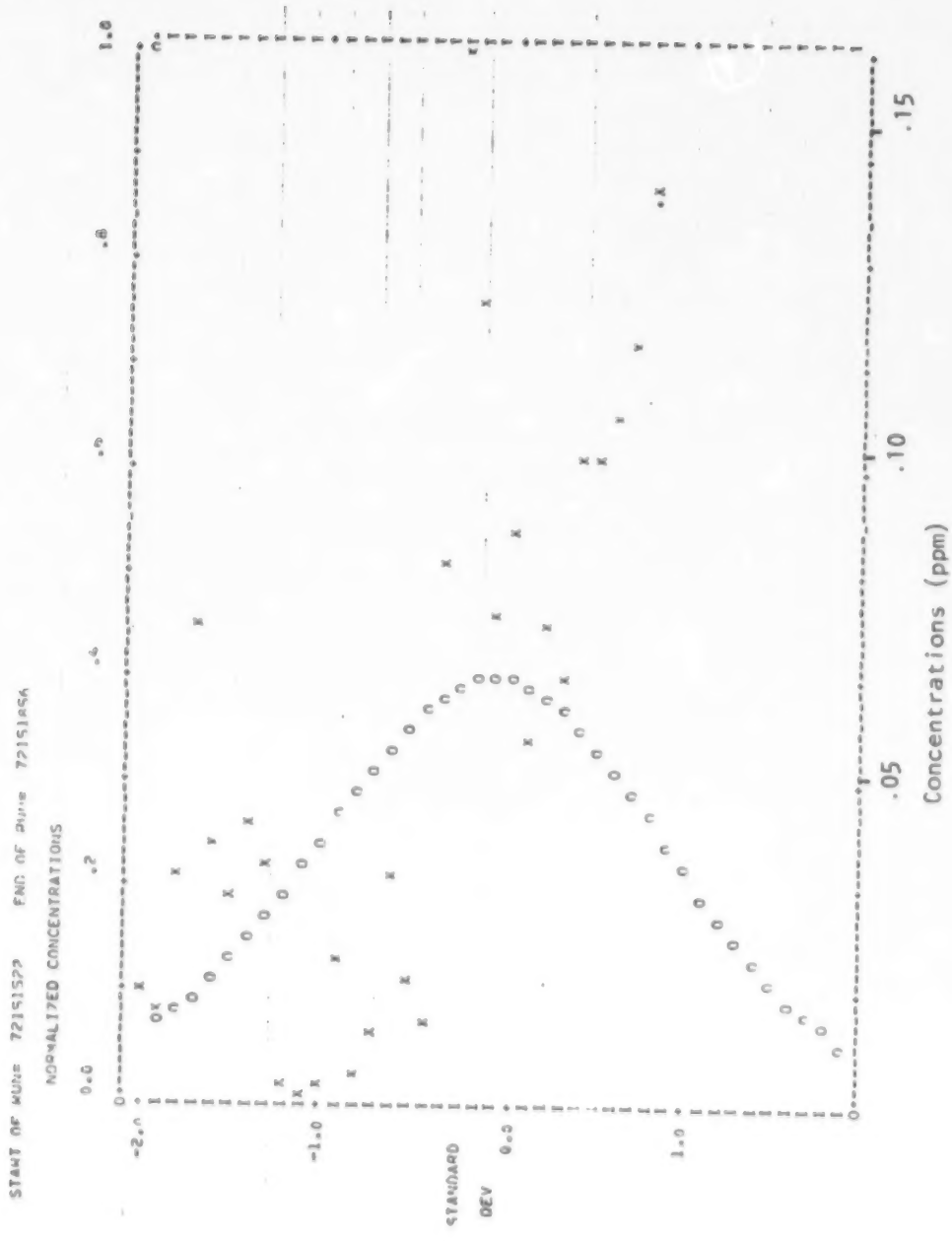
START OF RUN= 72151529 END OF RUN= 72151654
NORMALIZED CONCENTRATIONS
STANDARD DEV
Concentrations (ppm)
.05
.10
.15

Run No. 8

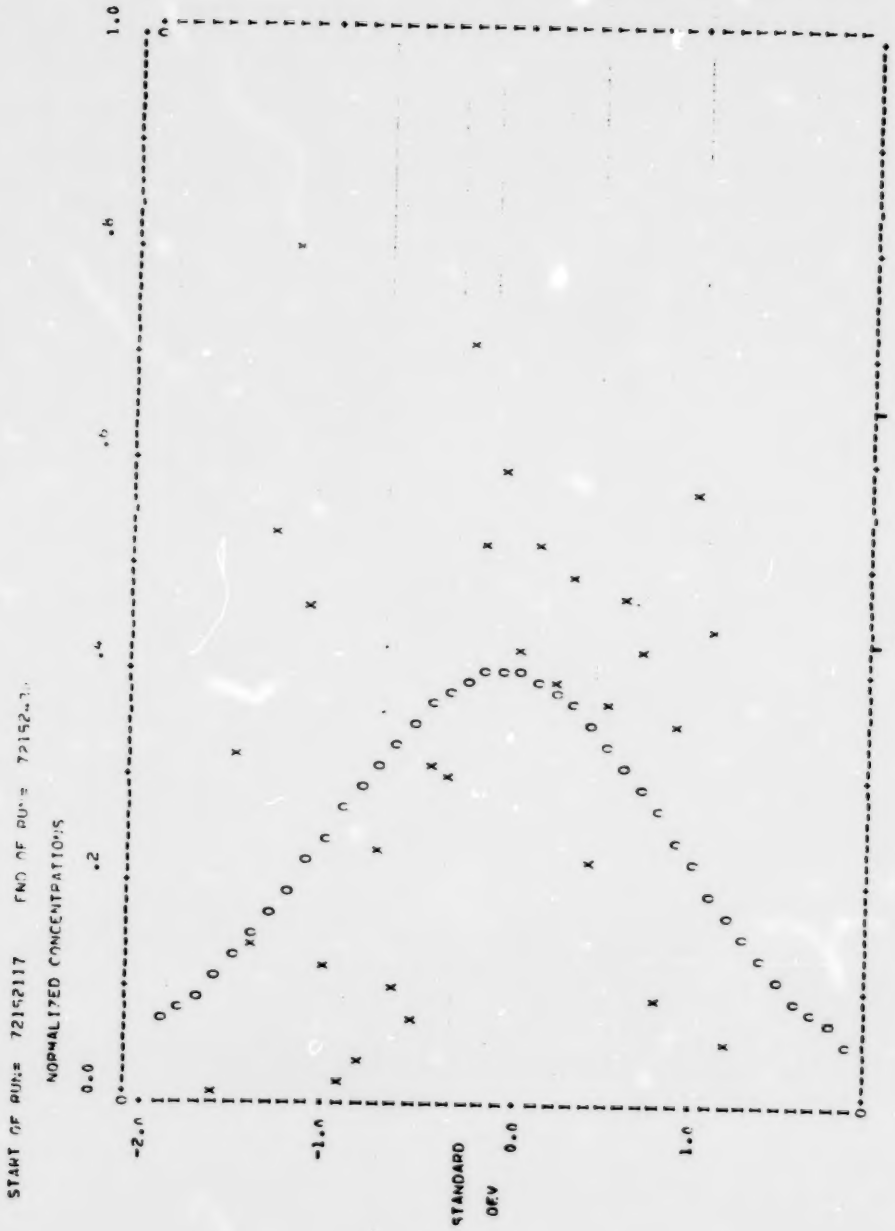
START OF RUN= 72152117 END OF RUN= 72152
NORMALIZED CONCENTRATIONS
0.0
.2
.4
.6
1.0
-2.0
-1.0
STANDARD
DEV
0.0
1.0
.05
.075
Concentrations (ppm)

Run No. 9

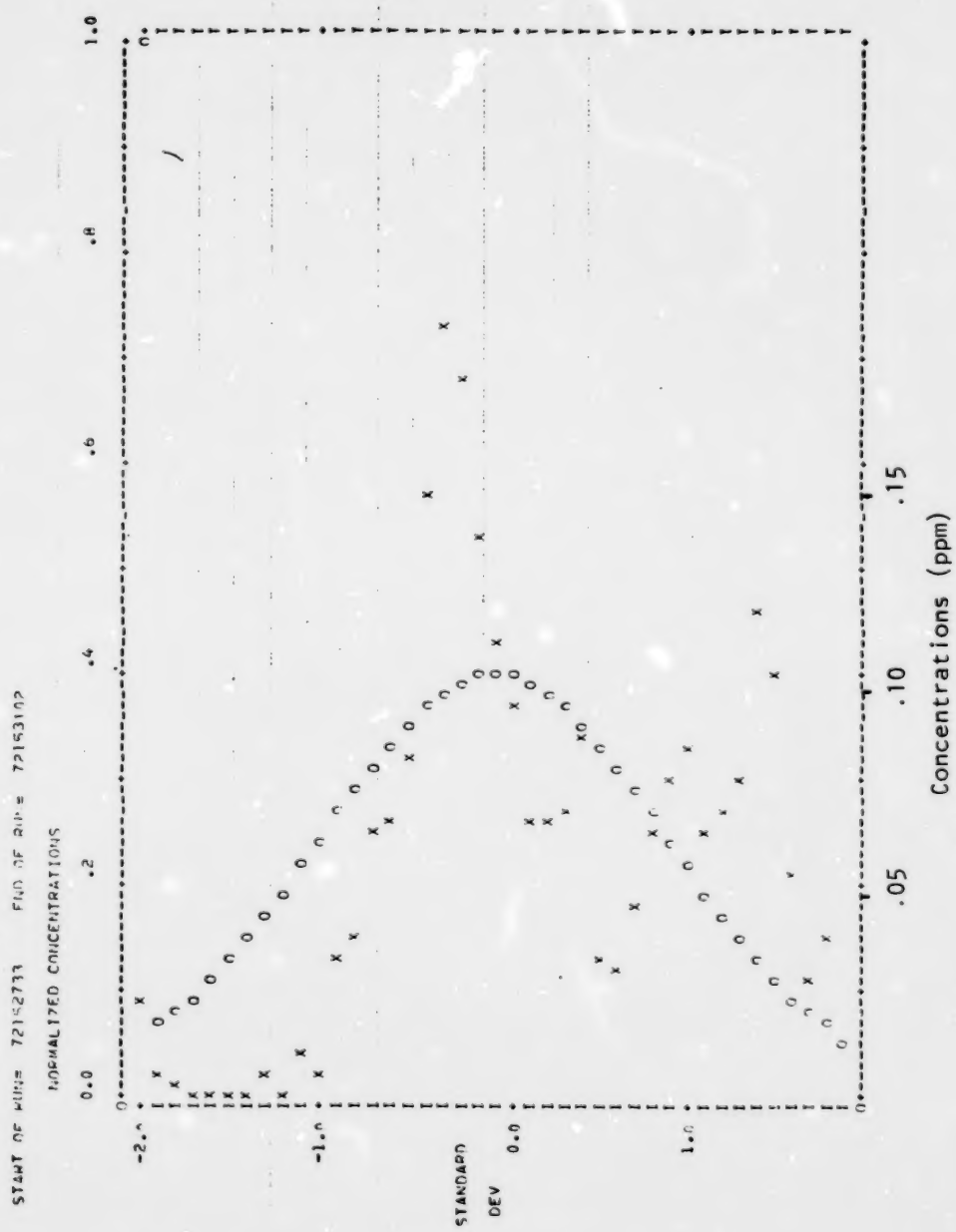
START OF RUN= 72152733 END OF RUN= 72153102
NORMALIZED CONCENTRATIONS
0.0
.2
.4
.6
.8
1.0
-2.0
-1.0
1.0
STANDARD
DEV
0.0
.05
.10
.15
Concentrations (ppm)

Run No. 10

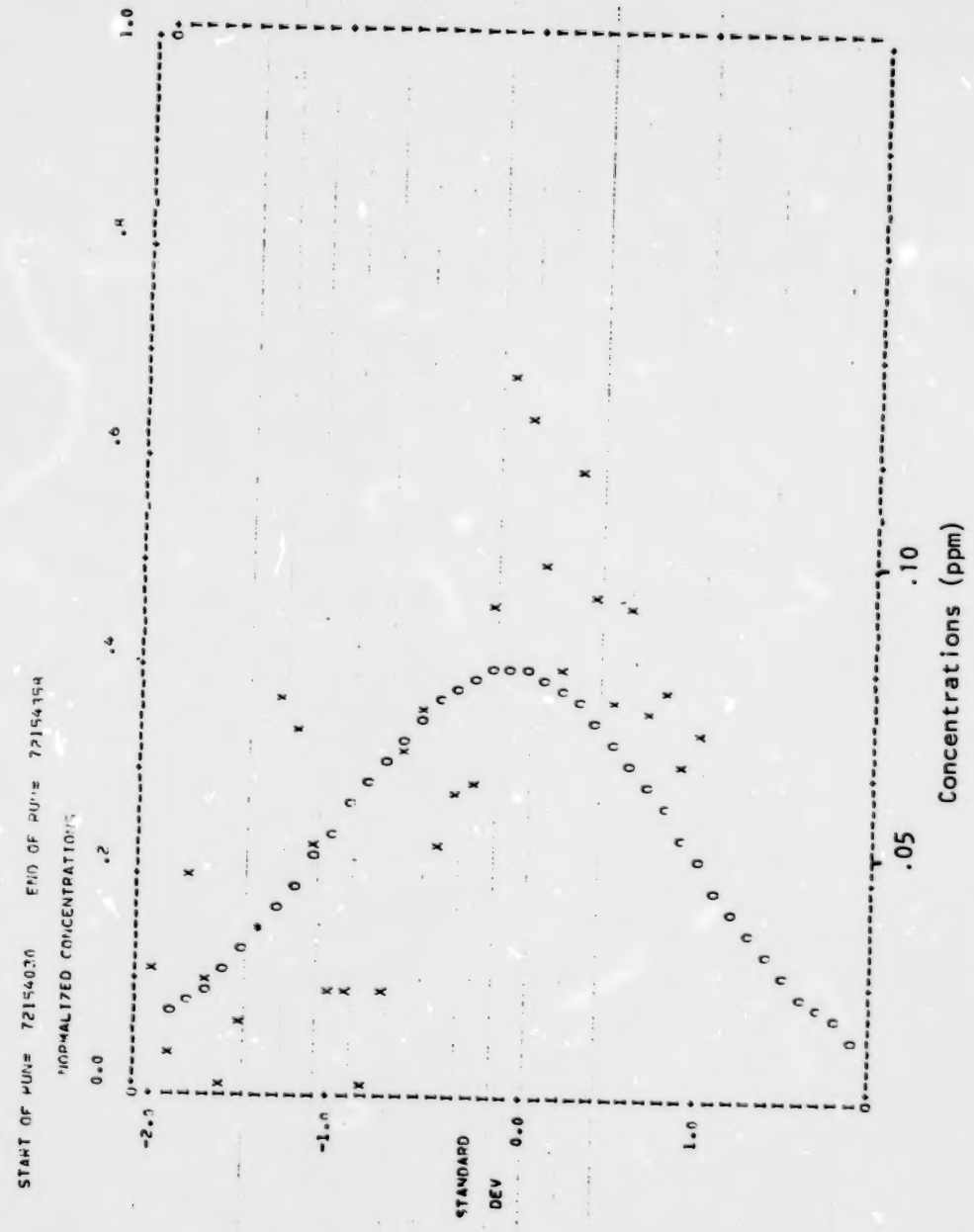
START OF RUN= 72154030 END OF RUN= 72154354
NORMALIZED CONCENTRATIONS
0.0
.2
.4
.6
.8
1.0
-2.0
-1.0
STANDARD DEV
0.0
1.0
.05
.10
Concentrations (ppm)

Run No. 12

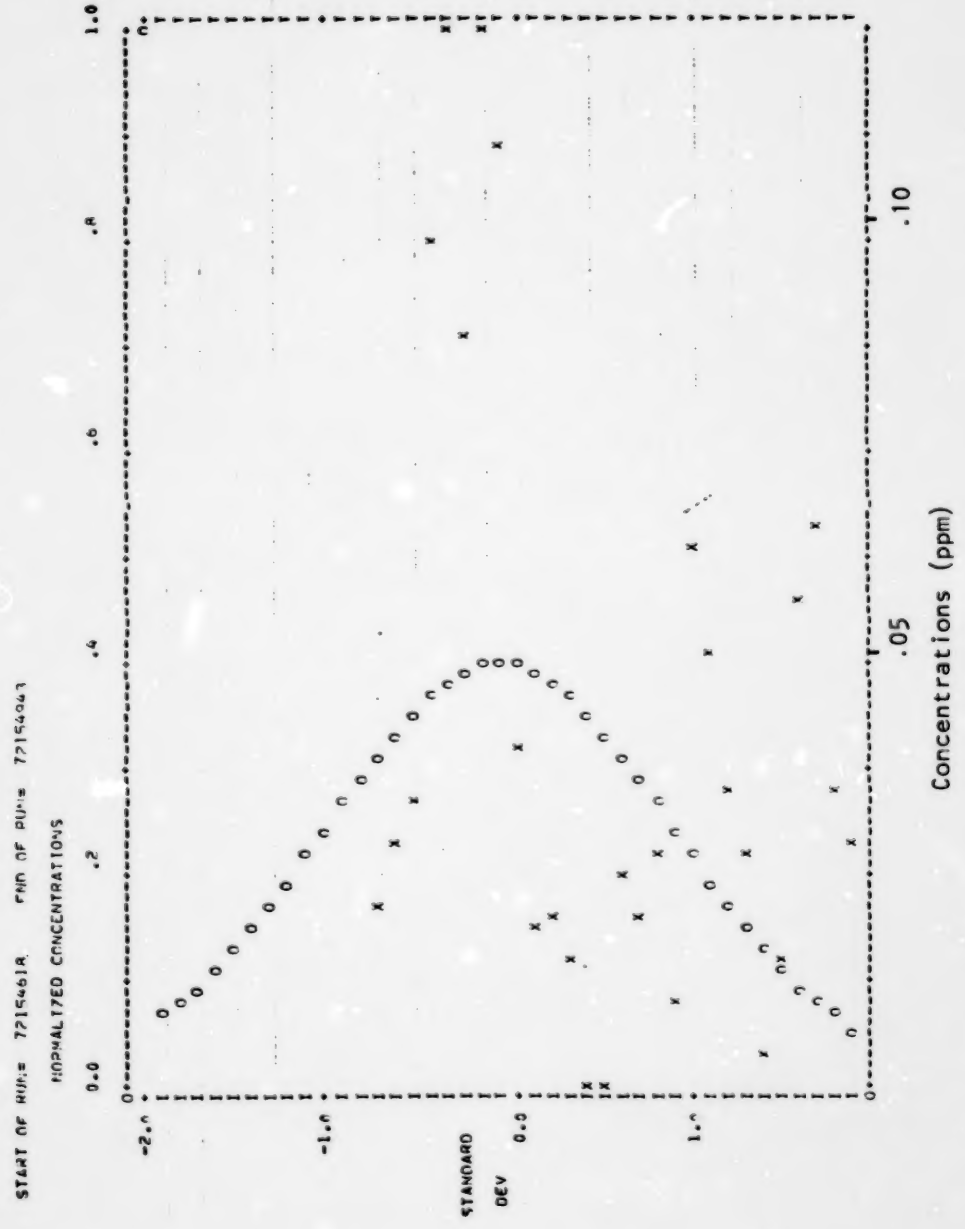
START OF RUN: 7215401R END OF RUN: 7215404J
NORMALIZED CONCENTRATIONS
STANDARD DEV
-2.0
-1.0
0.0
1.0
0.0
.2
.4
.6
.8
1.0
.05
.10
Concentrations (ppm)

Run No. 13

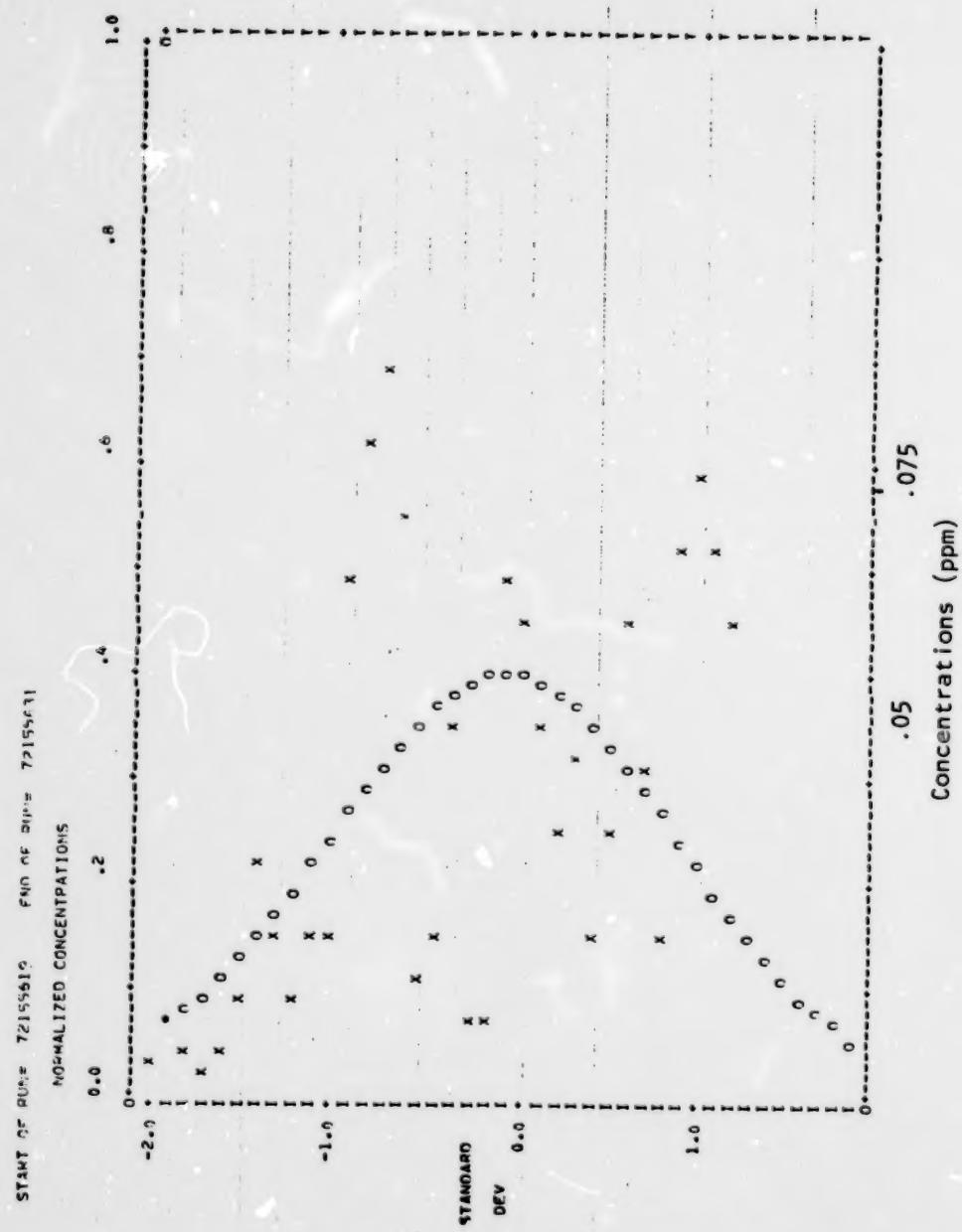
START OF RUN= 72155619 END OF RUN= 72155731
NORMALIZED CONCENTRATIONS
0.0
.2
.4
.6
.8
1.0
-2.0
-1.0
STANDARD
DEV
0.0
1.0
.05
.075
Concentrations (ppm)

Run No. 14

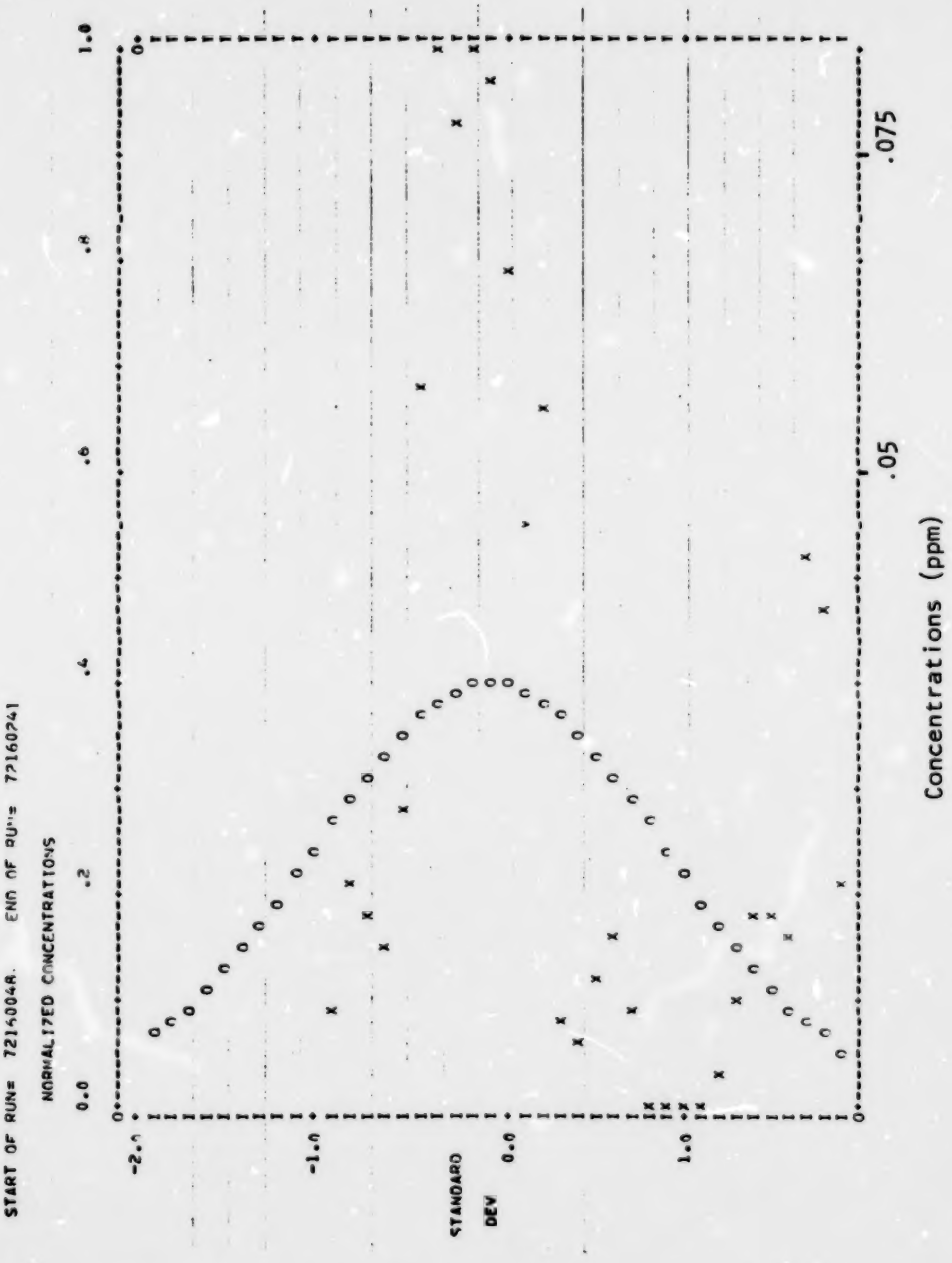
START OF RUN= 72160048. END OF RUN= 72160241
NORMALIZED CONCENTRATIONS
0.0
.2
.4
.6
.8
1.0
-2.0
-1.0
STANDARD
DEV
0.0
1.0
0
.05
.075
Concentrations (ppm)

Run No. 15

APPENDIX 5 SO_2 TRAVERSES FOR MARCH 15, 1976 AM (0740-0940).

This appendix contains the normalized SO_2 traverses for the flight of March 15, 1976 AM (0740-0940). The run information table for this flight is reproduced for convenience in interpreting each traverse.

TABLE Run information for flight of March 15, 1976 AM (0740-0940)

RUN NUMBER	TIME (MST)	ALTITUDE (m-MSL) ±20	DOWNWIND DISTANCE (km) ±0.3	σ_y (m) ±100	MAX CONC. (ppm) ±0.02	INTEGRATED CONC. (ppm-m) ±50	FLIGHT DIR. (From-to)
1	0800 - 0802	610	3.2	302	5.43	3730	NW-SE
2	0803 - 0805	610	8.0	405	4.08	3580	SE-NW
3	0807 - 0809	460	3.2	+	+	+	NW-SE
4	0811 - 0813	460	8.0	+	+	+	SE-NW
5	0815 - 0816	760	3.2	+	+	+	NW-SE
6	0820 - 0821	760	8.0	M	M	M	SE-NW
7	0823 - 0825	550	3.2	387	2.26	1550	NW-SE
8	0828 - 0830	550	8.0	473	6.12	6350	SE-NW
9	0831 - 0833	550	8.0	500	6.01	6030	NW-SE
10	0836 - 0838	520	3.2	2041	2.62	2890	SE-NW
11	0840 - 0842	520	8.0	1184	2.04	4740	NW-SE
12	0844 - 0846	670	3.2	518	2.34	1860	SE-NW
13	0848 - 0850	670	8.0	1514	0.24	270	NW-SE
14	0854 - 0901	610	-	T	T	T	S - N
15	0902 - 0912	610	-	T	T	T	N - S
16	0914 - 0920	610	9.7	T	T	T	SE-NW
17	0925 - 0929	610	8.0	T	T	T	NW-SE

T Turbulence run
\+ NO SO_2 detected on these traverses
M data lost due to system malfunction
\- run not crosswind

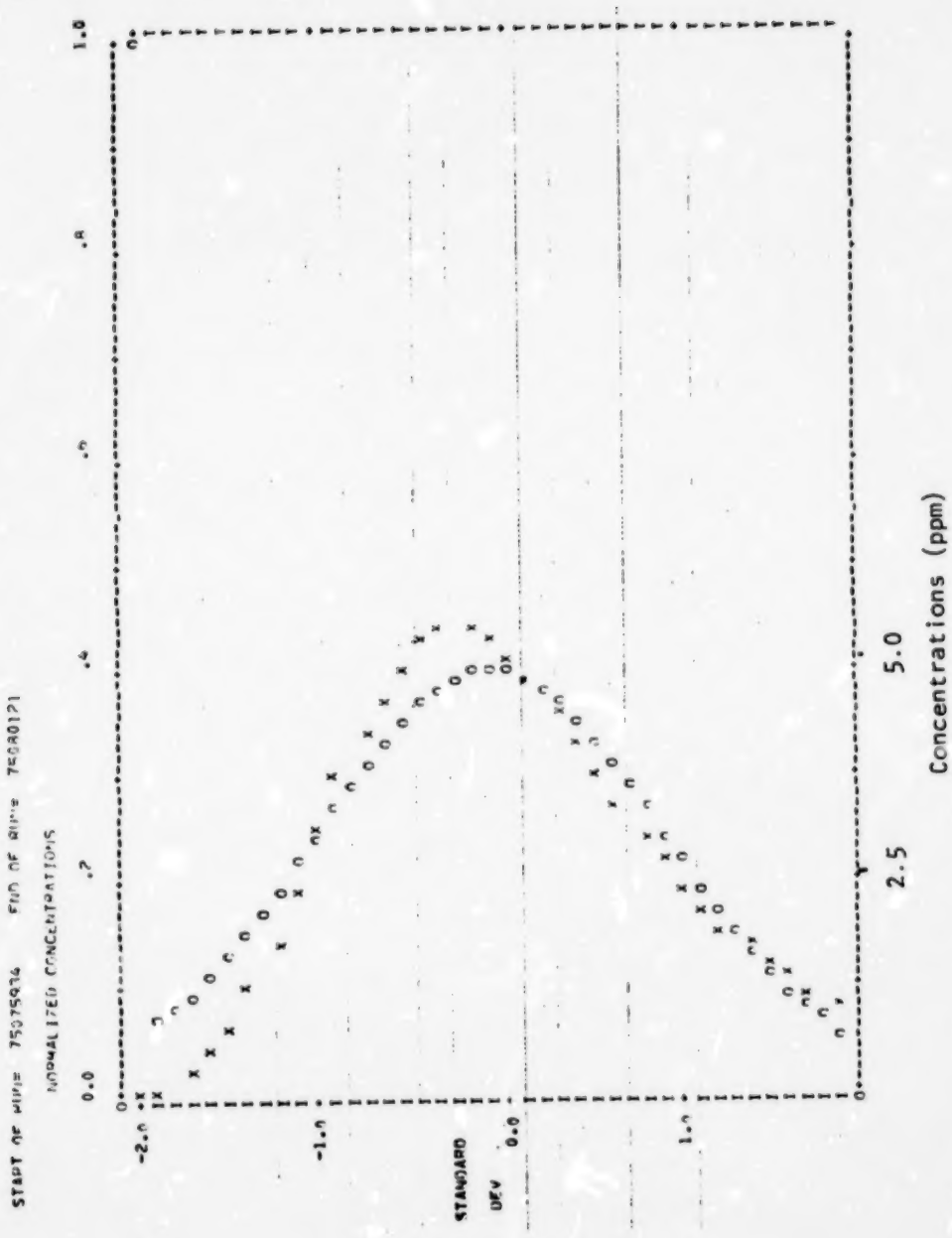
START OF RUN= 75075034 END OF RUN= 75080121
NORMALIZED CONCENTRATIONS
0.0
.2
.4
.6
.8
1.0
-2.0
-1.0
STANDARD
DEV 0.0
1.0
2.5
5.0
Concentrations (ppm)

Run No. 1

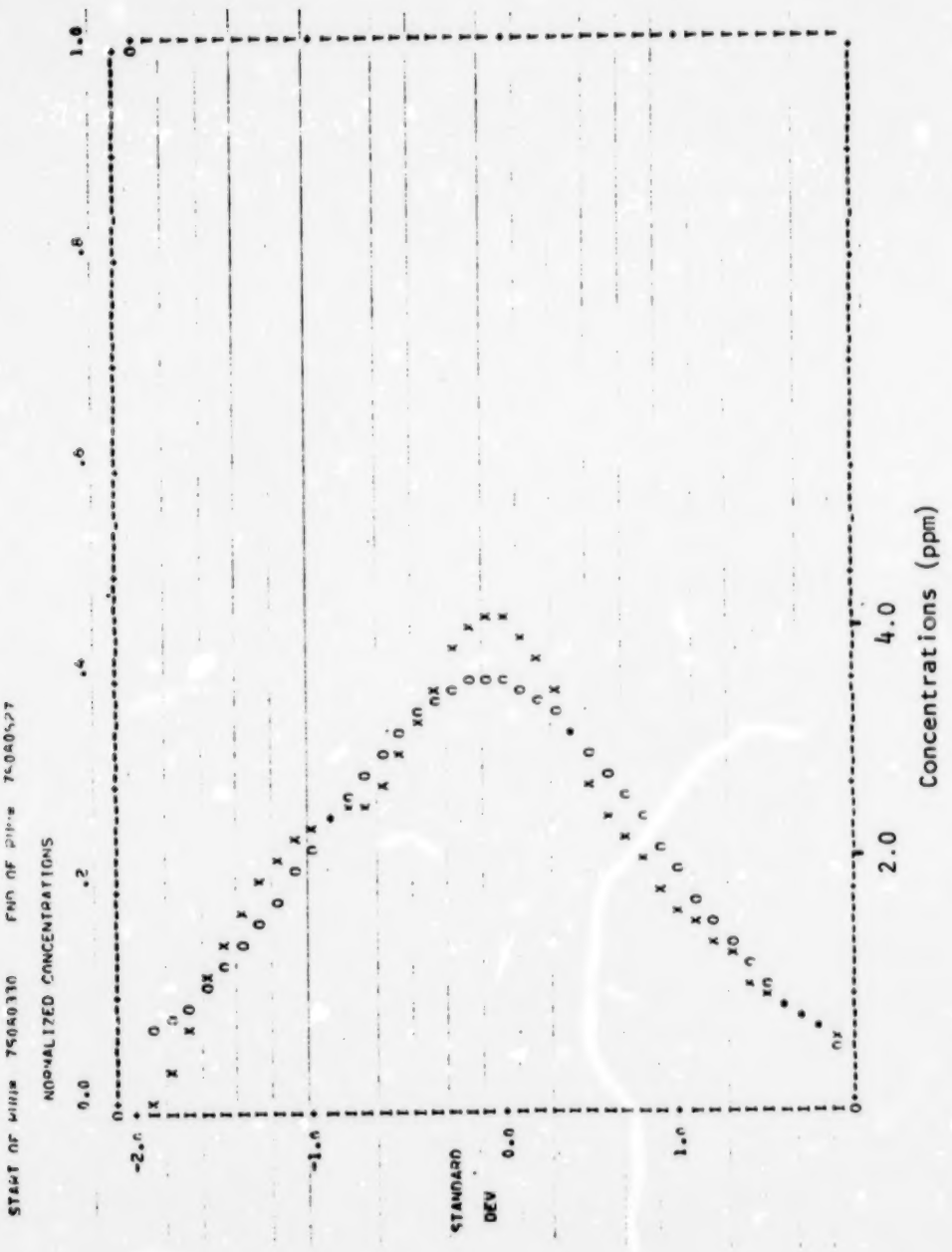
START OF RUN# 75080330 END OF RUN# 75080427
NORMALIZED CONCENTRATIONS
0.0
.2
.4
.6
.8
1.0
-2.0
-1.0
STANDARD
DEV
0.0
1.0
2.0
4.0
Concentrations (ppm)

Run No. 2

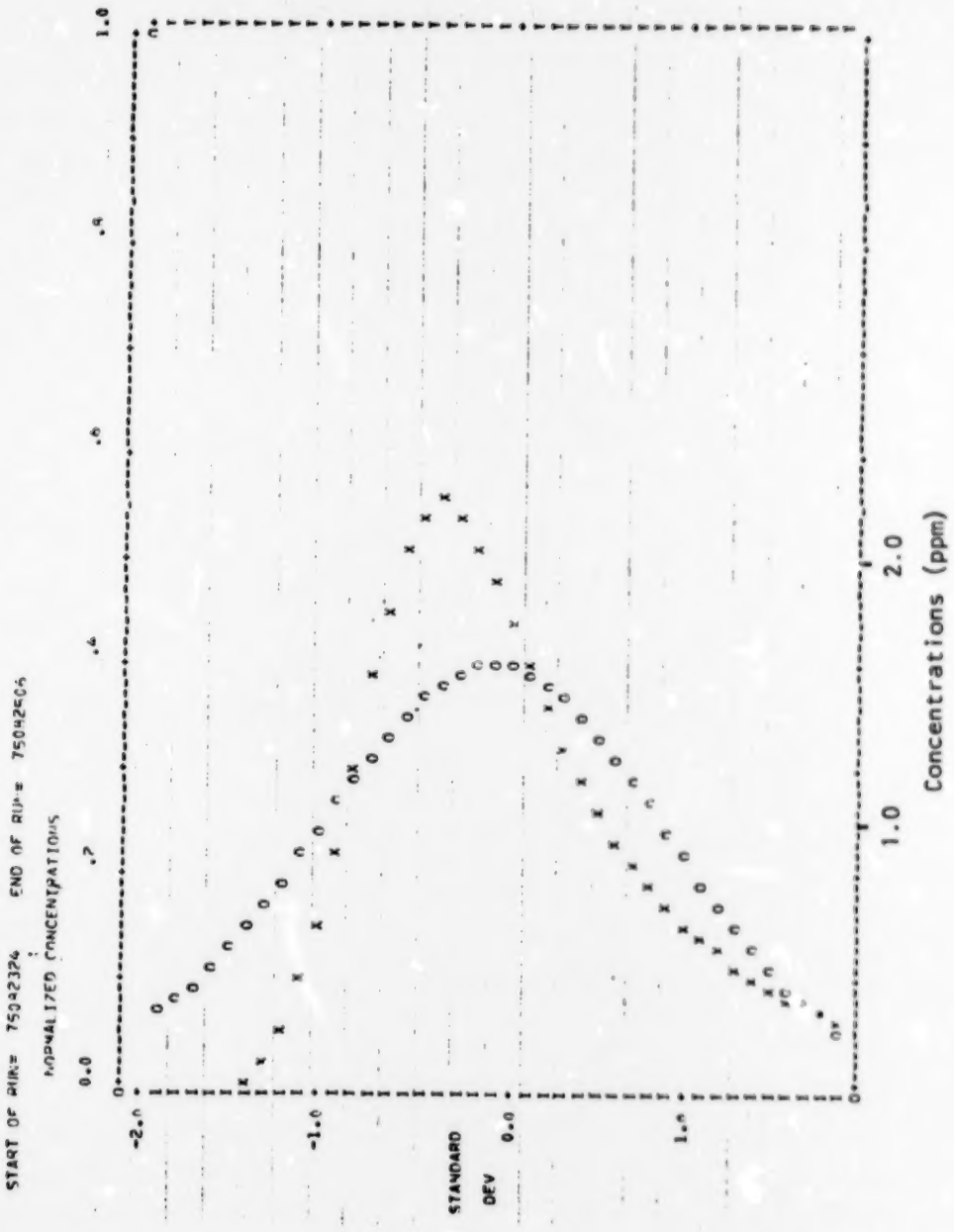
START OF RUN= 75042324 END OF RUN= 75042506
NORMALIZED CONCENTRATIONS
0.0
.2
.4
.6
.8
1.0
-2.0
-1.0
STANDARD
DEV
0.0
1.0
1.0
2.0
Concentrations (ppm)

Run No. 7

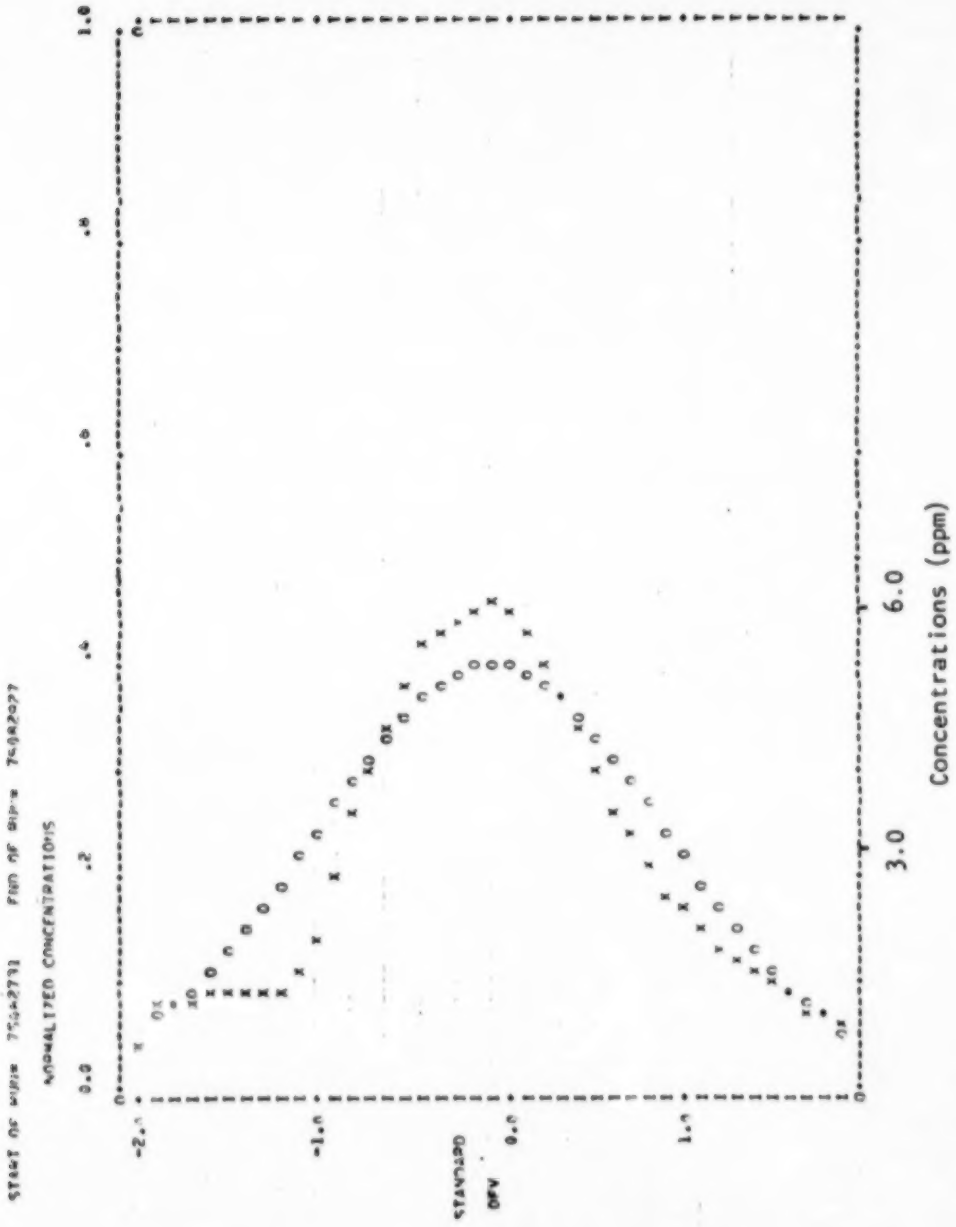
START OF WIND 75082791 END OF WIND 75082927
NORMALIZED CONCENTRATIONS
0.0
.2
.4
.6
.8
1.0
-2.0
-1.0
0.0
1.0
STANDARD
DEV
3.0
6.0
Concentrations (ppm)

Run No. 8

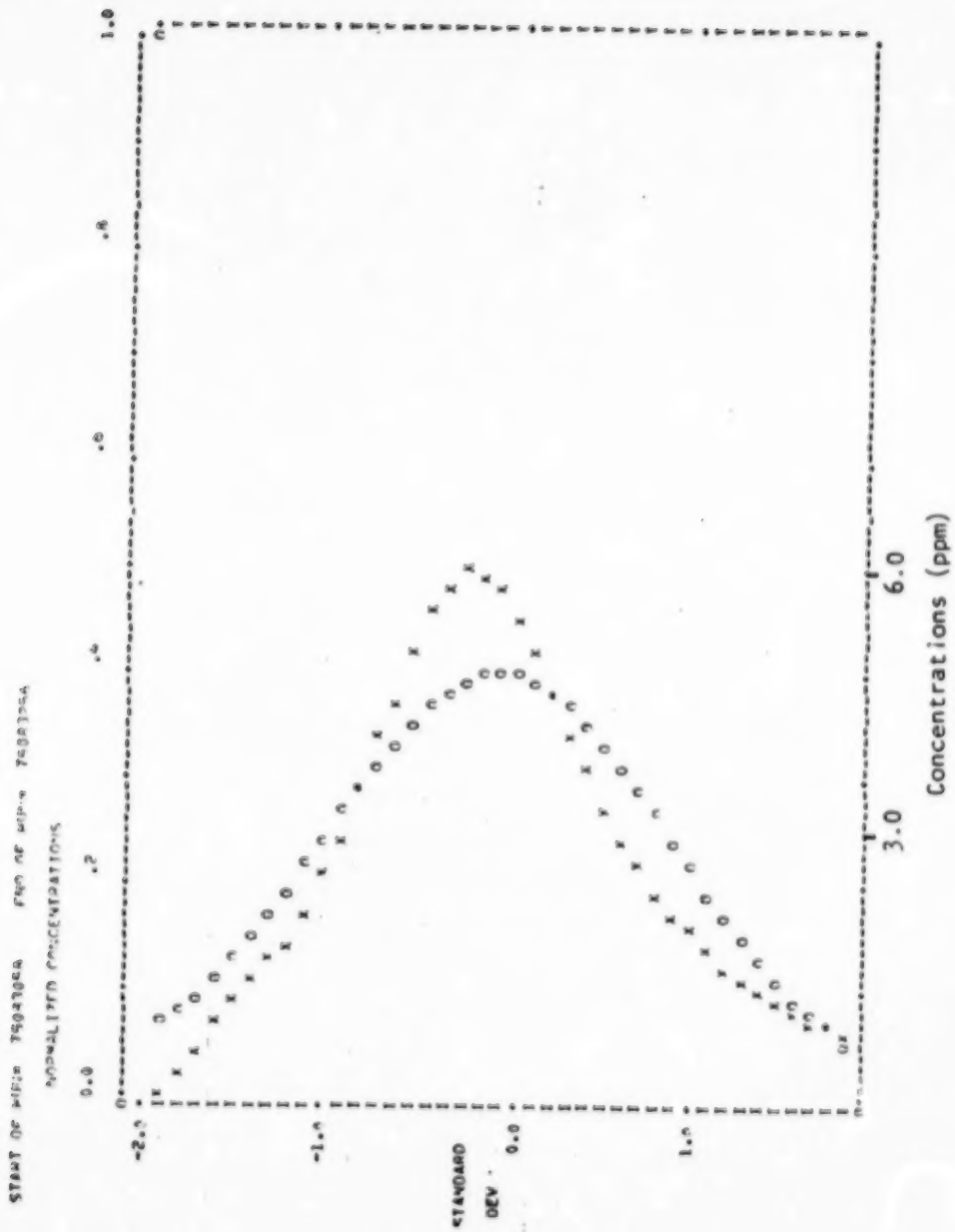

Run No. 9

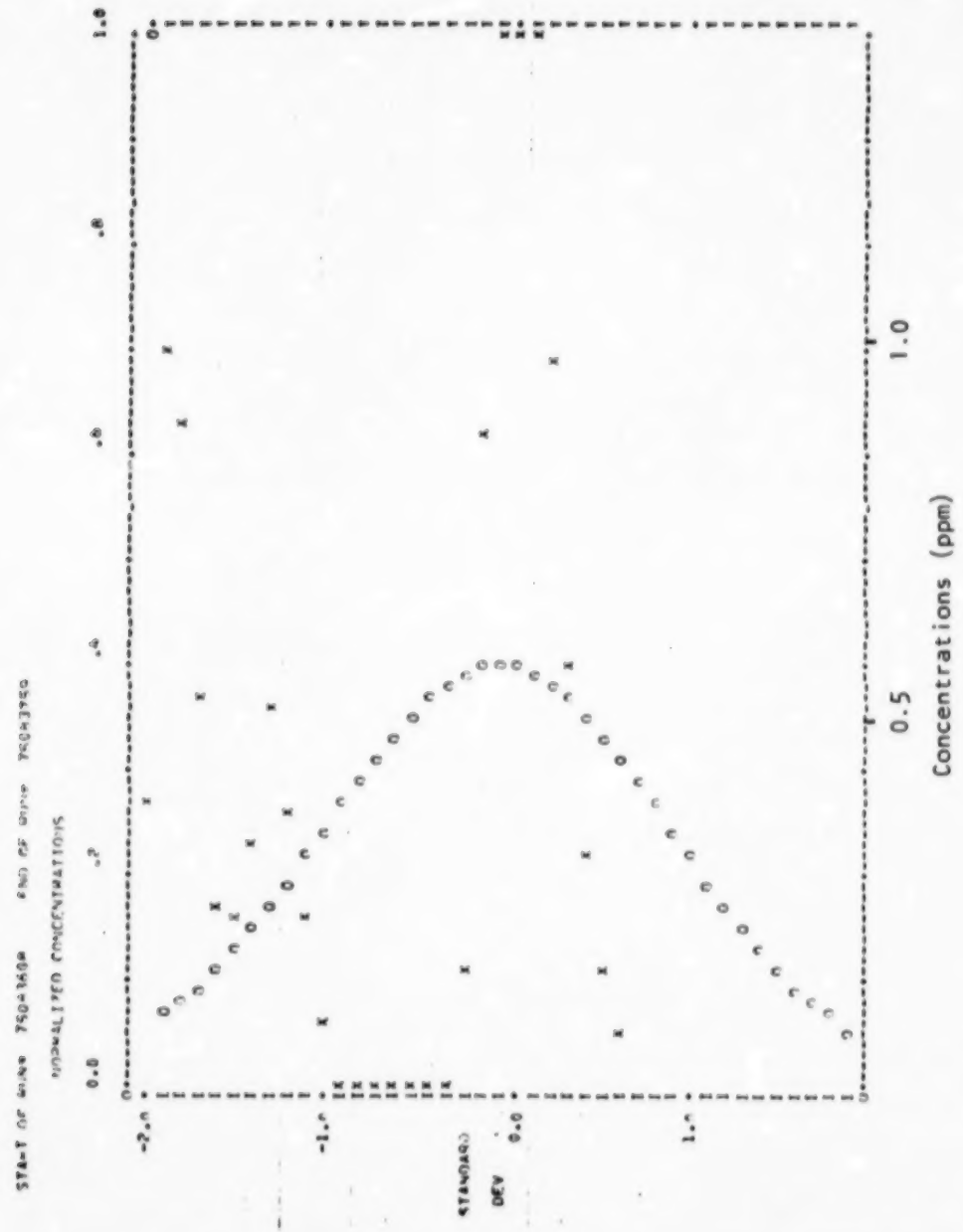
Concentrations (ppm)
0.5
1.0
-2.0
-1.0
0.0
1.0
0.0
.2
.4
.6
.8
1.0
NORMALIZED CONCENTRATIONS
STANDARD
DEV

Run No. 10

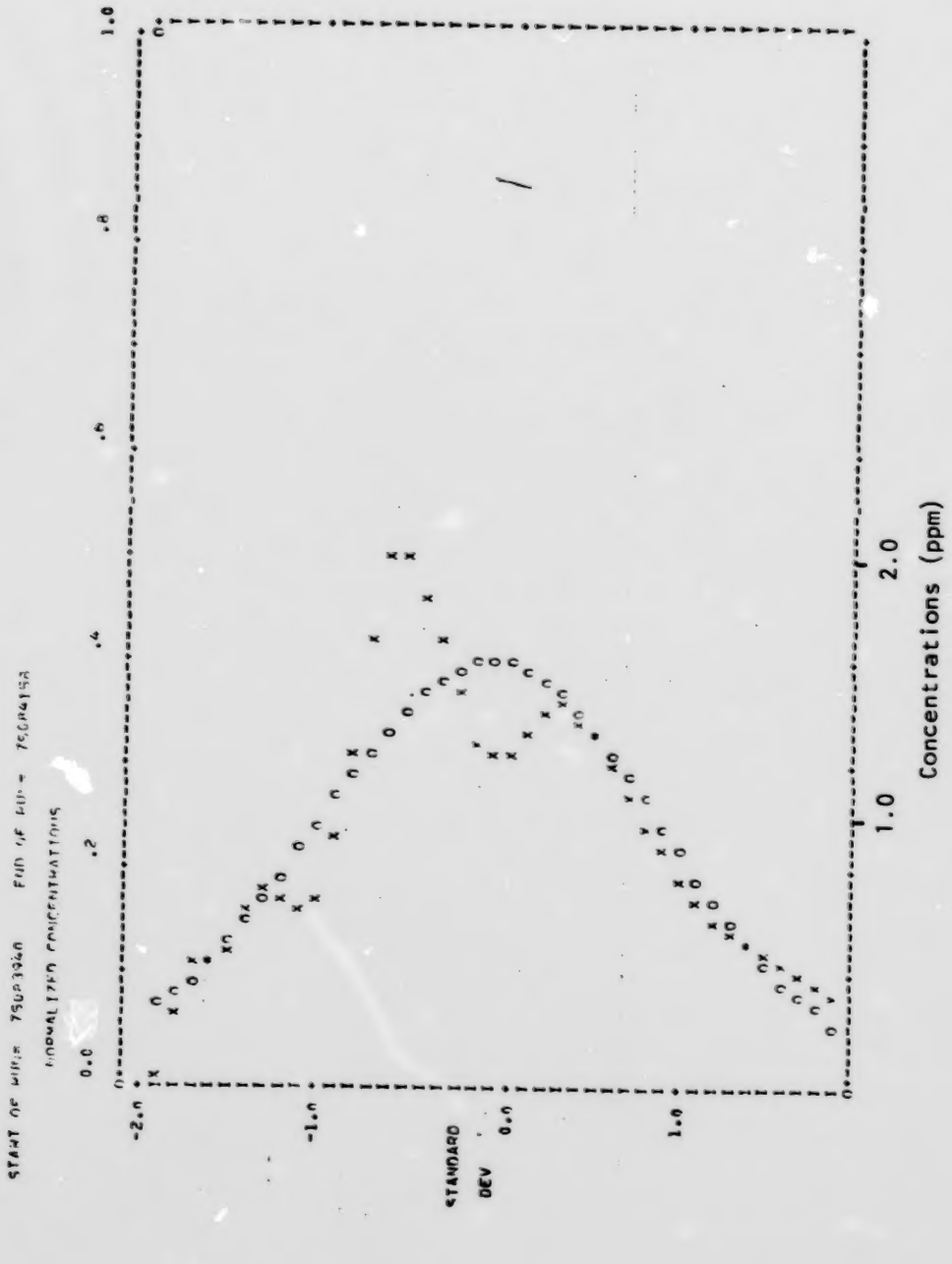
START OF RUN: 7503 1940 END OF RUN: 7503 1952
NORMALIZED CONCENTRATIONS
0.0
.2
.4
.6
.8
1.0
-2.0
-1.0
STANDARD
DEV
0.0
1.0
1.0
2.0
Concentrations (ppm)

Run No. 11

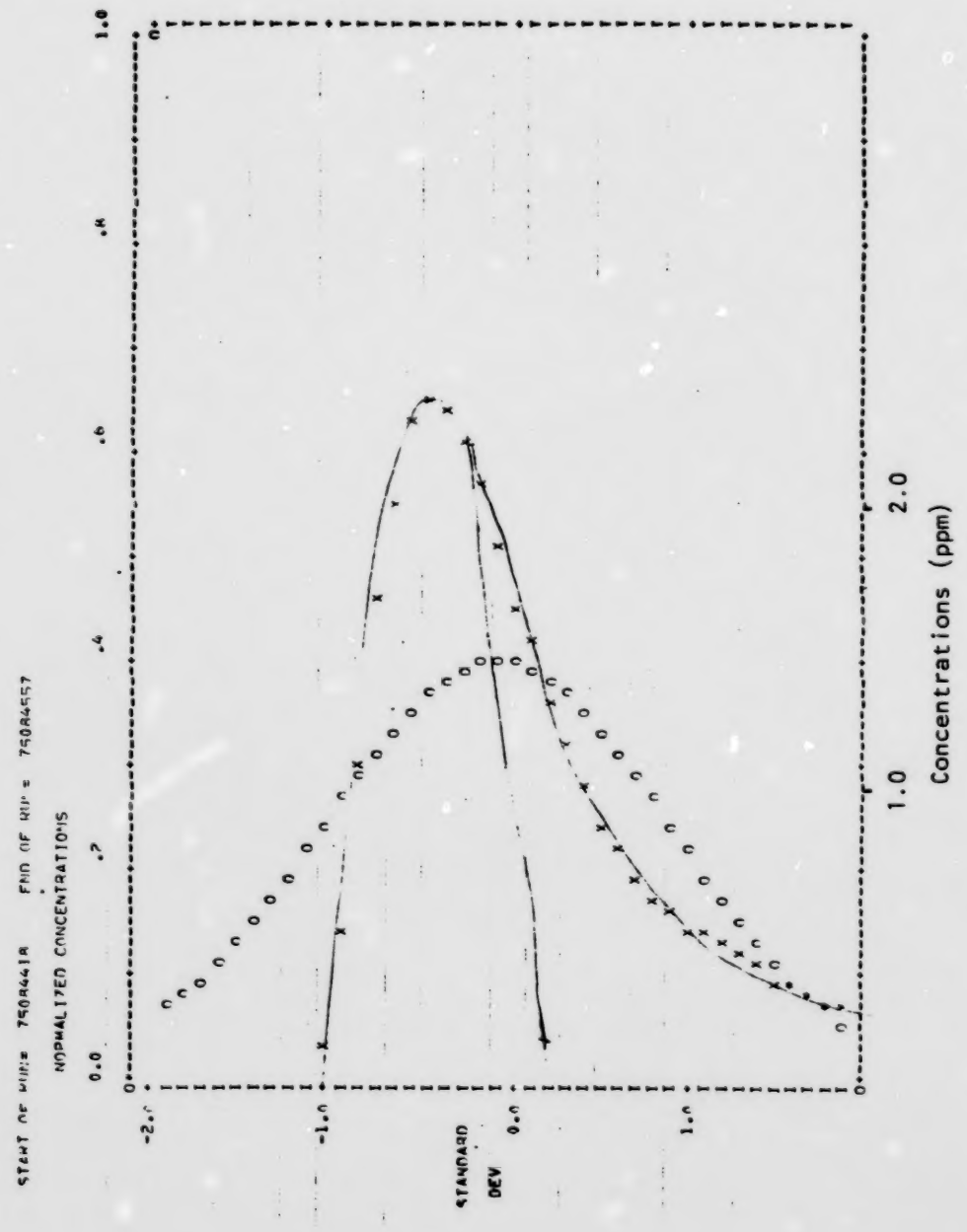
START OF RUN= 750R4418 END OF RUN= 750R4557
NORMALIZED CONCENTRATIONS
0.0
.2
.4
.6
.8
1.0
-2.0
-1.0
STANDARD DEV
0.0
1.0
1.0
2.0
Concentrations (ppm)

Run No. 12

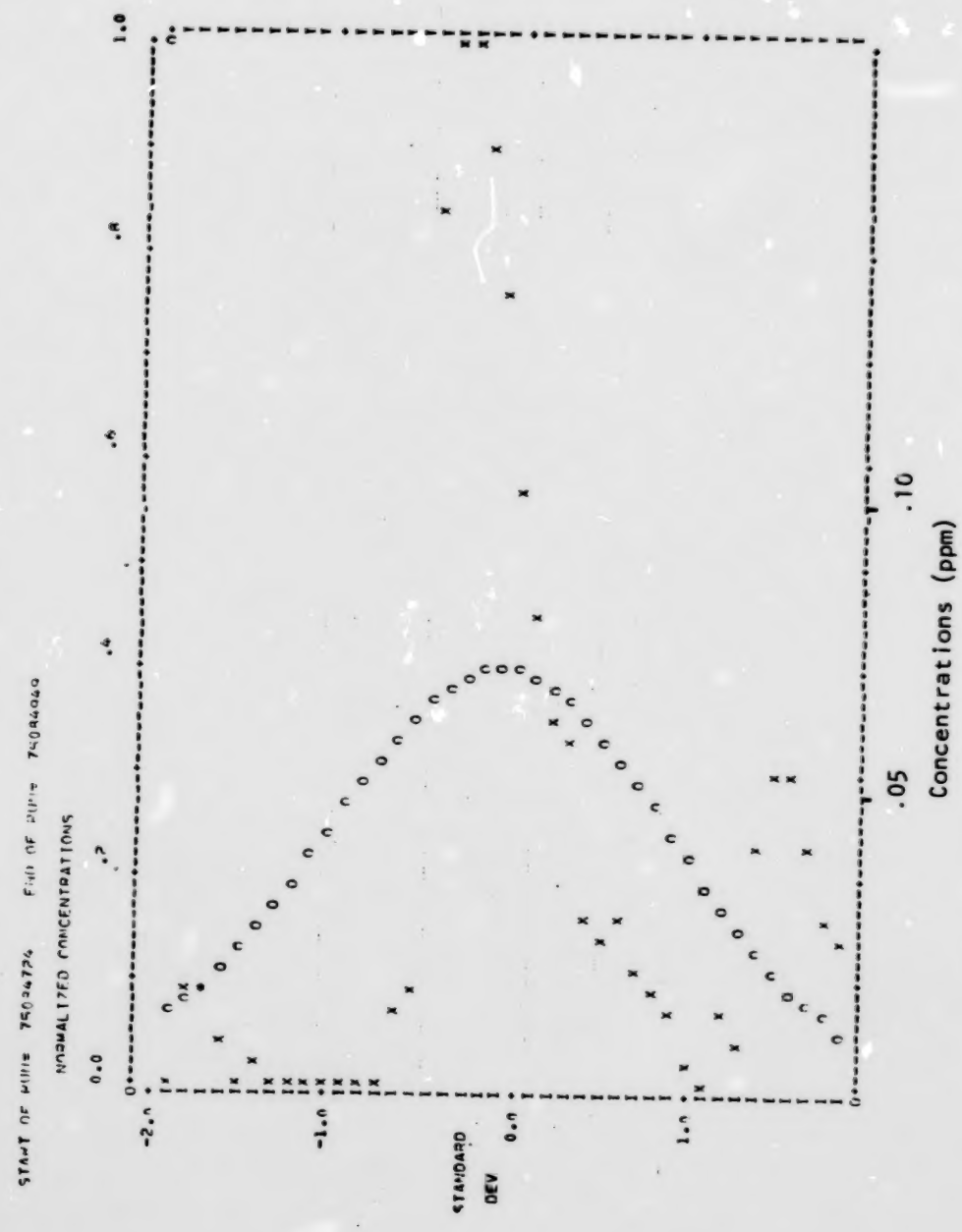
START OF RUN# 750924724 END OF RUN# 750924049
NORMALIZED CONCENTRATIONS
0.0
.2
.4
.6
.8
1.0
-2.0
-1.0
STANDARD
DEV
0.0
1.0
.05
.10
Concentrations (ppm)

Run No. 13

APPENDIX 6 EMISSION CHARACTERISTICS FROM GCOS PLANT

Emission characteristics used to calculate the plume rise were provided by Great Canadian Oil Sands Limited for the period of the field program. These are summarized for the two main stacks.

i) Incinerator stack

height	107 m
diameter	1.8 m
altitude of stack top	366 m MSL
exit temperature	603 ± 7°C
exit velocity	16.6 ±2.1 m/sec

ii) Powerhouse stack

height	107 m
diameter	5.8 m
altitude of stack top	366 m MSL
exit temperature	280 ± 18°C
exit velocity	20.1 ± 1.2 m/sec

APPENDIX 7 THE APPROPRIATE GAUSSIAN EQUATION FOR NORMALIZED AXIAL CENTER LINE CONCENTRATION

The observed normalized center line concentrations of SO_2 were compared with the predictions of a Gaussian model using dispersion coefficients commonly referred to as the Pasquill-Gifford coefficients. The time-averaged concentration field in the Gaussian model is given by (see for example, Pasquill (1971)):

$$\frac{\chi(x,y,z)\bar{U}}{Q} = \frac{1}{2\pi\sigma_y\sigma_z}\left[\exp\ -\frac{y^2}{2\sigma_y^2}\right] \cdot \left[\exp\ -\frac{(H-z)^2}{2\sigma_z^2} + \exp\ -\frac{(H+z)^2}{2\sigma_z^2}\right] \qquad \text{(A-1)}$$

where Q is the source strength and H the height of the source. The above formulations assumes complete "reflection" of the plume from the ground; the second term in the square brackets is a virtual source required to simulate the complete reflection at the surface.

Using the above model, the axial center line concentrations are given by

$$\frac{\chi(x,0,H)\bar{U}}{Q} = \frac{1}{2\pi\sigma_y\sigma_z}\left[1 + \exp\ -\frac{2H^2}{2\sigma_z^2}\right] \qquad \text{(A-2)}$$

Again, the second term in the square bracket simulates the complete reflection at the surface. Physically, it is clear that for downwind distances for which σ_z is less than or of a similar size to H, the effects of reflection of the plume at the surface cannot have a significant effect at plume center line. For large downwind distances, the second term due to the virtual source approaches unity.

If no virtual source is assumed, then the predicted concentration field at axial center line is given by

$$\frac{\chi(x,0,H)\bar{U}}{Q} = \frac{1}{2\pi\sigma_y\sigma_z} \qquad \text{(A-3)}$$

On physical grounds, it is clear that equation (A-3) is more appropriate than (A-2) for axial center line concentrations at downwind distances where σ_z is similar in size to or smaller than the effective plume height, or equivalently until the plume is well mixed in the vertical.

The Pasquill-Gifford σ_z values appropriate for the stability classes and downwind distances flow were always over a factor of two less than the observed effective stack height (see Table 22). The observed σ_z values, however, were generally a factor of two or three larger than the Pasquill-Gifford values. But even for these larger σ_z values, equation (A-3) without a virtual source is the appropriate equation for comparison of the observed axial concentrations to Gaussian predictions.

TABLE 22 A comparison of the effective stack heights with the Pasquill-Gifford σ_z values

Case Study	Assigned Stability Class (Table 21)	Observed Effective Stack Height (m)	Pasquill-Gifford σ_z value for 16 km downwind (m)
March 10	D	720	180
March 11 AM	E	350	100
March 11 PM	D	510	180
March 12	D	660 (1310)	180
March 15	F	310	56
*	C		790
*	B		2300

* no case studies had these stabilities; however the comparison of the Pasquill-Gifford σ_z values for unstable cases with observed stack heights for the neutral and stable cases is useful.

the non-bracketted value for the observed effective stack height on March 12 is for a downwind distance of 4.8 km; the bracketted value is for 11.3 km.